

**Eco-friendly Synthesis of Fly Ash and Volcanic Ash
Supported Solid Base Catalysts for Conventional
and Microwave Assisted Organic Transformations**

A Thesis

Submitted for the Award of

Doctor of Philosophy

Degree

In Chemistry

(Faculty of Science)

to the

UNIVERSITY OF KOTA, KOTA



Supervised by

Prof. Ashu Rani

Submitted by

Stuti Katara

Department of Pure & Applied Chemistry

University of Kota, Kota

2015



UNIVERSITY OF KOTA, KOTA
M.B.S. Marg, Near Kabir Circle, Kota (Raj.)

Prof. Ashu Rani
Head
Dept. of Pure & Applied Chemistry
University of Kota, Kota

Residence
2-m-1, Rangbari Scheme
Kota-324005 (Raj.) India
Ph: 0744-2420815
e-mail: ashu.uok@gmail.com

Date.....

CERTIFICATE

It is to certify that the

- i. Thesis entitled “*Eco-friendly Synthesis of Fly Ash and Volcanic Ash Supported Solid Base Catalysts for Conventional and Microwave Assisted Organic Transformations*” submitted by *Stuti Katara* is an original piece of research work carried out by the candidate under my supervision.
- ii. Literary presentation is satisfactory and the thesis is in a form suitable for publication.
- iii. Work evidences the capacity of the candidate for critical examination and independent judgment.
- iv. Candidate has put in at least 200 days of attendance every year.

Prof. Ashu Rani

Dedicated
To
My Parents

*“All of Science is nothing more than
the refinement of everyday thinking.”*

-Albert Einstein

ACKNOWLEDGEMENT

Words are often less to reveals one's deep regards. With an understanding that work like this can never be the outcome of a single person, I take this opportunity to express my profound sense of gratitude and respect to all those who helped me through the duration of this work.

First and foremost, praises and thanks to “**Shri Bade Mathuradhish Ji**” for his showers of blessings, for leading me in the right path and for giving me strength to cross the toughest situations.

I avail this opportunity to extend my hearty indebtedness to my research supervisor **Prof. Ashu Rani** for her invaluable guidance, untiring efforts, patience, constant motivation and regular monitoring and meticulous attention at all stages during my research work. I would also like to convey my deep regards for her apart from the subject of my research, I learnt a lot from her, which I am sure, will be useful in different stages of my life. She has provided many opportunities for me to increase my abilities as a researcher and responsibilities as a team member.

I am grateful to **Sh. Onkar Singh**, Vice Chancellor and **Prof. Madhusudan Sharma**, former Vice Chancellor, University of Kota, Kota, for allowing me to carryon my research work in his respective institute.

I would like to thank **Dr. Arun Kumar**, Lecturer, Department of Mathematics, Govt. College, Kota, faculty members of Department of Pure & Applied Chemistry, University of Kota, **Dr. Niloo Chauhan, Dr. Bhawani Singh, Dr. Shweta Vyas, Mr. Ankit Sharma, Dr. Sushil Sharma, Dr. Shweta Saxena, Dr. Bhartiya Sharma, Dr. Suman Khinchi** and official staff of Department, Research section and Accounts section of University of Kota, for immediate help and timely cooperation.

I would like to acknowledge **Dr. Mukul Gupta, Dr. T. Shripathi, Dr. D. M. Phase, Dr. Uday Deshpande** of UGC-DAE Consortium for Scientific Research, Indore, and technical staff of **University of Pune, Pune, IIT Bombay,**

Mumbai, **SAIF**, Chandigarh, **IIT-Roorkee**, Roorkee, **CDRI**, Lucknow for providing instrumentation facilities for sample analysis. I would like to thank **Mr. Rawat** and **Mr. Chauhan**, Indica Chem. Ind. Pvt. Ltd., Kotdwar (Uttarakhand) for providing me samples of volcanic ash. I would like to express my sincere thanks to **UGC** for giving me **Junior and Senior Research Fellowship** and **Fly Ash Mission Project**, sanctioned to **Prof. Ashu Rani** for providing me analytical support in my department.

I am grateful to my ex-colleagues **Dr. Deepti**, **Dr. Anita**, **Dr. Shefali**, my lab-mates **Sakshi**, **Renu**, **Khushboo**, **Niharika**, **Priyanka**, **Hari Om**, **Swarnima**, **Niranjan** and **Rajesh** for their unconditional support and friendly atmosphere in the lab throughout my research career.

The highest gratitude goes to my family. My family has always been a source of inspiration and encouragement. I wish to thank my father **Mr. Chandra Shekhar Katara** and my mother **Mrs. Anita Katara**, whom love, teachings and support have brought me this far. I wish to thank my elder brother **Mr. Hemant Katara** for his affection, understanding and support and my uncle **Dr. Rakesh Katara** for his guidance and sharing all the knowledge regarding research. I am deeply thankful to my uncle **Mr. Subhash Chaturvedi**, my Bhuaji **Mrs. Rama Sharma**, brother **Mr. Davesh Sharma** and my loving sister **Mrs. Sudhi Sharma**, for unconditional support and help. Last but not the least, I would also like to thank all members of **Katara** (paternal) and **Sharma** (maternal) families for their support, love and wishes.



Stuti Katara

INDEX

CHAPTERS	PAGE NO.
Chapter 1 : Introduction	1-27
1.1 Solid base catalysts	1
1.2 Generation of basic sites	2
1.3 Characterization of basic surfaces	4
1.4 Types of solid base catalysts	10
1.5 Fly ash	21
1.6 Volcanic ash	22
1.7 Scope of the work	23
1.8 References	23
Chapter 2 : Synthesis and Characterization of Solid Base Catalyst from Perlite and Its Catalytic Application in Cross- Aldol Condensation	28-54
Abstract	28
2.1 Introduction	29
2.2 Experimental	31
2.3 Catalyst characterization	32
2.4 Catalytic activity of KATP catalyst	34
2.5 Catalyst regeneration	35
2.6 Results and discussion	35
2.7 Catalytic activity	45
2.8 Reaction mechanism	48
2.9 Catalyst regeneration	51
2.10 Conclusion	53
2.11 References	53

Chapter 3 : Magnesium Nitrate Activated Perlite as Solid Base Catalyst for Microwave Assisted Nitroaldol Condensation Reaction **55-85**

Abstract	55
3.1 Introduction	56
3.2 Experimental	58
3.3 Catalyst characterization	60
3.4 Experimental setup	60
3.5 Catalytic activity of MTP catalyst	63
3.6 Catalyst regeneration	65
3.7 Results and discussion	65
3.8 Catalytic activity	75
3.9 Reaction mechanism	78
3.10 Catalyst regeneration	81
3.11 Conclusion	83
3.12 References	84

Chapter 4 : Strontium Nitrate Activated Fly Ash: An Efficient Solid Base Catalyst for Microwave Assisted Michael Addition Reaction **86-115**

Abstract	86
4.1 Introduction	87
4.2 Experimental	89
4.3 Catalyst characterization	90
4.4 Catalytic activity of SrTFA catalyst	92
4.5 Catalyst regeneration	93
4.6 Results and discussion	93
4.7 Catalytic activity	102
4.8 Reaction mechanism	106

4.9	Catalyst regeneration	109
4.10	Conclusion	112
4.11	References	113

**Chapter 5 : Barium Nitrate Activated Fly Ash: Synthesis,
Characterization and Its Catalytic Application**

116-146

Abstract		116
5.1	Introduction	117
5.2	Experimental	118
5.3	Catalyst characterization	119
5.4	Catalytic activity of BaTFA catalyst	119
5.5	Catalyst regeneration	122
5.6	Results and discussion	122
5.7	Catalytic activity	134
5.8	Reaction mechanism	138
5.9	Catalyst regeneration	138
5.10	Conclusion	143
5.11	References	144

**Chapter 6 : Silica Enrichment in Fly Ash and Synthesis of Solid
Base Catalyst for Claisen-Schmidt Condensation
Reaction**

147-171

Abstract		147
6.1	Introduction	148
6.2	Experimental	149
6.3	Catalyst characterization	150
6.4	Catalytic activity of CaSFA catalyst	150
6.5	Catalyst regeneration	152

6.6	Results and discussion	152
6.7	Catalytic activity	163
6.8	Reaction mechanism	166
6.9	Catalyst regeneration	169
6.10	Conclusion	170
6.11	References	170

ANNEXURE I **172-174**

ANNEXURE II **175-178**

Publications

Chapter 1

Introduction

Sir Humphrey Davy first observed the phenomenon of catalysis during the development of the mine safety lamp in 1816. In 1835, Jons Jakob Berzelius defined the term catalyst. A catalyst is a substance that increases the rate at which a chemical reaction will reach equilibrium, without itself being consumed in the reaction process [1]. The action of the catalyst is called catalysis and it comes from two Greek words: *Kata*- “down” and *lyein* “loosen”.

The use of a catalyst provides a higher reaction rate at the same given temperature without affecting the equilibrium of the reaction. The rate of the forward reaction is increased thus the rate of the back reaction is also increased. Hence the energy profile for a catalyzed reaction and an uncatalyzed reaction differ only in the height of the activation curve.

Catalysts are divided in two main forms, namely heterogeneous and homogeneous. Homogeneous catalysts exist in the same phase as that of the reactants whereas the former describes a system in which the catalyst exists in a different phase than that of the reactants. Usually heterogeneous catalysts exist in solid form while the reactants are liquids/gases.

1.1 Solid base catalysts

Solid base catalysts are originally defined as catalysts for which the color of an acidic indicator changes when it is chemically adsorbed. There are two types of solid bases: Bronsted and Lewis base. According to Bronsted and Lewis definitions, a Bronsted base is a proton acceptor and Lewis base is an electron-pair donor [2]. Because of the advantages over liquid bases, the use of solid base catalysts in organic synthesis is expanding. Solid bases are non-corrosive and easier to dispose than liquid bases, separation and recovery of products, catalysts recovery and reuse are easier in case of solid base catalyst. Furthermore, base-catalyzed reactions can be performed without using solvents and even in the gas phase, opening up more possibilities for discovering novel reaction systems [3]. Examples of the application of recyclable solid base catalysts are far fewer than for solid acids because a number of industrially important reactions are solid acid catalyzed therefore fewer efforts have been devoted to solid base catalysts [4].

Four reasons for recognizing certain materials as heterogeneous basic catalysts are as follows.

(1) Characterization of the surfaces indicates the existence of basic sites: characterizations of the surfaces by various methods such as color change of the acid-base indicators adsorbed, surface reactions, adsorption of acidic molecules, and spectroscopies (UV, IR, XPS, ESR etc.) indicate that basic sites exist on the surfaces.

(2) There is a parallel relation between catalytic activity and the amount and/or strength of the basic sites: The catalytic activities correlate well with the amount of basic sites or with the strength of the basic sites measured by various methods. Also, the active sites are poisoned by acidic molecules such as HCl, H₂O and CO₂.

(3) The material has similar activities to those of homogeneous basic catalysts for “base-catalyzed reactions” well-known in homogeneous systems. There are a number of reactions known as base-catalyzed reactions in homogeneous systems. Certain solid materials also catalyse these reactions to give the same products. The reaction mechanisms occurring on the surfaces are suggested to be essentially the same as those in homogeneous basic solutions.

(4) There are indications of anionic intermediates participating in the reactions: mechanistic studies of the reactions, product distributions and spectroscopic observations of the species adsorbed on certain materials indicate that anionic intermediates are involved in the reactions [5].

1.2 Generation of basic sites

Generally, the surface of solid base catalyst is covered with carbon dioxide, water, oxygen etc. and shows no activity for base-catalyzed reactions. Generation of basic sites requires high-temperature pre-treatment to remove adsorbed species and in some cases, alkaline earth oxides adsorb CO₂, H₂O and O₂ form carbonates, hydroxides and peroxides respectively. For removal of these adsorbed species from the surfaces high-temperature pre-treatment is essential to obtain the active metal oxide surfaces. Evolution of CO₂, H₂O and O₂ results in generation of basic sites on the surfaces which act as catalytically active sites for

several reaction types. The nature of the basic sites thus the change in catalytic activity depends on the severity of the pre-treatment.

As an example, the activity maxima of MgO appear at different pre-treatment temperatures for different reaction types: 800 K for 1-butene isomerization, 973 K for CH₄-D₂ exchange and amination of 1,3-butadiene with dimethylamine, 1273 K for hydrogenation of 1,3-butadiene and 1373 K for hydrogenation of ethylene.

As the pre-treatment temperature increases, the molecules covering the surfaces are successively desorbed according to the strength of the interaction with the surface sites. The molecules weakly interacting with the surfaces are desorbed at lower pre-treatment temperatures, and those strongly interacting are desorbed at higher temperatures. However, rearrangement of surface and bulk atoms also occurs during pre-treatment in addition to desorption of the molecules, which is evidenced by a decrease in the surface area with an increase in the pre-treatment temperature.

According to the proposal by *Coluccia* and *Tench*, there exist several Mg–O ion pairs of different co-ordination numbers on the surface of MgO catalyst as shown in **Figure 1.1**. Ion pairs of low coordination numbers exist at corners, edges and high Miller index surfaces. Different basic sites generated by increasing the pre-treatment temperature appear to correspond to the ion pairs of different coordination numbers. The correspondence between the catalytically active sites for different reaction types and the coordination number of the ion pairs, however, is not definite yet. Among the ion pairs of different coordination numbers, the ion pair of three-fold Mg²⁺ three-fold O²⁻ is most reactive and adsorbs CO₂ most strongly. To reveal the ion pair, the highest pre-treatment temperature is required. At the same time, the ion pair is most unstable and tends to rearrange easily at high temperature. The appearance of such highly unsaturated sites by the removal of CO₂ and the elimination by the surface rearrangement compete, which results in the activity maxima with change in the pre-treatment temperature. Such variations of catalytic activities with pre-treatment temperature as observed for MgO are common to those for other types of solid base catalysts too. It is essential to remove the adsorbed CO₂, H₂O and in some cases, O₂ from the surfaces to

generate basic sites, though proper pre-treatment temperatures vary with the types of catalysts and reactions [4].

It is important to know as exception that the surface basic sites generated on rare earth oxides, however, behave differently from those of the other heterogeneous base catalysts. The sites of rare earth oxides do not seem to vary in nature with pre-treatment temperature.

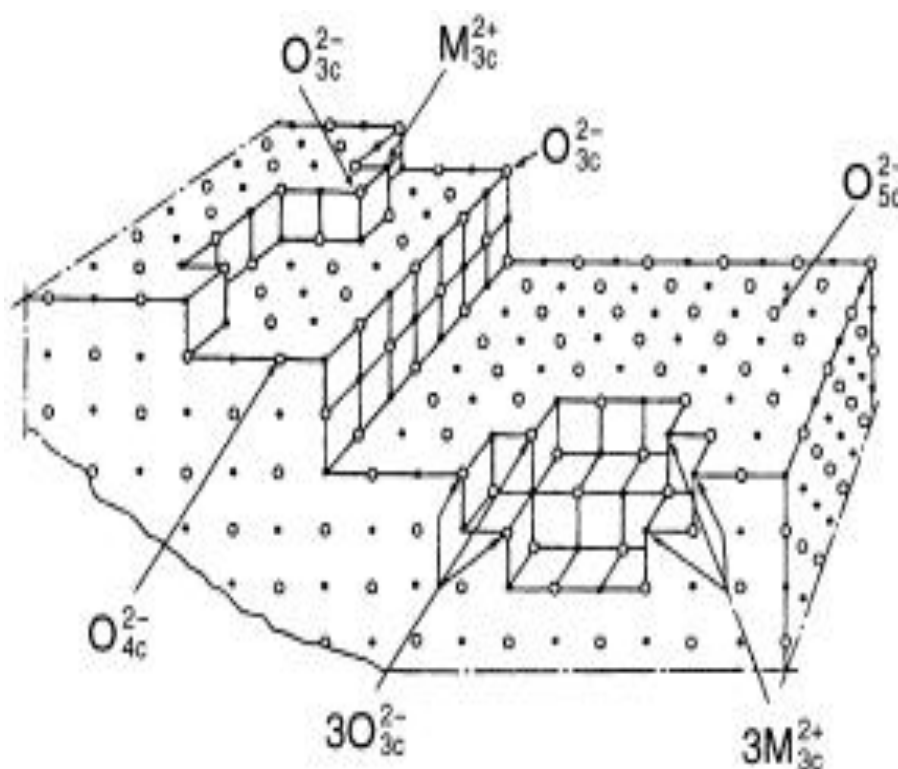


Figure 1.1: Ions in low coordination on the surface of MgO.

1.3 Characterization of basic surfaces

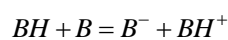
The surface properties of the heterogeneous basic catalysts have been studied by various methods by which existence of basic sites has been realized. Different characterization methods give different information about the surface properties. All the properties of basic sites cannot be measured by any single method. Integration of the results obtained by different characterizations interprets the structures, reactivities, strengths and amounts of the basic sites on the catalyst surfaces. In this section, some representative methods for characterization of the surface basic sites are described.

1.3.1 Indicator method

Acid-base indicators change their colors according to the strength of the surface sites and pK_{BH} values of the indicators. The strength of the surface sites are expressed by an acidity function (H_-) proposed by Paul and Long. The H_- function is defined by the following equation [6]:

$$H_- = pK_{BH} + \log [B^-]/[BH]$$

where $[BH]$ and $[B^-]$ are, respectively, the concentration of the indicator BH and its conjugated base and pK_{BH} is the logarithm of the dissociation constant of BH. The reaction of the indicator BH with the basic site \underline{B} is



The amount of basic sites of different strengths can be measured by titration with benzoic acid. A sample is suspended in a nonpolar solvent and an indicator is adsorbed on the sample in its conjugated base form. The benzoic acid titer is a measure of the amount of basic sites having a basic strength corresponding to the pK_{BH} value of the indicator used.

1.3.2 Temperature-programmed desorption (TPD) of carbon dioxide

This method is frequently used to measure the number and strength of basic sites. The strength and amount of basic sites are reflected in desorption temperature and the peak area, respectively, in a TPD plot. However, it is difficult to express the strength in a definite scale and to count the number of sites quantitatively. Relative strengths and relative numbers of basic sites on the different catalysts can be estimated by carrying out the TPD experiments under the same conditions. TPD plots of CO_2 desorbed from alkaline earth oxides are compared in **Figure 1.2** and the strength of basic sites is found to be in the increasing order of $MgO < CaO < SrO < BaO$ [7].

1.3.3 UV absorption and luminescence spectroscopies

UV absorption and luminescence spectroscopies give information about the coordination states of the surface atoms. High surface area MgO absorbs UV light and emits luminescence, which is not observed with MgO single crystal.

Ion pairs of low coordination numbers responsible for UV absorption and luminescence exist at corners, edges or high Miller index surfaces. The surface model for MgO shown in **Figure 1.1** was proposed on the basis of UV absorption and luminescence together with the effects of hydrogen adsorption on the luminescence spectrum [5]. Although the UV absorption and luminescence spectroscopies give us useful information about the coordination state, it is difficult to count the number of the sites of a certain coordination state.

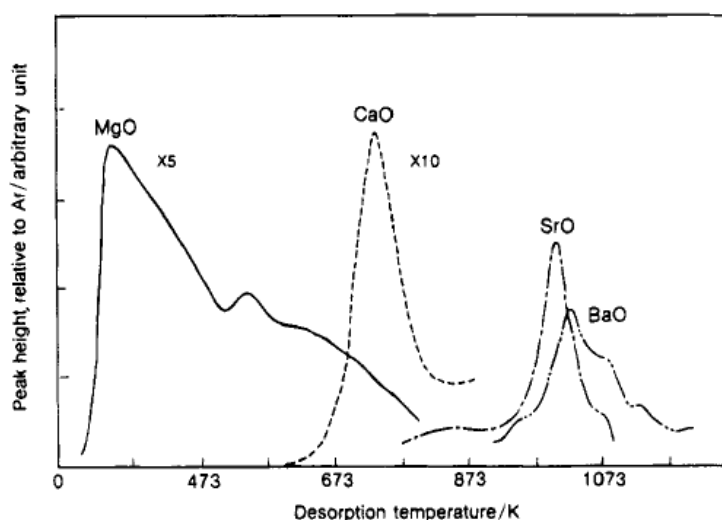


Figure 1.2: TPD plots of carbon dioxide desorbed from alkaline earth oxides.

1.3.4 Temperature-programmed desorption of hydrogen

This method gives information about the coordination state of the surface ion pairs when combined with the other methods such as UV absorption and luminescence spectroscopies. The number of each ion pair could be counted if TPD is accurately measured with a proper calibration method. This method has been applied only to the MgO surface. Hydrogen is heterolytically dissociated on the surface of MgO to form H^+ and H^- , which are adsorbed on the surface O^{2-} ion and Mg^{2+} ion, respectively. TPD plots of hydrogen adsorbed on MgO pre-treated at different temperatures are shown in **Figure 1.3**.

Seven desorption peaks appear in the temperature range 200-650 K. Appearance of the peaks varies with the pre-treatment temperature. Appearance of

the peaks at different temperatures indicates that several types of ion pairs with different coordination numbers exist on the surface of MgO (**Figure 1.1**) [5].

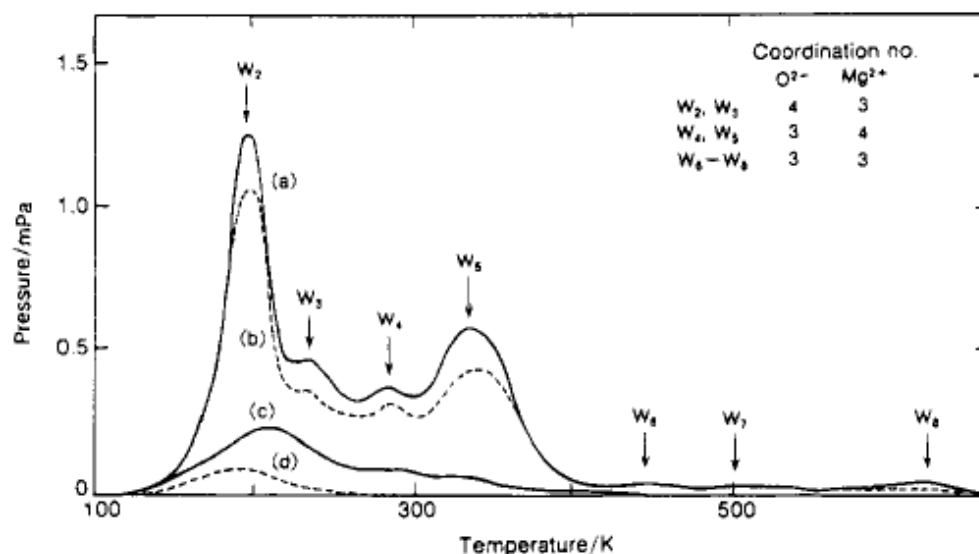
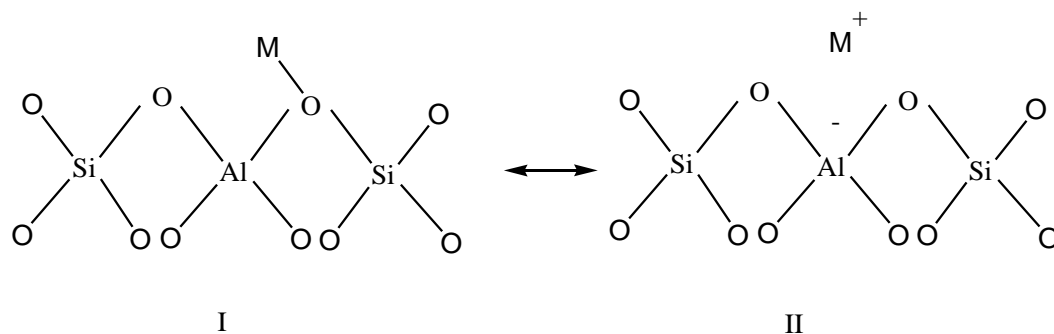


Figure 1.3: TPD plots for hydrogen adsorbed on MgO at various pre-treatment temperatures: (a) 1123 K (b) 973 K (c) 823 K (d) 673 K.

1.3.5 X-ray photoelectron spectroscopy

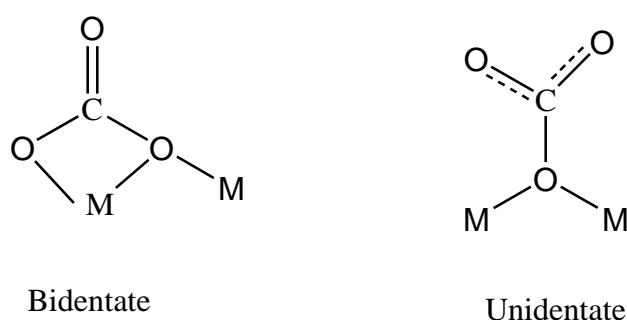
The XPS binding energy (BE) for oxygen reflects the basic strength of the oxygen. As the O_{1s} BE decreases, electron pair donation becomes stronger. The effects of zeolite composition and the type of cation on the BE of the constituent elements for X- and Y-zeolites ion-exchanged with a series of alkali cations have been studied [8]. With increasing cation electronegativity (χ), the O_{1s} BE increases. The O_{1s} BE of zeolite is directly delineated to the electron density of the framework oxygen. On the basis of XPS features of zeolite, Okamoto et al. proposed a bonding model of zeolite as shown in **Scheme 1.1**. Configurations I and II are in resonance. In configuration I, extra frame-work cations form covalent bonds with framework oxygens, while in configuration II, the cations form fully ionic bondings with the negatively charged zeolite lattice. As the electronegativity of the cation increases and approaches that of oxygen, the contribution of configuration I increases to reduce the net charges on the lattice. This explains the dependences of the O_{1s} BE on the electronegativity of the cation [8].



Scheme 1.1: Schematic bonding model of zeolite.

1.3.6 IR of carbon dioxide

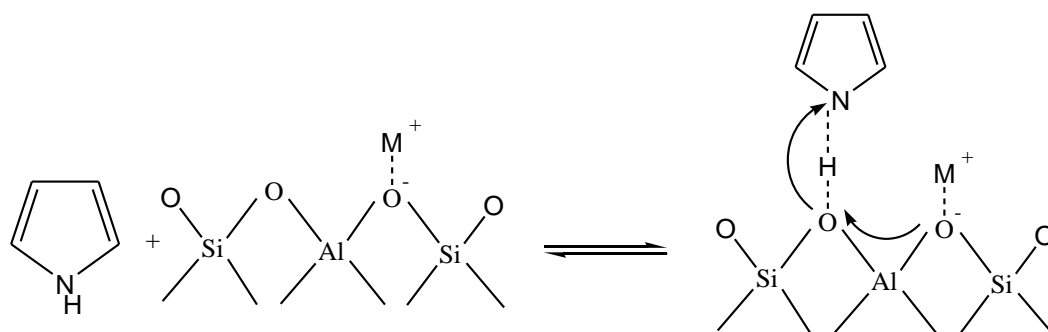
This method gives information about the adsorbed state of CO_2 on the base catalyst surface. Carbon dioxide interacts strongly with a basic site and therefore, the surface structures including basic sites are estimated from the adsorbed state of CO_2 . Carbon dioxide is adsorbed on MgO and other heterogeneous basic catalysts in different forms: bidentate carbonate, unidentate carbonate and bicarbonate (**Scheme 1.2**). For CaO , carbon dioxide is adsorbed in the form of bidentate carbonate. In the adsorption state of unidentate carbonate, only surface oxygen atoms participate, while the metal ion participate in the adsorption state of bidentate. In other words, the existence of only a basic site is sufficient for unidentate carbonate, but the existence of both a basic site and a metal cation is required for bidentate carbonate [5].



Scheme 1.2: Adsorbed forms of carbon dioxide.

1.3.7 IR of pyrrole

Pyrrole is proposed to be a probe molecule for measurement of the strength of basic sites. The IR band ascribed to the N-H stretching vibration shifts to a lower wavenumber on interaction of the H atom in pyrrole with a basic site (**Scheme 1.3**). The shift increases when the negative charge on the oxide ion increases. The negative charge is associated closely with the strength of the basic site. The basic strengths of alkali ion-exchanged zeolites are in the order $\text{CsX} > \text{NaX} > \text{KY} > \text{NaY}$, KL, Na-mordenite, Na-beta. According to the pyrrole IR basic strengths of the basic sites are found to be in the order $\text{CsX} > \text{RbX} > \text{KK X NaX} > \text{LiX}$ and $\text{CsY} > \text{RbY} > \text{KY} > \text{NaY} > \text{LiY}$.



Scheme 1.3: Model for pyrrole chemisorbed on a basic site.

1.3.8 Oxygen exchange between carbon dioxide and catalyst surface

This method gives information about the dynamic nature of interaction of adsorbed CO_2 with the surface ion pair. As described above, carbon dioxide is used as a probe molecule for the basic properties in IR and TPD. If ^{18}O -labeled, carbon dioxide is used, additional information about the nature of basic sites is obtained. Oxygen exchange between adsorbed CO_2 and the MgO surface takes place to a considerable extent. TPD desorption peak consisting mainly of C^{16}O_2 and $\text{C}^{16}\text{O}^{18}\text{O}$ after C^{18}O_2 adsorption on MgO and suggested that the adsorbed C^{18}O_2 interacts with the peroxy ion $(^{16}\text{O}_s)_2^{2-}$ on a defect in the MgO surface. It could be concluded that basic sites are not fixed on the surface but are able to move over the surface when carbon dioxide is adsorbed and desorbed. The position of the basic site (surface O atom) changes as CO_2 migrates over the basic site. In

addition, it became clear that not only O^{2-} basic sites but also adjacent Mg^{2+} sites participate in CO_2 adsorption. Therefore, it is reasonable to consider that the metal cations adjacent to the basic site participate in the base-catalyzed reactions.

1.4 Types of solid base catalysts

The types of heterogeneous basic catalysts are listed in **Table 1.1**. These materials act as a base toward most of the reagents and, therefore, are called heterogeneous basic catalysts or solid base catalysts [5]. The detail of different types of solid base catalysts is given below.

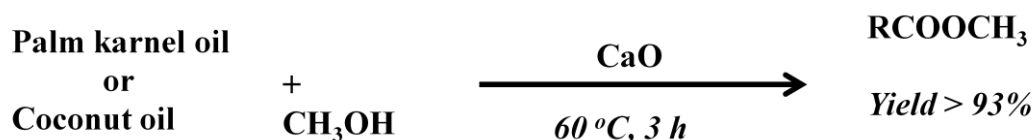
Table 1.1: Types of solid basic catalysts.

Type of solid base	Catalyst	Example
Single metal oxide	Alkali earth oxides	MgO, CaO, SrO and BaO
	Rare earth oxide	La_2O_3 and YbO_2
	Transition metal oxide	ZrO_2
Mixed Oxide	Mg-Al mixed oxide	MgO- Al_2O_3
	Mg-Ti mixed oxide	MgO- TiO_2
Supported catalyst	Catalyst: Na, K, KF, KNO_3 and K_2O	KF/ Al_2O_3 , Na/NaOH/ Al_2O_3
	Support: C, Al_2O_3 , SiO_2 , ZrO_2 and MgO	Na/MgO
Mesoporous material	Modified mesoporous material	MgO/SBA-15
	Functionalised mesoporous material	MCM-41 functionalised with amino groups
	Mesoporous silicon oxynitride	
Zeolite	Alkali ion exchanged zeolite	Cs-exchanged zeolite X, Y
	Alkali metal or metal oxide occluded zeolite	Cs-occluded zeolite X, Y
Clay and modified clay	Hydrotalcite, Chrysolite, Sepiolite	Magnesium silicate
	Hydrotalcite-calcined and rehydrated	Mg-Al hydrotalcites
Oxynitride	Silicon oxynitride	SiON

	Aluminophosphate oxynitride	AIPON
	Zirconophosphate oxynitride	ZrPON
Other	Modified natural phosphate (NP)	Calcined NaNO ₃ /NP

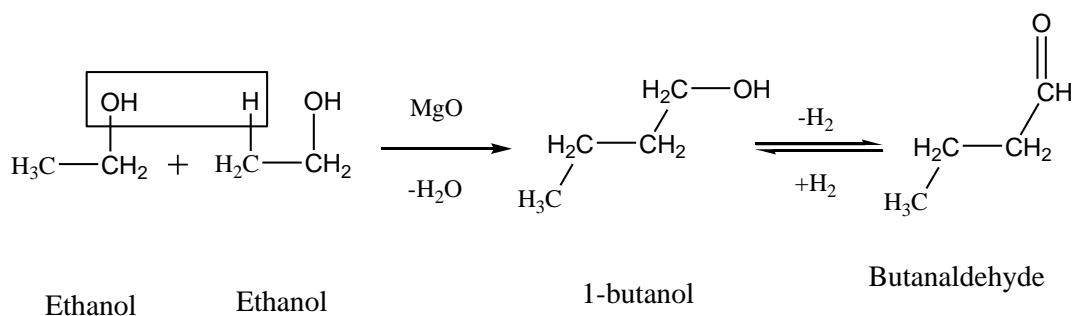
1.4.1 Alkali and alkaline earth metal oxide

Various supported and unsupported alkali and alkaline earth metal compound used as catalyst are well reported in the literature. **CaO**, **Al₂O₃** supported **Li₂O**, **Na₂O**, **K₂O**, **CaO**, **MgO** catalysts have been used in transesterification of palm kernel oil and coconut oil (**Scheme 1.4**) [9]. The calcination temperature was found to largely influence the catalytic activity of the resultant catalysts, except for **Mg(NO₃)₂/Al₂O₃** that exhibited very low methyl ester content at all temperatures. **Ca(NO₃)₂/Al₂O₃** and **LiNO₃/Al₂O₃** yielded the high methyl ester contents (>90%) when the calcination was performed at 450 °C. With increasing the temperature, the methyl ester contents were dropped due to the formation of inactive metal aluminates. On the contrary, the activities of **NaNO₃/Al₂O₃** and **KNO₃/Al₂O₃** catalysts were remarkably improved when the calcination was carried out at >550 °C [9].



Scheme 1.4: Transesterification of palm kernel oil and coconut oil over **CaO** catalyst.

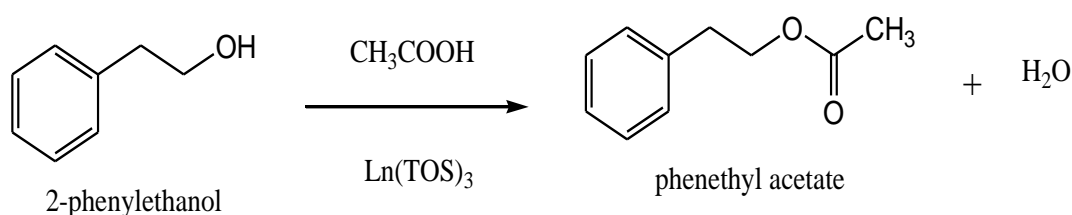
Dimerisation of ethanol to butanol over **MgO**, **CaO** and **BaO** solid-base catalysts is reported by Ndou et al. (**Scheme 1.5**) [10]. The dimerisation reaction does not proceed primarily through the aldol condensation reaction. The reaction is proposed to proceed through a mechanism in which a C–H bond in the β -position on ethanol is activated by the basic metal oxide and condenses with another molecule of ethanol by dehydration to form 1-butanol which is a crucial building block for acrylic acid and acrylic esters and is widely used as a solvent. It is also used as an additive to gasoline [10].



Scheme 1.5: Dimerisation of ethanol to 1-butanol.

1.4.2 Rare earth oxide

Lanthanide (III) complexes of p-toluenesulfonic acid (**Ln(TOS)₃**) catalysts for acylation of 2-phenylethanol have been reported and found a clear correlation between the ionic radius of the lanthanide (III) ion and the yield of the reaction product (**Scheme 1.6**). It is revealed that conversion or catalytic activity decreases with increase in ionic radius of lanthanide (III) ion [11].



Scheme 1.6: Acylation reaction over lanthanide (III) tosylate catalyst.

La, Cs-La, Sm, Cs-Sm, Ce, Cs-Ce phosphate catalysts for vapor phase O-alkylation of phenol to anisole [12] and **Eu₂O₃/Al₂O₃** catalyst for the transesterification of soybean oil with methanol to biodiesel have been reported [13].

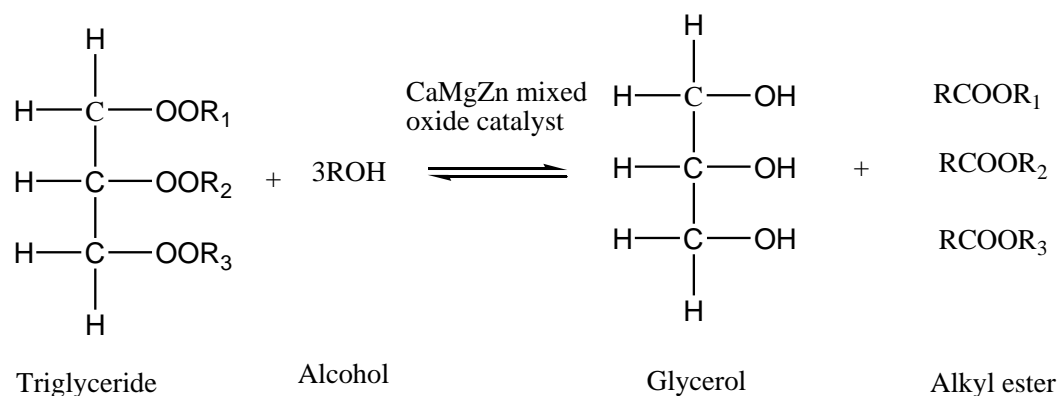
1.4.3 Mixed metal oxide

Mixed metal oxides (MMOs), contains alkali, alkaline, rare earth and noble metals. A variety of reactions such as reduction, oxidation, alkylation, Mannich, condensation, deprotection, cycloaddition, hydroxylation, dehydration, dehydrogenation, transesterification, reactions involving biomimetic

oxygen-evolving catalysts and other important C–C bond forming reactions are well reported on the surface of mixed metal oxides. The mixed metal oxides are important in organic reactions, industrial applications and green chemistry [14].

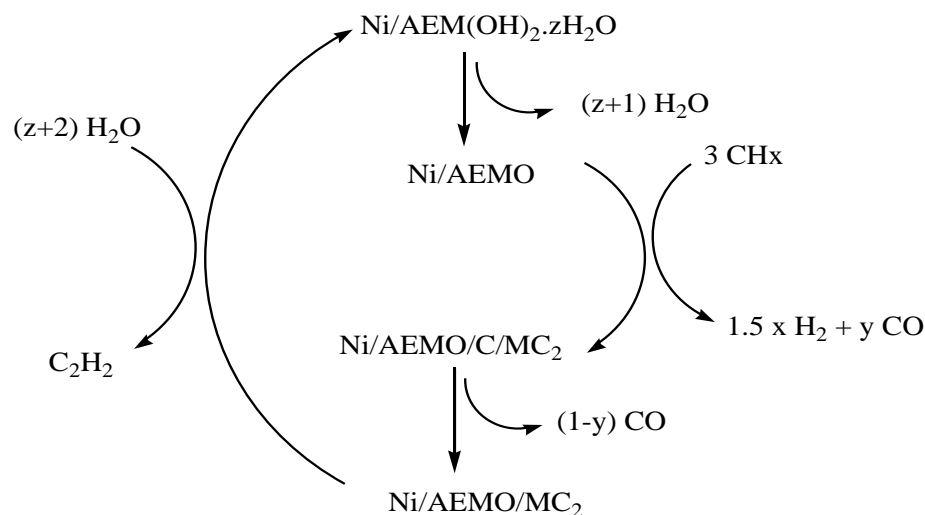
The KI impregnated Mg–Al mixed-metal oxide catalyst has base strength in the range of 9.8-15, efficiently catalyses transesterification of soybean oil with methanol with >90% conversion to biodiesel. Al–O–K sites are the basic site in the catalyst [15].

Biodiesel production from palm oil by **CaO–CeO₂** [16], palm kernel oil by **CaMgZn mixed oxide (Scheme 1.7)** [17], jatropha curcas oil by **K₂CO₃/ HT** [18], soyabean oil by **MgAlNi** [19] and rapeseed oil by hydrated tricalcium aluminate (**Ca₃Al₂O₆·6H₂O**) [20, 21].



Scheme 1.7: Biodiesel synthesis reaction.

Ni/SrO–CaO catalyst for the selective conversion of hydrocarbons to C₂H₂ and CO has been reported by Michael et al. (**Scheme 1.8**) [22]. **MgO–LaO** mixed oxide prepared by coprecipitation, was used to catalyse the reaction of cyclic carbonates and methanol at 150 °C for 2 h, to form dimethyl carbonate [23].



Scheme 1.8: A schematic process for the selective production of C_2H_2 and CO from gaseous hydrocarbons (CH_x) using Ni-modified alkaline earth metal oxide (AEMO) and metal carbide (MC_2) intermediates.

1.4.4 Zeolite

Zeolites are microporous, aluminosilicate minerals commonly used as commercial adsorbents and catalysts. The elementary building units of zeolites are SiO_4 and AlO_4 tetrahedra (**Figure 1.4**). Adjacent tetrahedra are linked at their corners via a common oxygen atom and resulted in an inorganic macromolecule with a structurally distinct three-dimensional framework. It is evident from this building principle that the net formula of the tetrahedra are SiO_2 and AlO_2^- , i.e. one negative charge resides at each tetrahedron in the framework which has aluminum in its center [24].

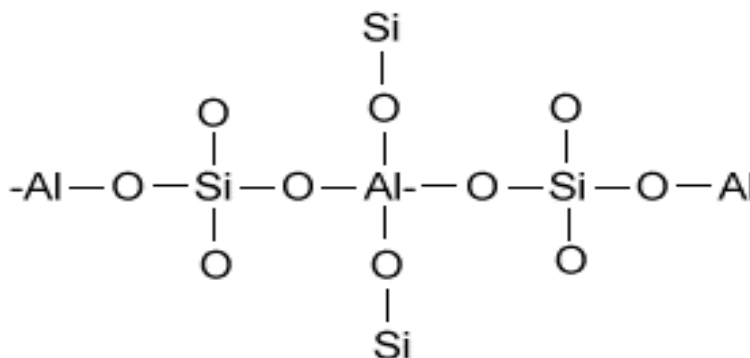


Figure 1.4: Basic zeolite structure.

The basic strength and density of basic sites in alkali ion exchanged zeolites decrease with an increase in framework Si/Al ratio, while basic strength increases with an increase in electropositivity of the counter cation in zeolites [25]. The characteristic features of zeolites are due to their ion exchange ability and specific pore structure.

Basic zeolites can be categorized in two categories:

- (i). Alkali ion-exchanged zeolite
- (ii). Alkali ion-added zeolite

(i) Alkali ion-exchanged zeolite

Zeolite possesses a net negative charge that is the result of the isomorphous replacement of Si^{4+} by Al^{3+} in the crystal lattice. This negative charge is balanced by cations (Na^+ , K^+ or Ca^{2+}) that are exchangeable with other cations in solution (**Figure 1.5**). Thus, zeolites have great selectivity for cation exchange, but little or no affinity for anions [26]. In alkali ion exchanged zeolites, the type of alkali ions used, affects the basic strength of the resulting zeolites. The effect of alkali ion on the basic strength follows the order $\text{Cs} > \text{Rb} > \text{K} > \text{Na} > \text{Li}$ [27]. Ion exchange, on **NaY** and **NaX** zeolites with alkali metal cations Li^+ , K^+ , Rb^+ and Cs^+ has been performed and catalytic efficiency has been studied by adsorption of CO_2 [28]. Cs exchanged **NaX** and **NaY** zeolite have been reported as effective catalysts for conversion of isopropanol to propene and acetone [29]. **Na⁺ ion exchange Y** and **ZSM-5** zeolites have been reported for catalytic oxidation of ethyl acetate [26].

(ii) Alkali ion-added zeolite

The zeolites having nanophase alkali metal oxides inside the zeolite cavities are known as alkali ion added zeolites [30]. In this category cesium oxide added faujasite zeolite has been synthesized by post-synthetic modification of basic **CsNaX** and **CsNaY** zeolites by impregnation with cesium acetate followed by thermal decomposition of the cesium acetate into oxide. The addition of metal oxides in zeolite cage structures generates additional basic sites responsible for improved catalytic activity [31].

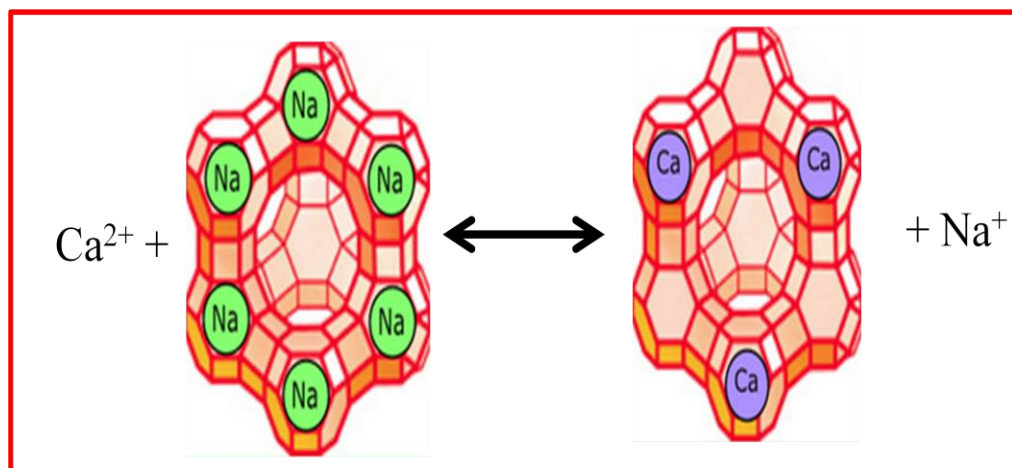


Figure 1.5: Alkali ion exchanged zeolite structure.

1.4.5 Supported solid base catalyst

Pure metal oxides own a poor specific surface area that seriously hinders their efficiency as catalysts. A convenient way to overcome this problem is to either coat a support with the metal oxide nanoparticles or to disperse them within a porous host that has a high surface area.

(i) Alumina supported base catalyst

Among alumina supported catalysts, **KOH** and **KF** supported on alumina are most widely studied. **KF/Al₂O₃**, **LiF/Al₂O₃**, **CsF/Al₂O₃** etc. catalysts are found to be suitable for a wide range of industrially important reactions. As shown in the catalyst model the O⁻ is found to be more basic than F⁻ (**Figure 1.6**) [32].

KF/Al₂O₃ catalyst has been used as a heterogenous base catalyst in a number of base-catalyzed reactions such as transesterification of canola oil and methanol to canola oil methyl ester [33], Suzuki-Miyaura reaction [34], Michael addition, aldol condensation and synthesis of diethyl carbonate by transesterification of ethylene carbonate at temperature 323 K under atmospheric pressure in liquid phase reaction condition [35,36].

KOH/Al₂O₃ is utilized for biodiesel production [37]. Sarda and co-workers reported synthesis of chalcone via Claisen Schmidt reaction is reported on **NaOH/Al₂O₃** [38]. The isomerization olefinic amines were carried out in a quartz reactor using **KNH₂/Al₂O₃** as the catalyst. The reactant was introduced to

the reactor from the side arm, after the catalyst was prepared. The isomerization of *N,N*-diethyl-3,7-dimethyloct-2-enylamine, was carried out at 353 K for 1 h. The product was corresponding enamine, which was obtained in a 91% yield with a 95% selectivity. The isomerized product has 100% *E* configuration. This proves that the catalyst $\text{KNH}_2/\text{Al}_2\text{O}_3$ is very effective for the isomerization of olefinic amines as well as simple alkenes [39].

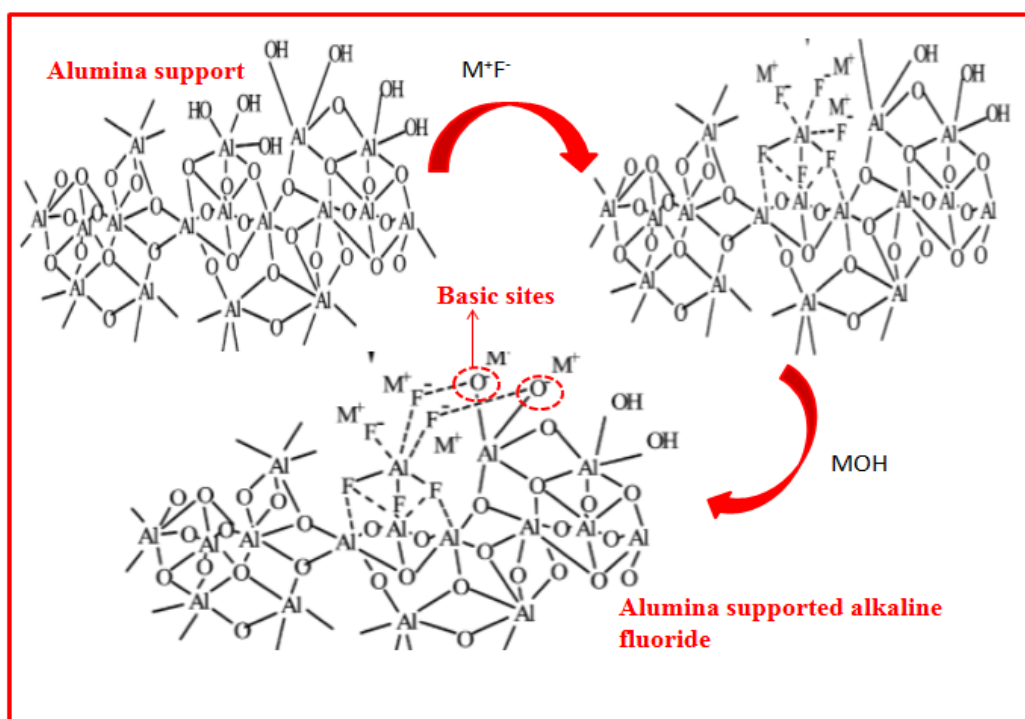
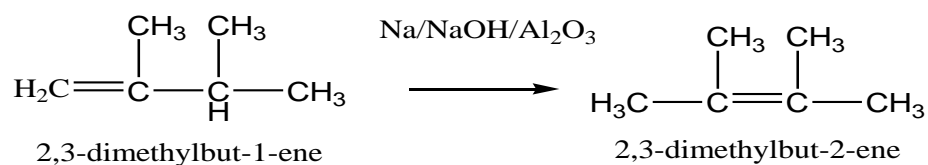


Figure 1.6: Alumina supported alkaline metal fluoride catalyst structure.

$\text{Na}/\text{NaOH}/\text{Al}_2\text{O}_3$ shows a very high catalytic activity for the isomerization of 2,3-dimethylbut-1-ene to 2,3-dimethylbut-2-ene, which is usable as an intermediate material for synthetic parathyroid. A 94% yield was obtained in 3 h at 293 K (**Scheme 1.9**) [39].



Scheme 1.9: Double bond isomerization reaction.

(ii) Silica supported base catalyst

The activity of Li/SiO_2 , Na/SiO_2 , K/SiO_2 , Cs/SiO_2 catalysts increases with the basicity of the metal ($\text{Cs} > \text{K} > \text{Na} > \text{Li}$). O-alkylation of 2-naphthol has been investigated in the vapor phase over alkali-loaded silica (**Figure 1.7**) [40].

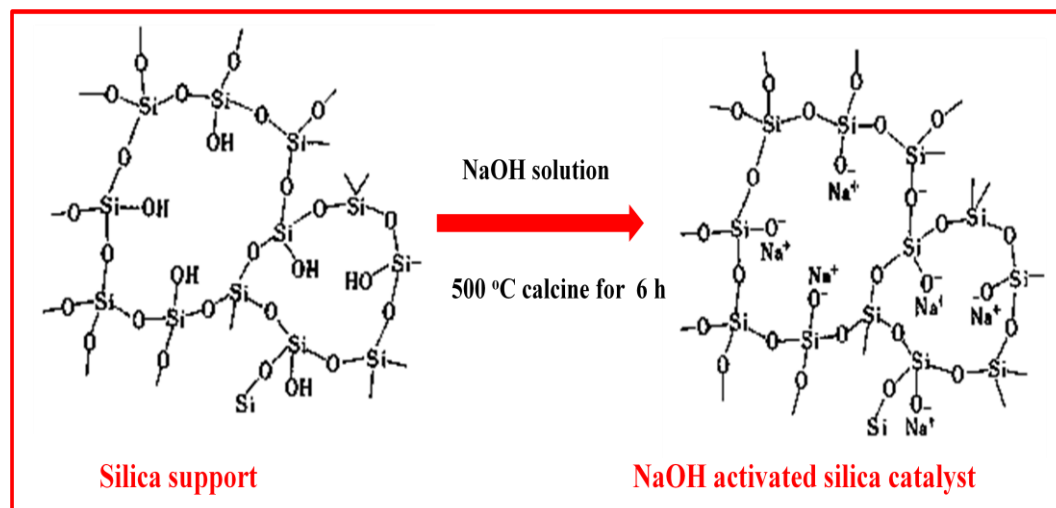
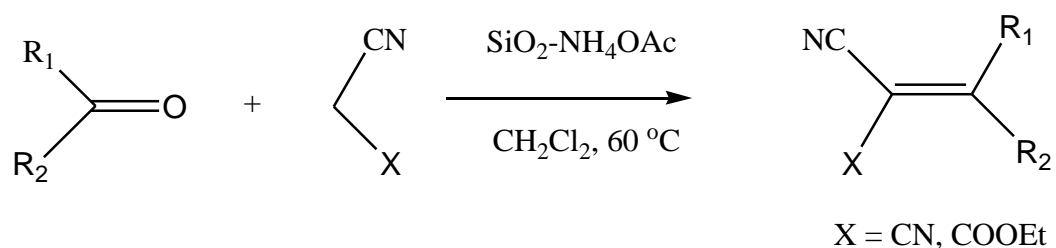


Figure 1.7: Synthesis of NaOH activated silica catalyst from silica.

Silica supported ammonium acetate is reported as an efficient and recyclable heterogeneous catalyst for Knoevenagel condensation between aldehydes or ketones and active methylene group in liquid phase (**Scheme 1.10**). The product has numerous applications in the elegant synthesis of fine chemicals, hetero Diels-Alder reactions and in the synthesis of carbocyclic as well as heterocyclic compounds of biological significance [41].



Scheme 1.10: Knoevenagel condensation between aldehydes or ketones and active methylene group.

Silica supported cinchona alkaloids as heterogeneous catalysts for asymmetric michael reaction is reported by Zhao et. al [42]. Oh et al. reported isomerization of 5-vinyl-2-norbornene using sodium-coated silica catalysts [43]. Crotonaldehyde production with the help of **MgO/SiO₂** catalyst has been reported [44].

(iii) Carbon supported base catalyst

Cs/nanoporous carbon catalyst provides cis-but-2-ene by isomerization of but-1-ene at 273 K [45]. **Cs-Ru/Carbon** catalyst prepared by impregnation has been reported as effective catalyst for ammonia synthesis [46]. Ammonia synthesis over **Ba-Co/graphitised carbon** is reported by Rarog-Pilecka et.al [47]. **CaO/SrO/BaO supported on carbon nano fibers** are reported as efficient catalysts for self condensation of acetone and transesterification reactions. These metal oxides on the carbon nanofibers are found to be amorphous in nature [48].

1.4.6 Solid super base catalyst

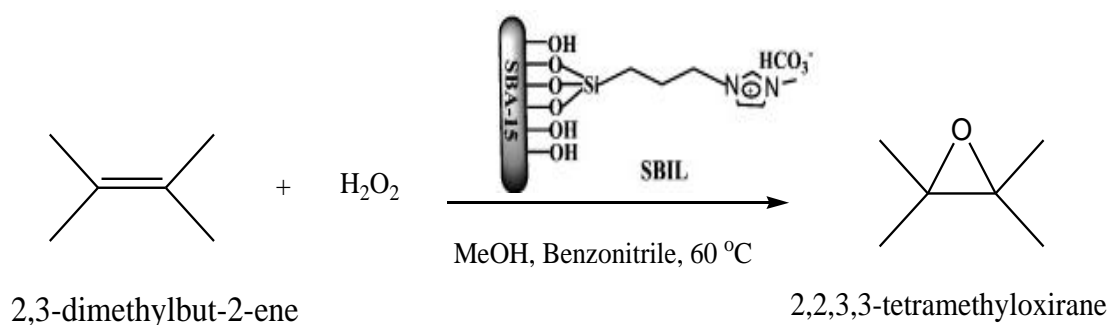
Normally, catalysts which possess base sites stronger than $pK_a = 26$ are called super base and all the metal deposited catalysts comes under the super base category. Solid super basic materials are highly promising for applications in environmentally friendly and economical catalytic processes, because they can catalyze diverse reactions under mild conditions and reduce waste production [49]. The generation of strong basic sites was also reported by the reaction of alkali metal with holes trapped on oxygen anions near to the cationic vacancy [50].

In the development of environment-benign processes, solid super bases are used as catalysts so that reactions can be conducted under mild conditions and without generation of much waste. In the past two decades, there were many reports on solid super bases such as **NaN₃/γ-Al₂O₃**, **Na/NaOH/γ-Al₂O₃**, **K/MgO**, **Eu₂O₃/γ-Al₂O₃**, **KNO₃/γ-Al₂O₃**, **KNO₃/ZrO₂**, **KOH/ZrO₂**, **KF/γ-Al₂O₃**, **K/KOH/γ-Al₂O₃** and **Ca(NO₃)₂/SBA-15** [50]. Recently, we found that the solid super bases **Na₂SnO₃** and **KOH/La₂O₃-MgO** showed excellent catalytic efficiency towards some organic reactions at room temperature [51].

1.4.7 Mesoporous material as base catalyst

Mesoporous materials with high surface area, controllable pore size and narrow pore distribution are interesting in applications as shape selective catalysis and shape selective adsorption. The most common types of mesoporous materials are **MCM-41** and **SBA-15**. Promising solid base catalyst **N/MgO/MCM-41** is prepared by nitridation of MgO-loaded mesoporous MCM-41. Basic species, bridging –NH– and terminal –NH₂ groups, are introduced into the framework of MgO/MCM-41 by nitridation. Prepared catalyst has been used in Knoevenagel condensation reaction and Claisen–Schmidt reaction [52]. **Ca/MCM-41** is reported as a solid base catalyst for transesterification of palm olein [53]. Magnetic iron oxide nanoparticles are incorporated in MCM-41 and organic amines (i.e. propylamine and propyl diethylene amine) are grafted to obtain magnetic mesoporous catalysts for the Knoevenagel condensation reactions. The catalyst can be easily dispersed into solution and rapidly removed by a magnet for recovery and reuse [54].

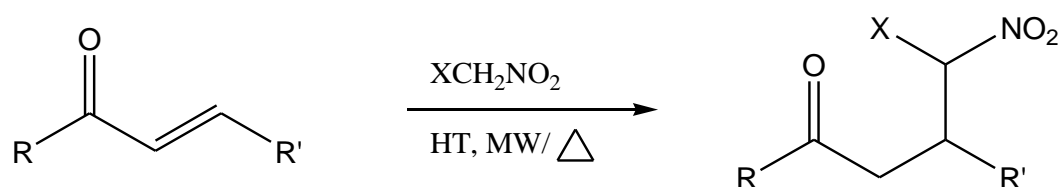
Biodiesel production by transesterification using tetraalkylammonium hydroxides immobilized onto **SBA-15** as a solid catalyst has been reported by Xie et al. [55]. Transesterification of canola oil as biodiesel over **Na/Zr-SBA-15** catalyst has been reported by Chen et al.[56]. Basic ionic liquid supported on mesoporous SBA-15 has been reported as efficient heterogeneous catalyst for epoxidation of olefins with H₂O₂ as oxidant (**Scheme 1.11**) [57].



Scheme 1.11: Epoxidation of olefins with H₂O₂ as oxidant over ionic liquid supported SBA-15.

1.4.8 Clay based catalytic material

Clay is a fine-grained natural rock or soil material that combines one or more clay minerals with traces of metal oxides and organic matter. Clays are distinguished from other fine-grained soils by differences in size and mineralogy. Unmodified hydrotalcites (HTs, a basic anionic clay), as catalyst in the Michael addition reaction between nitromethane and α,β -unsaturated ketones under MW has been reported by Kumae et al. (**Scheme 1.12**) [58].



Scheme 1.12: Hydrotalcite catalyzed microwave assisted Michael addition.

KF/clay, a material with excellent stability and high catalytic activity is reported for the conversion of soybean oil into biodiesel in the presence of methyl alcohol [59]. **Sepiolite** – a naturally-porous hydrated magnesium silicate with the highest surface area among all clay minerals, modified by loading 10–50wt.% of K_2CO_3 , was found to be very active in the catalysis of the transesterification reaction of canola oil with methanol [60].

1.5 Fly ash

Fly ash, a major residue arising from the combustion of pulverized coal, is one of the main wastes generated in coal-fired power plants. The chemical composition of fly ash with high percentage of silica (60– 65%), alumina (25– 30%), magnetite, Fe_2O_3 (6–15%) make it useful for the synthesis of zeolite, catalyst and precipitated silica [61]. The other important physicochemical characteristics of fly ash, such as surface area $2.57\text{ m}^2/\text{g}$, bulk density $0.994\text{ g}/\text{cm}^3$, average particle size $17.02\text{ }\mu\text{m}$, porosity, water holding capacity and surface area make it suitable for use as an adsorbent [62–65]. Fly ash after appropriate activation has been converted into solid acid and solid base catalyst.

1.5.1 Fly ash supported solid base catalysts

Fly ash supported aminopropylatedtrimethoxysilane (**APTMS/FA**) has been used as recyclable catalyst for the synthesis of ethyl(cyclohexylidene) cyanoacetate by Knoevenagel condensation reaction [66]. **Fly ash loaded NaOH** [67], **CaO** [68], **MgO** [69] and **KF/Al₂O₃** [70] have been reported as efficient catalysts for the synthesis of 1,1'-dibenzylidenecyclohexanone, ethyl(E)- α -cyanocinnamate, 4-methoxy-2'-hydroxychalcone and 2'-hydroxy chalcone, respectively by various condensation reactions.

1.6 Volcanic ash

Volcanic ash also known as perlite, is a silicious and volcanic glass lava containing crystal water, falling into the category of igneous rock. After calcination at high temperature 760-1100 °C, crystal water in the rocks evaporates, and the perlite may undergo a 15–20 times volume expansion. This expansion is due to the presence of 2-6% combined water in the crude perlite rock. Since perlite is a form of amorphous aluminosilicate, it is classified as chemically inert and has a pH of approximately 7. Perlite has bulk density 0.125 g cm⁻³, particle size 0.2-1 mm, porosity 80-90% and BET surface area 2.4 m² g⁻¹ [71]. Due to these physicochemical properties perlite has been used mostly in ceramic material and as adsorbent. Few researches have been done in the field of perlite supported catalyst synthesis also.

1.6.1 Perlite supported catalysts

Perlite has been converted into catalyst after chemical or physical modification. **ZSM-5** zeolite from expanded perlite as catalyst in FCC gasoline aromatization [72], perlite granules coated with indium doped TiO₂ for gas-phase photocatalytic decomposition of ethylbenzene [73], immobilization of α -Amylase on modified mesostructure perlite, prepared by sol gel method [74], Ag coated bulgarian natural glass perlite via spray pyrolysis for decomposition of ozone [75], **BNi/perlite** catalyst for nitro-benzene hydrogenation reaction [76] and **Ag/perlite** for ozone decomposition [77] have been reported. **TiO₂/perlite** composite prepared by flame spray pyrolysis for photocatalytic applications [78]

and nanosized iron oxide coated perlite for arsenate removal [79] have been reported while the researches regarding perlite supported solid base catalysts synthesis and its catalytic applications are not reported in the literature.

1.7 Scope of the work

The aim of this work is to study preparation and characterization of innovative fly ash and perlite supported solid base catalysts and to evaluate their catalytic applications in liquid phase condensation reactions. Fly ash and perlite both are siliceous waste materials, non toxic and have external surface which can be activated during the chemical activation according to the demand of the reaction. In this study catalysts are prepared by activating with KOH/Al₂O₃, Mg(NO₃)₂, Sr(NO₃)₂, Ba(NO₃)₂ and Ca(NO₃)₂ over mechanically and thermally activated support materials, characterized by using different analytical techniques like FTIR spectroscopy, X-ray diffraction, Scanning electron microscopy, Transmission electron microscopy, Thermo gravimetric analysis and N₂ adsorption-desorption etc. The basicity and basic strength of prepared catalysts were measured by Hammett indicator method. The prepared catalyst serves as potential solid base catalysts for several condensation reactions, which is evidenced by high yield and conversion. Thus the present research study reports new solid base catalysts for the replacement of liquid bases in important reactions and introduces new catalysts for organic synthetic chemistry. This catalytic study explores the wide application of fly ash and perlite as solid base catalysts in pharmaceutical, petrochemical and fine chemical industries.

1.8 References

- [1] B. Lindström, L.J. Pettersson, *Cattech* 7 (2003) 130.
- [2] M.J. Climent, A. Corma, S. Iborra, A. Velty, *J. Mol. Catal. A Chem.* 182-183 (2002) 327.
- [3] D. Wu, X. Fu, F. Xiao, J. Li, N. Zhao, W. Wei, Y. Sun, *Catal. Commun.* 9 (2008) 680.
- [4] H. Hattori, *Appl. Catal. A Gen.* 222 (2001) 247.
- [5] H. Hattori, *Chem. Rev.* 95 (1995) 537.

-
- [6] M.A. Paul, F.A. Long, *Chem. Rev.* 57 (1957) 1.
- [7] G. Zhang, H. Hattori, K. Tanabe, *Appl. Catal.* 36 (1988) 189.
- [8] Y. Okamoto, *J. Catal.* 112 (1988) 427.
- [9] S. Benjapornkulaphong, C. Ngamcharussrivichai, K. Bunyakiat, *Chem. Eng. J.* 145 (2009) 468.
- [10] A.S. Ndou, N. Plint, N.J. Coville, *Appl. Catal. A Gen.* 251 (2003) 337.
- [11] T.N. Parac-vogt, K. Deleersnyder, K. Binnemans, *Eur. J. Org. Chem.* (2005) 1810.
- [12] G.S. Devi, D. Giridhar, B.M. Reddy, *J. Mol. Catal. A Chem.* 181 (2002) 173.
- [13] A.A. Refaat, *Int. J. Environ. Sci. Technol.* 8 (2011) 203.
- [14] M.B. Gawande, R.K. Pandey, R. V. Jayaram, *Catal. Sci. Technol.* 2 (2012) 1113.
- [15] J. Tantirungrotechai, P. Chotmongkolsap, M. Pohmakotr, *Microporous Mesoporous Mater.* 128 (2010) 41.
- [16] W. Thitsartarn, S. Kawi, *Green Chem.* 13 (2011) 3423.
- [17] S. Limmanee, T. Naree, K. Bunyakiat, C. Ngamcharussrivichai, *Chem. Eng. J.* 225 (2013) 616.
- [18] G. Teng, L. Gao, G. Xiao, H. Liu, J. Lv, *Appl. Biochem. Biotechnol.* 162 (2010) 1725.
- [19] Y. Wang, J. Jehng, *Chem. Eng. J.* 175 (2011) 548.
- [20] B. Wang, S. Li, S. Tian, R. Feng, Y. Meng, *Fuel* 104 (2013) 698.
- [21] D.-W. Lee, Y.-M. Park, K.-Y. Lee, *Catal. Surv. from Asia* 13 (2009) 63.
- [22] M.C.J. Bradford, M. Te, M. V. Konduru, A. Pollack, D.X. Fuentes, *Catal. Today* 123 (2007) 23.
- [23] C. Murugan, H.C. Bajaj, *Indian J. Chem.* 52 (2013) 459.
- [24] J. Weitkamp, *Solid State Ionics* 131 (2000) 175.
- [25] R. Davis, *J. Catal.* 216 (2003) 396.
- [26] B. Silva, H. Figueiredo, O.S.G.P. Soares, M.F.R. Pereira, J.L. Figueiredo, a. E. Lewandowska, M. a. Bañares, I.C. Neves, T. Tavares, *Appl. Catal. B Environ.* 117-118 (2012) 406.
- [27] P.E. Hathway, M.E. Davis, *J. Catal.* 119 (1989) 497.

- [28] K.S. Walton, M.B. Abney, M.D. Levan, *Microporous Mesoporous Mater.* 91 (2006) 78.
- [29] C. Jia, D. Herein, N. Pfander, H.G. Karge, F.C. Jentoft, *J. Mol. Catal. A Chem.* 162 (2000) 227.
- [30] M. Wallau, U. Schuchardt, *J. Brazilian Chem. Soc.* 6 (1995) 393.
- [31] M. Laspras, H. Cambon, D. Brunel, I. Rodriguez, P. Geneste, *Microporous Mater.* 7 (1996) 61.
- [32] M. Verziu, M. Florea, S. Simon, V. Simon, P. Filip, V.I. Parvulescu, C. Hardacre, *J. Catal.* 263 (2009) 56.
- [33] N. Boz, M. Kara, O. Sunal, N. Degirmenbasi, *Turkish J. Chem.* 33 (2009) 433.
- [34] F. Bernhardt, R. Trotzki, T. Szuppa, A. Stolle, B. Ondruschka, Beilstein *J. Org. Chem.* 6 (2010) 7.
- [35] P. Qiu, B. Yang, C. Yi, S. Qi, *Catal. Letters* 137 (2010) 232.
- [36] H. Kabashima, H. Tsuji, S. Nakata, Y. Tanaka, H. Hattori, *Appl. Catal. A Gen.* 194-195 (2000) 227.
- [37] L. Čapek, M. Hájek, P. Kutálek, L. Smoláková, *Fuel* 115 (2014) 443.
- [38] S.R. Sarda, W.N. Jadhav, S.R. Bhusare, S.K. Wasmatkar, S.A. Dake, R.P. Pawar, *Int. J. ChemTech Res.* 1 (2009) 265.
- [39] Y. Ono, T. Baba, *Catal. Today* 38 (1997) 321.
- [40] R. Bal, K. Chaudhari, S. Sivasanker, *Catal. Letters* 70 (2000) 75.
- [41] R. Gupta, M. Gupta, S. Paul, R. Gupta, *Bull. Korean Chem. Soc.* 30 (2009) 2419.
- [42] W. Zhao, Y. Zhang, C. Qu, L. Zhang, J. Wang, Y. Cui, *Catal. Letters* (2014).
- [43] J.H. Oh, B.S. Ahn, J. Han, S.D. Lee, S.W. Kim, H. Lee, *Bull. Korean Chem. Soc.* 29 (2008) 2202.
- [44] A. Corma, S. Iborra, *Adv. Catal.* 49 (2006) 239.
- [45] M.G. Stevens, H.C. Foley, *Chem. Commun.* (1997) 519.
- [46] W. Raróg-pilecka, E. Miskiewicz, S. Jodzis, J. Petryk, D. Łomot, Z. Kaszukur, Z. Karpinski, Z. Kowalczyk, *J. Catal.* 239 (2006) 313.

- [47] W. Raróg-pilecka, E. Miskiewicz, L. Kepinski, Z. Kaszkur, K. Kielar, Z. Kowalczyk, *J. Catal.* 249 (2007) 24.
- [48] A.M. Frey, J. Yang, C. Feche, N. Essayem, D.R. Stellwagen, F. Figueras, K.P. de Jong, J.H. Bitter, *J. Catal.* 305 (2013) 1.
- [49] T. Li, L. Sun, L. Gong, X. Liu, X. Liu, *J. Mol. Catal. A. Chem.* 352 (2012) 38.
- [50] H. Ma, S. Li, B. Wang, R. Wang, S. Tian, *J. Am. Oil Chem. Soc.* 85 (2008) 263.
- [51] S.-G. Zhang, S.-F. Yin, Y.-D. Wei, S.-L. Luo, C.-T. Au, *Catal. Letters* 142 (2012) 608.
- [52] T. Wang, G. Wu, N. Guan, L. Li, *Microporous Mesoporous Mater.* 148 (2012) 184.
- [53] J. Tantirungrotechai, P. Thananupappaisal, B. Yoosuk, *Catal. Commun.* 16 (2011) 25.
- [54] X. Chen, M. Arruebo, K.L. Yeung, *Catal. Today* 204 (2013) 140.
- [55] W. Xie, M. Fan, *Chem. Eng. J.* 239 (2014) 60.
- [56] W.-K. Chen, H.-H. Tseng, M.-C. Wei, E.-C. Su, I.-C. Chiu, *Int. J. Hydrogen Energy* 39 (2014) 19555.
- [57] C. Yuan, Z. Huang, J. Chen, *Catal. Commun.* 24 (2012) 56.
- [58] S. Vijaikumar, K. Pitchumani, *Indian Acad. Chem.* 49 (2010) 469.
- [59] H.J. Alves, A.M. da Rocha, M.R. Monteiro, C. Moretti, M.D. Cabrelon, C.A. Schwengber, M.C. Milinsk, *Appl. Clay Sci.* 91-92 (2014) 98.
- [60] N. Degirmenbasi, N. Boz, D.M. Kalyon, *Appl. Catal. B Environ.* 150-151 (2014) 147.
- [61] O. Babajide, N. Musyoka, L. Petrik, F. Ameer, *Catal. Today* 190 (2012) 54.
- [62] K.N. Ismail, K. Hussin, M.S. Idris, *J. Nucl. Relat. Technol.* Vol. 4 (2007) 47.
- [63] M. Ahmaruzzaman, *Prog. Energy Combust. Sci.* 36 (2010) 327.
- [64] H.K. Venkatanarayanan, P.R. Rangaraju, *Cem. Concr. Compos.* 43 (2013) 54.
- [65] S. Kumar, R. Kumar, *Ceram. Int.* 37 (2011) 533.
- [66] D. Jain, M. Mishra, A. Rani, *Fuel Process. Technol.* 95 (2012) 119.

- [67] D. Jain, C. Khatri, A. Rani, *Fuel* 90 (2011) 2083.
- [68] D. Jain, C. Khatri, A. Rani, *Fuel Process. Technol.* 91 (2010) 1015.
- [69] D. Jain, A. Rani, *Am. Chem. Sci. J.* 1 (2011) 37.
- [70] D. Jain, R. Hada, A. Rani, *J. Catal.* 2013 (2013) 1.
- [71] D. Bastani, A.A. Safekordi, A. Alihosseini, V. Taghikhani, *Sep. Purif. Technol.* 52 (2006) 295.
- [72] P. Wang, B. Shen, J. Gao, *Catal. Surv. from Asia* 125 (2007) 155.
- [73] M. Hinojosa-reyes, S. Arriaga, L.A. Diaz-torres, V. Rodríguez-gonzález, *Chem. Eng. J.* 224 (2013) 106.
- [74] A. Karimi, S.M. Mousavi, B. Ghiasi, J.R. Grace, *Am. J. Sci. Res.* 32 (2011) 107.
- [75] K. Genov, I. Stambolova, M. Shipochka, I. Boevski, S. Vassilev, V. Blaskov, *J. Univ. Chem. Technol. Metall.* 46 (2011) 363.
- [76] D. Acosta, J. Martinez, C. Carrera, E. Erdmann, E. Gonzo, H. Destéfanis, *Lat. Am. Appl. Res.* 36 (2006) 317.
- [77] K. Genov, V. Georgiev, T. Batakliiev, D.K. Sarker, *World Acad. Sci. Eng. Technol.* 80 (2011) 1015.
- [78] M. Giannouri, T. Kalampaliki, N. Todorova, T. Giannakopoulou, N. Boukos, D. Petrakis, T. Vaimakis, C. Trapalis, *Int. J. Photoenergy* 2013 (2013) 1.
- [79] M.G. Mostafa, Y. Chen, J. Jean, C. Liu, Y. Lee, *J. Hazard. Mater.* 187 (2011) 89.

*Synthesis and Characterization of
Solid Base Catalyst from Perlite
and Its Catalytic Application in
Cross-Aldol Condensation*

Abstract

A new type of solid base catalyst [KOH/Al₂O₃/Thermally activated perlite (KATP)] has been synthesized by thermal and chemical activation of perlite, a material formed by cooling of volcanic eruption. Initially perlite was thermally activated at 800 °C for 3 h followed by chemical activation by loading of alumina (15 wt%) then treated with an aqueous solution of KOH (10 wt%). The physico-chemical properties of catalytic materials were monitored by N₂ adsorption-desorption study, Thermo gravimetric analysis, FTIR spectroscopy, X-ray diffraction, Scanning electron microscopy and Transmission electron microscopy. The basic strength of the catalyst was measured by Hammett indicator method. KATP catalyst was effectively used in liquid phase, solvent free, Cross-aldol condensation of 4-methoxybenzaldehyde with 2-hydroxyacetophenone and gave higher conversion (89%) to desired product 2-hydroxy-4'-methoxychalcone, up to seven reaction cycles. This excellent conversion shows that KATP catalyst has sufficient active basic sites, both on the surface and in the bulk, which are not lixiviated in reaction solution and make the catalyst reusable. Moreover, this catalyst may replace conventional, environmentally hazardous homogeneous liquid bases by creating solvent free, eco-friendly and solid base catalyzed process. This application of perlite to synthesize a solid base catalyst finds a novel way to use this silica enriched abundant waste material.

2.1 Introduction

Perlite is a light grey colored glassy volcanic rock with rhyolitic composition, having numerous concentric cooling cracks which give rise to a perlitic structure (concentric onion-like partings). Perlite ranges in color from light gray to almost black and has a waxy to pearly luster. Perlite is formed by rapid cooling of viscous lava or magma [1]. SiO_2 , Al_2O_3 , K_2O , Na_2O are major constituents of perlite while TiO_2 , CaO , MgO , Fe_2O_3 and unburned carbon are present as minor constituents with 2-5% combined water [2]. Perlite expands in temperature range of 760–1100 °C up to 15-20 times of volume of the rock, due to removal of combined water and converts into light weight, white colored and fluffy material that resembles pumice [1], with approximate bulk density 0.125 g cm^{-3} , particle size 0.2–1 mm and porosity 80–90% [4]. Huge amount of solid waste perlite is available in the world, it is reported that approximately 3 million metric tons of perlite was produced in 15 countries during 2012 [3]. As far as bulk application of perlite is concerned, due to being inert and non-hazardous material, it is widely used as fire resistive material, soil conditioner, fillers, extenders in paints, resins, enamels, rubber, as abrasives and in filtration [1], yet limited reports are available for utilization of perlite in catalytic applications, perlite is reported to be used for photocatalysis [4] and ozone decomposition [5] etc. However, more research is required in testing and model the performance of this material.

Perlite is an amorphous aluminosilicate with high content of silica more than 70%. Inorganic support materials, including silica gel, alumina, zeolite and perlite are focused due to their thermal and mechanical stability, non-toxicity and high resistance against microbial attacks and organic solvents. Lots of inorganic support materials, however, have too expensive cost because of being synthesized from organosilicon compounds, such as recently developed materials MCM-41, SBA-15, meso-cellular foams. Here the advantage of perlite instead of the other supports is that, this is naturally occurring siliceous material so inexpensive than the other supports. So, due to being rich siliceous material, perlite is thought to be explored as efficient and economical support material for heterogeneous catalyst synthesis.

For organic synthesis, base catalysis is an important area of fundamental industrial importance in fine chemical, petrochemical and pharmaceutical industries. Commercially the base catalyzed reactions are largely carried out by using homogeneous bases like NaOH, Ca(OH)₂, KOH etc. [6, 7]. These bases are harmful, required in more than stoichiometric amount, having high operating cost. Some serious environmental issues associated with these bases are neutralization, product separation, purification, corrosion and waste generation which motivate substantial efforts towards the development of processes mediated by solid base catalysts.

Solid base catalyst seems to be a promising candidate for replacing a homogeneous process for solving the above said problems of homogeneous bases as well as for the suppression of side reactions that include self-condensation and oligomerization, which results in better selectivity and product yield by developing desired basic strength as required for the reaction [7]. Solid base catalysts such as metal oxides viz. CaO, MgO [8], supported catalysts viz LiOH/Al₂O₃ [9], Na/SiO₂, Cs/MCM-41 [10] and KF/activated carbon [11] are well reported in the literature for different organic transformations. The main advantages of heterogeneous catalysts over homogeneous ones include easier catalyst recovery and recycling resulting in mitigation of the adverse environmental impacts, such as waste water treatment and elimination of corrosion problems.

Cross-aldol condensation reaction of aromatic aldehydes with cyclic ketones is an important synthetic reaction for the preparation of α,β -unsaturated ketone or chalcone. The compounds with the backbone of chalcones have been reported to possess various biological activities such as antimicrobial, anti-inflammatory, analgesic, antiplatelet, antiulcerative, antimalarial, anticancer, antiviral etc. [12].

We have recently reported fly ash supported base catalysts viz. NaOH/Fly ash [13], CaO/Fly ash [14], amino propylated/Fly ash [15], MgO/Fly ash [16], KF/Fly ash [17] applicable for various types of condensation reactions. Perlite being rich in silica (72-75%) and alumina (12-15%) [18], is thought to be explored as an efficient siliceous support material to synthesize novel, recyclable,

eco-friendly and cost effective solid base catalyst for Cross-aldol condensation of 2-hydroxyacetophenone and 4-methoxybenzaldehyde. Perlite after suitable thermal and chemical activation has been converted into an effective solid base catalyst and reused up to six reaction cycles for synthesis of 2-hydroxy-4'-methoxychalcone in single step, liquid phase and solvent free reaction conditions possessing various pharmaceutical applications.

2.2 Experimental

2.2.1 Materials

Perlite was collected from Indica Chemical Industries Pvt. Limited, Kotdwar (Uttarakhand). KOH (95%), $\text{Al}(\text{NO}_3)_3 \cdot 9\text{H}_2\text{O}$ (98%), NH_4CO_3 (95%) and NH_4OH (98%) were purchased from Sigma Aldrich and 4-methoxybenzaldehyde (98%) and 2-hydroxyacetophenone (99%) were purchased from S.D. Fine Chemical Ltd., India. All the purchased reagents were of analytical grade and used as such.

2.2.2 Catalyst synthesis

As received perlite (P) was thermally activated at 800 °C for 3 h to form thermally activated perlite (TP) consequently C, S, moisture and other impurities also get removed [19]. Several catalytic materials synthesized during the study are reported below.

a) Al_2O_3 /Thermally activated perlite (ATP)

An aqueous solution of aluminum nitrate (for 15 wt% alumina loading) was added into 10 g TP at constant stirring followed by dropwise addition of aqueous solution of $(\text{NH}_4)_2\text{CO}_3$ (0.05 mol) and the pH was maintained close to 8.0 by the addition of appropriate amount of NH_4OH . Resultant slurry was aged for 1 h then filtered and washed with double distilled water up to pH 7 to remove leached compounds, air dried at 110 °C for 24 h and calcined at 700 °C for 3 h in a muffle furnace under static conditions to form TP supported Alumina material (ATP). Pure Al_2O_3 powder was synthesized by adopting the similar process without involving TP [17].

b) KOH/Al₂O₃ (KA)

KA was prepared by dropwise addition of an aqueous solution of KOH (10 wt%) into 10 g pure Al₂O₃ powder at constant stirring. The slurry was aged at 110 °C for 24 h then filtered and washed with double distilled water up to pH 7 to remove leached compounds, air dried at 110 °C for 24 h and calcined at 400 °C for 3 h in a muffle furnace under static conditions.

c) KOH/Thermally activated perlite (KTP)

KTP was prepared by dropwise addition of an aqueous solution of KOH (10 wt%) into 10 g TP at constant stirring. The slurry was aged at 110 °C for 24 h then filtered and washed with double distilled water up to pH 7 to remove leached compounds, air dried at 110 °C for 24 h and calcined at 400 °C for 3 h in a muffle furnace under static conditions.

d) KOH/Al₂O₃/Thermally activated perlite (KATP)

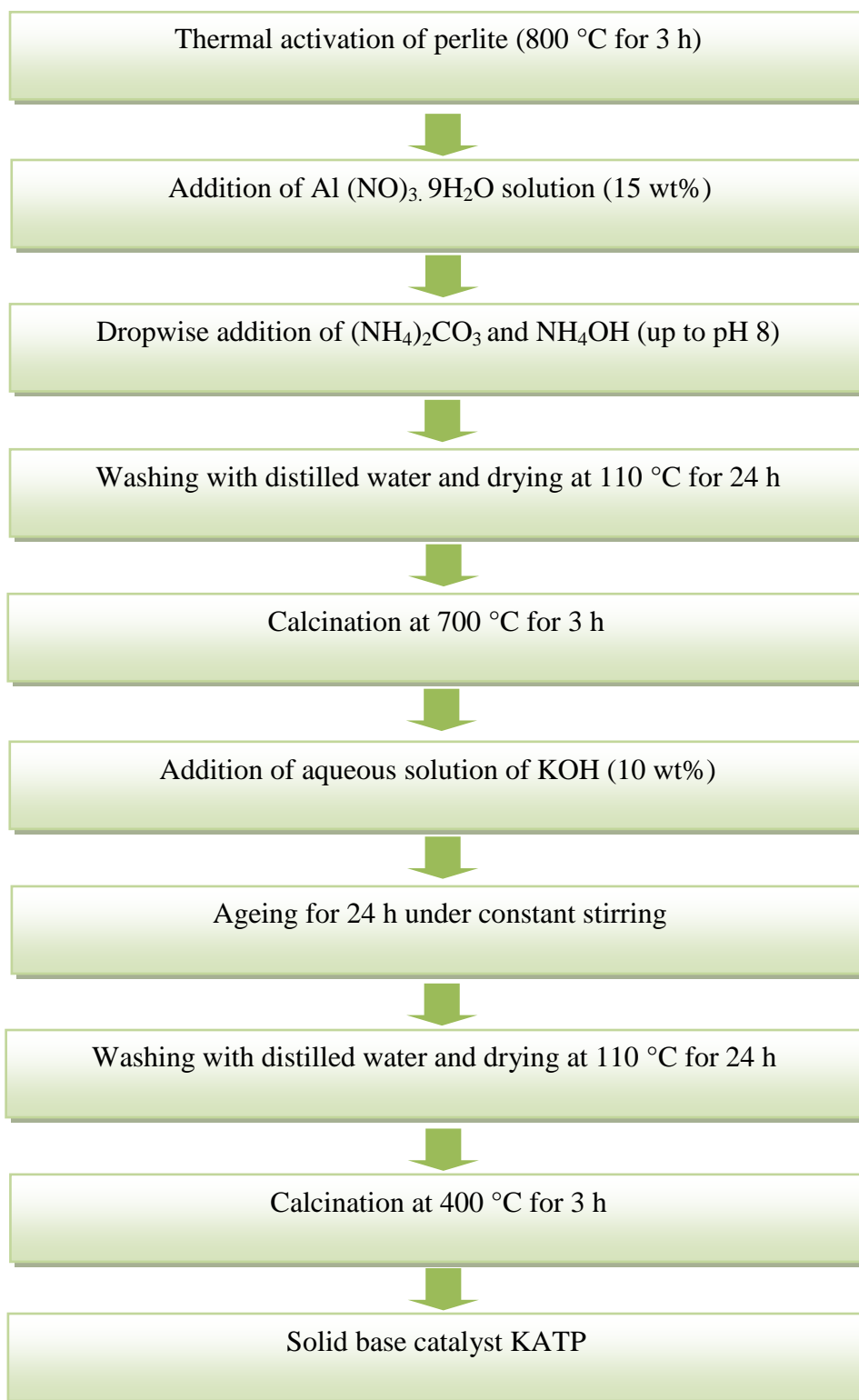
KATP was prepared by dropwise addition of an aqueous solution of KOH (10 wt%) into 10 g ATP, at constant stirring. The slurry was aged at 110 °C for 24 h then filtered and washed with double distilled water up to pH 7 to remove leached compounds, air dried at 110 °C for 24 h and calcined at 400 °C for 3 h in a muffle furnace under static conditions (**Scheme 2.1**).

2.3 Catalyst characterization

P, ATP, KA, KTP and KATP were characterized by N₂ adsorption-desorption study, TGA, FTIR, XRD, SEM and TEM. Instruments detail and operating conditions during the characterization are given in **Annexure I**.

2.3.1 Basic strength and basicity measurement

The basic strength of the catalyst was determined by using Hammett indicators like phenolphthalein (pK_a = 8.2), Nile blue (pK_a = 9.8), 2,4,6-trinitroaniline (pK_a = 12.2), 2,4-dinitroaniline (pK_a = 15) and 4-nitroaniline (pK_a = 18.4). 25 mg KATP catalyst was stirred with 1 mL of the solution of Hammett indicator diluted in methanol and left to equilibrate for 2 h [20].



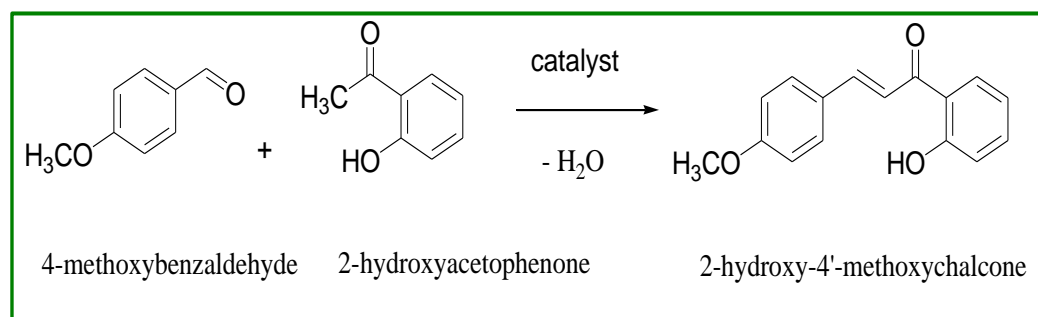
Scheme 2.1: Synthesis of solid base catalyst KATP.

If the indicator exhibits a color change, then the catalyst is labelled as stronger than the indicator and if not, then the catalyst was said to be weaker than the indicator.

Basicity of the catalysts was determined by benzoic acid titration method using phenolphthalein indicator. In benzoic acid titration method, 0.1 g of the catalyst was suspended in 2 mL of phenolphthalein indicator solution (0.01 mg/mL toluene). It was then stirred for 0.5 h and titrated against 0.01 M benzoic acid in toluene solution until the pink colour changed to colourless [20].

2.4 Catalytic activity of KATP catalyst

Catalytic activity of all catalytic materials was tested by Cross-aldol condensation of 4-methoxybenzaldehyde with 2-hydroxyacetophenone in solvent-free, single step, liquid phase reaction conditions as shown in **Scheme 2.2**.



Scheme 2.2: Cross-aldol condensation of 4-methoxybenzaldehyde with 2-hydroxyacetophenone over various catalytic materials.

2.4.1 Cross-aldol condensation

The condensation of 4-methoxybenzaldehyde with 2-hydroxyacetophenone was performed in a liquid phase batch reactor consisting of 250 mL round bottom flask equipped with digital magnetic stirrer and glass condenser, immersed in a constant temperature oil bath. A mixture of 4-methoxybenzaldehyde and 2-hydroxyacetophenone was taken in a round bottom flask. The desired amount of catalytic material, taken according to substrate/catalyst weight ratio ranging from 10:1 to 2.5:1, was preheated at appropriate temperature for 2 h prior to adding in the reaction mixture. The

reaction was carried out at different molar ratio of substrate ranging from 2:1 to 1:3 at different temperatures in the range of 60 to 160 °C for time ranging from 1 to 8 h. After completion of the reaction, the solid catalyst was filtered and the product was analyzed by Gas Chromatograph.

The conversion of 4-methoxybenzaldehyde and yield were calculated by using weight percent method.

$$\text{Conversion (wt\%)} = 100 \times (\text{Initial wt\%} - \text{Final wt\%}) / \text{Initial wt\%}$$

Yield % of 2-hydroxy-4'-methoxychalcone obtained =

$$100 \times \frac{\text{g of 2-hydroxy-4'-methoxychalcone obtained experimentally}}{\text{g of 2-hydroxy-4'-methoxychalcone obtained theoretically}}$$

2.5 Catalyst regeneration

After initial use, spent catalyst from the reaction mixture was recovered by filtration and regenerated for further use. The recovered catalyst was washed thoroughly with acetone, dried in oven at 110 °C for 12 h and thermally activated at 400 °C for 2 h in static condition before reuse in next reaction cycle under similar reaction conditions as earlier.

2.6 Results and discussion

2.6.1 Chemical composition of P and KATP catalyst

The Chemical composition of as received perlite (P) and KATP as determined by SEM-EDX, are given in **Table 2.1**. The chemical composition of perlite reveals that major components of perlite are SiO₂ and Al₂O₃. Some minor components are also present in it. Al and K contents in KATP are increased considerably up to 6.59% and 3.32% respectively while Si percentage is decreased slightly. The thermal activation of perlite at 800 °C for 3 h removes C, S, moisture and other impurities. Loss on ignition (LOI) was determined by heating a certain weighed quantity of perlite in muffle furnace at 800 °C for 3 h, LOI was found to be 4.1 wt%.

Table 2.1: Chemical composition of P and KATP.

Elements	P (Wt%)	KATP (Wt%)
O	73.70	71.56
Si	18.83	16.78
Al	3.72	6.59
K	1.44	3.32
Na	1.61	1.19
Mg	0.21	0.15
Ca	0.19	0.13
Fe	0.10	0.10
Zn	0.13	0.11
Ti	0.07	0.07

2.6.2 Surface area results

Specific surface areas of P and KATP catalyst were calculated to be 2.3 m²/g and 1.5 m²/g respectively (**Table 2.2**). A slight decrease in the surface area of the catalyst is observed after the effective chemical treatment of P with Al₂O₃ and KOH. Decrement in the surface area is due to the blockage of small pores of the P [21]. In the present catalytic system the change in the surface area results into increased surface active catalytic sites (hydroxyl groups), which is accounted for the high catalytic activity.

Table 2.2: Surface area of P and KATP.

Catalyst	Specific surface area (m ² /g)
P	2.3
KATP	1.5

2.6.3 Thermogravimetric analysis

The TGA curve of P, as shown in **Figure 2.1**, is having weight loss of 4.3% within the temperature range 50-400 °C. TGA curve of KATP shows weight loss of 6.6 % within the temperature range 30-1000 °C (**Figure 2.1**). The weight loss in P and KATP indicates the removal of moisture content with some volatile materials. This weight loss would correspond to the removal of moisture content, burning of carbonaceous materials and volatilization of some trace metal oxides present in P and KATP [22].

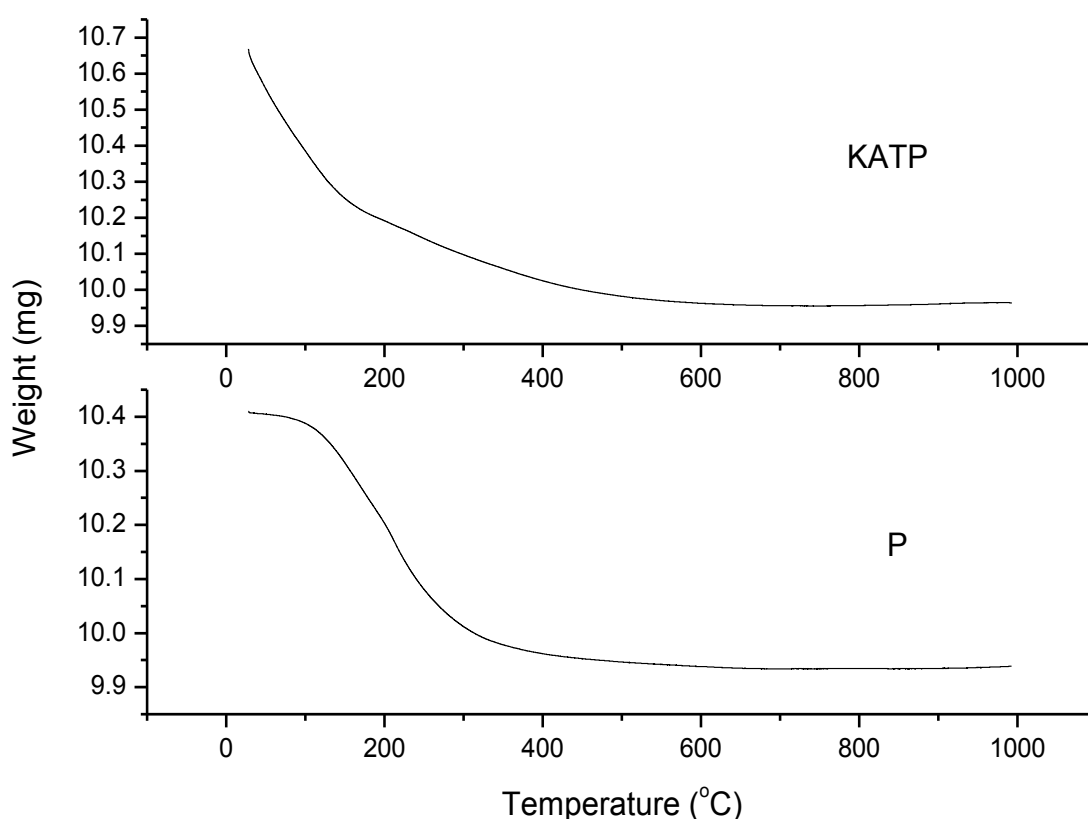


Figure 2.1: TGA curves of P and KATP.

2.6.4 FTIR studies

The surface of perlite is covered with hydroxyl groups and physically adsorbed water. On thermal activation initially the physically adsorbed water is removed, resulting in the formation of surface siloxane bridges (Si–O–Si), which on chemical activation with KOH results in increased surface silanols thus basicity. Each FTIR spectrum (**Figure 2.2**) shows a broad band between 3600-

3200 cm^{-1} , which is attributed to surface $-\text{OH}$ groups of $-\text{Si}-\text{OH}$ on the silica surface [16]. The broadness of band indicates the presence of strong hydrogen bonding [23]. Intensity and broadness reduce in case of TP (**Figure 2.2b**) confirms loss of water from perlite during thermal activation which again increases in case of ATP (**Figure 2.2c**), may be due to the presence of surface $-\text{Al}-\text{OH}$. Loaded Al_2O_3 in ATP facilitates and provides suitable active sites for further activation by KOH , thus hydroxyl groups increases in case of KATP catalyst (**Figure 2.2d**), which is also evidenced by a broad, intense band at 3600-3200 cm^{-1} . Each spectrum (**Figure 2.2, 2.3, Table 2.3**) shows a peak around 1630 cm^{-1} attributed to bending mode ($\delta_{\text{O-H}}$) of water molecules [24].

Perlite mainly comprises of amorphous silica, which is normally assumed to be formed by a continuous network of Q^4 units $[\text{Si}(\text{SiO}_4)_4]$, gives broadband in the range of 1100-1040 cm^{-1} due to $\text{Si}-\text{O}-\text{Si}$ asymmetric stretching vibration modes (**Figure 2.2a**) [14]. The increased $-\text{OH}$ species in case of ATP and KATP in the form of $-\text{Si}-\text{OH}$ and $-\text{Si}-\text{O}-\text{Al}-\text{OH}$ groups (**Figure 2.2c, 2.2d**), shift the position of $\text{Si}-\text{O}-\text{Si}$ band towards lower wave number indicating the transformation of amorphous silica Q^4 units $[\text{Si}(\text{SiO}_4)_4]$ to Q^3 units $[\text{Si}(\text{OH})(\text{SiO}_4)_3]$ [25]. The band appears at 794 cm^{-1} in TP due to symmetric $\text{Si}-\text{O}-\text{Si}$ stretching vibration [13] is shifted towards lower wave number in ATP (**Figure 2.2c**) and KATP (**Figure 2.2d**) at 789 and 785 cm^{-1} (**Table 2.3**) respectively, which also could be an evidence for increased $-\text{OH}$ groups on surface due to Al_2O_3 loading and surface activation by KOH . Al_2O_3 loading in ATP is also confirmed by $\text{Si}-\text{O}-\text{Al}$ stretching peak, appearing at 602 cm^{-1} [26]. Few K^+ ions could replace the protons of the surface hydroxyl groups present on fully hydroxylated alumina which is also proved by the peak around 1400 cm^{-1} conferring the presence of $\text{Al}-\text{O}-\text{K}$ bond in KATP (**Figure 2.2d**) [21].

Band due to $-\text{OH}$ stretching vibration appearing between 3600-3200 cm^{-1} is least broad in case of KTP (**Figure 2.3a**) representing lesser number of surface silanol groups on KTP surface. This band is broader and sharper in case of KATP (**Figure 2.3b**) due to the presence of $-\text{Si}-\text{O}-\text{Al}-\text{OH}$ species and hydrogen bonding among hydroxyl groups while KA (**Figure 2.3c**) also shows broad band in this region reflecting the abundance of strong hydrogen bonding in hydroxyl

groups. KA and KATP both show peaks centered at 1400 cm^{-1} indicating the presence of Al–O–K species [21].

Table 2.3: The observed transmission frequencies (cm^{-1}) of Fourier transform infrared spectra of P, TP, ATP, KA, KTP, KATP and reused KATP and their assignments.

Peak Assignments	P	TP	ATP	KA	KTP	KATP	Reused KATP	Ref.
Si-O-Al stretching vibration	597	572	602	–	–	612	590	26
Si-O-Si symm. stretching vibration	797	794	789	–	794	785	789	13
Si-O-Si asymm. stretching vibration	1054	1059	1044	–	1042	1056	1052	14
Al-O-K stretching vibration	–	–	–	1400	–	1400	–	21
H-O-H bending vibration	1626	1630	1631	1634	1634	1636	1632	24
-O-H stretching vibration	3632	3598	3630	3482	3601	3469	3452	16

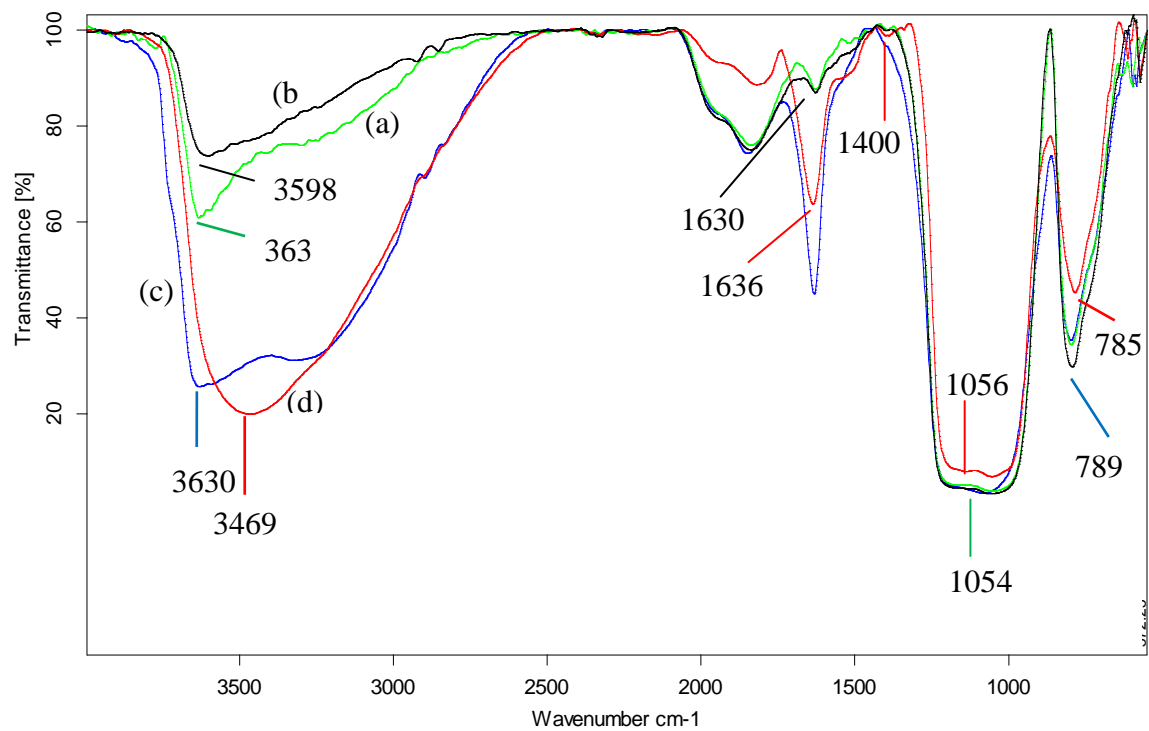


Figure 2.2: FTIR spectra of (a) P, (b) TP, (c) ATP and (d) KATP.

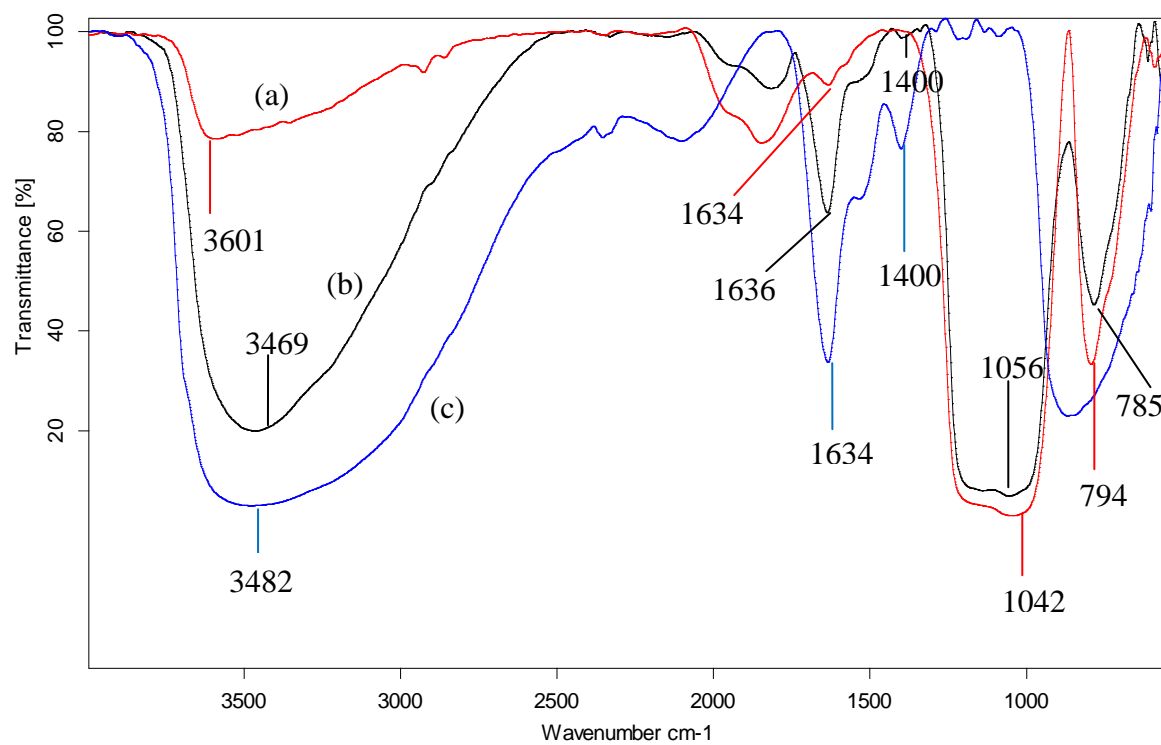


Figure 2.3: FTIR spectra of (a) KTP, (b) KATP and (c) KA.

2.6.5 X-ray diffraction studies

XRD analysis was carried out to study the effect of different activation procedures on perlite. The XRD pattern of perlite shows its amorphous nature (**Figure 2.4a**) while after thermal activation, a small peak is observed at $2\theta = 26.7^\circ$ (**Figure 2.4b**) due to formation of quartz crystalline phase [13]. **Figure 2.5b** shows that alumina loaded on perlite surface is amorphous in nature [27] resulting in disappearance of small crystalline peak visible in **Figure 2.5a**. On treatment with KOH, phase of potassium aluminum silicate (KAlSiO_4) is observed at $2\theta = 28.6^\circ$ (**Figure 2.5c**) in KATP (PDF-180987) [28].

2.6.6 SEM analysis results

The SEM micrographs of P and TP show particles of different irregular shapes and sizes, whereas the SEM micrograph of KATP (**Figure 2.6**) shows agglomerated particles with some loaded potassium aluminum species on perlite surface. In KATP increased amount of Al and K confirms the successful loading of alumina and KOH in the above mentioned forms on P surface.

2.6.7 TEM analysis results

The small dark spherical spots in the TEM image (**Figure 2.7b**) of each particle of the catalyst are proposed as nano crystalline potassium aluminosilicate (KAlSiO_4) phase referred as a super basicity center of the catalyst which is absent in P (**Figure 2.7a**).

2.6.8 Basic strength and basicity measurement

Basic strength and basicity of KATP catalyst were determined by the Hammett indicator method using phenolphthalein - benzoic acid titration. KATP shows basic strength $15 > \text{H}_+ > 9.8$ and basicity 1.07 mmol/g which shows quite resemblance with reported literature [29].

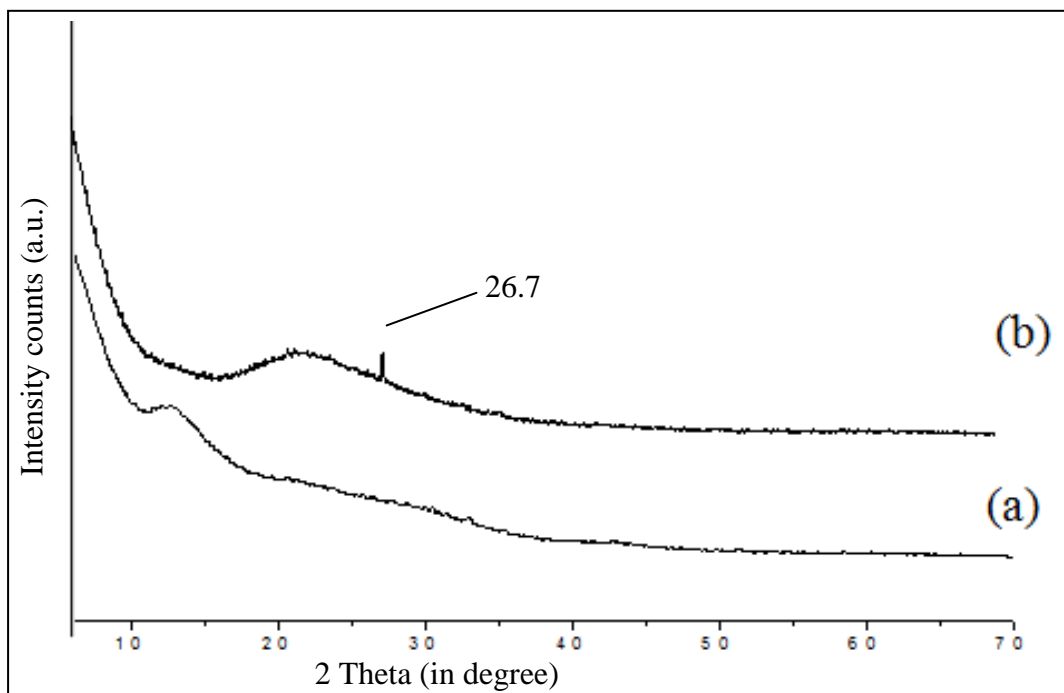


Figure 2.4: X ray diffraction patterns of (a) P and (b) TP.

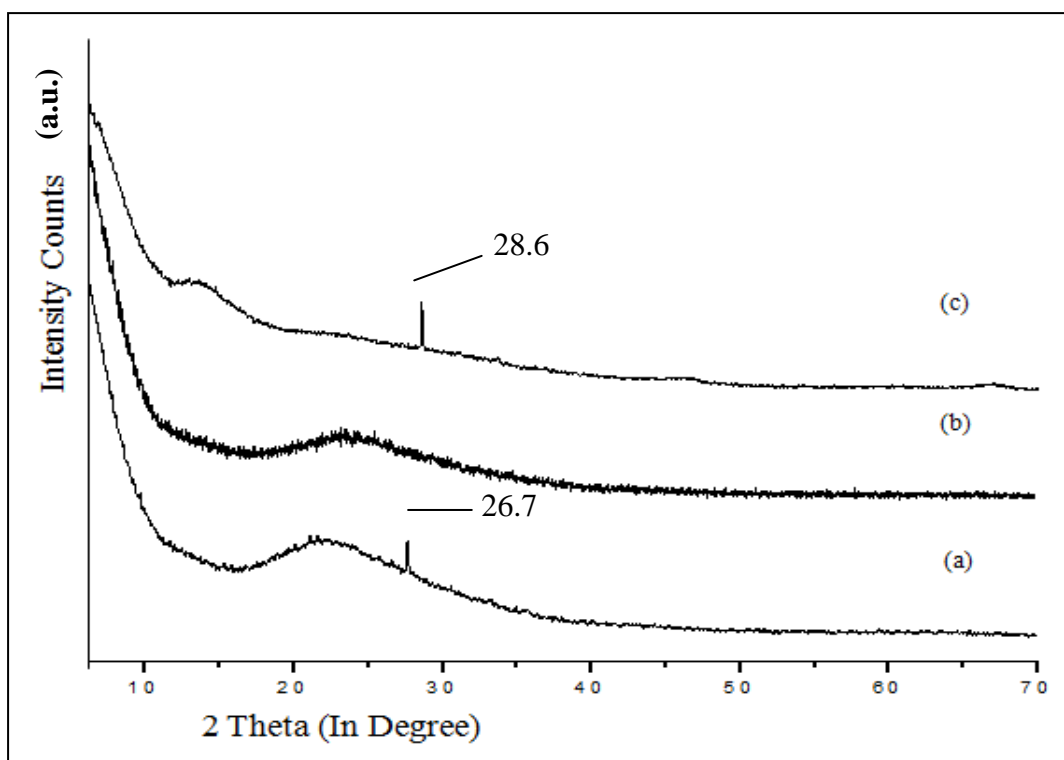


Figure 2.5: X-ray diffraction pattern of (a) TP, (b) ATP and (c) KATP.

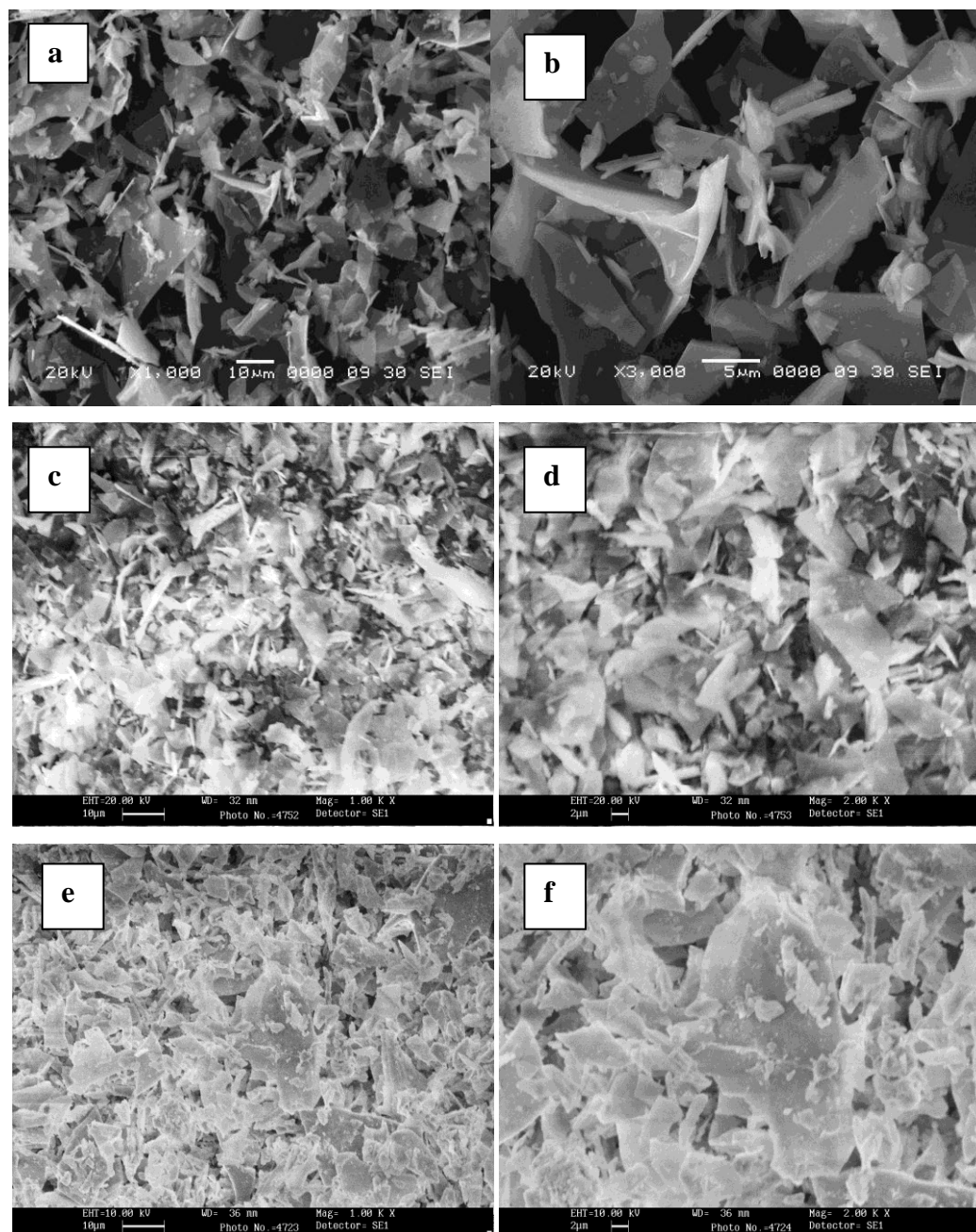


Figure 2.6: SEM micrographs of (a-b) P, (c-d) TP and (e-f) KATP.

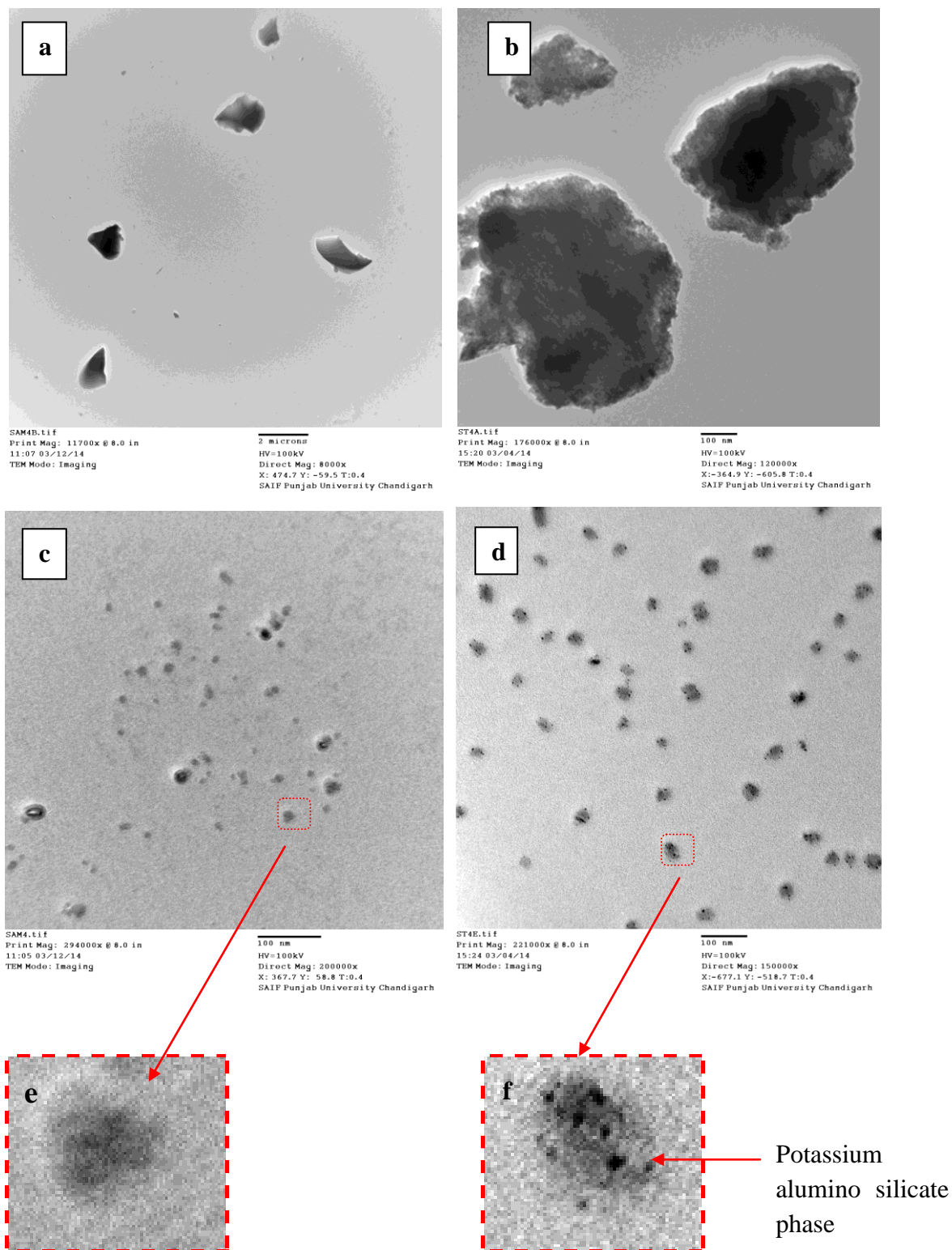


Figure 2.7: TEM images of (a, c) P, (b, d) KATP (e) P (magnified) and (f) KATP (magnified).

2.7 Catalytic activity

A comparison of catalytic activity of different catalytic materials has been made, which were synthesized at various stages of KATP synthesis. For this purpose the condensation of 4-methoxybenzaldehyde and 2-hydroxyacetophenone with different catalytic materials like TP, ATP, Pure Al₂O₃, KA, KTP and KATP was carried out at 110 °C for 2 h, taking 4-methoxybenzaldehyde\2-hydroxyacetophenone molar ratio 1:1 and 4-methoxybenzaldehyde to catalyst weight ratio of 5:1. As indicated in **Table 2.4**, KATP has given highest conversion in given reaction conditions and selected as catalyst for optimization of reaction parameters for highest conversion.

Table 2.4: Catalytic activities of different catalysts for Cross-aldol condensation reaction.

Catalyst	Conversion % of 4-methoxy benzaldehyde	Yield % of 2-hydroxy-4'-methoxychalcone
TP	Nil	Nil
ATP	Nil	Nil
Pure Al ₂ O ₃	Nil	Nil
KA	50	44
KTP	35	30
KATP	63	57

Reaction conditions: Temperature 110 °C, Time 2 h, 4-methoxybenzaldehyde/2-hydroxyacetophenone molar ratio 1:1, substrate/catalyst weight ratio 5:1.

2.7.1 Effect of reaction time

In order to check the effect of reaction time, the reaction was carried out at 110 °C for different times ranging from 1 to 8 h taking 4-methoxybenzaldehyde\2-hydroxyacetophenone in 1:1 molar ratio and 4-methoxybenzaldehyde to catalyst weight ratio of 5:1. Conversion was observed to increase maximum up to 89% with increasing reaction time up to 4 h. On further increasing the reaction time, conversion remained constant as shown in **Figure 2.8**. From the above results, the

optimum reaction time was found to be 4 h for highly selective synthesis of 2-hydroxy-4'-methoxychalcone over KATP.

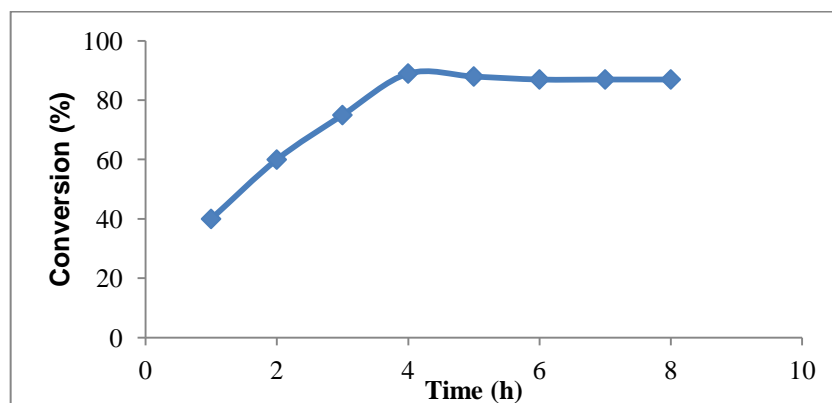


Figure 2.8: Variation of conversion (%) of 4-methoxybenzaldehyde with time.

Reaction conditions: Temperature 110 °C, Time 1 – 8 h, substrate/catalyst weight ratio 5:1, 4-methoxybenzaldehyde/2-hydroxyacetophenone molar ratio 1:1.

2.7.2 Effect of substrate/catalyst weight ratio

The effect of substrate to catalyst weight ratio on conversion of 4-methoxybenzaldehyde was studied by varying the amount of KATP under optimized reaction conditions. As indicated from **Table 2.5**, at lower catalyst amount, i.e. 4-methoxybenzaldehyde/KATP weight ratio 10:1, only 65% conversion of 4-methoxybenzaldehyde was observed. On increasing 4-methoxybenzaldehyde/KATP weight ratio to 5:1, conversion of 4-methoxybenzaldehyde increased up to 89%. The increase in the conversion with increase in the catalyst weight can be attributed to an increase in the availability of number of catalytic active sites required for this reaction. On further increasing the amount of catalyst no change in conversion is observed.

2.7.3 Effect of reaction temperature

Optimization of reaction temperature to give maximum conversion of 4-methoxybenzaldehyde was studied at temperature ranging from 60 to 160 °C for 4 h taking 4-methoxybenzaldehyde/2-hydroxyacetophenone in molar ratio 1:1 and 4-methoxybenzaldehyde to catalyst weight ratio of 5:1. Conversion was observed

to increase on increasing reaction temperature ranging from 60 to 110 °C as revealed from **Figure 2.9**. The results show that the maximum conversion (89%) of 4-methoxybenzaldehyde to 2-hydroxy-4'-methoxychalcone was found at 110 °C, after which conversion remained almost steady till 160 °C.

Table 2.5: Effect of substrate/catalyst weight ratio on conversion (%) of 4-methoxybenzaldehyde to 2-hydroxy-4'-methoxychalcone over KATP.

4-methoxybenzaldehyde/KATP Weight ratio	Conversion % of 4-methoxybenzaldehyde
10:1	65
5:1	89
2.5:1	89

Reaction conditions: Temperature 110 °C, Time 4 h, 4-methoxybenzaldehyde/2-hydroxyacetophenone molar ratio 1:1.

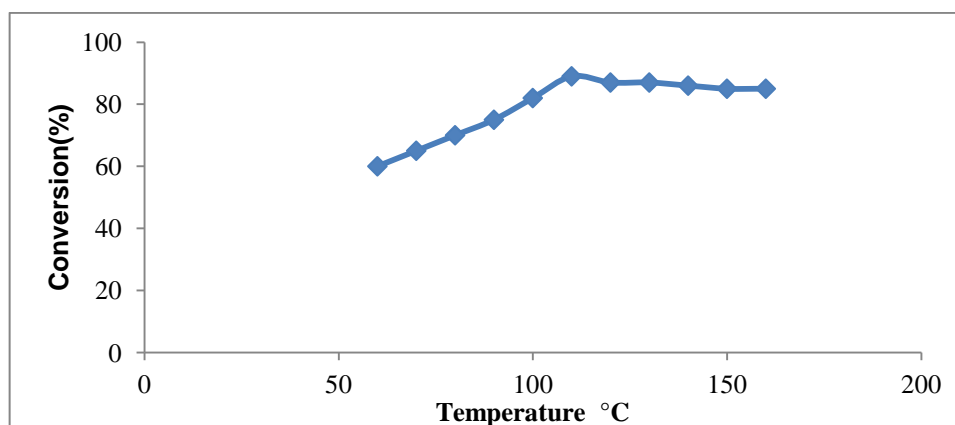


Figure 2.9: Variation of conversion (%) of 4-methoxybenzaldehyde with temperature.

Reaction conditions: Temperature 60 – 160 °C, Time 4 h, substrate/catalyst weight ratio 5:1, 4-methoxybenzaldehyde/2-hydroxyacetophenone molar ratio 1:1.

2.7.4 Effect of reactant molar ratio

The synthesis of 2-hydroxy-4'-methoxychalcone was carried out at 110 °C with various molar ratios of reactants for 4 h over KATP catalyst. As indicated by **Table 2.6**, 78% conversion of 4-methoxybenzaldehyde was observed at 2:1 molar ratio of 4-methoxybenzaldehyde to 2-hydroxyacetophenone. This may be due to an insufficient quantity of the reactants to react with each other. There was an increase in conversion up to 89% at 1:1 molar ratio of 4-methoxybenzaldehyde to 2-hydroxyacetophenone at the same reaction conditions. This may be due to equilibrating of each reactant quantity on the basic sites on the surface of the KATP catalyst. The conversion decreased from 80% to 77% on further increasing the molar ratio from 1:2 to 1:3.

Table 2.6: Effect of molar ratio of 4-methoxybenzaldehyde/2-hydroxyacetophenone on conversion (%) of 4-methoxybenzaldehyde to 2-hydroxy-4'-methoxychalcone over KATP.

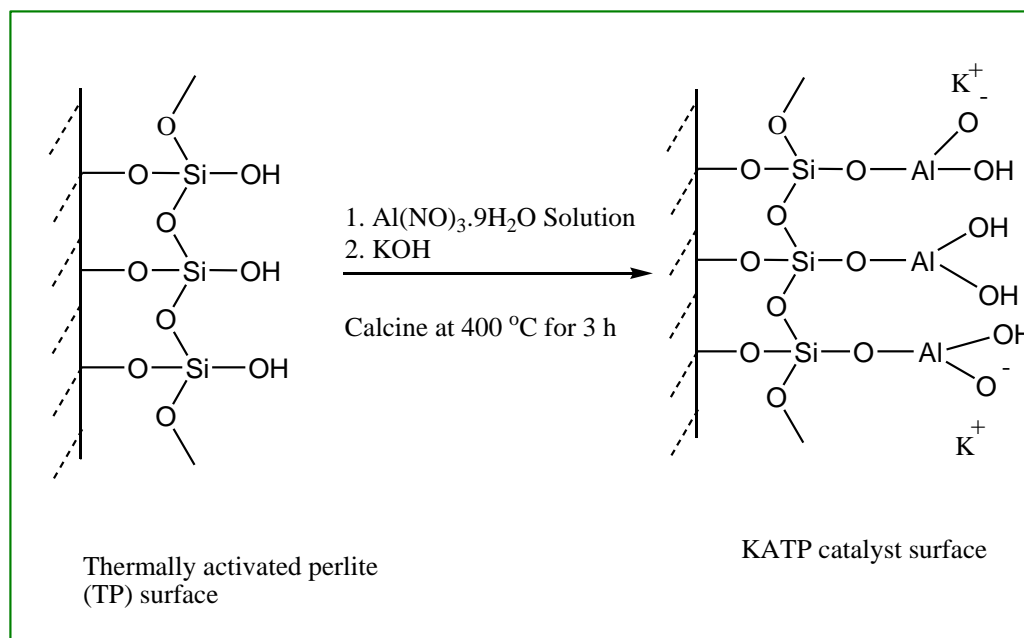
Molar ratio	Conversion % of 4-methoxybenzaldehyde
2:1	78
1:1	89
1:2	80
1:3	77

Reaction conditions: Temperature 110 °C, Time 4 h, substrate/catalyst weight ratio 5:1.

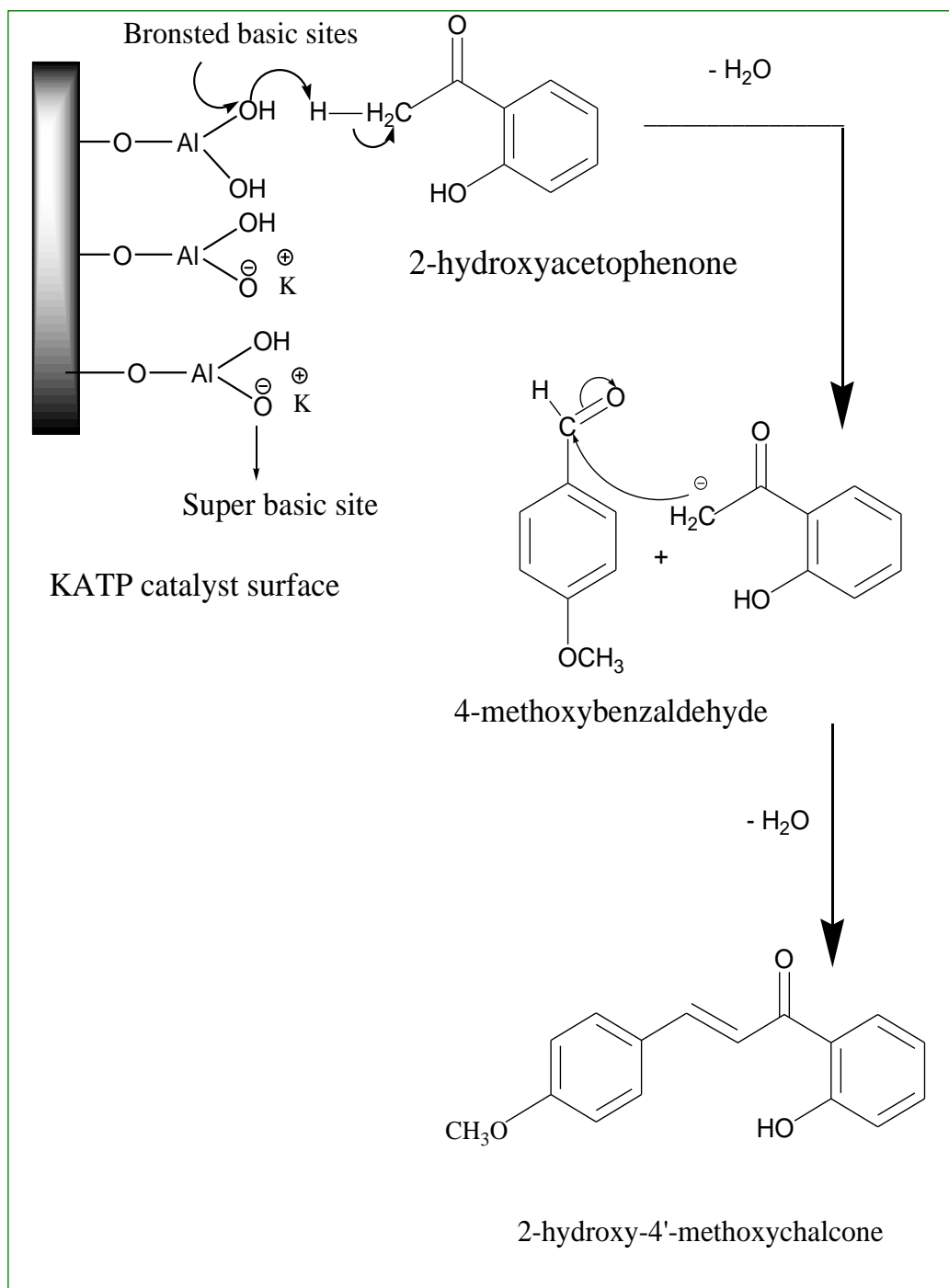
2.8 Reaction mechanism

The plausible structure for active basic sites of the KATP catalyst is shown in **Scheme 2.3**. The reaction mechanism over KATP catalyst shows (**Scheme 2.4**) that the surface basic sites of the KATP catalyst initiate the reaction by abstracting the proton from 2-hydroxyacetophenone resulting in the formation of carbanion.

This generated carbanion attacks on the C atom of the carbonyl group of 4-methoxybenzaldehyde and forms condensation product 2-hydroxy-4'-methoxychalcone with water removal by the nucleophilic addition reaction.



Scheme 2.3: The schematic presentation of chemical activation of perlite with $\text{Al}(\text{NO}_3)_3 \cdot 9\text{H}_2\text{O}$ and KOH solutions and proposed structure of KATP.



Scheme 2.4: Proposed mechanism for Cross-aldol condensation of 2-hydroxyacetophenone and 4-methoxybenzaldehyde over KATP.

2.9 Catalyst regeneration

The KATP catalyst was recovered from the reaction mixture by simple filtration, washed thoroughly with acetone, dried in oven at 110 °C for 12 h followed by thermal activation at 400 °C for 2 h under static conditions. The regenerated catalyst was used for the next reaction cycle under similar reaction conditions to first reaction cycle. The FTIR spectrum of reused KATP catalyst after seven reaction cycles (**Figure 2.10b**) resembles that of fresh KATP catalyst (**Figure 2.10a**) indicating the stability of surface hydroxyl groups responsible for Bronsted basic catalytic activity. Due to the stability of these basic sites KATP catalyst was found efficient up to seven reaction cycles, giving conversion in the range of 89–75% as shown from **Table 2.7**. The significant decrease in conversion after seven reaction cycles is due to the deposition of carbonaceous material on the external surface of the reused catalyst which may block the active basic sites present on the catalyst surface.

Table 2.7: Cross-aldol condensation of 2-hydroxyacetophenone and 4-methoxybenzaldehyde over fresh and regenerated KATP.

Reaction cycle	Conversion % of 4-methoxybenzaldehyde	Yield % of 2-hydroxy-4'-methoxychalcone
I	89	80
II	81	75
III	81	75
IV	80	72
V	78	70
VI	76	66
VII	75	64

Reaction conditions: Temperature 110 °C, Time 4 h, 4-methoxybenzaldehyde /2-hydroxyacetophenone ratio 1:1, substrate/catalyst weight ratio 5:1.

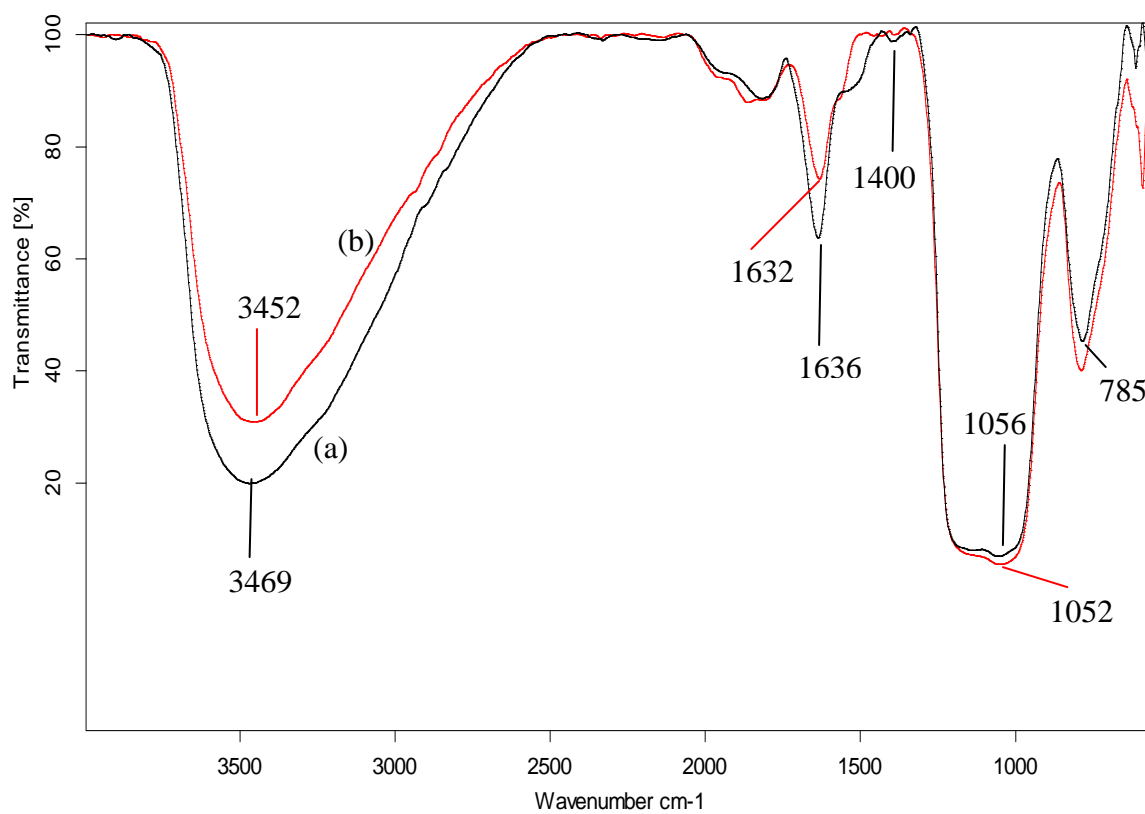


Figure 2.10: FTIR spectra of (a) KATP and (b) reused KATP.

2.10 Conclusion

This study provides a new solid support perlite which is least explored in catalytic applications. An effective solid base catalyst has been prepared through thermal and chemical activation. The perlite based catalyst KATP serves as a potential solid base catalyst for Cross-aldol condensation reaction as evidenced from higher conversion of 4-methoxybenzaldehyde (89%). KATP catalyst possesses higher basicity due to increase in Bronsted basic sites, i.e. Si/Al–OH content. The reaction was carried out in solvent free conditions and the catalyst can be easily separated by simple filtration, regenerated and reused up to several times with almost equal efficiency, thus produces no waste and makes the process economic. It is thus confirmed that under experimental conditions, the leaching of active basic sites or deactivation of the catalyst is almost negligible. This investigation brings into light the structural aspects of a novel perlite supported solid base catalyst which is cost effective, eco-friendly and recyclable and can be used in solvent free organic transformations.

2.11 References

- [1] M. Alkan, M. Karadas, M. Dogan, O. Demirbaş, *Colloids Surfaces A Physicochem. Eng. Asp.* 259 (2005) 155.
- [2] D. Bastani, A.A. Safekordi, A. Alihosseini, V. Taghikhani, *Sep. Purif. Technol.* 52 (2006) 295.
- [3] W.P. Bolen, *U.S. Geol. Surv. U.S.*, Oct. (2013) 55.1.
- [4] M. Giannouri, T. Kalampaliki, N. Todorova, T. Giannakopoulou, N. Boukos, D. Petrakis, T. Vaimakis, C. Trapalis, *Int. J. Photoenergy* 2013 (2013) 1.
- [5] K. Genov, I. Stambolova, M. Shipochka, I. Boevski, S. Vassilev, V. Blaskov, *J. Univ. Chem. Technol. Metall.* 46 (2011) 363.
- [6] A. Corma, S. Hamid, S. Iborra, A. Velty, *J. Catal.* 234 (2005) 340.
- [7] S. Abello, D. Vijaya-Shankar, J. Perez-Ramirez, *Appl. Catal. A Gen.* 342 (2008) 119.
- [8] H. Kabashima, H. Tsuji, T. Shibuya, H. Hattori, *J. Mol. Catal. A Chem.* 155 (2000) 23.

- [9] Y. Fu, T. Baba, Y. Ono, *Appl. Catal. A Gen.* 166 (1998) 425.
- [10] R. Bal, K. Chaudhari, S. Sivasanker, *Catal. Letters* 70 (2000) 75.
- [11] B.H. Hameed, C.S. Goh, L.H. Chin, *Fuel Process. Technol.* 90 (2009) 1532.
- [12] Y.R. Prasad, A.L. Rao, R. Rambabu, *E-Journal Chem.* 5 (2008) 461.
- [13] D. Jain, C. Khatri, A. Rani, *Fuel* 90 (2011) 2083.
- [14] D. Jain, C. Khatri, A. Rani, *Fuel Process. Technol.* 91 (2010) 1015.
- [15] D. Jain, M. Mishra, A. Rani, *Fuel Process. Technol.* 95 (2012) 119.
- [16] D. Jain, A. Rani, *Am. Chem. Sci. J.* 1 (2011) 37.
- [17] D. Jain, R. Hada, A. Rani, *J. Catal.* 2013 (2013) 1.
- [18] L. Meesuk, S. Seammai, *Sci. Asia* 36 (2010) 33.
- [19] K. Kordatos, S. Gavela, A. Ntziouni, K.N. Pistiolas, A. Kyritsi, V.K. Rigopoulou, *Microporous Mesoporous Mater.* 115 (2008) 189.
- [20] R. Rahul, J.K. Satyarthi, D. Srinivas, *Indian J. Chem.* 50 (2011) 1017.
- [21] H. Ma, S. Li, B. Wang, R. Wang, S. Tian, *J. Am. Oil Chem. Soc.* 85 (2008) 263.
- [22] M.M.A. Sekkina, R.M. Issa, A.E.-D.M. Bastawisy, W.A. El Helece, *Int. J. Chem.* 2 (2010) 81.
- [23] C. Khatri, A. Rani, *Fuel* 87 (2008) 2886.
- [24] S. Kabra, S. Katara, A. Rani, *Int. J. Innov. Res. Sci. Eng. Technol.* 2 (2013) 4319.
- [25] M.E. Simonsen, C. Sonderby, Z. Li, E.G. Sogaard, *J. Mater. Sci.* 44 (2009) 2079.
- [26] M.E.G. Frances I. Hurwitz, Denisse V. Aranda, in: *Am. Chem. Soc. 236th Natl. Meet. Philadelphia, PA, August 20, 2008, 2008.*
- [27] J. Temuujin, K. Okada, K.J. MacKenzie, *Appl. Clay Sci.* 21 (2002) 125.
- [28] J. V. Smith, O.F. Tuttle, *Am. J. Sci.* 255 (1957) 282.
- [29] O. Ilgen, A.N. Akin, *Turkish J. Chem.* 33 (2009) 281.

*Magnesium Nitrate Activated
Perlite as Solid Base Catalyst for
Microwave Assisted Nitroaldol
Condensation Reaction*

Abstract

The synthesis of highly active perlite supported solid base catalyst (MTP) has been carried, with the aim of being used as heterogeneous catalyst in nitroaldol condensation reaction. The MTP catalyst was characterized for determining structural, textural and morphological properties using some analytical techniques viz. N₂ adsorption-desorption study, Thermogravimetric analysis, FTIR spectroscopy, X-ray diffraction analysis, Scanning electron microscopy, Energy dispersive X-ray analysis and Transmission electron microscopy. The basic strength of the catalyst was measured by Hammett indicator method. The catalytic activity of MTP was tested by microwave irradiated, liquid phase, single step and solvent free nitroaldol condensation of nitroethane with propionaldehyde, giving higher conversion (95%) and selectivity (97%) to desired product 1-nitro-3-pentanol. Nitroaldol condensation products 'nitroalcohols' can be converted to pharmacologically important chemicals such as chloramphenicol and ephedrine antibiotics. The nitroaldol condensation reaction was further carried out by taking nitroethane or nitromethane with number of carbonyl compounds. The MTP catalyst can be regenerated and reused up to 3 reaction cycles with almost equal efficiency. The conversion results show that the catalyst possesses sufficient stable active basic sites responsible for the catalytic activity. The work reports an innovative use of solid waste perlite as an effective solid base catalyst.

3.1 Introduction

Base catalyzed condensation and addition reactions are some of the important reaction steps employed for making large and complex molecules that characterize many of the fine chemicals and pharmaceutical products. Other reactions such as trans-esterification and isomerisation have applications, mainly in food and cosmetic industries [1].

The nitroaldol or Henry reaction is easily recognizable as one of the classical name reactions in organic synthesis. It is a coupling reaction between a carbonyl compound and an alkylnitro compound bearing a hydrogen atom. The overall transformation enables the formation of a carbon-carbon bond with the concomitant generation of a new difunctional group, namely the nitroalcohol [2]. The reaction involves the C–C bond formation, which is important in organic synthesis. The products, nitroalcohols, can be converted by hydrogenation to β -aminoalcohols, which are then converted to pharmacologically important chemicals such as chloramphenicol and ephedrine antibiotics [3]. Generally the nitroaldol reaction has been carried out in the presence of the Mg–Al hydrotalcite, diamino-functionalised MCM-41 [4], KOH, NH_4OAc [2], KF/alumina, MgO, $\text{Mg}(\text{OH})_2$, MgCO_3 , CaO, CaCO_3 , SrO, SrCO_3 , BaCO_3 , BaO, KOH/alumina [3], DABCO, Et_3N etc.[5].

Catalysts are majorly characterized as homogeneous and heterogeneous catalysts. Homogeneous bases such as alkali metal oxide, alkaline earth metal oxides, hydroxides and liquid bases are majorly used as homogeneous catalysts in organic reactions including isomerization [6], C–C bond formation, addition, cyclization, oxidation and condensation [7]. These bases are unsafe, required in more than stoichiometric amount, have high operating cost and some serious environmental issues attached with base neutralization, product separation and purification, corrosion and waste generation, thus motivate the considerable efforts towards the development of processes mediated by heterogeneous base catalysts. Replacing the homogeneous bases with heterogeneous base catalysts can lead to harmless and cleaner productions. Side reactions that include self-condensation and polymerization are suppressed by using heterogeneous catalyst resulting in better selectivity and product yield [8]. The use of heterogeneous base

catalyst keeps away the complex neutralization and separation steps, needed to recover the homogeneous base catalysts from the reaction mixture [9]. The recovered solid catalysts can be easily regenerated and reused in further reaction cycles.

Microwave irradiation has got recognition in the past decade as a powerful tool for rapid and efficient synthesis of a variety of compounds because of selective absorption of microwave energy by polar molecules [10]. Microwave radiation utilizes wavelengths of 0.001 – 1 m and frequencies of 0.3 – 300 GHz [11].

Microwave-enhanced chemistry is based on the efficient heating of materials by “microwave dielectric heating” effects. This phenomenon is dependent on the ability of a specific material (solvent or reagent) to absorb microwave energy and convert it into heat. The electric component of an electromagnetic field causes heating by two main mechanisms: dipolar polarization and ionic conduction [12]. The main advantages of non conventional ‘Microwave heating’ over the conventional heating include highly accelerated rate of the reaction, reduction in reaction time with an improvement in the yield and quality of the product, superheating (temperature more than boiling point) and high heating rate. Microwave irradiations abide by the green chemistry principles, which states that a reaction should be environmentally friendly, conducted under solvent free conditions, having minimal or no by-products formations with maintaining the atom economy [13].

The present work elaborates the synthesis of magnesium nitrate activated perlite catalyst to have high basicity and catalytic activity for nitroaldol condensation reaction. As one of the main constituent of perlite is silica (72%), possesses insufficient catalytic activity, which is enhanced by treatment with $\text{Mg}(\text{NO}_3)_2$ loading and consequently generation of forsterite and enstatite phases of MgO-SiO_2 with high basicity and catalytic activity [14]. Chemical activation was performed on thermally activated perlite by precipitation method. Nitroaldol condensation between carbonyl compound and a nitroalkane compound to get nitroalcohols were taken as a test reaction for testing the catalytic activity of $\text{Mg}(\text{NO}_3)_2$ activated perlite catalyst under microwave atmosphere.

3.2 Experimental

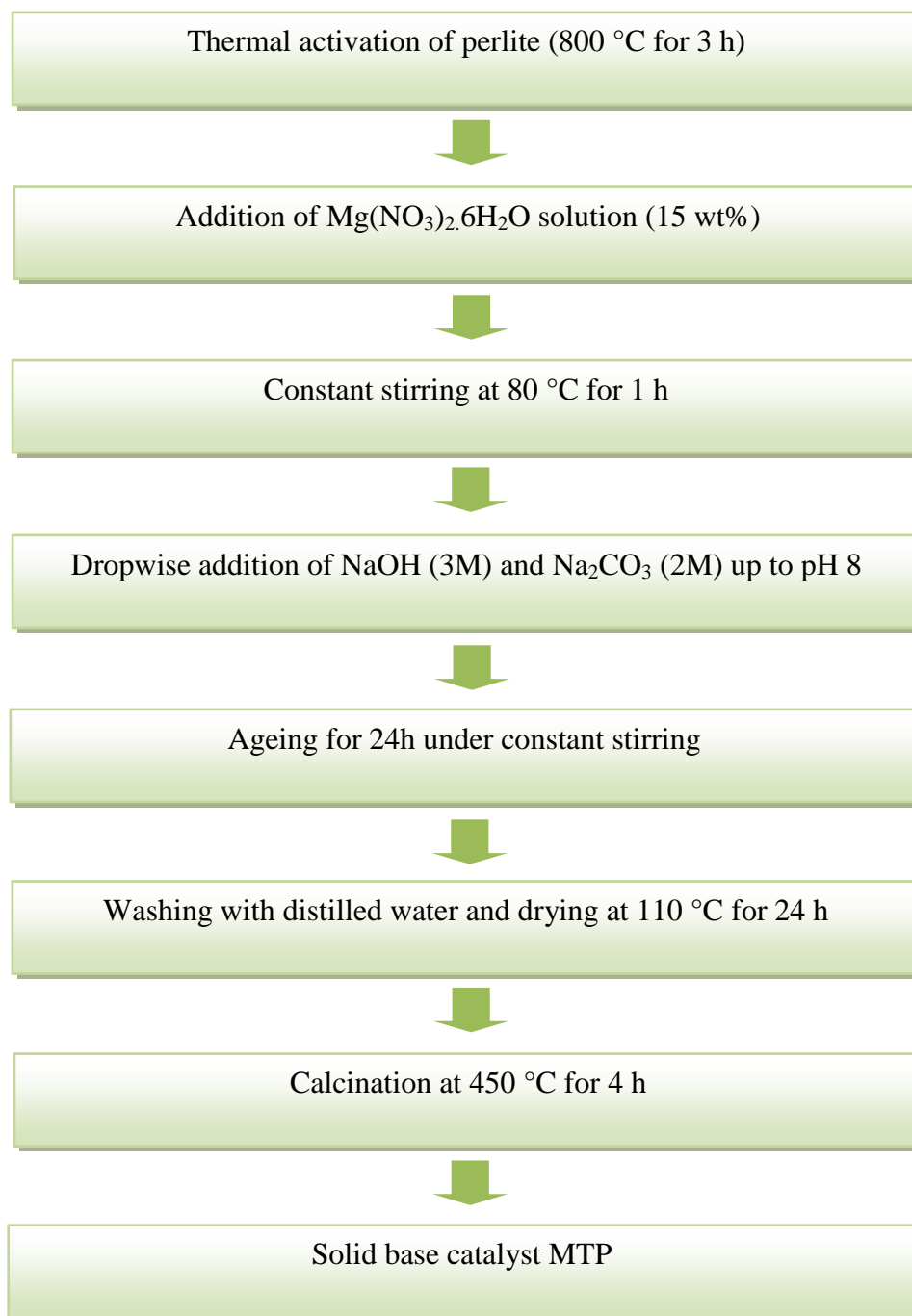
3.2.1 Materials

Perlite was collected from Indica Chemical Industries Pvt. Limited, Kotdwar (Uttarakhand). $\text{Mg}(\text{NO}_3)_2 \cdot 6\text{H}_2\text{O}$ (98%), NaOH (98%), Na_2CO_3 (99%) were purchased from Sigma Aldrich and nitroethane (98%), nitromethane (98%) and various carbonyl compounds were purchased from S.D. Fine Chemical Ltd., India. All reagents used, were of analytical grade and were used without any further purification.

3.2.2 Catalyst synthesis

As received perlite (P) was thermally activated at 800 °C for 3 h to form thermally activated perlite (TP) consequently C, S, moisture and other impurities also get removed [15].

Solid base catalyst $\text{Mg}(\text{NO}_3)_2 \cdot 6\text{H}_2\text{O}$ activated TP (MTP) was prepared by dropwise addition of an aqueous solution of $\text{Mg}(\text{NO}_3)_2 \cdot 6\text{H}_2\text{O}$ (15 wt%) into TP, at constant stirring. The resulted slurry was aged at 80 °C temperature for 1 h followed by drop wise addition of a mixed solution of NaOH (3M) and Na_2CO_3 (2M) (in 1:1 ratio) up to pH 8, resulted slurry was again aged for 24 h then washed with double distilled water, dried at 110 °C for 24 h and then calcined at 450 °C for 4 h at controlled heating rate under inert conditions to form MTP solid base catalyst. Pure MgO was synthesized by adopting similar synthetic procedure without involving TP (**Scheme 3.1**).



Scheme 3.1: Synthesis of solid base catalyst MTP.

3.3 Catalyst characterization

P, TP and synthesized catalyst MTP were characterized by N₂ adsorption-desorption study, TGA, FTIR, XRD, SEM and TEM. Instruments detail and operating conditions during characterization are given in **Annexure I**. Basic strength of the MTP catalyst was determined using Hammett indicators like phenolphthalein ($pK_a = 8.2$), Nile blue ($pK_a = 9.8$), 2,4,6-trinitroaniline ($pK_a = 12.2$), 2,4-dinitroaniline ($pK_a = 15$) and 4-nitroaniline ($pK_a = 18.4$). Basicity was measured by benzoic acid titration method using phenolphthalein indicator [16]. The methods for evaluating basic strength and basicity are given in detail in **Chapter 2**.

3.4 Experimental setup

The microwave reaction was carried out in CEM Focused Microwave™ Synthesis System, Model Discover (**Figure 3.1**). The system is designed to enhance the ability to perform chemical reactions under controlled conditions on a laboratory scale. The System facilitates either homogeneous or heterogeneous solution phase chemistry, solid phase chemistry or chemistry conducted on solid supports. It accommodates vessels ranging in volume from 5 mL to 125 mL for reactions performed under atmospheric conditions and a 10 mL vessel with septa for reactions performed at elevated temperatures and pressures. Primary uses of the Discover are in the discovery and optimization phases of the new product development process. The Discover system consists of microwave power delivery system with operator selectable power output from 0 - 300 watts, operational temperature range from 25 - 250 °C and operational pressure range from 0 – 300 psi (0 – 21 bar).

Microwave energy is applied to the vessel contents (reactants, catalysts, salts, solvents and solid supports) to accelerate the chemical reaction. The microwave absorption properties of some liquid and solid materials, due to their polar and ionic characteristics, have the capability to significantly enhance chemical reactions relative to traditional energy application (heating) techniques. The microwave interaction properties with the reactants, intermediates, catalysts, solid supports and salts provide unique opportunities for the synthetic chemist.



Figure 3.1: CEM Discover microwave synthesizer.

The CEM Discover model is a single mode cavity instrument, having a sample cavity possessing multiple entry points for the microwave energy to enter the cavity (**Figure 3.2**).

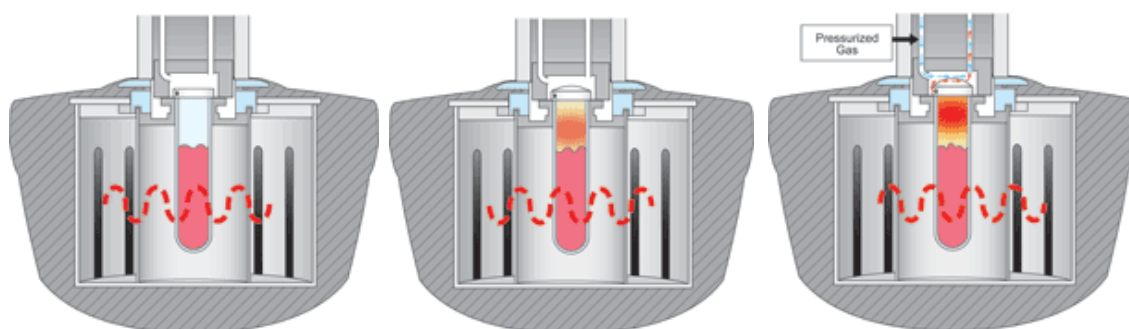


Figure 3.2: Cutaway view of sample cavity with multiple entry points for microwave energy.

The microwave synthesizer possesses Intellivent pressure control system to control the pressure during reaction (**Figure 3.3**). This pressure control system consists of a load cell to enable pressure measurement and control of the reaction environment that senses changes in the external deflection of the septa on top of the sealed pressure vial. The sensor housing incorporates a capture and release mechanism that secures the reaction vessel in the cavity.

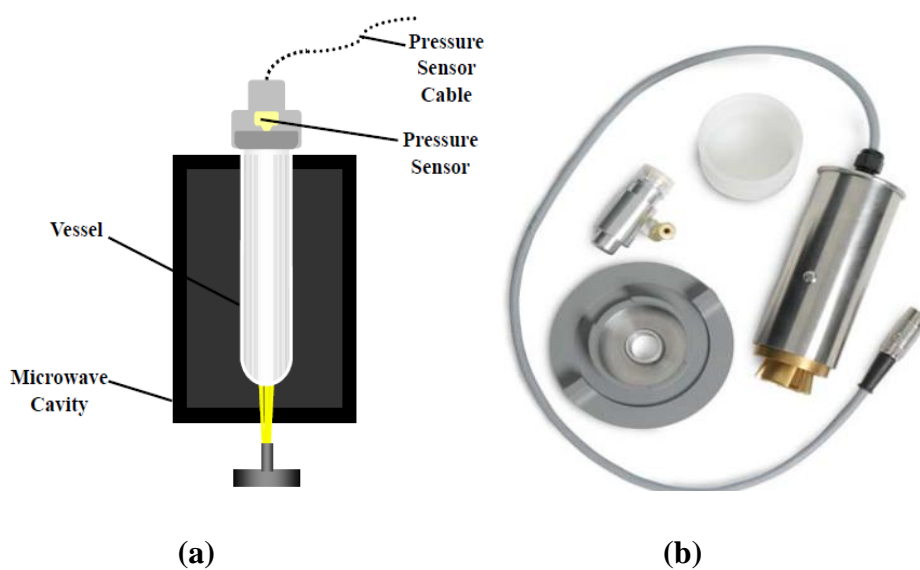


Figure 3.3: (a) IntelliVent pressure sensor assembly (b) Cutaway view of IntelliVent pressure sensor.

The standard infrared temperature control system for the microwave synthesizer consists of a non-contact infrared sensor which monitors and controls the temperature conditions of the reaction vessel located in the instrument cavity (**Figure 3.4**). The temperature sensor is centrally located beneath the cavity floor and “looks” up at the bottom of the vessel. A lens is positioned between the sensor and the cavity floor to protect the sensor.

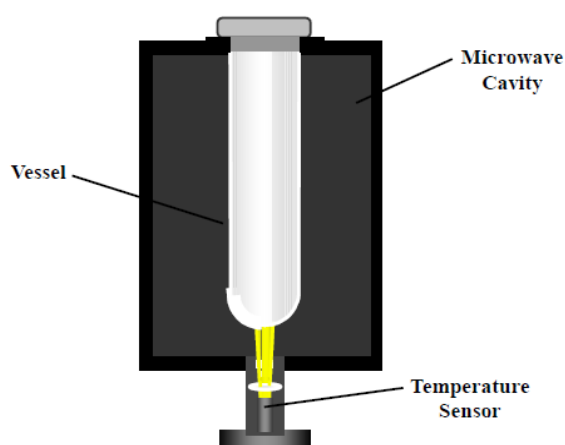


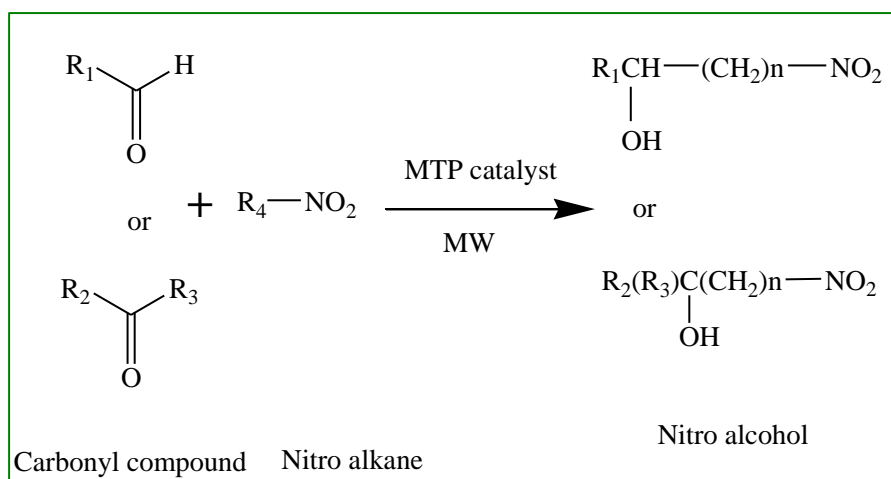
Figure 3.4: Cutaway view of infrared temperature sensor.

3.4.1 Working methodology

To run a microwave reaction, a specific method including all the conditions during the reaction like temperature, hold time, pressure and power according to reaction requirement, was prepared (**Figure 3.5**). Reaction mixture, activated catalyst and magnetic bar were taken in a glass vial (10 mL capacity) then sealed with a septum and put into the microwave cavity where the vial was again sealed with pressure lock then the vial was microwave irradiated by pushing the start key after selecting the required parameters of time, temperature, pressure and power. After the completion of the reaction (as monitored by TLC) the time v/s temperature/power/pressure were recorded on the monitor using synergy software. The catalyst was filtered out and the product was analyzed by Gas Chromatograph to know the conversion %. The experiments for optimization of various reaction parameters and conditions were performed by adopting the similar procedure.

3.5 Catalytic activity of MTP catalyst

The catalytic activity of the MTP was tested by the nitroaldol condensation reaction of carbonyl compound with nitroalkane in solvent-free, liquid phase reaction conditions, under microwave irradiation as shown in **Scheme 3.2**.



Scheme 3.2: Nitroaldol condensation of nitroalkane with carbonyl compound over MTP.

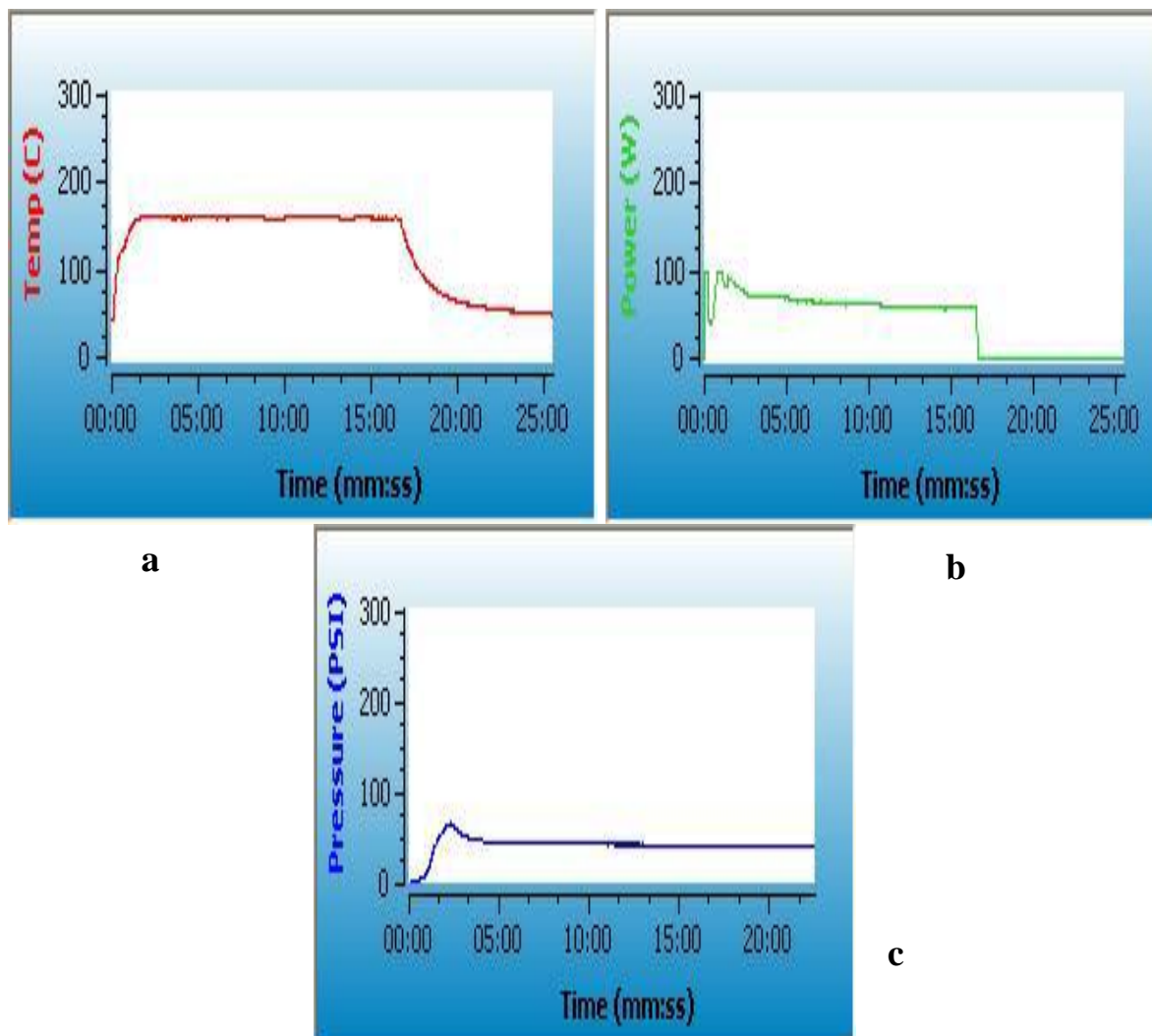


Figure 3.5: Reaction controlling parameters graphs generated by microwave synthesizer (a) Temperature v/s time (b) Power v/s time (c) Pressure v/s time.

3.5.1 Reaction procedure: Nitroaldol condensation

For nitroaldol condensation, a mixture of nitroalkane and carbonyl compound in 2:1 to 1:3 molar ratios was taken in presence of MTP catalyst (preheated at 450 °C for 2 h) in a glass vial (capacity 10 mL) with magnetic stirring. The vial was sealed with a septum and placed into the microwave cavity where it was again sealed with a pressure lock and microwave irradiated in a CEM Focused Microwave™ Synthesis System, model Discover. The reaction was carried out at different molar ratio of substrate having various substrates to

catalyst weight ratio ranging from 10:1 to 2.5:1 at different temperatures in the range of 40–100 °C. The reaction mixture was treated with microwaves for time ranging from 5 to 30 minutes, at power ~ 70 W and pressure 50 Psi. The reaction was monitored by thin layer chromatography, stopped after completion of the reaction and cooled to room temperature. After completion of the reaction the catalyst was filtered and the product was analyzed by Gas Chromatograph.

The conversion and selectivity were calculated as follows:

$$\text{Conversion (wt \%)} = 100 \times (\text{Initial wt\%} - \text{Final wt\%}) / \text{Initial wt\%}$$

$$\text{Selectivity of product (wt\%)} = 100 \times \frac{\text{GC peak area \% of nitro alcohol}}{\text{Total GC peak area \% for all the products}}$$

3.6 Catalyst regeneration

The used catalyst was washed thoroughly with acetone and dried in oven at 110 °C for 12 h, thermally activated at 450 °C for 2 h before reuse in next reaction cycle under similar reaction conditions as in the first reaction cycle.

3.7 Results and discussion

3.7.1 Chemical composition of P and MTP catalyst

The chemical compositions of as P and MTP as determined by SEM – EDX, are given in **Table 3.1**. Loss on ignition (LOI) was found to be 4.1 wt%, by heating a certain weighed quantity of perlite in muffle furnace at 800 °C for 3 h. LOI would also correspond to the burning of carbonaceous materials and volatilization of some trace metal oxides present in P and MTP catalyst [15]. In P, negligible amount of Mg is present, while the increased amount of Mg incorporated in the catalyst was found to be 5.15%, while Si and Al percentage is slightly decreased, as evaluated by SEM– EDX. The increase in Mg is responsible for various MgO-SiO₂ phases in MTP catalyst resulting in increased basicity and catalytic activity for condensation reaction.

Table 3.1: Chemical composition of P and MTP.

Elements	P (Wt%)	KATP (Wt%)
O	73.70	71.97
Si	18.83	17.62
Al	3.72	2.12
K	1.44	1.26
Na	1.61	1.47
Mg	0.21	5.15
Ca	0.19	0.13
Fe	0.10	0.10
Zn	0.13	0.11
Ti	0.07	0.07

3.7.2 Surface area results

Specific surface area of P is slightly decreased on thermal and chemical activation and reaches 2.3 m²/g to 1.7 m²/g for MTP (**Table 3.2**). The slight decrease in surface area could be assigned to the blockage of the small pores of P surface by loading various Mg species. Mg may load on TP surface in various forms like MgCO₃, Mg(OH)₂, MgO and Mg-SiO₂. It seems that an increase in the amount of these Mg forms contribute to the blockage of mesopores of small diameter and making them unapproachable for N₂ molecules [17]. In MTP catalyst, decrease in the surface area results in increased surface active catalytic sites (-OH groups), responsible for the high catalytic activity.

Table 3.2: Surface area of P and MTP.

Catalyst	Specific surface area (m ² /g)
P	2.3
MTP	1.7

3.7.3 Thermogravimetric analysis

TGA profiles of P and MTP catalyst are given in **Figure 3.6**. The TGA curve of P shows 4.3% weight loss within the temperature range 50-400 °C, indicates the removal of moisture content and some volatile materials [18]. The TGA curve of as prepared MTP (uncalcined), shows weight loss of 8% within the temperature range 0-1000 °C. It can be concluded that precursor $\text{Mg}(\text{NO}_3)_2 \cdot 6\text{H}_2\text{O}$, during the catalyst preparation converts into $\text{Mg}(\text{OH})_2$ and MgCO_3 . The weight loss in temperature range 270 – 370 °C and 400 – 550 °C are assigned to decomposition of $\text{Mg}(\text{OH})_2$ and MgCO_3 respectively [19] as well as burning of carbonaceous materials and volatilization of some trace metal oxides present in as prepared MTP catalyst.

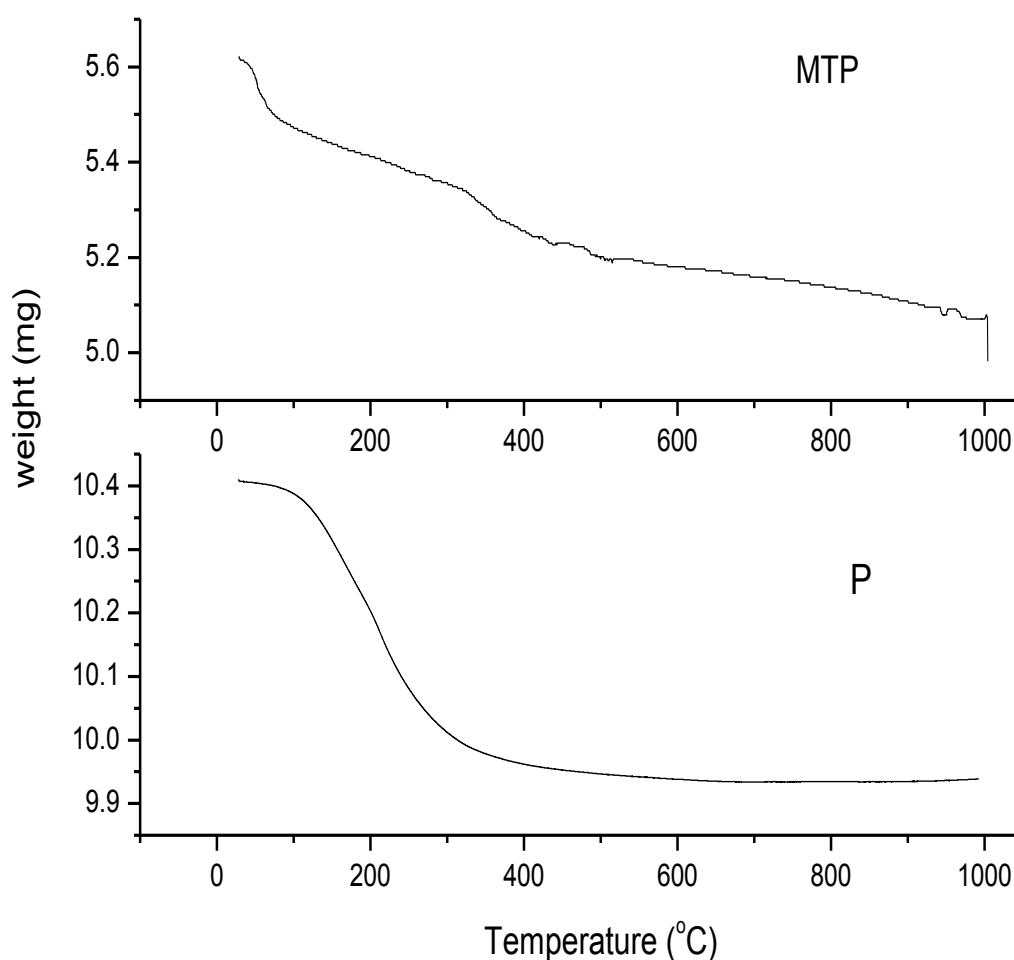


Figure 3.6: TGA curves of P and MTP.

3.7.4 FTIR studies

Silica is the major component of perlite, which is totally roofed by hydroxyl groups and physically adsorbed water. Physically adsorbed water is removed on thermal activation resulting in the formation of surface siloxane bridges on silica surface [20] which helps in increasing surface hydroxyl groups on further chemical activation and hence increases surface basicity and catalytic activity of the material. Each FTIR spectrum (**Figure 3.7**) shows a broad band between 3600-3200 cm^{-1} , which is attributed to $-\text{OH}$ species of surface silanol groups ($-\text{Si}-\text{OH}$) and adsorbed water molecules on the surface [21]. Strong hydrogen bonding between $-\text{OH}$ species is responsible for the broadness of this band [22]. Intensity and broadness reduce in case of TP (**Figure 3.7b**) confirming the loss of water in perlite during thermal activation, which again increases in case of MTP, probably due to increased $-\text{Si}-\text{O}-\text{Mg}-\text{OH}$ groups on TP surface.

All spectra (**Figure 3.7**) show a peak around 1630 cm^{-1} attributed to bending mode ($\delta_{\text{O-H}}$) of water molecules [23]. A small band centered at 1521 cm^{-1} present in MTP and reused MTP, is due to $(\text{CO}_3)^{2-}$ stretching vibration of MgCO_3 and show an agreement with the TGA result [24].

Amorphous silica is the major component of perlite, which is normally assumed to be formed by a continuous network of Q^4 units $[\text{Si}(\text{SiO}_4)_4]$ [25], gives broad band in the range of 1100-1040 cm^{-1} due to $\text{Si}-\text{O}-\text{Si}$ asymmetric stretching vibration modes (**Figure 3.7a**) [26]. The increased $-\text{OH}$ species in case of MTP in the form of $-\text{Si}-\text{OH}$ and $-\text{Si}-\text{O}-\text{Mg}-\text{OH}$ groups (**Figure 3.7c**), shift the position of $\text{Si}-\text{O}-\text{Si}$ band towards lower wave number indicating the transformation of amorphous silica Q^4 units $[\text{Si}(\text{SiO}_4)_4]$ to Q^3 units $[\text{Si}(\text{OH})(\text{SiO}_4)_3]$ [25]. Band appearing at 797 cm^{-1} in P due to symmetric $\text{Si}-\text{O}-\text{Si}$ stretching vibration [7] gets shifted towards lower wave number in MTP (**Figure 3.7c and Table 3.3**) at 792 cm^{-1} could be an evidence for increased silanol groups on MTP surface. A small peak at 572 cm^{-1} is due to the stretching vibration of $\text{Si}-\text{O}-\text{Al}$ group [23].

Band due to $-\text{OH}$ stretching vibration is appeared between 3600-3200 cm^{-1} , is least broad in case of TP (**Figure 3.7b**) representing the lesser number of $\text{Si}-\text{OH}$ groups on the catalyst surface. This band is broader and sharper in case of

MTP (Figure 3.7c) due to –Si–O–Mg–OH groups and hydrogen bonding among hydroxyl groups.

Table 3.3: The observed transmission frequencies (cm^{-1}) of FTIR spectra of P, TP, MTP and reused MTP and their assignments.

Peak Assignments	P	TP	MTP	Reused MTP	Ref.
Si-O-Al stretching vib.	572	572	572	595	23
Si-O-Si Symm. stretching vib.	797	794	792	795	7
Si-O-Si asymm. stretching vib.	1054	1059	1013	1022	26
(CO₃)²⁻ – stretching vibration	-	-	1521	1522	24
H-O-H bending mode	1626	1630	1635	1634	23
-O-H stretching vib.	3632	3598	3594	3669	21

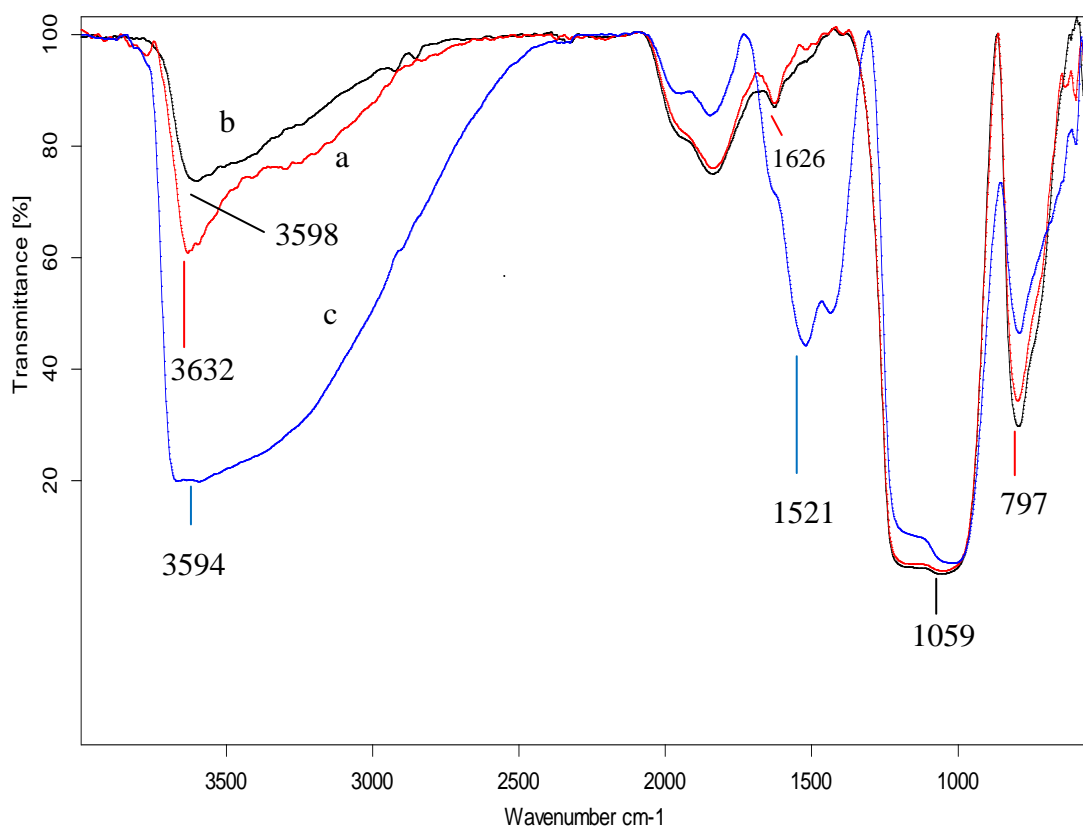


Figure 3.7: FTIR spectra of (a) P, (b) TP and (d) MTP.

3.7.5 X-ray diffraction studies

The XRD diffraction patterns for P, TP, Pure MgO and MTP are displayed in **Figure 3.8**. The analysis was carried out to study the effect of activation on perlite surface. The XRD pattern of perlite in **Figure 3.8a** depicts its purely amorphous nature of silica while after thermal activation at 800 °C for 3 h, a small peak is observed at $2\theta = 26.7^\circ$ (**Figure 3.8b**) corresponding to the crystalline phase of quartz [27]. The XRD pattern of pure MgO (**Figure 3.8c**) shows diffraction peaks at $2\theta = 36^\circ, 42^\circ, 62^\circ$ [28]. All of the diffraction peaks can be indexed as the known periclase (MgO) structure (JCPDS 87-0653) [28]. The XRD pattern of MTP catalyst shows new small broad humps at around $2\theta = 36^\circ, 42^\circ, 61^\circ$ which could be assigned to forsterite (Mg_2SiO_4) (JCPDS data file No. 34-0189) and enstatite (MgSiO_3) (JCPDS data file No. 11-0273) [29] mineral phases which confirms the effective functionalization of amorphous silica with MgO loading (**Figure 3.8d**).

3.7.6 SEM analysis results

The surface morphology of the P, TP and MTP as examined using SEM technique, is shown in **Figure 3.9** which demonstrate particles of different sizes, having irregular faces in all materials. MTP shows shiny agglomerated areas on TP particles due to loaded MgO as well as due to newly formed phases like enstatite and forsterite [29].

3.7.7 TEM analysis studies

TEM images of P and MTP catalyst are given in **Figure 3.10**. SAED pattern of MTP shows diffuse rings, which indicates amorphous structure of MTP catalyst (**Figure 3.10c**). Bright field micrographs of MTP catalyst (**Figure 3.10d-f**) show dark spots on the TP surface which represents the loading of Mg species in various forms on TP surface.

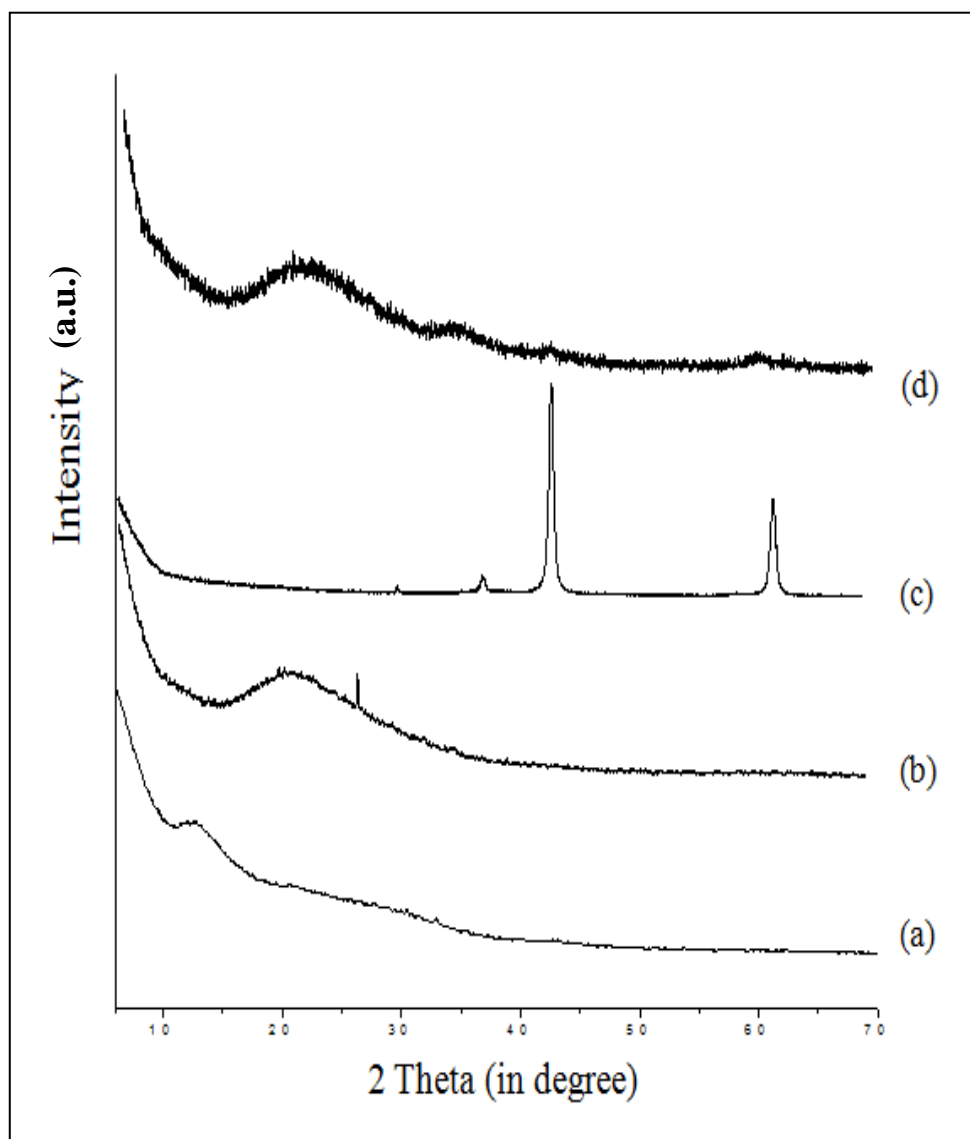


Figure 3.8: X-ray diffraction patterns of a) P, (b) TP, (c) Pure MgO and (d) MTP.

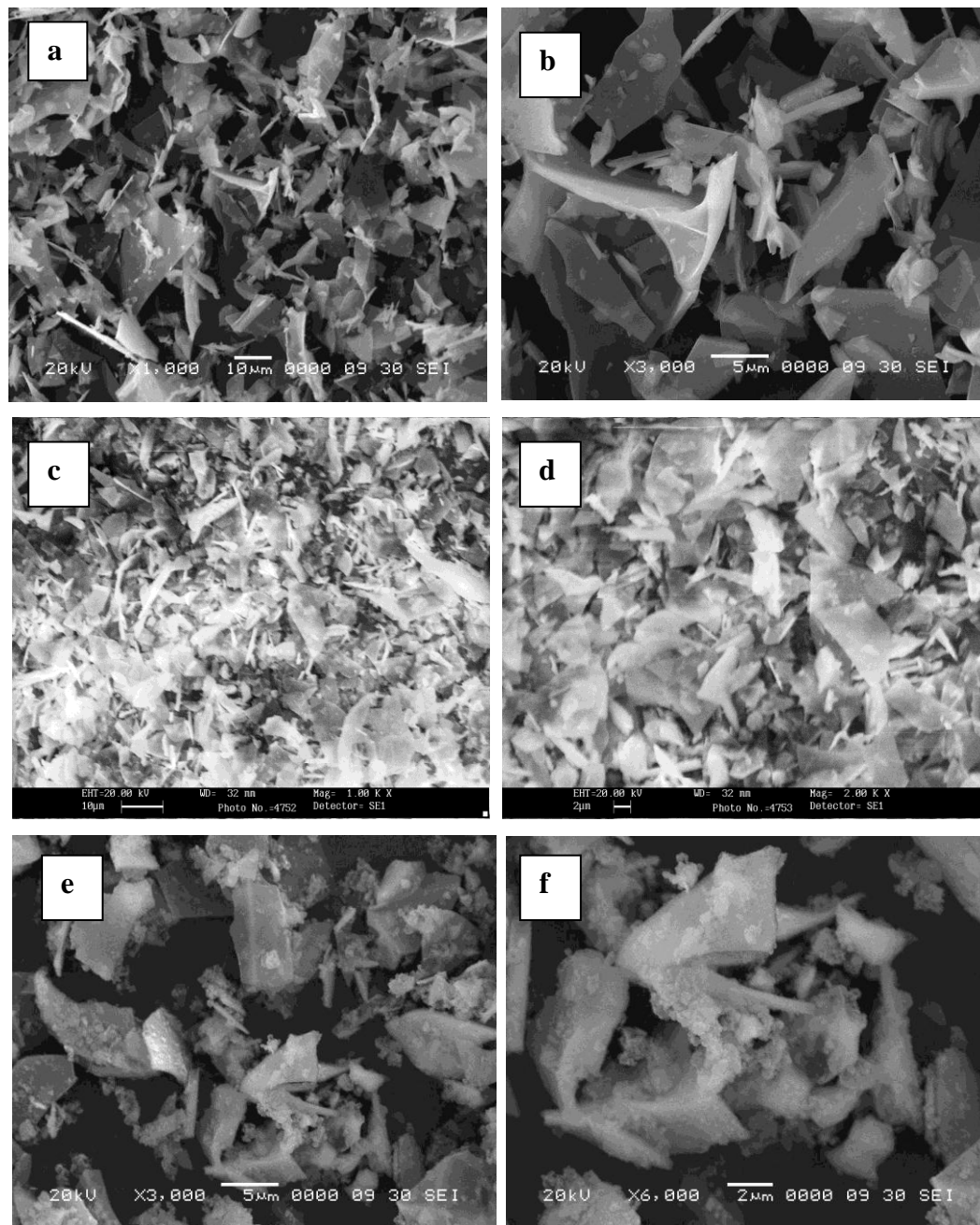


Figure 3.9: SEM micrographs of (a) P, (b) P (magnified), (c) TP, (d) TP (magnified), (e) MTP and (f) MTP (magnified).

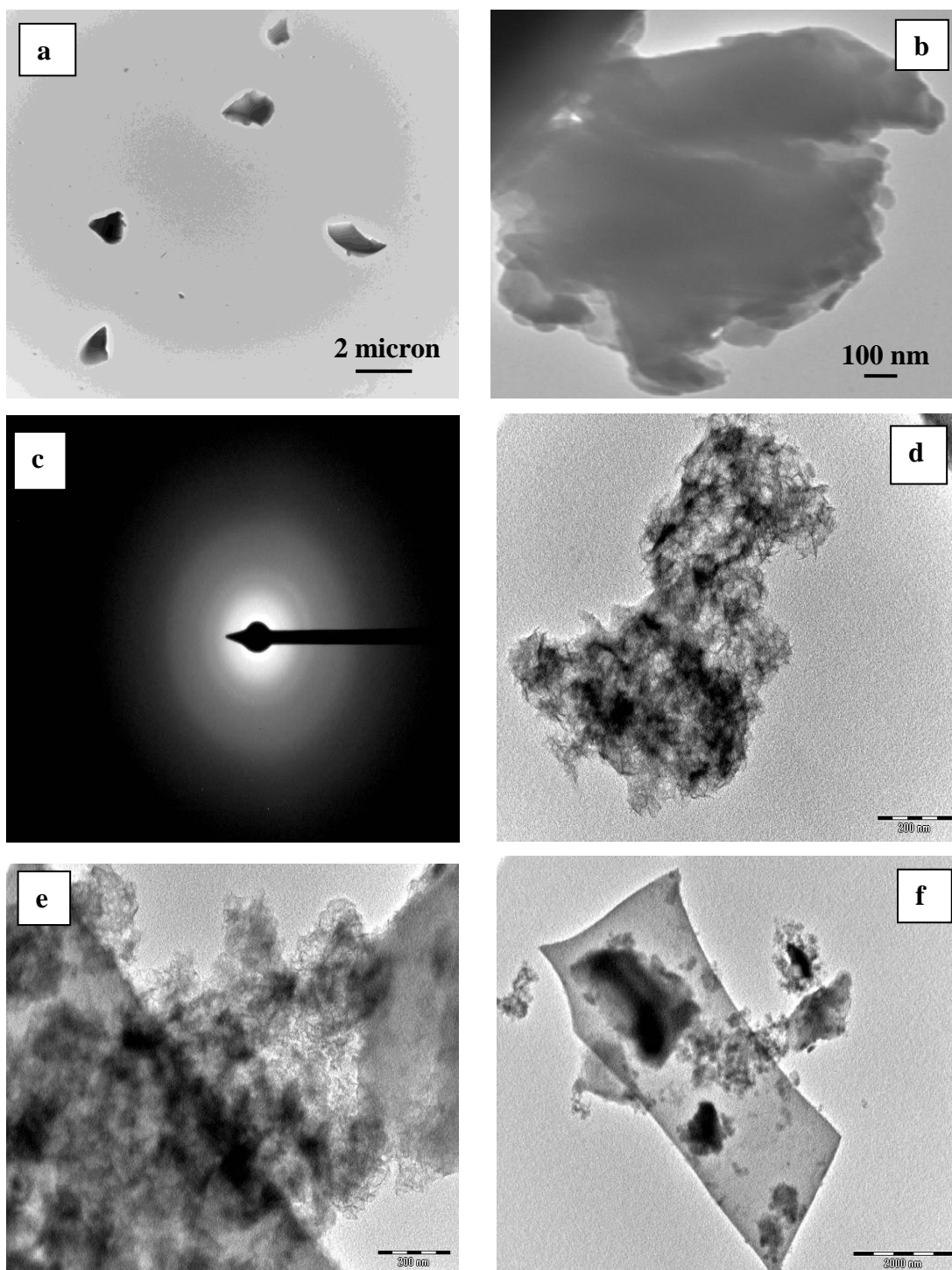


Figure 3.10: TEM images of (a-b) P, (c) SAED pattern of MTP and (d-f) bright field micrograph of MTP in the range 2000 nm to 200 nm scales.

3.7.8 Basic strength and basicity measurement

The basic strength of the MTP catalyst was determined by using Hammett indicators and found to be $15 > H_{-} > 9.8$. The total basicity was determined by benzoic acid titration method and found to be 1.02 mmol/g.

3.8 Catalytic activity

The catalytic activity of MTP catalyst was measured by a single step, liquid phase, solvent free and microwave irradiated nitroaldol condensation reaction of propionaldehyde with nitroethane under optimized reaction conditions. Results given in **Table 3.4** show that both perlite (P) and thermally activated perlite (TP) do not possess any catalytic activity for studied reaction. MTP catalyst under the given conditions, showed maximum activity. Parameters such as reactant molar ratio, amount of catalyst, reaction time and temperature were optimized in order to achieve the maximum catalytic activity and good conversion and selectivity of desired product.

Table 3.4: Catalytic activity of P, TP and MTP for nitroaldol condensation reaction of nitroethane with propionaldehyde.

Catalyst	Conversion (%) of nitroethane	Selectivity (%) for 1-nitro-3-pentanol
P	Nil	Nil
TP	Nil	Nil
MTP	78	82

Reaction conditions: Temperature 80 °C, Time 15 minute, nitroethane/propionaldehyde molar ratio 1:1, substrate/catalyst weight ratio 5:1.

3.8.1 Effect of reaction time

In order to find the reaction time to get highest conversion and selectivity over MTP catalyst, the reaction was carried out at 80 °C for different time intervals ranging from 5 minutes to 30 minutes taking nitroethane/propionaldehyde molar ratio 1:1 and nitroethane to catalyst weight ratio 5:1. It was found that in first 15 minutes of the reaction period the

conversion and selectivity increase linearly up to 95% and 97% respectively which remained constant upto 30 minutes (**Figure 3.11**). The optimized reaction time was found to be 15 minutes, in which MTP catalyst gave highest conversion 95% of nitroethane to 1-nitro-3-pentanol with 97% selectivity.

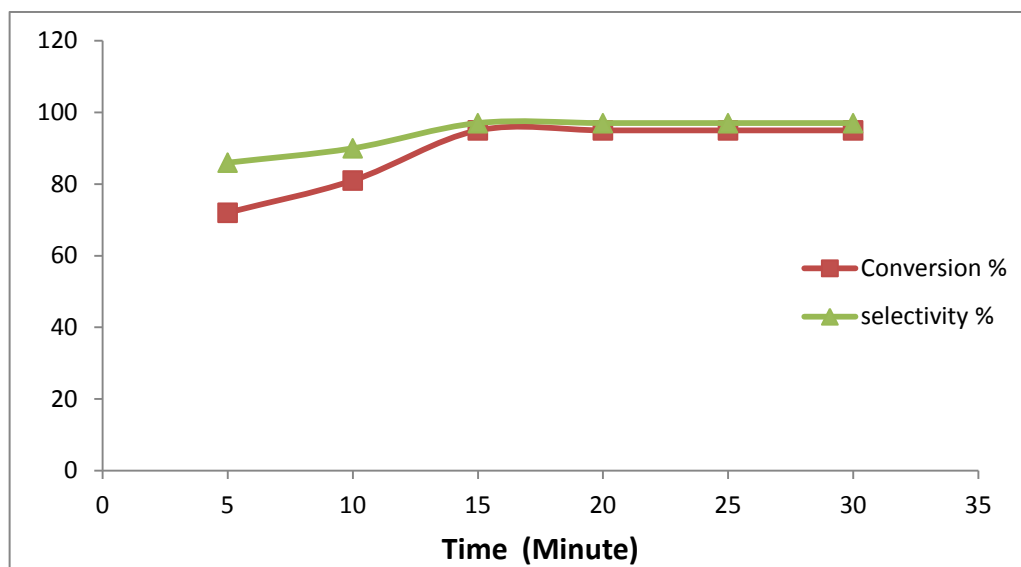


Figure 3.11: Variation in conversion (%) of nitroethane and selectivity (%) for 1-nitro-3-pentanol with time.

Reaction conditions: Temperature 80 °C, nitroethane/propionaldehyde molar ratio 1:1, substrate/catalyst weight ratio 5:1.

3.8.2 Effect of reaction temperature

Optimization of reaction temperature to give maximum conversion and selectivity was carried out at temperature ranging from 40 °C to 100 °C for 15 minutes taking nitroethane/propionaldehyde molar ratio of 1:1 while substrate to catalyst weight ratio was 5:1. Conversion and selectivity were observed to increase on increasing reaction temperature ranging from 40 °C to 80 °C as inferred from **Figure 3.12**. The results show that the maximum conversion (95%) of nitroethane and selectivity (97%) for 1-nitro-3-pentanol was found at 80 °C, after which conversion and selectivity remain almost steady till 100 °C.

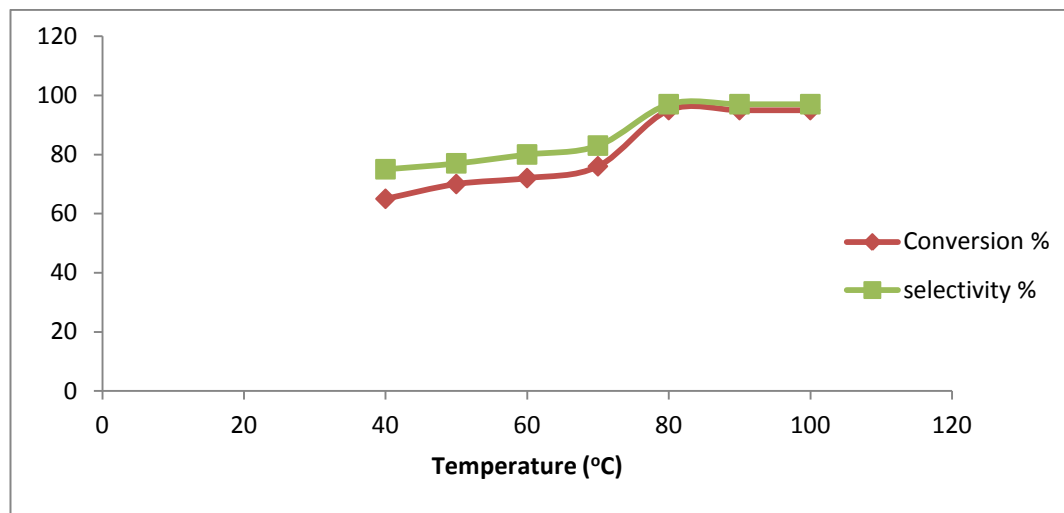


Figure 3.12: Variation in conversion (%) of nitroethane and selectivity (%) for 1-nitro-3-pentanol with temperature.

Reaction conditions: Time 15 minute, nitroethane/propionaldehyde molar ratio 1:1, substrate/catalyst weight ratio 5:1.

3.8.3 Effect of substrate/catalyst weight ratio

The influence of substrate to catalyst weight ratio on conversion and selectivity were investigated by varying the amount of MTP catalyst under optimized reaction conditions. It can be seen from **Table 3.5**, only 71% conversion of nitroethane is achieved at nitroethane/MTP weight ratio 10:1. On increasing nitroethane/MTP weight ratio to 5:1, conversion of nitroethane is increased up to 95% while selectivity for 1-nitro-3-pentanol is increased up to 97%. The increase in selectivity and conversion, with increase in the catalyst weight can be attributed to an increase in the availability of number of catalytic active sites required for condensation reaction. On further increase in the amount of catalyst no changes in conversion and selectivity are observed.

3.8.4 Effect of reactant molar ratio

The synthesis of 1-nitro-3-pentanol was carried out at 80 °C with various molar ratios of reactants for 15 minutes over MTP catalyst. As indicated by **Table 3.6**, 72% conversion of nitroethane was observed at 2:1 molar ratio of nitroethane to propionaldehyde. This may be due to insufficient quantity of the reactants to

react with each other. There was an increase in conversion up to 95% with selectivity 97% at 1:1 molar ratio of nitroethane to propionaldehyde at the same reaction conditions. This may be due to equilibrating of each reactant quantity on the basic sites of the MTP catalyst surface. The conversion decreased from 82% to 75% on further increasing the molar ratio from 1:2 to 1:3 which could be attributed to the self aldol addition reaction of the excessively present propionaldehyde.

Table 3.5: Effect of substrate/catalyst weight ratio on conversion (%) of nitroethane and selectivity (%) for 1-nitro-3-pentanol over MTP.

nitroethane /MTP weight ratio	Conversion (%) of nitroethane	Selectivity (%) for 1-nitro-3-pentanol
10:1	71	74
5:1	95	97
2.5:1	95	97

Reaction conditions: Temperature 80 °C, Time 15 minutes, nitroethane/propionaldehyde molar ratio 1:1.

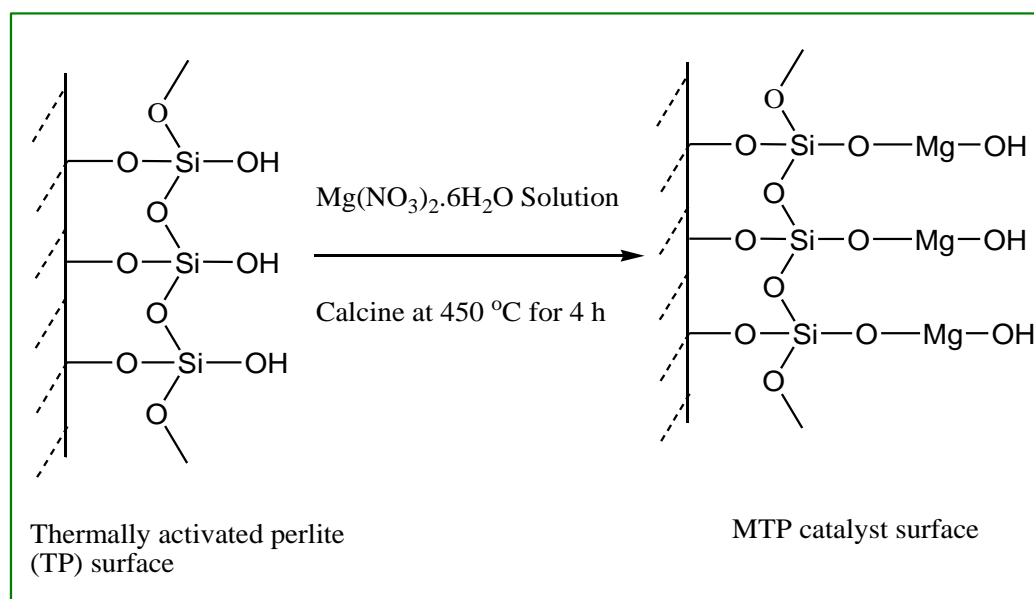
3.9 Reaction mechanism

The plausible structure for active basic sites of the MTP catalyst is shown in (Scheme 3.3). The reaction mechanism over MTP catalyst shows (Scheme 3.4) that the surface basic sites (hydroxyl groups) of the MTP catalyst initiate the reaction by abstracting the proton from nitroethane, resulting in the formation of carbanion. The formed nitroethanion again attack on the electron deficient carbon atom of the carbonyl group of propionaldehyde with loss of water and form condensation product by simple nucleophilic addition reaction.

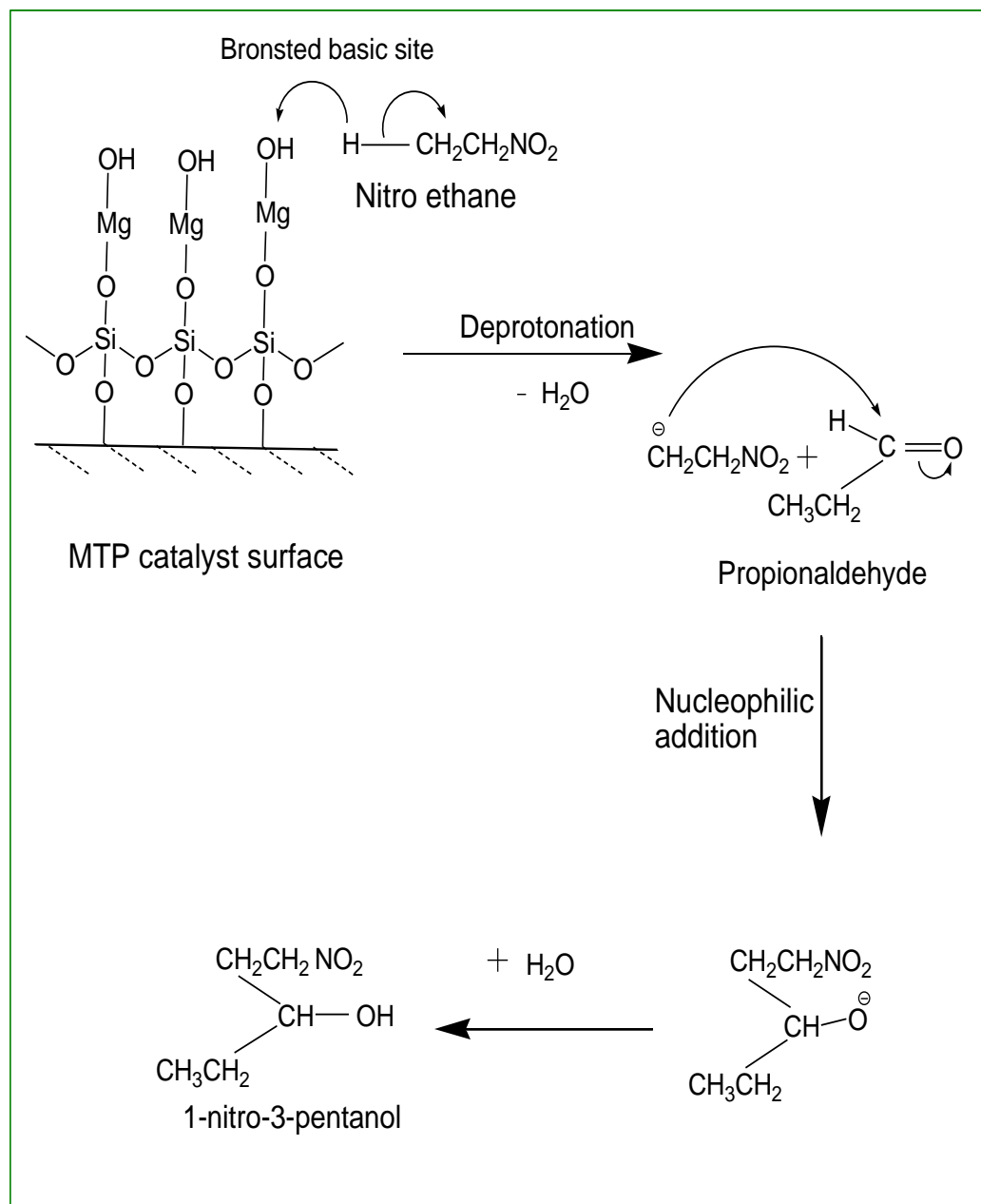
Table 3.6: Effect of molar ratio of nitroethane/propionaldehyde on conversion (%) of nitroethane and selectivity (%) for 1-nitro-3-pentanol over MTP.

Molar ratio	Conversion (%) of nitroethane	Selectivity (%) for 1-nitro-3-pentanol
2:1	72	93
1:1	95	97
1:2	82	90
1:3	75	89

Reaction conditions: Temperature 80 °C, Time 15 minutes, substrate/catalyst weight ratio 5:1.



Scheme 3.3: The schematic presentation of chemical activation of perlite with $\text{Mg}(\text{NO}_3)_2 \cdot 6\text{H}_2\text{O}$ and proposed structure of MTP.



Scheme 3.4: Proposed mechanism for Nitroaldol condensation of nitroethane and propionaldehyde over MTP.

3.10 Catalyst regeneration

The spent catalyst was filtered out from the reaction mixture, washed with acetone, dried in oven at 110 °C for 12 h followed by thermal activation at 450 °C for 2 h under static condition. The regenerated MTP catalyst was reused in the next reaction cycles under similar reaction conditions as to first reaction cycle. The FTIR spectrum of reused MTP catalyst after four reaction cycles (**Figure 3.13b**) matches with the fresh MTP catalyst (**Figure 3.13a**). The catalyst was found to be equally efficient up to four reaction cycles, giving an approximately similar conversion and selectivity for 1-nitro-3-pentanol (**Table 3.7**). During the course of the reaction, the catalyst loses its catalytic activity due to the deposition of organic molecules on the catalyst surface. The possibility of organic molecules, entering the interstices of the catalyst cannot be ruled out, which is confirmed by the successively quite decreased conversion % after regeneration, leading to deactivation of the catalyst [30].

Table 3.7: Nitroaldol condensation of nitroethane and propionaldehyde over fresh and regenerated MTP.

Reaction cycle	Conversion % of nitroethane	Selectivity % for 1-nitro-3-pentanol
I	95	97
II	89	92
III	86	92
IV	80	85

Reaction conditions: Temperature 80 °C, Time 15 minute, nitroethane/propionaldehyde molar ratio 1:1, substrate/catalyst weight ratio 5:1.

The study of nitroaldol condensation reaction was then extended to the several substituted aromatic and nonaromatic aldehydes with nitroethane and nitromethane using the MTP catalyst through microwave irradiation. All the reactions occurred in solvent free conditions within 15 minutes at 80 °C maintaining the reactant molar ratio 1:1, substarte/catalyst weight ratio 5:1. The results are summarized in the **Table 3.8**.

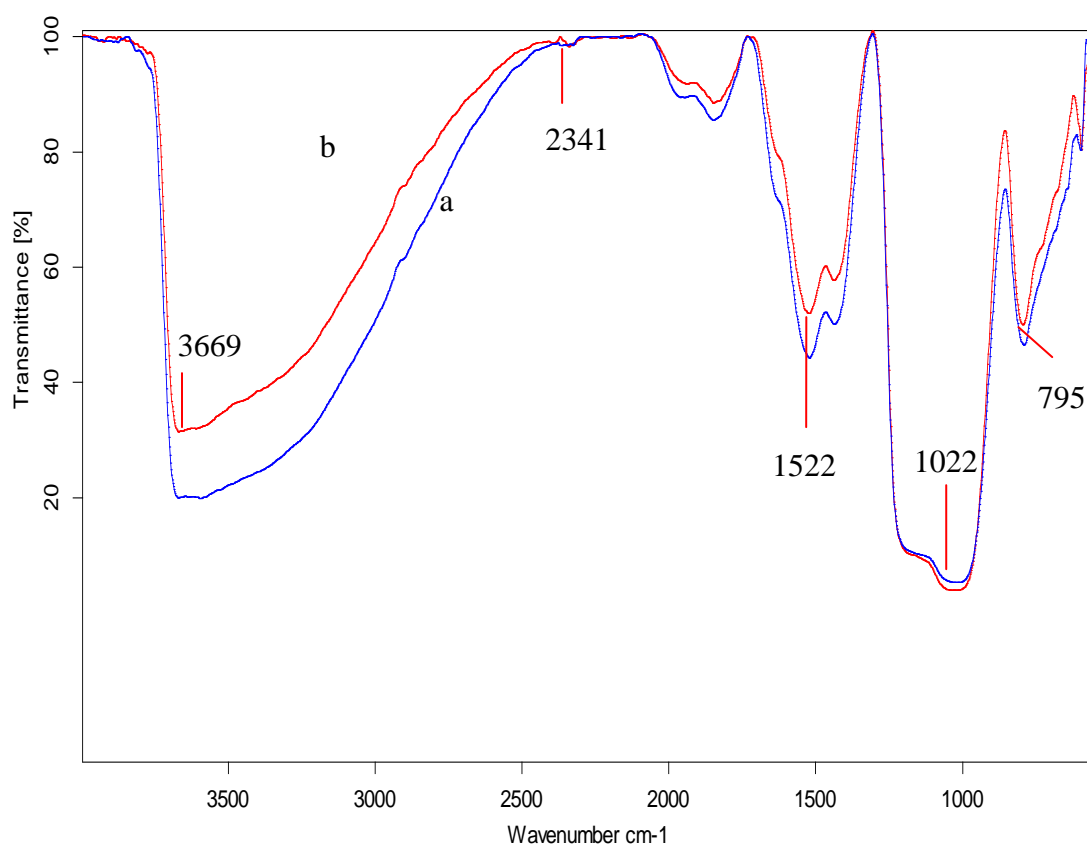


Figure 3.13: FTIR spectra of (a) MTP and (b) reused MTP.

Table 3.8: Nitroaldol condensation of nitro alkane with various aromatic and nonaromatic aldehydes in presence of MTP.

S.No.	Carbonyl compound	Nitro compound	Conversion (%)
1	Acetone	Nitromethane	46
2	Benzaldehyde	Nitromethane	39
3	Isobutyraldehyde	Nitromethane	62
4	Methylpropionate	Nitromethane	34
5	p-chlorobenzaldehyde	Nitromethane	76
6	p-nitrobenzaldehyde	Nitromethane	83
7	Acetone	Nitroethane	54
8	Benzaldehyde	Nitroethane	43
9	Isobutyraldehyde	Nitroethane	79
10	Methylpropionate	Nitroethane	32
11	p-chlorobenzaldehyde	Nitroethane	85
12	p-nitrobenzaldehyde	Nitroethane	87

Reaction conditions: Temperature 80 °C, Time 15 minutes, substrate molar ratio 1:1, substrate/catalyst weight ratio 5:1.

3.11 Conclusion

The present work provides a brief report on the catalytic application of a new solid support perlite which is least explored till now. An effective solid base catalyst has been prepared through thermal and chemical activation. The prepared MTP catalyst acts as efficient heterogeneous base catalyst for nitroaldol

condensation reaction under optimized reaction conditions with giving conversion of 95% and selectivity 97%. MTP catalyst possesses higher basicity due to increase in Bronsted basic sites i.e. Si–OH and Si-O-Mg-OH content. The reaction was carried out in solvent free conditions under microwave irradiations and the catalyst can be easily separated by simple filtration, regenerated and reused up to three times with almost equal efficiency, thus produces no waste and makes the process profitable. The efficient reuses of the catalyst confirm the stability of the surface active basic sites. This investigation brings into light an innovative application of perlite in cost effective, eco-friendly and recyclable catalyst synthesis for different important organic reactions.

3.12 References

- [1] A. Corma, S. Iborra, *Adv. Catal.* 49 (2006) 239.
- [2] F.A. Luzzio, *Tetrahedron* 57 (2001) 915.
- [3] K. Akutu, H. Kabashima, T. Seki, H. Hattori, *Appl. Catal. A Gen.* 247 (2003) 65.
- [4] B.M. Choudary, M.L. Kantam, K.K. Rao, F. Figueras, A.A. Einstein, *Green Chem.* (1999) 187.
- [5] Z.W. Changsheng Gan, Xing Chen, Guoyin Lai, *Synlett* 3 (2006) 387.
- [6] C.G. Hartung, C. Breindl, M. Beller, 56 (2000) 5157.
- [7] D. Jain, C. Khatri, A. Rani, *Fuel Process. Technol.* 91 (2010) 1015.
- [8] J. Weitkamp, M. Hunger, U. Rymsa, *Microporous Mesoporous Mater.* 48 (2001) 255.
- [9] X. Zhang, E.S.M. Lai, R. Martin-aranda, K.L. Yeung, *Appl. Catal. A Gen.* 261 (2004) 109.
- [10] K.R.D. Madhvi A. Surati, Smita Jauhari, *Sch. Res. Libr.* 4 (2012) 645.
- [11] F.K. Macdonald, K.M.M. Carneiro, I.R. Pottie, *Tetrahedron Lett.* 52 (2011) 891.
- [12] C.O. Kappe, *Angew Chem Int Edu* 43 (2004) 6250.
- [13] H.S.P. Rao, S. Jothilingam, *J. Chem. Sci* 117 (2005) 323.
- [14] F. Tavangarian, R. Emadi, *Mater. Res. Bull.* 45 (2010) 388.

- [15] K. Kordatos, S. Gavela, A. Ntziouni, K.N. Pistiolas, A. Kyritsi, V.K. Rigopoulou, *Microporous Mesoporous Mater.* 115 (2008) 189.
- [16] R. Rahul, J.K. Satyarthi, D. Srinivas, *Indian J. Chem.* 50 (2011) 1017.
- [17] H. Ma, S. Li, B. Wang, R. Wang, S. Tian, *J. Am. Oil Chem. Soc.* 85 (2008) 263.
- [18] M.M.A. Sekkina, R.M. Issa, A.E.-D.M. Bastawisy, W.A. El Helece, *Int. J. Chem.* 2 (2010) 81.
- [19] R.E.O. Neill, L. Vanoye, C. De Bellefon, F. Aiouache, "Applied Catal. B, Environ. 144 (2014) 46.
- [20] F. Adam, J. Nelson, A. Iqbal, *Catal. Today* 190 (2012) 2.
- [21] D. Jain, A. Rani, *Am. Chem. Sci. J.* 1 (2011) 37.
- [22] D. Jain, C. Khatri, A. Rani, *Fuel* 90 (2011) 2083.
- [23] S. Katara, S. Kabra, A. Sharma, R. Hada, A. Rani, *Int. Res. J. Pure Appl. Chem.* 3 (2013) 299.
- [24] H. Handa, T. Baba, H. Sugisawa, Y. Ono, *J. Mol. Catal. A Chem.* 134 (1998) 171.
- [25] M.E. Simonsen, C. Sonderby, Z. Li, E.G. Sogaard, *J. Mater. Sci.* 44 (2009) 2079.
- [26] B.J. Saikia, G. Parthasarathy, N.C. Sarmah, G.D. Baruah, *Indian Acad. Sci.* 31 (2008) 155.
- [27] A. Sharma, K. Srivastava, V. Devra, A. Rani, *Am. Chem. Sci. J.* 2 (2012) 177.
- [28] W. Wang, X. Qiao, J. Chen, H. Li, *Mater. Lett.* 61 (2007) 3218.
- [29] F. Tavangarian, R. Emadi, *J. Alloys Compd.* 485 (2009) 648.
- [30] P. Forzatti, L. Lietti, *Catal. Today* 52 (1999) 165.

*Strontium Nitrate Activated
Fly Ash: An Efficient Solid Base
Catalyst for Microwave Assisted
Michael Addition Reaction*

Abstract

Fly ash is converted into an efficient solid base catalyst: strontium nitrate activated fly ash, by treating with strontium nitrate on mechanically and thermally activated fly ash. The catalytic application of prepared catalyst was evaluated by Michael addition reaction under microwave irradiations. The synthesized catalyst was highly active for solvent free synthesis of Michael adducts through conjugate addition of 2-cyclohexenone with nitromethane or active methylene compounds. The microwave assisted synthesis resulted in increased yield of the products (92%) at a significantly lower reaction temperature (90 °C) and reaction time (15 minute) than the synthesis by thermal heating (78% yield, at 120 °C, for time range 120 minute). The physico-chemical properties of catalyst were investigated by N₂ adsorption-desorption study, TGA, FTIR, XRD, SEM-EDX and TEM analytical techniques. The basic strength was measured by Hammett indicator method. The catalyst could be easily regenerated and reused up to four reaction cycles with almost similar efficiency. The work reports an alternative pathway for utilization of waste fly ash by using it in the development of novel, cost effective and recyclable solid base catalyst for industrially important Michael addition reaction.

4.1 Introduction

Coal-fired power plants are taking a prominent part in the energy production today. These plants produce a large number of by-products during coal burning, also known as coal combustion products (CCPs) viz. fly ashes (FAs), bottom ashes (BAs), boiler slags (BS), fluidised bed combustion ashes (FBCAs), semi dry adsorption (SDA) products and flue gas desulphurisation (FGD) gypsum [1]. The physical, chemical and micro structural properties of fly ash depend on coal category viz. anthracite, bituminous and lignite as well as on combustion conditions [2]. Worldwide annual production of coal fly ash is estimated around 800 million tonnes [3], constituting about 75–80% of the total CCPs production [4]. Therefore, development of innovative methodology for utilization of this industrial waste in various value added materials has become an essential objective of the present research and development work related with fly ash management and utilization. SiO_2 and Al_2O_3 are major constituents of fly ash while Fe_2O_3 , CaO , MgO , TiO_2 , Na_2O and K_2O are present as minor constituents [5]. Fly ash has a specific surface area $\sim 17 \text{ m}^2/\text{g}$, mesoporosity $\sim 0.06 \text{ cm}^3/\text{g}$ and macroporosity $0.65 \text{ cm}^3/\text{g}$ [6]. According to ASTM Standard C 618, fly ash is divided into two categories Class F and Class C. The fly ash generally resulted from the burning of higher-rank bituminous and anthracite coals containing $>70\%$ SiO_2 , Al_2O_3 and Fe_2O_3 with low amount of calcium is classified as Class F fly ash. On the other hand, Class C fly ash contains $>50\%$ SiO_2 , Al_2O_3 and Fe_2O_3 with high amount of calcium, is mostly produced from the burning of low-rank lignite and sub-bituminous coals [4,7]. As far as bulk application of fly ash is concerned, besides concrete industry, there are a number of uses and utilization areas of fly ash such as structural fill, waste solidification and stabilization, roadway and pavement utilization, metallurgy and valuable metal extraction, agriculture, environmental engineering and adsorption of heavy metals and dye from industrial effluents [4]. Studies report that being aluminosilicate rich material fly ash can be used as an alternative silica source in synthetic organic chemistry.

Among the well known solid base catalysts, SrO has been reported as an active heterogeneous base transesterification catalyst due to its high basicity and

insolubility in methanol, vegetable oil and FAMEs [8]. The Strontium based catalysts can be divided into 6 categories such as neat **1.** SrO [9], **2.** Strontium salts eg. SrCO₃, Sr(OH)₂.8H₂O [10], Sr(NO₃)₂, SrSO₄, SrCl₂ [11], **3.** Doped SrO eg. strontium doped silica supported silver catalyst [(x)SrO Ag(y)/SiO₂] [12], Sr(NO₃)₂ doped ZnO [13], **4.** Mixed oxides nanocomposite eg. Sr₃Al₂O₆, **5.** Thin films eg. barium strontium titanate thin films [14], **6.** Supported catalysts eg. Sr(NO₃)₂/γ-Al₂O₃, Sr(NO₃)₂/ZrO₂ [13], SrO/MgO [15], SrO/Carbon nano fiber [16], SrO/SiO₂, SrO/CaO [17], Sr-Co/Al₂O₃, Sr/FeSi [18].

Commercially the base catalyzed reactions are largely carried out in fine chemical, petrochemical, agrochemical and pharmaceutical industries by using homogeneous bases like NaOH, Ca(OH)₂, KOH etc. [19]. Harsher reaction conditions, corrosion, tedious post reaction work up, environmental problems are the main disadvantages of homogeneous base catalysis. Consequently, solid base catalysis has been intensively investigated as a replacement for homogeneous base catalysis. Solid base catalysis presents several advantages over homogeneous catalysis such as no corrosion, ease of separation from reaction mixture and lesser environmental issues. Solid base catalysts such as hydrotalcite, KF/Al₂O₃, MgO, MCM-41 [20], LiOH/Al₂O₃ [21], Na/SiO₂ [22] and KF/activated carbon [23] etc. are well reported in the literature for different organic transformations. Supporting a desired catalyst on a suitable support not only increases the number of active sites, but also leads to various changes in the surface morphology. The dispersion ability of a catalyst in reaction will be promoted after supporting the catalyst on a suitable support [17]. Properly and homogeneously dispersed catalyst plays a significant role in catalyzing a reaction. Fly ash being rich in silica (60%) and alumina (32%) [24], is thought to be explored as an efficient siliceous support material to synthesize novel, recyclable, eco-friendly and cost effective solid base catalyst. Previously, we have reported fly ash supported base catalysts viz. NaOH/Fly ash [19], CaO/Fly ash [5], amino propylated/Fly ash [25], MgO/Fly ash [26], KF/Fly ash [27] applicable for various types of condensation reactions.

Michael addition is one of the most important reactions for C-C bond formation through conjugate addition mechanism [28]. Generally Michael

additions are performed in an appropriate solvent in the presence of bases like $\text{Ba}(\text{OH})_2$, MgO , $\text{KF}/\text{Al}_2\text{O}_3$, $\text{Na}/\text{NaOH}/\text{Al}_2\text{O}_3$ [29], MgLa mixed oxides [30], piperidine [31] etc. under conventional reaction conditions. To overcome the disadvantages of conventional reaction conditions like prolonged reaction time, lower product yield and tedious work-ups, new non-conventional procedure ‘microwave irradiation’ is found to facilitate the Michael addition. Microwave irradiations also satisfied the “green chemistry” protocol, which states that a reaction should be performed under solvent free conditions, having minimal or no by-products formations with maintaining the atom economy [32]. To the best of our knowledge, strontium salts activated fly ash has not been explored as a solid base catalyst, applicable for Michael additions.

Thus, the aim of this work is to synthesize an efficient, cost-effective, microwave stable solid base catalyst- Strontium nitrate activated fly ash, for microwave mediated Michael addition of 2-cyclohexenone with a number of active methylene compounds. Michael adducts possess various applications in polymerization [33], carbohydrate synthesis [34], biologically active heterocycles [35], pharmaceutical and fine chemical industries [29]. Fly ash after suitable mechanical, thermal and chemical activation has been converted into an effective solid base catalyst. Michael addition was carried out under microwave irradiations in a single step, liquid phase and solvent free reaction conditions and catalyst was reused up to four reaction cycles with almost similar product yield. Thus, the synthesized strontium nitrate activated fly ash catalyst gives a solution to overcome the disadvantages of homogeneous and commercial heterogeneous catalysts and also suggests an alternative pathway for utilization of solid waste fly ash as a support material in synthesis of solid base catalyst for industrially important microwave assisted Michael addition reactions.

4.2 Experimental

4.2.1 Materials

Fly ash was collected from Jamshedpur Thermal Power Station, Jamshedpur (Jharkhand). All chemicals $\text{Sr}(\text{NO}_3)_2$ (99%), NaOH (98%), Na_2CO_3 (99%) were purchased from Sigma Aldrich and 2-cyclohexenone (98%) and

active methylene compounds were purchased from S.D. Fine chemical Ltd., India. All reagents used were of analytical grade and used as such.

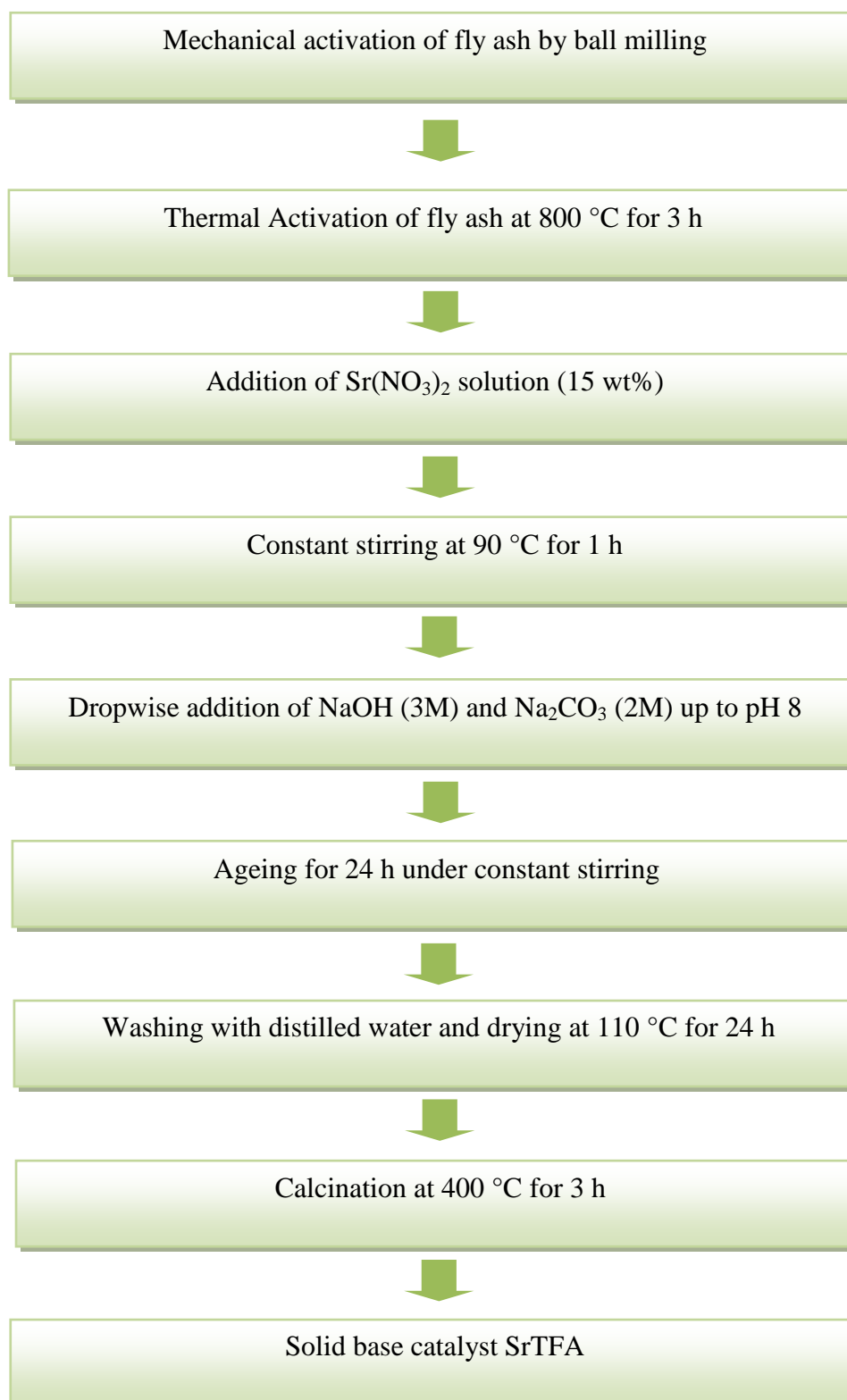
4.2.2 Catalyst synthesis

As received fly ash (FA) was mechanically activated by using high energy planetary ball mill (Retsch PM-100, Germany) in an agate jar with 5mm diameter agate balls for 10 h, 20 h and 30 h at 250 rotation/minute speed to increase the surface area as well as surface active sites. 30 h milled FA showed the higher specific surface area, also called as mechanically activated fly ash (MFA), was selected for further activations. The agate jar was loaded with ball to powder weight ratio of 10:1. MFA was thermally activated at 800 °C for 3 h to form thermally activated fly ash (TFA), consequently C, S, moisture and other impurities also get removed [36]. An aqueous solution of $\text{Sr}(\text{NO}_3)_2$ (15 wt% loading) was added into 10 g TFA and constantly stirred for 1 h at 90 °C. Precipitation was done by dropwise addition of mixture of NaOH (3M) and Na_2CO_3 (2M) solution (in 1:1 ratio) up to pH 8 in the above mixture. Resultant slurry was aged for 24 h then filtered and washed with double distilled water up to pH 7 to remove leached compounds, air dried at 110 °C for 24 h and calcined at 400 °C for 3 h in a muffle furnace under static conditions to form strontium nitrate activated fly ash catalyst (SrTFA) (**Scheme 4.1**).

4.3 Catalyst characterization

Physicochemical properties of FA, MFA, TFA and SrTFA were studied by N_2 adsorption- desorption study, TGA, FTIR, XRD, SEM-EDX and TEM techniques. Instruments detail and operating conditions during the characterization are given in **Annexure I**.

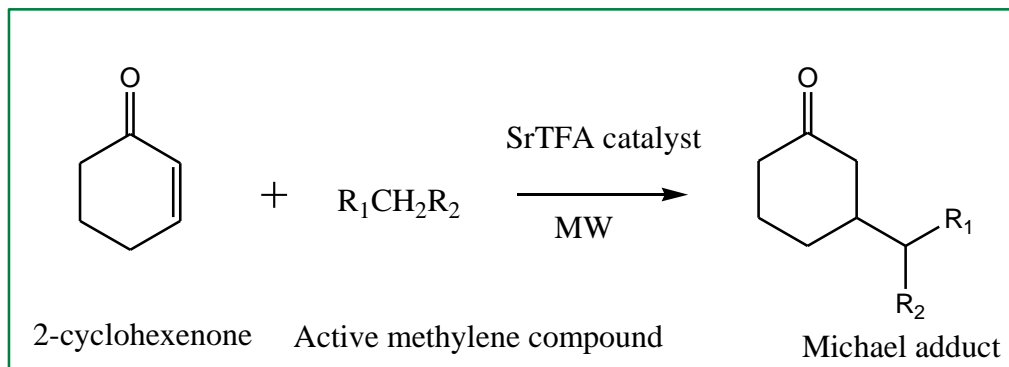
Basic strength of SrTFA was determined using Hammett indicators like phenolphthalein ($\text{pK}_a=8.2$), Nile blue ($\text{pK}_a=9.8$), 2,4,6-trinitroaniline ($\text{pK}_a=12.2$), 2,4-dinitroaniline ($\text{pK}_a=15$) and 4-nitroaniline ($\text{pK}_a=18.4$). Basicity was measured by a benzoic acid titration method using phenolphthalein indicator [37]. The methods for evaluating basic strength and basicity are given in detail in **Chapter 2**.



Scheme 4.1: Synthesis of solid base catalyst SrTFA.

4.4 Catalytic activity of SrTFA catalyst

The catalytic activity of SrTFA was tested by the Michael addition reaction under microwave irradiations **Scheme 4.2**.



Scheme 4.2: Michael addition reaction of 2-cyclohexenone with active methylene compound over SrTFA.

The reaction mixture for Michael addition of nitromethane (Michael donor) with 2-cyclohexenone (Michael acceptor) in 2:1 to 1:3 molar ratios was taken with SrTFA (preheated at 400 °C for 2 h) during the study. The substrate (2-cyclohexenone) to catalyst weight ratio ranged from 10:1 to 2.5:1. Synthesis of Michael adducts were performed in a glass vial (capacity 10 ml) with magnetic stirring, in microwave unit (CEM Discover) (**Microwave synthesis system is described in Chapter 3**). The vial was sealed with a septum and placed into the microwave cavity where it was again sealed with a pressure lock. The reaction mixture was microwave irradiated for time ranging from 5 to 30 minutes, at power ~ 70 W, for temperature ranging from 60-120 °C and pressure 50 Psi.

After completion of the reaction (TLC monitoring), the mixture was cooled and the solid catalyst was filtered out. The crude product was extracted with $CHCl_3$ solvent and excessive solvent was later removed by evaporation. The product was analyzed by Gas Chromatograph.

The conversion of active methylene compound was calculated as follows:

$$\text{Conversion (wt \%)} = 100 \times (\text{Initial wt\%} - \text{Final wt\%}) / \text{Initial wt\%}$$

The isolated yield (%) of Michael adduct was calculated by using weight percent method.

$$\% \text{ Isolated yield of Michael adduct obtained} = \frac{\text{g of Michael adduct obtained experimentally}}{\text{g of Michael adduct obtained theoretically}} \times 100$$

4.5 Catalyst regeneration

The used catalyst was filtered out by simple filtration method then washed with acetone. After washing catalyst was dried in oven at 110 °C for 12 h and thermally activated at 400 °C for 2 h in muffle furnace before reuse in next reaction cycles under similar reaction conditions as earlier.

4.6 Results and discussion

4.6.1 Chemical composition of FA and SrTFA catalyst

The chemical compositions of as received FA and synthesized SrTFA catalyst as determined by SEM-EDX are given in **Table 4.1**. Loss on ignition (LOI) was found to be 5 wt%, by heating a certain weighed quantity of FA in muffle furnace at 800 °C for 3 h. As depicted from **Table 4.1** SrO is not present in FA or it may be present in FA but beyond the instrument detection limit. In SrTFA SrO is detectable and found 4.91%. Treatment of FA with Sr(NO₃)₂ proved to be effective in removing some metals to a lower level and hence increasing the Sr content in the prepared catalyst. The increased Sr is accountable for the generation of a number of Sr-SiO₂/CO₃/OH phases, thus increased catalytic activity and basicity in the SrTFA catalyst for Michael addition reaction.

4.6.2 Surface area results

Specific surface area results of all samples are given in **Table 4.2**. Specific surface area of FA 9.18 m²/g, considerably increases after mechanical activation and reaches up to 30.02 m²/g for MFA while it decreases after thermal activation

and reaches up to 28.47 m²/g. During the mechanical activation breaking of FA spherical particles takes place which results in increased surface area.

The chemical activation of TFA results into decreased surface area due to the blockage of its small pores by loading of different Sr species [38]. In SrTFA catalyst, decrease in the surface area facilitates the generation of surface active basic sites thus catalytic activity.

Table 4.1: Chemical composition of FA and SrTFA.

Chemical components	FA (Wt%)	SrTFA (Wt%)
SiO ₂	59.42	58.90
Al ₂ O ₃	18.79	17.23
Fe ₂ O ₃	6.91	6.48
CaO	2.56	2.10
MgO	1.84	1.52
K ₂ O	2.37	1.98
Na ₂ O	3.84	3.42
TiO ₂	1.27	0.96
SrO	-	4.91
Other elements	3	2.5

Table 4.2: Specific surface area of all catalytic materials.

Catalyst	Specific surface area (m ² /g)
FA	9.18
FA (10 h milled)	15.14
FA (20 h milled)	22.54
MFA	30.02
TFA	28.47
SrTFA	23.54

4.6.3 Thermogravimetric analysis

TGA curves of FA and SrTFA (**Figure 4.1**) show weight loss of 5.96% and 11.23% respectively, within the temperature range 50-1000°C, are attributed to water loss and burning of carbonaceous materials and volatilization of some trace metal oxides and other impurities [39]. Precursor $\text{Sr}(\text{NO}_3)_2$ would be converted into $\text{Sr}(\text{OH})_2$ and SrCO_3 during the catalyst synthesis. So the considerable weight loss in SrTFA may be assigned to the decomposition of $\text{Sr}(\text{NO}_3)_2$, $\text{Sr}(\text{OH})_2$ and SrCO_3 .

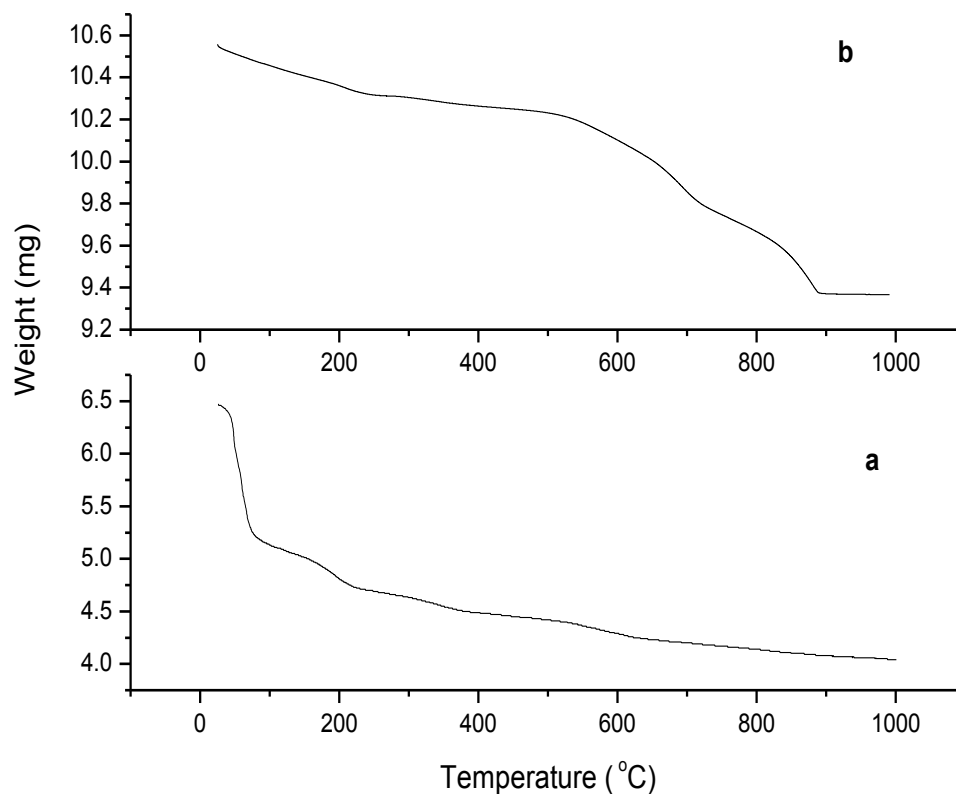


Figure 4.1: TGA curve of (a) FA and (b) SrTFA.

4.6.4 FTIR studies

The FTIR spectra of FA, MFA, TFA are given in the **Figure 4.2**. All spectra show a broad band between $3000\text{-}3600\text{ cm}^{-1}$, which is attributed to -O-H stretching vibration of surface silanol groups (Si-OH) [26]. Intensity and broadness increase in case of MFA is an evidence for the breaking of spherical

silica particles and formation of Si-OH groups and the presence of strong H-bonding which again decreases after thermal activation due to loss of adsorbed water in TFA [19]. A peak centered at 1608 cm^{-1} , present in all samples is assigned to bending mode ($\delta_{\text{O-H}}$) of water molecule (**Figure 4.2, 4.3**) [7]. A small peak around 2830 cm^{-1} is assigned to -C-H stretching vibration of organic contaminants present in fly ash sample (**Table 4.3**) [40]. Peaks around 1986 and 1872 cm^{-1} (**Figure 4.2, Table 4.3**) are assigned to SiO_2 as possible quartz [41]. Peaks centered at 1521 and 1681 cm^{-1} are due to $(\text{CO}_3)^{2-}$ stretching vibration, visible in all spectra, show the highest intensity in FA and get reduced after thermal activation confirming the removal of carbonate or carbonate like species during thermal activation [40,42]. A broad band between 1103 - 1168 cm^{-1} is attributed to Si-O-Si asymmetric stretching vibration [40]. A peak at approx $\sim 600\text{ cm}^{-1}$ is attributed to Si-O-Al stretching vibration (**Figure 4.2, 4.3**) [43].

FTIR spectrum of SrTFA (**Figure 4.3b**) shows the broader and much intense band in the region of 3000 - 3600 cm^{-1} as compared to TFA. The increased intensity could be assigned to generation of Si-OH groups as well as to Si-O-Sr-OH groups during the chemical activation while H-bonding is responsible for the broadness of the band between these groups. The increased OH groups are responsible for the Bronsted basic sites which initiate the reaction by abstracting the proton from active methylene group [44].

There is also possibility of SrO, $\text{Sr}(\text{OH})_2$ and SrCO_3 formation on TFA surface [15]. Some of the basic sites generated by SrO, would be due to the presence of $\text{Sr}^{+2}\text{-O}^{-2}$ ion pairs in different coordination environments [15]. $\text{Sr}(\text{OH})_2$ and SrCO_3 formation could be assigned due to the absorption of water vapour [45] and CO_2 from environment [16] by SrO compound.

Table 4.3: The observed transmission frequencies (cm-1) of Fourier transform infrared spectra of FA, MFA, TFA, SrTFA and reused SrTFA and their assignments.

Assignments	FA	MFA	TFA	SrTFA	Reused SrTFA	Ref.
Si-O-Al stretching vibration	602	601	594	602	600	44
Si-O-Si asymm. Stretching vibration	1151	1103	1129	1168	1106	41
(CO₃)²⁻ stretching vibration	1521, 1681	1521	1521, 1679	1521	1521	41, 43
H-O-H bending Vibration	1609	1616	1608	1617	1614	7
-C-H stretching vibration	2830	2854	2827	-	-	41
-O-H stretching vibration	3539	3442	3553	3444	3566	26

4.6.5 X-ray diffraction studies

The XRD patterns of FA, MFA, TFA and SrTFA are given in **Figure 4.4**. Peaks at $2\theta = 20.7^\circ$, 26.5° , 40.66° and 49.96° are attributed to quartz (SiO₂, ICDD pdf number 000- 46-1045) while peaks at $2\theta = 33.4^\circ$ and 16.4° confirm the presence of calcite (CaCO₃, ICDD pdf number, 47-1743) and mullite (Al₆Si₂O₁₃, ICDD pdf number 000-15-0776) respectively in all XRD patterns. Thermal activation plays an important role in the crystallization and modification of previously present crystalline phases as shown from **Figure 4.4c** that after thermal activation number of crystalline phases like quartz, mullite and calcite become more intense and sharper while magnetite (Fe₃O₄, ICDD pdf number, 19-

0629) peak at $2\theta = 34.85^\circ$ (**Figure 4.4a-b**) tends to disappear and converts into hematite phase (Fe_2O_3 , ICDD pdf number, 33-0664) at high temperature treatment (**Figure 4.4c**). Mechanical activation of FA results in decrease in peak intensities of crystalline phase like quartz, mullite and calcite (**Figure 4.4b**). In SrTFA, presence of a crystalline peak at $2\theta = 32.3^\circ$ confirms availability of crystalline strontium silicate ($\alpha\text{-Sr}_2\text{SiO}_4$, JCPDS 076-1493) phase [46], which is also consistent with the TEM, SEM and FTIR results.

4.6.6 SEM analysis results

SEM micrographs (**Figure 4.5**) show the surface morphologies of fly ash in comparison with the mechanically, thermally and chemically activated fly ash samples. It can be seen that fly ash mainly consists of spherical particles with smooth outer surfaces and irregularly shaped unburned carbon particles. The smooth aluminosilicate spherical particles are formed as a result of thermochemical transformations of mineral particles during coal combustion process, where the minerals melt to form small droplets, which upon sudden cooling and action of surface tension forces adopt the spherical shape [47]. During mechanical activation spherical shape particles break into irregular shape particles as shown by **Figure 4.5b** which during thermal activation form clumps and convert into agglomerated particles **Figure 4.5c**, this agglomeration is the main reason of additional crystallinity which is clearly visible in the XRD pattern of TFA. Shiny clumps of strontium based species on TFA surface (**Figure 4.5d**) confirm effective chemical activation, which is also in good agreement with FTIR and XRD results. EDX results are showing the microchemistry of FA and SrTFA, given in **Table 4.1**. In SrTFA increased amount of Sr confirms the successful loading of different Sr species in the above mentioned forms on TFA surface.

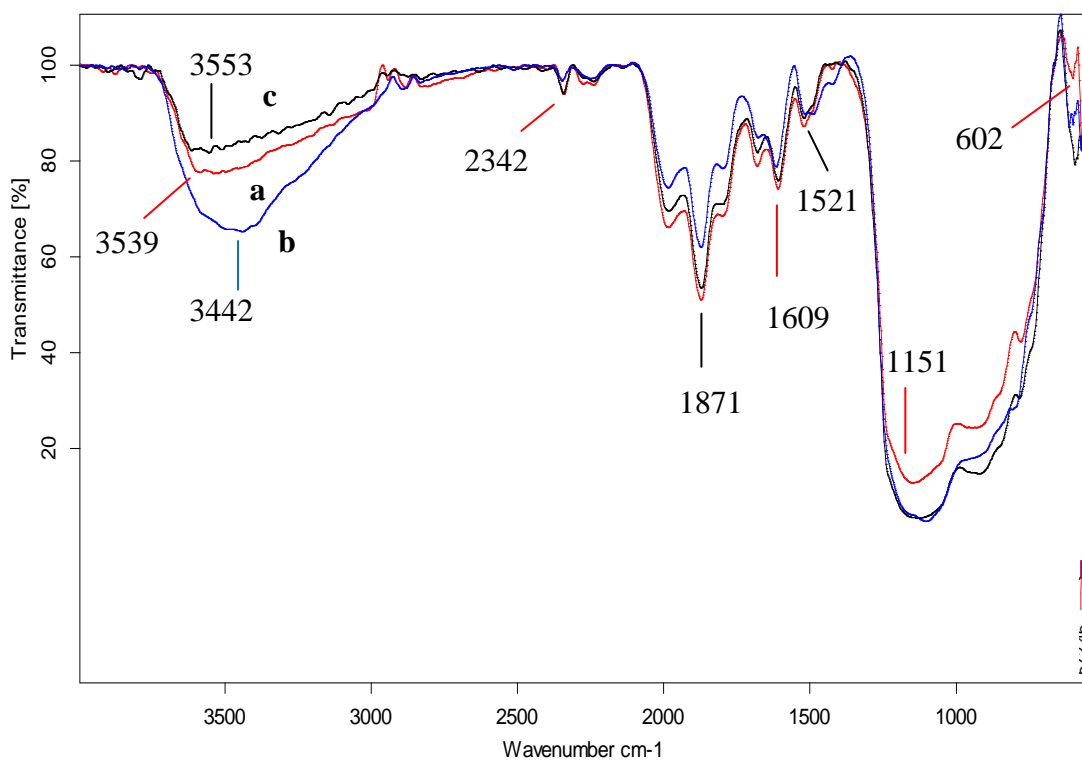


Figure 4.2: FTIR spectra of (a) FA, (b) MFA and (c) TFA.

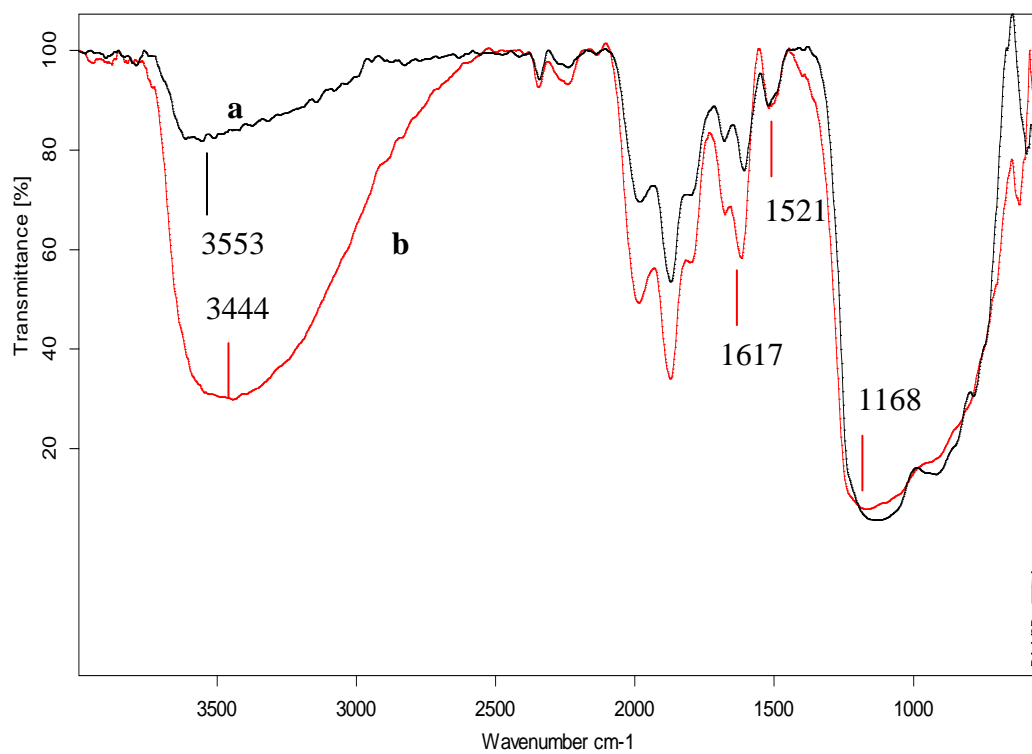


Figure 4.3: FTIR spectra of (a) TFA and (b) SrTFA.

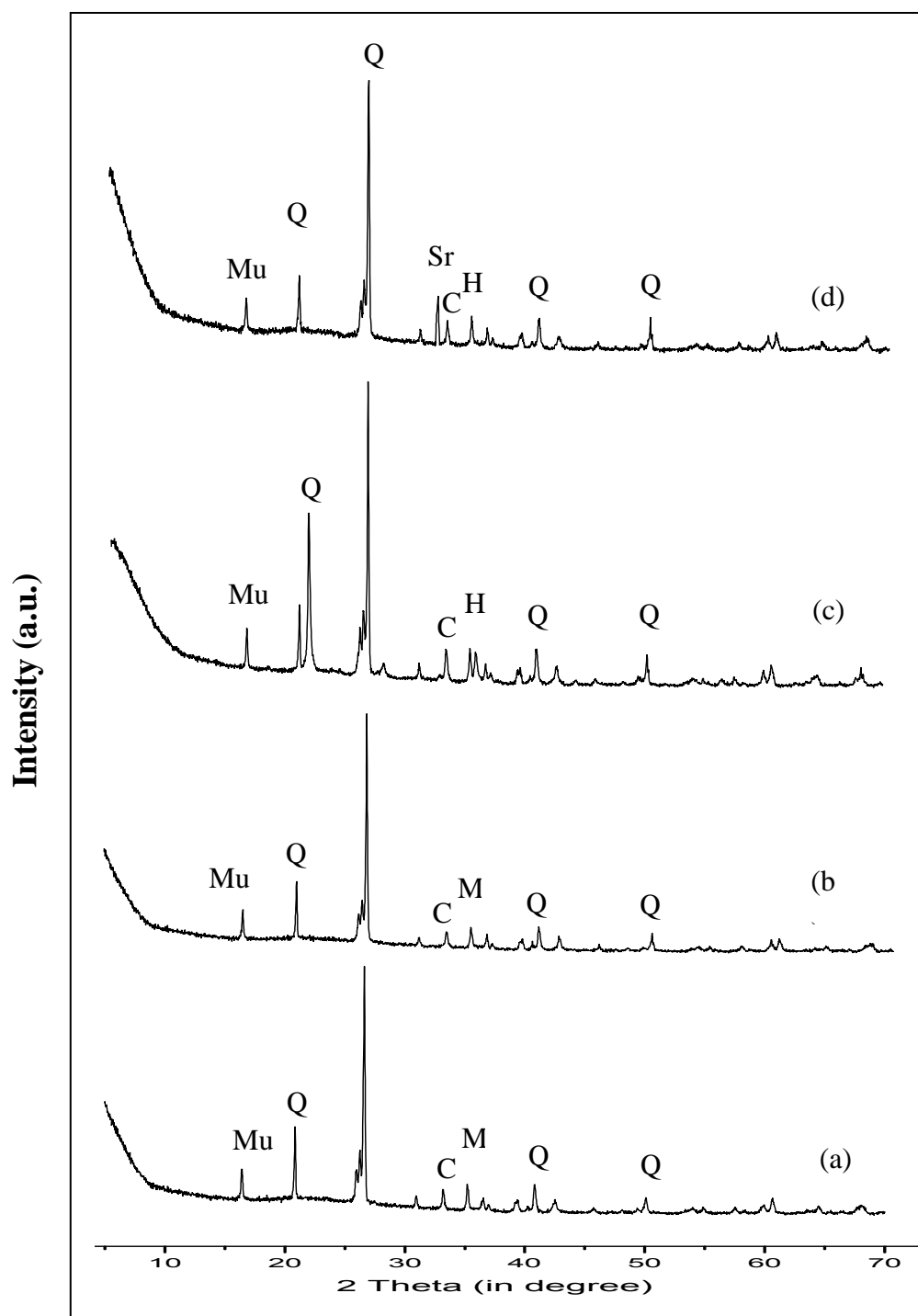


Figure 4.4: X-ray diffraction patterns of (a) FA, (b) MFA, (c) TFA and (d) SrTFA.

(Mu = Mullite, Q = Quartz, C = Calcite, M = Magnetite, H = Hematite, Sr = Strontium silicate)

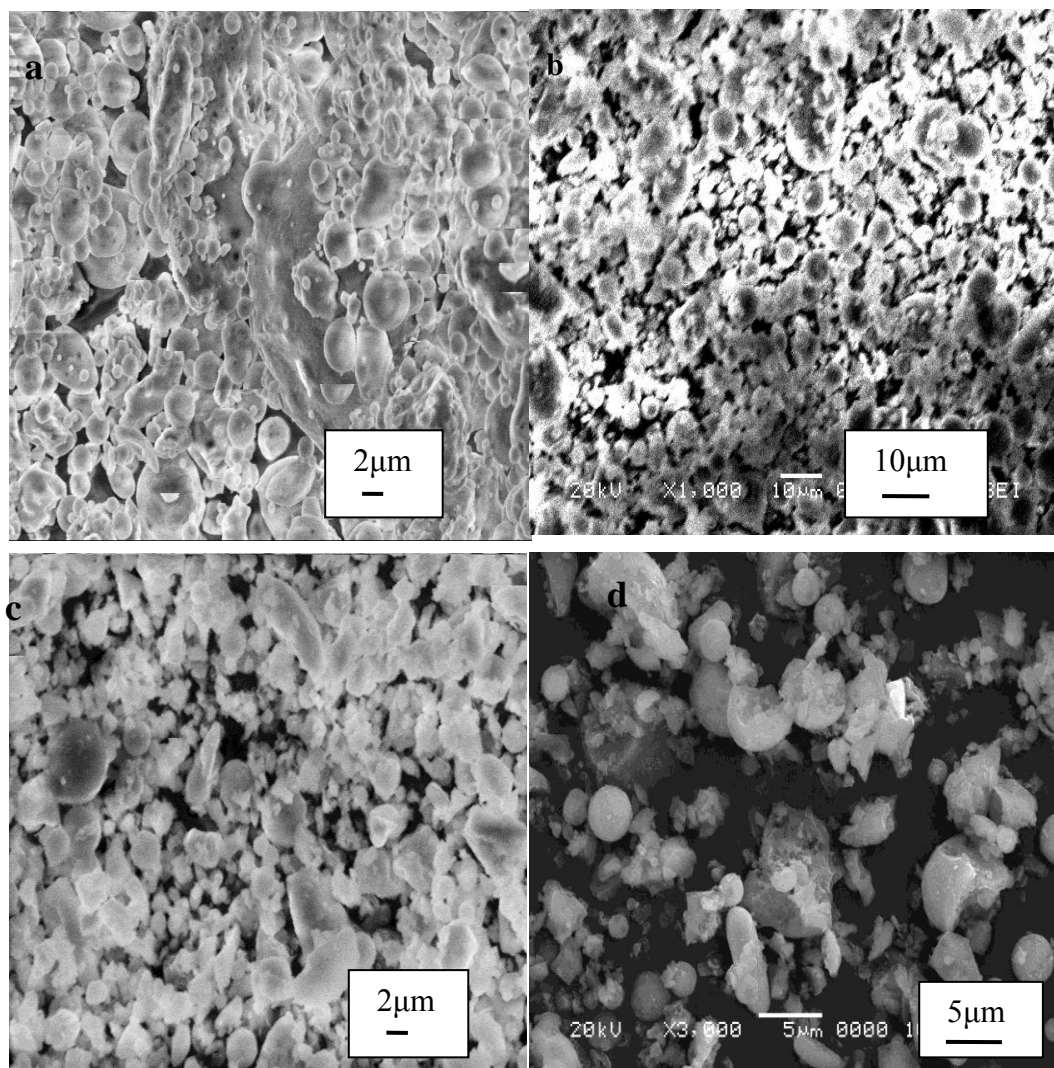


Figure 4.5: SEM micrographs of (a) FA, (b) MFA, (c) TFA and (d) SrTFA.

4.6.7 TEM analysis results

TEM image of FA shows a completely spherical, fine and smooth particle of fly ash which has been reduced in size after mechanical activation (**Figure 4.6b**). So, mechanical activation is accountable for the complete removal of smoothness and sphericity of spherical silica particles. TEM image of SrTFA (**Figure 4.6**) shows dark spots of crystalline strontium silicate phase while the needle like structure may be attributed to the SrCO₃ phase [15] .

4.6.8 Basic strength and basicity measurement

The base strength and basicity of SrTFA were determined by the Hammett indicator method. SrTFA shows basic strength $15 < H_{-} < 18.4$ and basicity was found to be 1.6 mmol/g.

4.7 Catalytic activity

The catalytic activity of SrTFA catalyst was measured by a single step, liquid phase, solvent free, microwave irradiated Michael addition reaction of 2-cyclohexenone with nitromethane under optimized reaction conditions.

Results given in **Table 4.4** show that FA, MFA and TFA do not possess any catalytic activity for Michael addition reaction. SrTFA catalyst under the given reaction conditions, showed maximum activity. Parameters such as reactant molar ratio, amount of catalyst, reaction time and temperature were optimized in order to attain the maximum catalytic activity, conversion and yield of desired product.

4.7.1 Effect of reaction time

In order to find the reaction time to get highest conversion over SrTFA catalyst, the reaction was carried out at 90 °C for different time intervals ranging from 5 minutes to 30 minutes taking nitromethane/2-cyclohexenone molar ratio 2:1 and 2-cyclohexenone to catalyst weight ratio 5:1. It was found that in first 15 minutes of the reaction period the conversion increases linearly up to 96% which remains unchanged up to 30 minutes (**Figure 4.7**). The optimized reaction time was found to be 15 minutes, in which SrTFA catalyst gave highest conversion 96% of nitromethane to 3-nitromethyl cyclohexanone.

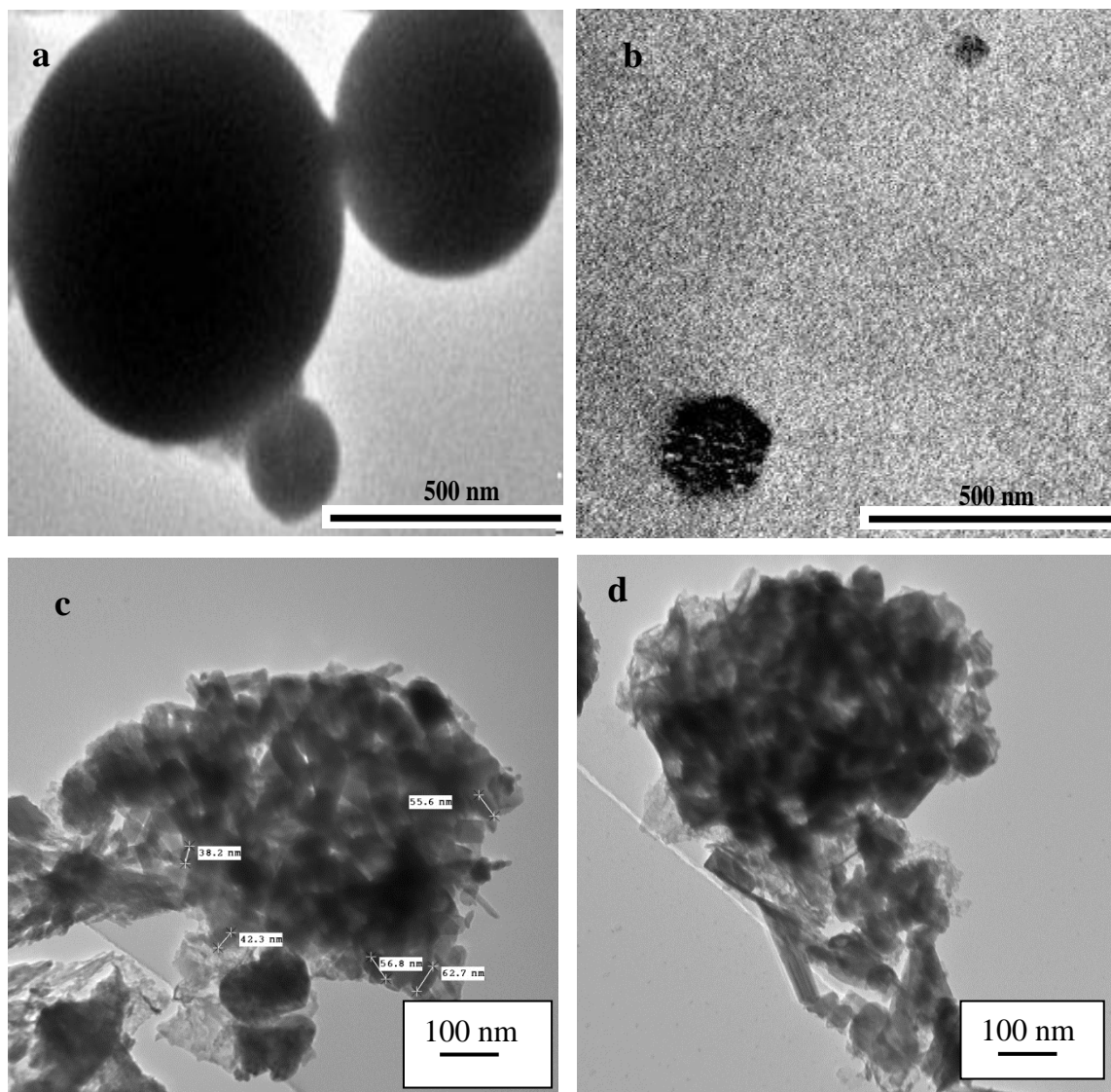


Figure 4.6: TEM images of (a) FA, (b) MFA and (c-d) SrTFA.

Table 4.4: Catalytic activity of FA, MFA, TFA and SrTFA for Michael addition reaction of 2-cyclohexenone with nitromethane.

Catalyst	Conversion (%) of nitromethane	Isolated yield (%) of 3-nitromethyl cyclohexanone
FA	Nil	Nil
MFA	Nil	Nil
TFA	Nil	Nil
SrTFA	84	76

Reaction conditions: Temperature 90 °C, Time 10 minute, nitromethane/2-cyclohexenone molar ratio 2:1, substrate/catalyst weight ratio 5:1.

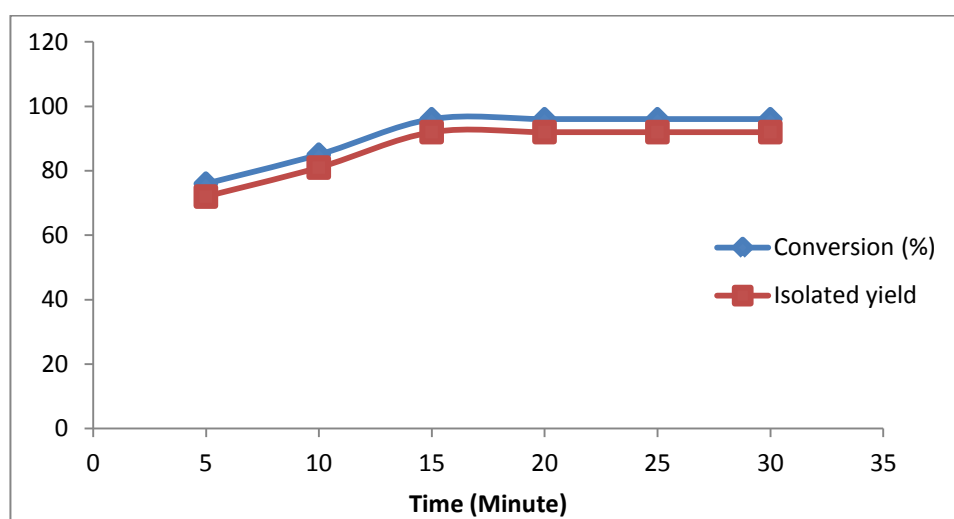


Figure 4.7: Effect of time on conversion (%) of nitromethane and isolated yield (%) of 3-nitromethyl cyclohexanone over SrTFA.

Reaction conditions: Temperature 90 °C, nitromethane/2-cyclohexenone molar ratio 2:1, substrate/catalyst weight ratio 5:1.

4.7.2 Effect of reaction temperature

Optimization of reaction temperature to give maximum conversion and isolated yield (%) was carried out at temperature ranging from 60 °C to 120 °C for 15 minutes taking nitromethane/2-cyclohexenone molar ratio of 2:1 while substrate to catalyst weight ratio was 5:1. Conversion and yield were observed to

increase on increasing reaction temperature ranging from 60 °C to 90 °C as depicted from **Figure 4.8**. The results show that the maximum conversion (96%) of nitromethane and isolated yield (92%) of 3-nitromethyl cyclohexanone was found at 90 °C, after which conversion and isolated yield (%) remain almost steady till 90 °C.

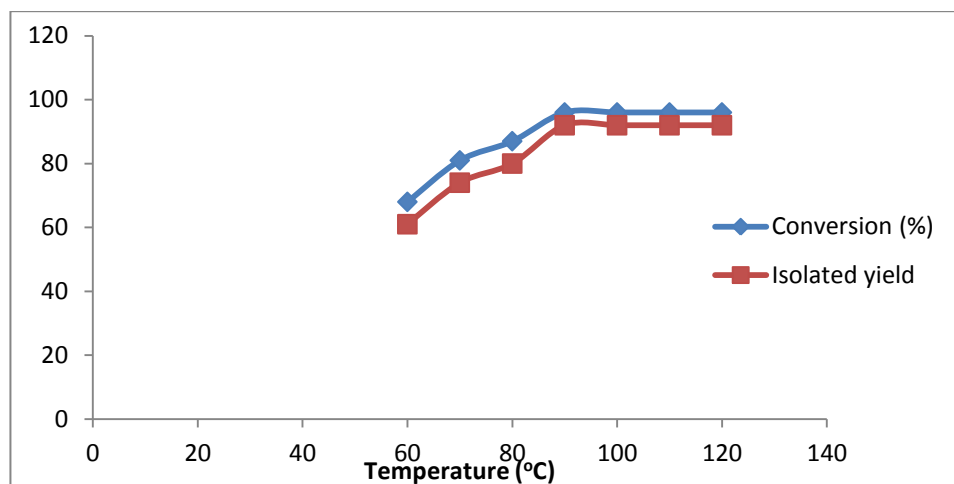


Figure 4.8: Effect of temperature on conversion (%) of nitromethane and isolated yield (%) of 3-nitromethyl cyclohexanone over SrTFA.

Reaction conditions: Time 15 minutes, nitromethane/2-cyclohexenone molar ratio 2:1, substrate/catalyst weight ratio 5:1.

4.7.3 Effect of substrate/catalyst weight ratio

The influence of substrate to catalyst weight ratio on conversion and isolated yield (%) was investigated by varying the amount of SrTFA catalyst under optimized reaction conditions. It can be seen from **Table 4.5**, only 72% conversion of nitromethane is achieved at 2-cyclohexenone/SrTFA weight ratio 10:1. On increasing 2-cyclohexenone/SrTFA weight ratio to 5:1, conversion of nitromethane is increased up to 96% while isolated yield (%) of 3-nitromethyl cyclohexanone is increased up to 92%. The increase in conversion, with increase in the catalyst weight can be attributed to an increase in the availability of number of catalytic active sites required for Michael addition reaction reaction. On further increase in the amount of catalyst no changes in conversion and isolated yield (%) are observed.

Table 4.5: Effect of substrate/catalyst weight ratio on conversion (%) of nitromethane and isolated yield (%) of 3-nitromethyl cyclohexanone over SrTFA.

nitromethane /SrTFA weight ratio	Conversion (%) of nitromethane	Isolated yield (%) of 3-nitromethyl cyclohexanone
10:1	72	70
5:1	96	92
2.5:1	96	92

Reaction conditions: Temperature 90 °C, Time 15 minutes, nitromethane/2-cyclohexenone molar ratio 2:1.

4.7.4 Effect of reactant molar ratio

The synthesis of 3-nitromethyl cyclohexanone was carried out at 90 °C with various molar ratios of reactants for 15 minutes over SrTFA catalyst under microwave irradiations. As indicated by **Table 4.6**, 70% conversion of nitromethane was observed at 3:1 molar ratio of nitromethane to 2-cyclohexenone. This may be due to insufficient quantity of the reactants to react with each other. There was an increase in conversion up to 96% at 2:1 molar ratio of nitromethane to 2-cyclohexenone at the same reaction conditions. This may be due to satisfactory reactant quantity on the basic sites of the SrTFA catalyst surface. The conversion decreased from 72% to 35% on further increasing the molar ratio from 1:1 to 1:3 which could be attributed to the lacking of nitromethane for the Michael addition reaction.

4.8 Reaction mechanism

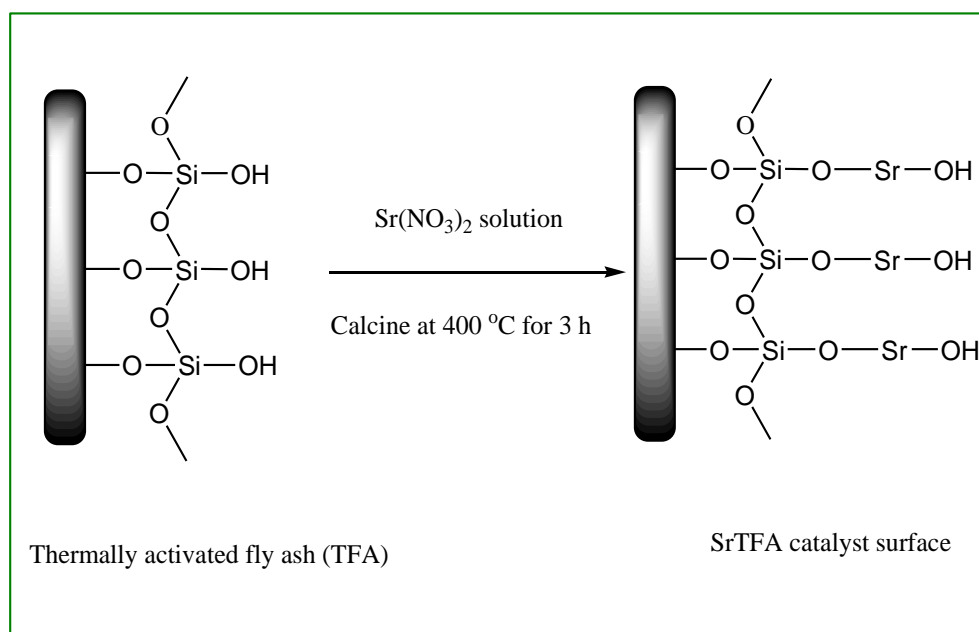
The plausible structure for active basic sites of the SrTFA catalyst is shown in **Scheme 4.3**. The reaction mechanism over SrTFA catalyst shows that Michael addition is an addition of active methylene compounds to α , β -unsaturated carbonyl compounds (2-cyclohexenone) (**Scheme 4.4**). Surface active bronsted basic sites ($-\text{Sr}-\text{OH}$) abstract proton from nitromethane and form

anion. The conjugate addition of the formed anion to the 2-cyclohexenone, followed by the acceptance of a proton produces Michael adduct [48].

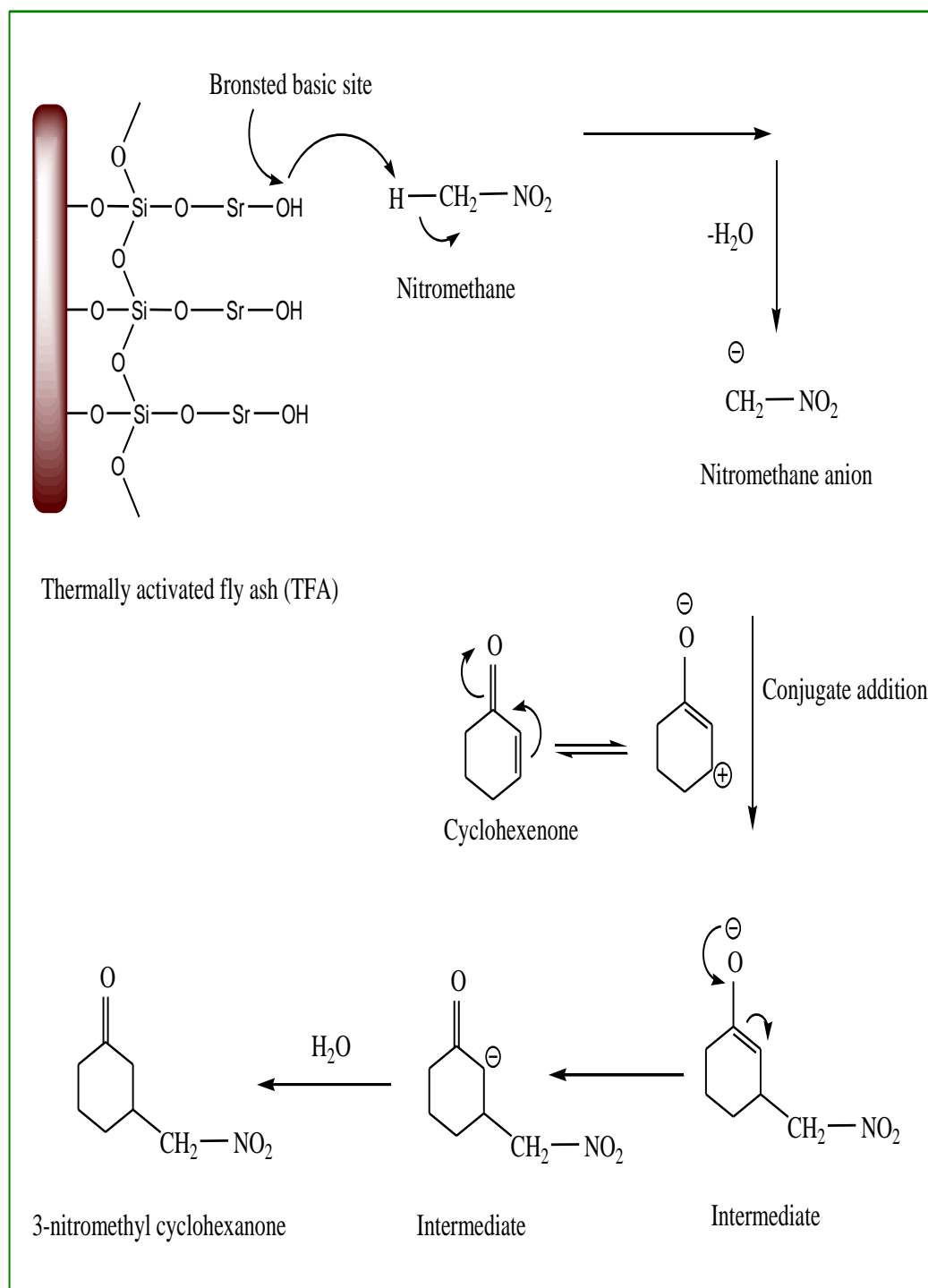
Table 4.6: Effect of molar ratio of nitromethane/2-cyclohexenone on conversion (%) of nitromethane and isolated yield (%) of 3-nitromethyl cyclohexanone over SrTFA.

Molar ratio	Conversion (%) of nitromethane	Isolated yield (%) of 3-nitromethyl cyclohexanone
3:1	70	65
2:1	96	92
1:1	72	70
1:2	48	45
1:3	35	31

Reaction conditions: Temperature 90 °C, Time 15 minutes, substrate/catalyst weight ratio 5:1.



Scheme 4.3: The schematic presentation of chemical activation of TFA with $\text{Sr}(\text{NO}_3)_2$ and proposed structure of SrTFA.



Scheme 4.4: Proposed mechanism for Michael addition reaction of 2-cyclohexenone and nitromethane over SrTFA.

4.9 Catalyst regeneration

After completion of the reaction the catalyst was filtered out by simple filtration method, washed with acetone and dried in oven at 110 °C for 12 h followed by thermal activation at 400 °C for 2 h. The regenerated SrTFA catalyst was used in the next cycle for the synthesis of Michael adduct under microwave irradiation, to evaluate the reusability of the catalyst. The regenerated catalyst was found to be having similar activity as fresh catalyst for consecutive four reaction cycles, giving 92-80% yield in microwave irradiation (**Table 4.7**) for Michael addition of 2-cyclohexenone with nitromethane. The FTIR spectrum of reused SrTFA catalyst after five reaction cycles (**Figure 4.9b**) resembles that of fresh SrTFA catalyst (**Figure 4.9a**) indicating the stability of surface hydroxyl groups responsible for Bronsted basic sites thus catalytic activity. Due to the stability of these basic sites SrTFA catalyst was found efficient up to five reaction cycles giving almost similar yield. The significant decrease in yield after five reaction cycles is due to the deposition of carbonaceous material on the external surface of the reused catalyst which may block the active basic sites present on SrTFA surface.

Table 4.7: Catalytic activity of fresh and regenerated SrTFA catalyst for Michael addition of 2-cyclohexenone with nitromethane.

Reaction Cycle	Isolated yield (%)
I	92
II	88
III	85
IV	81
V	80

Reaction conditions: Temperature 90 °C, Time 15 minutes, substrate/catalyst weight ratio 5:1, nitromethane/2-cyclohexenone molar ratio 2:1.

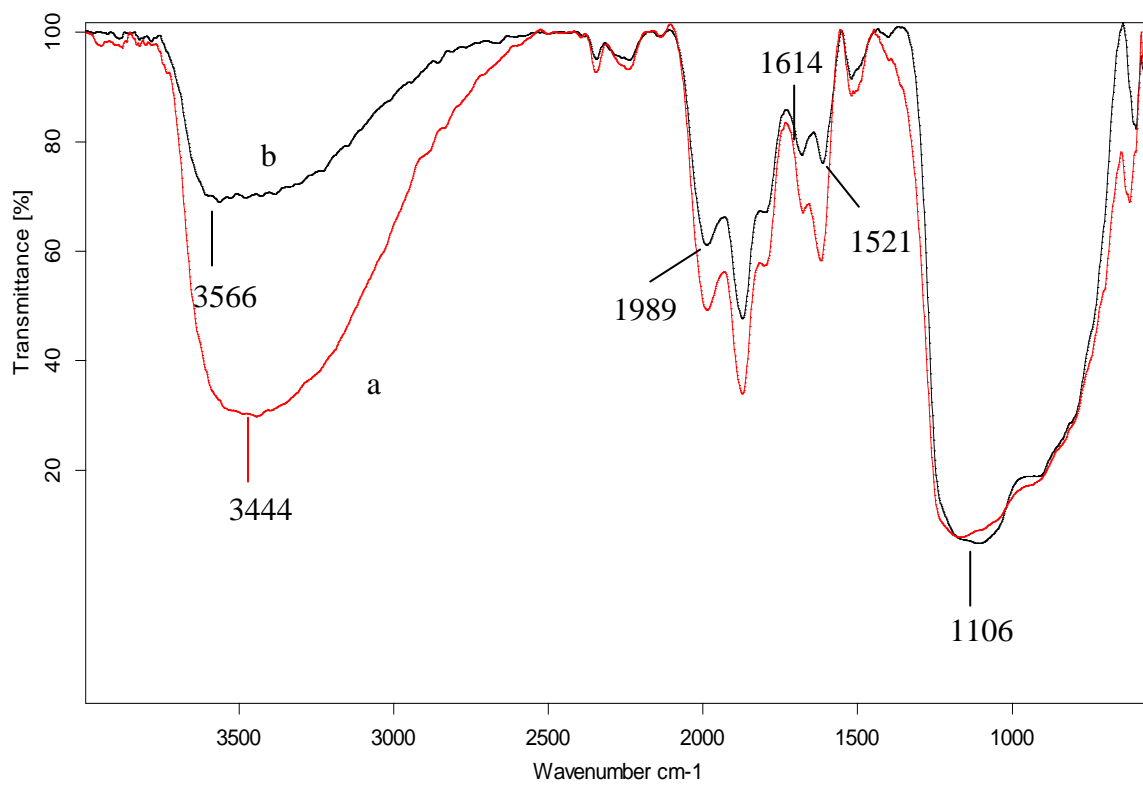
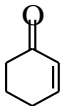
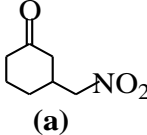
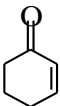
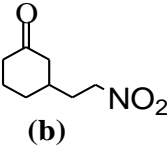
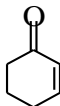
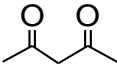
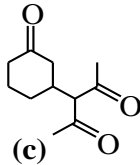
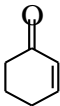
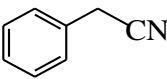
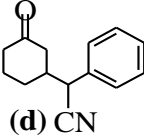


Figure 4.12: FTIR spectra of (a) SrTFA and (b) Reused SrTFA.

The study of Michael addition reaction was then further extended to the several active methylene compounds with 2-cyclohexenone using SrTFA catalyst under microwave irradiations as well as thermal heating conditions. The results are summarized in **Table 4.8**. It is observed by the results (**Table 4.8**) that in the synthesis of Michael adduct, yield is considerably increased by microwave irradiations as compare to thermal heating. Moreover, the microwave synthesis could be done easily and efficiently at lower temperature in shorter time than in the thermal heating condition.

Table 4.8: Michael addition of 2-cyclohexenone with active methylene compounds in presence of SrTFA catalyst under microwave irradiation and thermal heating.

Entry	Michael acceptors	Michael donar	Product	Isolated Yield (%)	
				MW	Thermal
1		CH ₃ -NO ₂		90	78
2		C ₂ H ₅ -NO ₂		92	79
5				91	79
6				92	80

Reaction conditions: Temperature 90 °C (MW), 120°C (thermal heating), Time 15 minutes (MW), 120 minutes (thermal heating), substrate/catalyst weight ratio 5:1, active methylene compound/2-cyclohexenone molar ratio 2:1.

Products were characterized by comparison of their spectroscopic data (^1H NMR) with those reported in the literature.

NMR data of products-

(a). **3-(1-Nitromethyl)cyclohexanone**: Colorless oil, ^1H -NMR (400 MHz, CDCl_3): δ 1.43-1.56 (m, 1H, CH_2), 1.67-1.87 (m, 1H, CH_2), 1.94-2.03 (m, 1H, CH_2), 2.07-2.17 (m, 2H, CH_2), 2.24-2.33 (m, 1H, CH_2), 2.40-2.53 (m, 2H, CH_2), 2.58-2.71 (m, 1H, CH), 4.26 (d, $J = 7.0$ Hz, 1H, CH_2NO_2), 4.35 (d, $J = 6.2$ Hz, 1H, CH_2NO_2).

(b). **3-(1-Nitroethyl)cyclohexanone**: Colorless oil, ^1H -NMR (400 MHz, CDCl_3): δ 1.40-1.48 (m, 2H, CH_2), 1.57 (d, $J = 9.6$ Hz, 6H, CH_3), 1.85-1.90 (m, 2H, CH_2), 1.91-1.97 (m, 2H, CH_2), 2.08-2.20 (m, 4H, CH_2), 2.25-2.32 (m, 2H, CH_2), 2.39-2.44 (m, 4H, CH_2), 2.46-2.48 (m, 2H, CH), 4.44-4.53 (m, 2H, CHNO_2).

(c). **3-(3-Oxocyclohexyl)pentan-2,4-dione**: Yellow solid, ^1H -NMR (400 MHz, CDCl_3): δ 1.30-1.40 (m, 1H, CH_2), 1.62-1.74 (m, 1H, CH_2), 1.75-1.82 (m, 1H, CH_2), 1.98-2.06 (m, 2H, CH_2), 2.14 (s, 3H, CH_3), 2.16 (s, 3H, CH_3), 2.20-2.31 (m, 2H, CH_2), 2.35-2.41 (m, 1H, CH_2), 2.61-2.71 (m, 1H, CHCH_2), 3.61 (d, $J = 10.4$ Hz, 1H, $\text{CH}(\text{COCH}_3)_2$).

(d). **3-Oxocyclohexylphenylacetonitrile**: Yellow oil, ^1H -NMR (400 MHz, CDCl_3): δ 1.48-1.63 (m, 4H, CH_2), 1.90-1.93 (m, 2H, CH_2), 1.96-2.14 (m, 2H, CH_2), 2.15-2.24 (m, 7H, CH_2), 2.30-2.35 (m, 3H, CH and CH_2), 3.69 (d, $J = 4.4$ Hz, 1H, CH-CN), 3.83 (d, $J = 4.4$ Hz, 1H, CH-CN), 7.19-7.25 (m, 4H, ArH), 7.28-7.34 (m, 6H, ArH).

4.10 Conclusion

In summary, we have synthesized the efficient, reusable and novel strontium nitrate activated fly ash catalyst through mechanical, thermal and chemical activation of fly ash, for microwave mediated Michael addition of 2-cyclohexenone with number of active methylene compounds in solvent free reaction conditions. The prepared catalyst possesses higher basicity due to increase in stable Bronsted basic sites i.e. $-\text{Sr}-\text{OH}$ content, was recovered and reused with small changes in the yield, confirming almost negligible leaching of

active basic sites or deactivation of the catalyst under the mentioned reaction conditions. The salient features of this protocol are reusability, cost effectiveness, eco-friendly nature, absence of solvent, shorter reaction time than conventional reaction condition, operational simplicity and easy product separation in high yield. The work investigates the structural properties of a novel fly ash supported solid base catalyst for microwave assisted Michael addition reactions in solvent free reaction conditions.

4.11 References

- [1] M. Gross, M. Soulard, P. Caullet, I. Saude, *Microporous Mesoporous Mater.* 104 (2007) 67.
- [2] M. Ahmaruzzaman, *Prog. Energy Combust. Sci.* 36 (2010) 327.
- [3] D. Zeng, S. Liu, W. Gong, J. Qiu, H. Chen, G. Wang, *Fuel* 119 (2014) 202.
- [4] I. Acar, M.U. Atalay, *Fuel* 106 (2013) 195.
- [5] D. Jain, C. Khatri, A. Rani, *Fuel Process. Technol.* 91 (2010) 1015.
- [6] M. Gross-lorgouilloux, M. Soulard, P. Caullet, J. Patarin, E. Moleiro, I. Saude, *Microporous Mesoporous Mater.* 127 (2010) 41.
- [7] S. Katara, S. Kabra, A. Sharma, R. Hada, A. Rani, *Int. Res. J. Pure Appl. Chem.* 3 (2013) 299.
- [8] J. Tantirungrotechai, S. Thepwatee, B. Yoosuk, *Fuel* 106 (2013) 279.
- [9] M. Koberg, R. Abu-Much, A. Gedanken, *Bioresour. Technol.* 102 (2011) 1073.
- [10] H. Kabashima, T. Katou, H. Hattori, *Appl. Catal. A Gen.* 214 (2001) 121.
- [11] C. Liu, J. Wang, Y. Li, *J. Mol. Catal. A Chem.* 258 (2006) 367.
- [12] H. Atia, M. Richter, U. Armbruster, R. Eckelt, A. Martin, in: *11 Eur. Congr. Catal. -EuropaCat-XI, Lyon, France, 2013*, pp. 5–6.
- [13] Z. Yang, W. Xie, *Fuel Process. Technol.* 88 (2007) 631.
- [14] M. Nargis, H. Jin, M. Bismillah, S. Oh, S. Park, *Applied Catal. A, Gen.* 413-414 (2012) 205.
- [15] A.P.S. Dias, J. Bernardo, P. Felizardo, M.J.N. Correia, *Fuel Process. Technol.* 102 (2012) 146.

- [16] A.M. Frey, J. Yang, C. Feche, N. Essayem, D.R. Stellwagen, F. Figueras, K.P. de Jong, J.H. Bitter, *J. Catal.* 305 (2013) 1.
- [17] C.-L. Chen, C.-C. Huang, D.-T. Tran, J.-S. Chang, *Bioresour. Technol.* 113 (2012) 8.
- [18] J. Li, C. Zhang, X. Cheng, M. Qing, J. Xu, B. Wu, Y. Yang, Y. Li, *Appl. Catal. A Gen.* 464-465 (2013) 10.
- [19] D. Jain, C. Khatri, A. Rani, *Fuel* 90 (2011) 2083.
- [20] J. Climent, A. Corma, S. Iborra, A. Velty, *J. Mol. Catal. A Chem.* 183 (2002) 327.
- [21] T. Baba, *Catal. Surv. from Japan* 4 (2000) 17.
- [22] R. Bal, K. Chaudhari, S. Sivasanker, *Catal. Letters* 70 (2000) 75.
- [23] S. Sandesh, G. V Shanbhag, *Catal. Letters* 143 (2013) 1226.
- [24] K.T. Paul, S.K.S. Manna, I. Manna, K.K. Chakraborty, N. G B, *Nanoscale Res Lett.* 2 (2007) 397.
- [25] D. Jain, M. Mishra, A. Rani, *Fuel Process. Technol.* 95 (2012) 119.
- [26] D. Jain, A. Rani, *Am. Chem. Sci. J.* 1 (2011) 37.
- [27] D. Jain, R. Hada, A. Rani, *J. Catal.* 2013 (2013) 1.
- [28] H. Hattori, *Chem. Rev.* 95 (1995) 537.
- [29] H.A. Prescott, Z. Li, E. Kemnitz, A. Trunschke, J. Deutsch, 234 (2005) 119.
- [30] H. Keipour, M.A. Khalilzadeh, A. Hosseini, *Chinese Chem. Lett.* 23 (2012) 537.
- [31] J. Li, G. Chen, W. Xu, T. Li, *Ultrason. Sonochemistry* 10 (2003) 115.
- [32] H.S.P. Rao, S. Jothilingam, *J. Chem. Sci.* 117 (2005) 323.
- [33] B.D. Mather, K. Viswanathan, K.M. Miller, T.E. Long, *Prog. Polym. Sci.* 31 (2006) 487.
- [34] C. Mukherjee, Anup Kumar Misra, *J. Carbohydr. Chem.* 26 (2007) 213.
- [35] V. Padmavathi, D.R.C.V. Subbaiah, A. Balaiah, B.C.O. Reddy, A. Padmaja, *Indian J. Chem.* 44 (2005) 2569.
- [36] K. Kordatos, S. Gavela, A. Ntziouni, K.N. Pistiolas, A. Kyritsi, V.K. Rigopoulou, *Microporous Mesoporous Mater.* 115 (2008) 189.
- [37] R. Rahul, J.K. Satyarthi, D. Srinivas, *Indian J. Chem.* 50 (2011) 1017.

- [38] H. Ma, S. Li, B. Wang, R. Wang, S. Tian, *J. Am. Oil Chem. Soc.* 85 (2008) 263.
- [39] M.M.A. Sekkina, R.M. Issa, A.E.-D.M. Bastawisy, W.A. El Helece, *Int. J. Chem.* 2 (2010) 81.
- [40] B.J. Saikia, G. Parthasarathy, N.C. Sarmah, G.D. Baruah, *Indian Acad. Sci.* 31 (2008) 155.
- [41] T. Sugama, L. Ecker, T. Butcher, in: *Energy Sci. Technol. Dep. Brookhaven Natl. Lab. ,Upton, NY 11973-5000, United States, 2010*, pp. 1–23.
- [42] H. Handa, T. Baba, H. Sugisawa, Y. Ono, *J. Mol. Catal. A Chem.* 134 (1998) 171.
- [43] M.E.G. Frances I. Hurwitz, Denisse V. Aranda, in: *Am. Chem. Soc. 236th Natl. Meet. Philadelphia, PA, August 20, 2008, 2008*.
- [44] D. Kishore, S. Kannan, *J. Mol. Catal. A Chem.* 223 (2004) 225.
- [45] B. Yoosuk, P. Krasae, B. Puttasawat, P. Udomsap, N. Viriya-empikul, K. Faungnawakij, *Chem. Eng. J.* 162 (2010) 58.
- [46] I. Baginskiy, R.S. Liu, C.L. Wang, R.T. Lin, Y.J. Yao, *J. Electrochem. Soc.* 158 (2011) P118.
- [47] S.M. Nyale, O.O. Babajide, G.D. Birch, N. Böke, L.F. Petrik, *Procedia Environ. Sci.* 18 (2013) 722.
- [48] H. Hattori, *Appl. Catal. A Gen.* 222 (2001) 247.

*Barium Nitrate Activated Fly
Ash: Synthesis, Characterization
and Its Catalytic Application*

Abstract

Barium nitrate activated fly ash catalyst (BaTFA) has been synthesized by successive mechanical, thermal and chemical activation of fly ash. The prepared catalyst was characterized by using various activation techniques viz. N₂ adsorption-desorption study, Thermo gravimetric analysis, FTIR spectroscopy, X-ray diffraction analysis, Scanning electron microscopy, Energy dispersive X-ray analysis and Transmission electron microscopy. Hammett indicator method was used to determine the basic strength of the prepared catalyst. The catalytic behaviour of catalyst was investigated by Claisen-Schmidt condensation reaction of 4-chlorobenzaldehyde with acetophenone under optimized reaction conditions. The catalyst gave high conversion (90%) of 4-chlorobenzaldehyde. The BaTFA catalyst can be regenerated and reused up to four reaction cycles with almost equal efficiency. The conversion results show that the catalyst possesses sufficient stable active basic sites responsible for the catalytic activity.

5.1 Introduction

The Claisen-Schmidt reaction is a condensation reaction of aldehydes and carbonyl compounds leading to chalcones or α,β -unsaturated ketone compounds which possess diverse pharmacological activities [1]. Chalcones are potentially important synthetic intermediates for the preparation of flavonoids and various heterocyclic compounds. They also exhibit biological activities, including antimitotic, antimalarial, anticancer and anti-inflammatory activity [2].

The Claisen-Schmidt condensation reaction has been reported using a number of acid and base catalysts. The various types of base catalysts used are NaOH, KOH, Ba(OH)₂, LiHMDS, LiOH.H₂O and acids such as RuCl₃, TiCl₄, BF₃.OEt, dry HCl, SOCl₂-EtOH, Zn(bpy)(OAc)₂, ZrCl₄, bam-boo char sulfonic acid, BiCl₃, clay, ionic liquids and sulfonic acid-functional ionic liquids [3].

As far as alkaline earth metals are considered, basic strength and catalytic activity of respective metal oxides are found to be following order: BaO > SrO > CaO > MgO [4]. Various barium species has been reported as valuable catalytic material for a number of organic reactions viz. oxidative dehydrogenation of propane by barium hydroxyapatite [5], barium oxide as oxygen-selective adsorbent [6], rapeseed oil transesterification over barium-aluminium oxide catalyst [7], ammonia synthesis over Ba-Co/carbon catalyst [8], Wittig-Horner reaction and crossed Cannizzaro reaction using barium hydroxide etc. [9].

Most of the organic reaction mechanisms, for fine-chemical synthesis, involve carbanion intermediates. They are formed by abstraction of a proton from a C-H bond of an organic molecule by a base. Many organic reactions often require a stoichiometric amount of liquid base to generate carbanions. A number of drawbacks are associated with the use of liquid bases such as difficult separation from the reaction mixture after reaction, disposal problems, corrosive and harmful nature and tedious post reaction work up.

On the other hand heterogeneous base catalysts possess fewer disposal problems, easier separation from the reaction medium and easier recovery of the products. A fundamental feature from an industrial point of view is that they are non corrosive hence offer environmentally benign and more economical pathways for the synthesis of fine chemicals. Because of these advantages, now researchers

are focusing on the solid base catalyzed synthesis of fine chemicals and other industrially important organic compounds.

The properties and qualities of fly ash have been described in detail in **Chapter 4**. Studies report that fly ash; a silico–aluminate material could be a hopeful siliceous support material for solid base catalyst synthesis. So the present chapter deals with the synthesis and characterization of barium nitrate activated fly ash solid base catalyst. The catalytic activity of the prepared catalyst has been investigated by Claisen-Schmidt condensation reaction of 4-chlorobenzaldehyde with acetophenone. Mechanically, thermally and chemically activated fly ash has been converted into atom-efficient, stable, recyclable and easily separable solid base catalyst. The Claisen-Schmidt reaction was carried out in a conventional batch reactor in single step, liquid phase and solvent free reaction conditions and catalyst was reused up to four reaction cycles with approximately similar efficiency. Thus the prepared catalyst could be a promising candidate to provide a new path for the use of extensively available fly ash in synthesis of proficient solid base catalyst.

5.2 Experimental

5.2.1 Materials

Fly ash was collected from Jamshedpur Thermal Power Station, Jamshedpur (Jharkhand). All chemicals $\text{Ba}(\text{NO}_3)_2$ (99%), NaOH (98%), Na_2CO_3 (98%) were purchased from Sigma Aldrich and various aldehydes and carbonyl compounds were purchased from S.D. Fine Chemical Ltd., India. All reagents used were of analytical grade and used as such.

5.2.2 Catalyst synthesis

As received fly ash (FA) was mechanically activated by using high energy planetary ball mill. 30 h milled FA showed the higher specific surface area, also called as mechanically activated fly ash (MFA), was selected for further activations. Thermally activated fly ash (TFA) was formed by thermally activating MFA at 800 °C for 3 h, consequently C, S, moisture and other impurities also get removed [10]. An aqueous solution of $\text{Ba}(\text{NO}_3)_2$ (15 wt%

loading) was added into 10 g TFA. Then the mixture was constantly stirred for 1 h at 90 °C. Precipitation was done by dropwise addition of mixture of NaOH (3M) and Na₂CO₃ (2M) solution (in 1:1 ratio) up to pH = 8 in the above mixture. The resultant slurry was aged for 24 h then filtered and washed with double distilled water up to a pH 7 to remove leached compounds, air dried at 110 °C for 24 h and calcined at 400 °C for 3 h in a muffle furnace under static conditions to form barium nitrate activated fly ash catalyst (BaTFA) (**Scheme 5.1**).

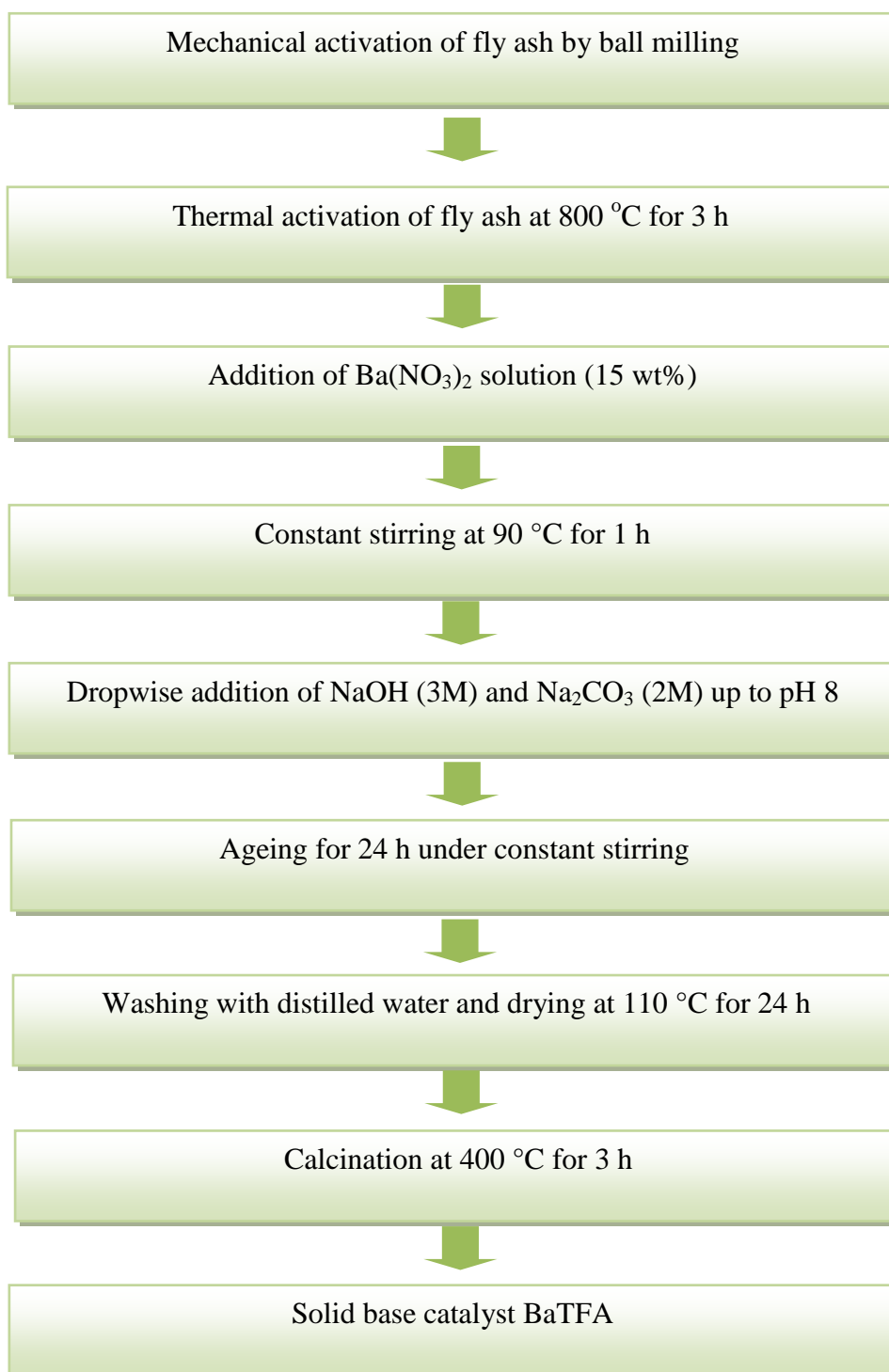
5.3 Catalyst characterization

The synthesized FA, MFA, TFA and BaTFA were characterized by N₂ adsorption-desorption, TGA, FTIR, XRD, SEM-EDX and TEM techniques. Instruments details and operating conditions during the characterization are given in **Annexure I**.

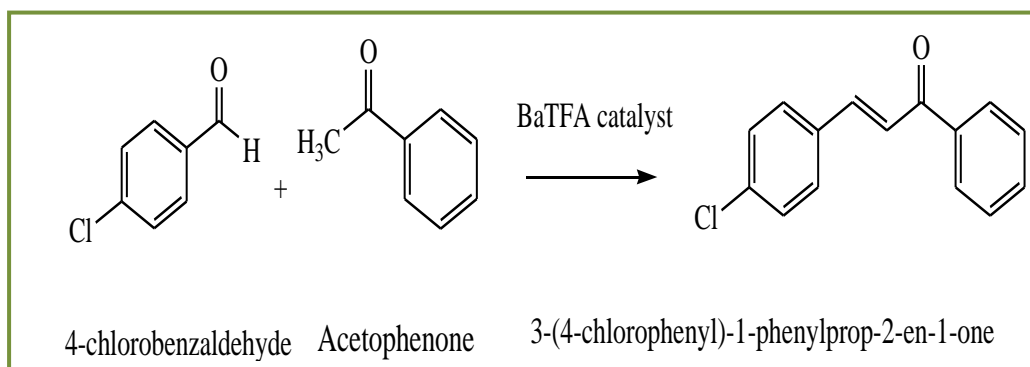
Hammett indicators like phenolphthalein (pK_a=8.2), Nile blue (pK_a=9.7), 2,4,6-trinitroaniline (pK_a=12.2), 2,4-dinitroaniline (pK_a=15) and 4-nitroaniline (pK_a=18.4) were used to evaluate the basic strength of BaTFA. Basicity was measured by a benzoic acid titration method using phenolphthalein indicator [11]. The methods for evaluating basic strength and basicity are given in detail in **Chapter 2**.

5.4 Catalytic activity of BaTFA catalyst

The catalytic activity of BaTFA was investigated by Claisen-Schmidt condensation reaction of 4-chlorobenzaldehyde with acetophenone as shown in **Scheme 5.2**. The reaction produces 3-(4-chlorophenyl)-1-phenylprop-2-en-1-one also known as 4-chlorochalcone. The reaction was carried out in a liquid phase batch reactor under optimized reaction conditions.



Scheme 5.1: Synthesis of solid base catalyst BaTFA.



Scheme 5.2: Claisen-Schmidt condensation reaction of 4-chlorobenzaldehyde with acetophenone over BaTFA.

In the procedure, 4-chlorobenzaldehyde and acetophenone in 2:1 to 1:3 molar ratios were taken in a 250 mL round bottom flask, equipped with magnetic stirrer and condenser, immersed in a constant temperature oil bath. The activated solid base catalyst BaTFA (preheated at 400 °C for 2 h) during the study was added to the reaction mixture. The substrate (acetophenone) to catalyst weight ratio ranged from 10:1 to 2.5:1. The reaction mixture was heated at required reaction temperature ranging from 90-150 °C and time from 1-5 h at atmospheric pressure in solvent free liquid phase reaction conditions.

After completion of the reaction (TLC monitoring), the mixture was cooled and filtered to separate the catalyst. The product was analyzed by Gas Chromatograph.

The conversion of 4-chlorobenzaldehyde and yield were calculated by using weight percent method.

$$\text{Conversion (wt\%)} = 100 \times (\text{Initial wt\%} - \text{Final wt\%}) / \text{Initial wt\%}$$

$$\text{Yield \% of 3-(4-chlorophenyl)-1-phenylprop-2-en-1-one obtained} =$$

$$100 \times \frac{\text{g of 3-(4-chlorophenyl)-1-phenylprop-2-en-1-one obtained experimentally}}{\text{g of 3-(4-chlorophenyl)-1-phenylprop-2-en-1-one obtained theoretically}}$$

5.5 Catalyst regeneration

The spent catalyst was filtered out by simple filtration method, thoroughly washed with acetone and dried at 110 °C for 12 h followed by thermal activation at 400 °C for 2 h in muffle furnace before reuse in next reaction cycles under reaction conditions similar to previous cycle.

5.6 Results and discussion

5.6.1 Chemical composition of FA and BaTFA catalyst

The chemical compositions of fly ash (FA) and BaTFA as determined by SEM-EDX are given in **Table 5.1**. The LOI of FA has been found to be 5 wt%, by heating a certain weighed quantity of FA in muffle furnace at 800 °C for 3 h. As it is clear from **Table 5.1** that BaO present in FA is beyond the detection limit of the instrument but in Case of BaTFA, due to the significant role of chemical activation, BaO percentage was increased up to 4.45%. The chemical activation results in the loss of other components slightly during the treatment with Ba(NO₃)₂, other constituents may be dissolved and leached during the catalyst preparation. The increased Ba is accountable for the generation of a number of Ba-SiO₂/CO₃/Al-SiO₂/OH phases, thus increases the catalytic activity and basicity in the BaTFA catalyst for Claisen-Schmidt condensation reaction.

Table 5.1: Chemical composition of FA and BaTFA.

Chemical components	FA (Wt%)	BaTFA (Wt%)
SiO ₂	59.42	58.82
Al ₂ O ₃	18.79	16.96
Fe ₂ O ₃	6.91	6.57
CaO	2.56	2.38
MgO	1.84	1.72
K ₂ O	2.37	1.93
Na ₂ O	3.84	3.66
TiO ₂	1.27	0.92
BaO	-	4.45
Other elements	3	2.5

5.6.2 Surface area results

Specific surface areas of all sample determined by N₂ adsorption-desorptions are given in **Table 5.2**. Specific surface area of FA is considerably increased on mechanical activation and reaches upto 30.02 m²/g for MFA while it decreases after thermal activation and reaches up to 28.47 m²/g. Spherical particles of FA break during the mechanical activation which results in increased surface area. The crystallite size of FA and MFA were found to be 33 nm and 18 nm respectively.

As it is clear from the pore distribution curve and obtained result that MFA contains mesopores and macropores (**Figure 5.1**). But the presence of mesopores are found to be greater than the macropores. Average pore volume of MFA is 4.76 nm, depicts its mesoporous nature, but the presence of macropores upto a limit can not be ignored totally. This interesting results are confirming the transition of macropores to mesopores during mechanical activation step.

As far as isotherm is considered, it is showing a resemblance with Type II and III, and conferring the transition of macroporous to mesoporous behaviour. For fly ash, it is not possible to get any of the ideal type of isotherm due to availability of heterogeneous particles with large variation in size, shape and porosity arrangements (**Figure 5.2**) [12].

The BET plots are observed with linear fragment/range for saturation pressure range (0.08- 0.32) i.e. the pressure observed over (P/P₀ value) for the BET equation, which resembles to most of the inorganic silica material (**Figure 5.3**).

The chemical activation of TFA results into decreased surface area due to the blockage of its small pores by loading of Ba species [13]. In BaTFA catalyst, decrease in the surface area facilitates the generation of surface active basic sites thus catalytic activity (**Figure 5.4**).

Table 5.2: Surface area of all catalytic materials.

Catalyst	Specific surface area (m ² /g)
FA	9.18
FA (10 h milled)	15.14
FA (20 h milled)	22.54
MFA	30.02
TFA	28.47
BaTFA	23.77

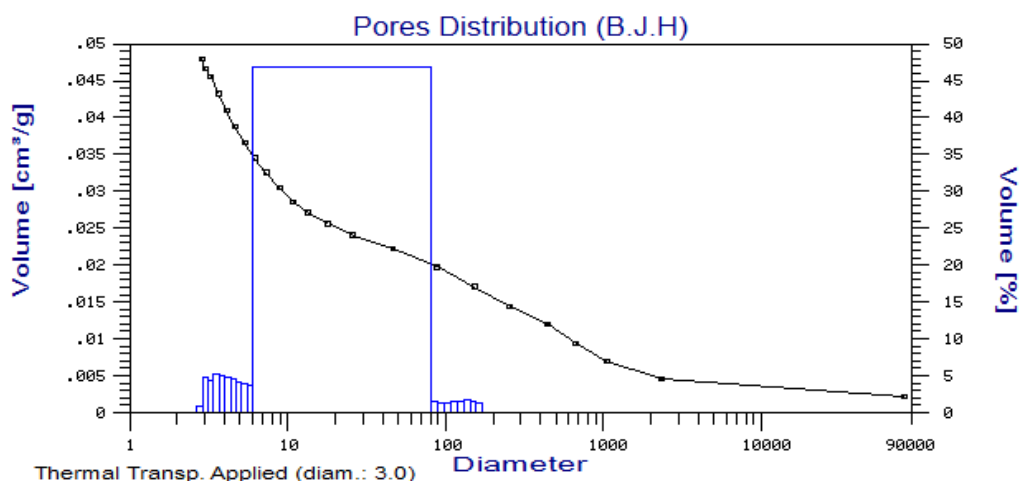


Figure 5.1: Pore distribution curve (B.J.H.) of MFA.

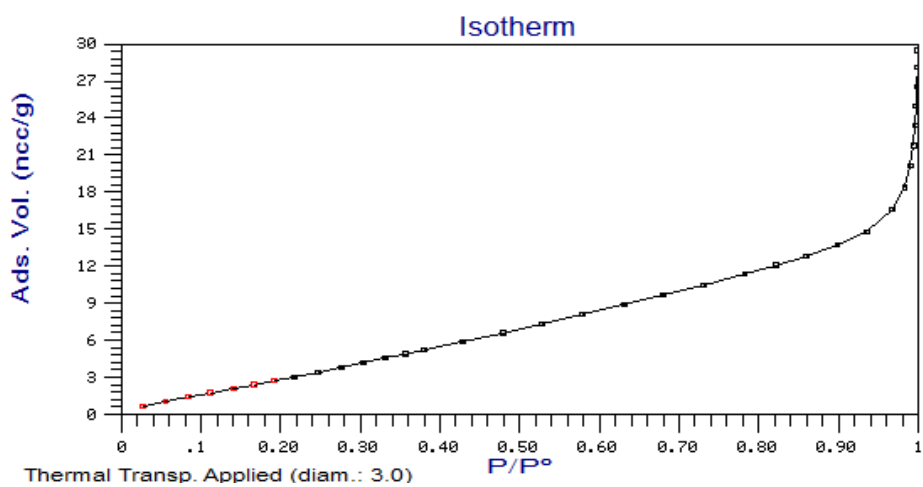


Figure 5.2: Isotherm curve of MFA.

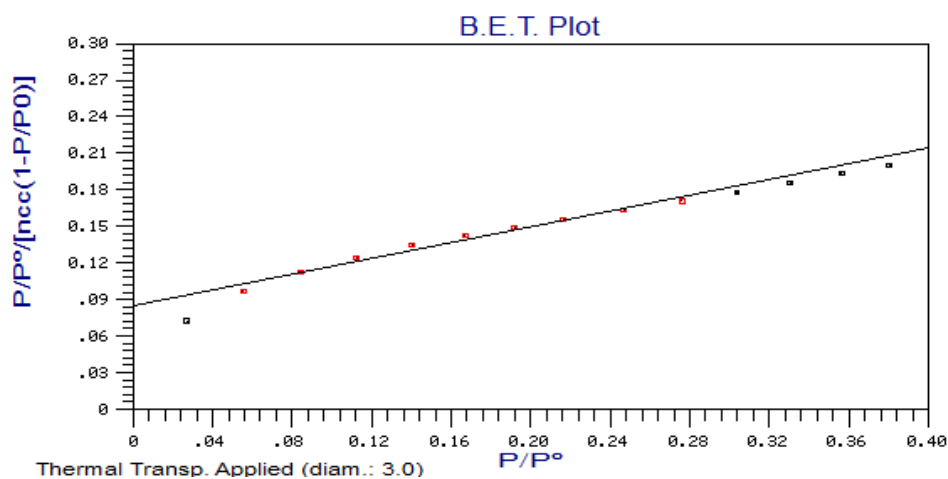


Figure 5.3: B.E.T. plot of MFA.

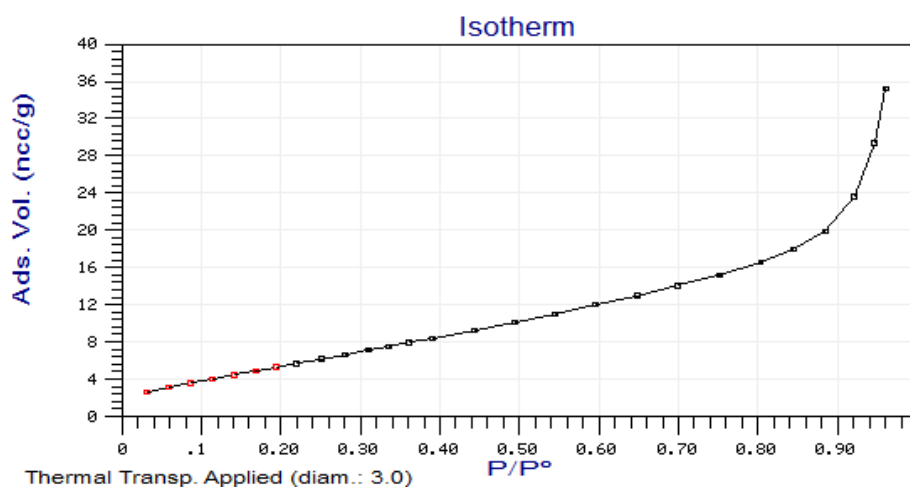


Figure 5.4: Isotherm curve of BaTFA.

5.6.3 Thermogravimetric analysis

TGA curves of FA and BaTFA (Figure 5.5) show weight loss of 5.96% and 2% respectively, within the temperature range 50-1000°C, are attributed to water loss and burning of carbonaceous materials and volatilization of some trace metal oxides and other impurities [14]. Precursor $\text{Ba}(\text{NO}_3)_2$ can attain any of the phases like $\text{Ba}(\text{OH})_2$, BaO , $\text{Ba-SiO}_2/\text{Al-SiO}_2$ and BaCO_3 during the catalyst synthesis. So the slight weight loss in BaTFA may be assigned to the decomposition of $\text{Ba}(\text{NO}_3)_2$, $\text{Ba}(\text{OH})_2$ and BaCO_3 .

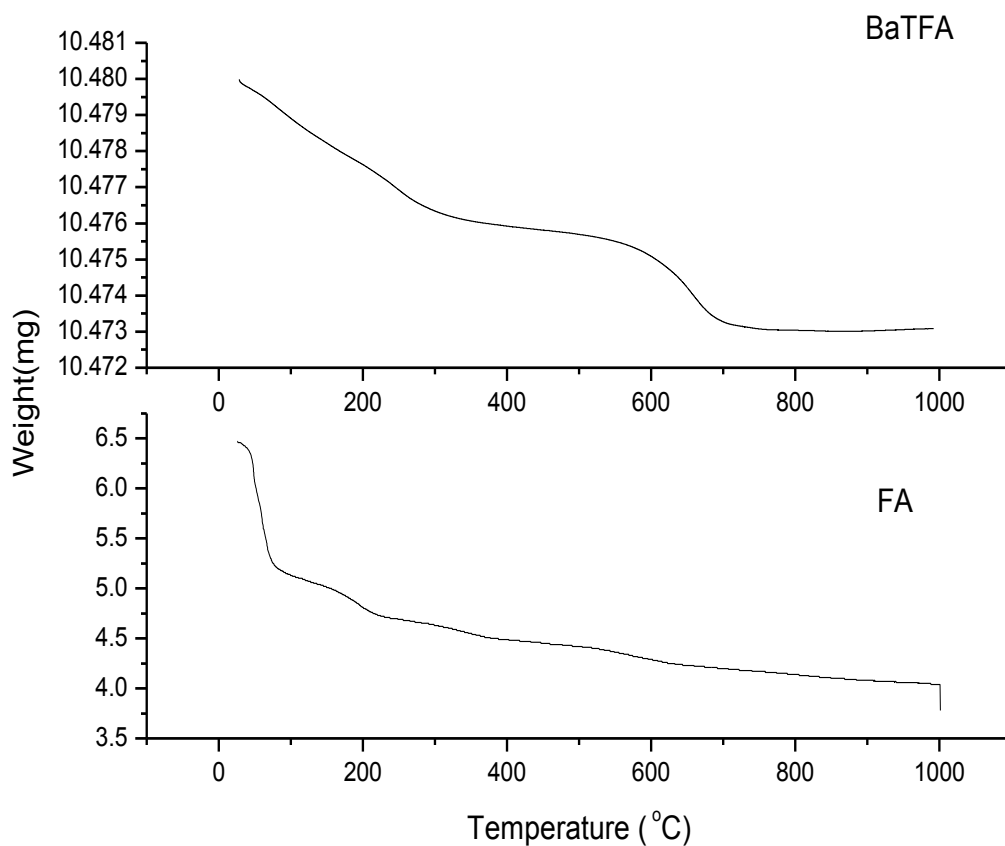


Figure 5.5: TGA curves of (a) FA and (b) BaTFA.

5.6.4 FTIR studies

The FTIR spectra of FA, MFA and TFA are given in the **Figure 5.6**. All spectra show a broad band between $3000\text{--}3600\text{ cm}^{-1}$, attributed to --O-H stretching vibration of surface silanol groups (Si-OH) [15]. Increase in intensity and broadness of this region in case of MFA is an evidence for the breaking of spherical silica particles and formation of Si-OH groups and the presence of strong H- bonding after milling [16]. Thermal activation causes the decrease in intensity and broadness due to loss of adsorbed water in TFA [17]. A peak centered at 1608 cm^{-1} , present in all samples is assigned to bending mode ($\delta_{\text{O-H}}$) of water molecules (**Figure 5.6, 5.7**) [18]. A small peak around 2830 cm^{-1} is assigned to --C-H stretching vibration of organic contaminants present in all the samples (**Table 5.3**) [19]. Peaks at 1986 and 1872 cm^{-1} (**Figure 5.6, Table 5.3**) are assigned to silica as possible quartz [20]. Peaks centered at 1521 and 1681 cm^{-1} are due to $(\text{CO}_3)^{2-}$ stretching vibration, visible in all spectra, show the highest

intensity in FA and get reduced after thermal activation confirming the removal of carbonate or carbonate like species during thermal activation [21,22]. A broad band between 1103-1165 cm^{-1} is attributed to Si-O-Si asymmetric stretching vibration [22]. A peak at approx $\sim 600 \text{ cm}^{-1}$ is attributed to Si-O-Al stretching vibration (**Figure 5.6, 5.7**) [23].

FTIR spectrum of BaTFA (**Figure 5.7b**) shows the broader and much intense band in the region of 3000-3600 cm^{-1} as compared to TFA. The increased intensity could be assigned to generation of Si-OH groups as well as to Si/Al-O-Ba-OH groups during the chemical activation while H-bonding is responsible for the broadness of the band between these groups. The increased OH groups are responsible for the Bronsted basic sites which initiate the reaction by abstracting the proton from methyl group [24]. There is also possibility of BaO, Ba(OH)₂ and BaCO₃ formation on TFA surface [25]. In BaTFA clearly visible sharp band centered at 1435 cm^{-1} is assigned to different Ba species, confirms the proper loading of Ba in different chemical phases [26]. Ba(OH)₂ and BaCO₃ formation could be assigned due to the absorption of water vapour [27] and CO₂ from environment [28] by BaO compound or they may generate during the catalyst synthesis step.

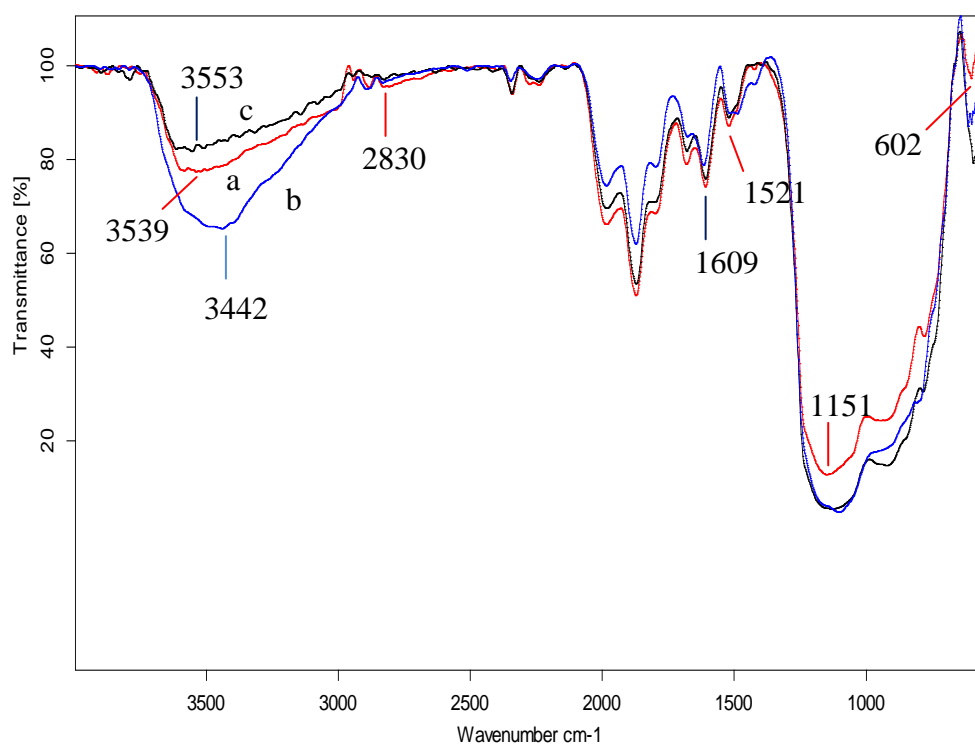


Figure 5.6: FTIR spectra of (a) FA, (b) MFA and (c) TFA.

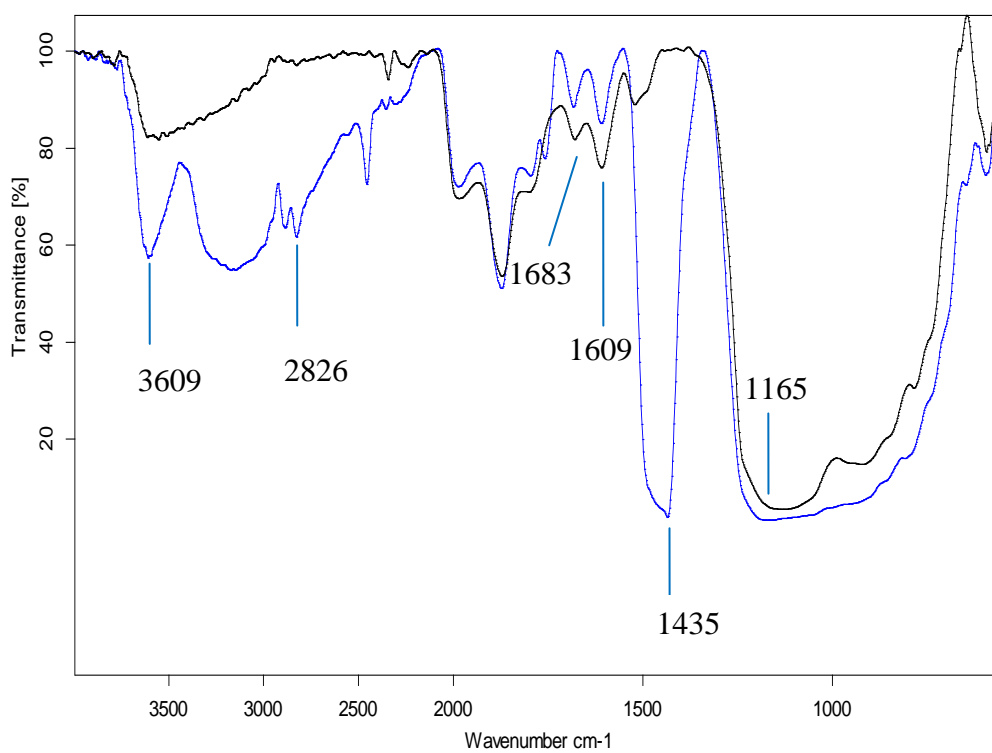


Figure 5.7: FTIR spectra of (a) TFA and (b) BaTFA.

Table 5.3: The observed transmission frequencies (cm^{-1}) of Fourier transform infrared spectra of FA, MFA, TFA, BaTFA and reused BaTFA and their assignments.

Assignments	RFA	MFA	TFA	BaTFA	Reused BaTFA	Ref.
Si-O-Al stretching vibration	602	601	594	596	595	23
Si-O-Si asymm. stretching vibration	1151	1103	1129	1165	1118	22
(CO₃)²⁻ stretching vibration	1521, 1681	1521	1521, 1679	1683	1680	21, 22
H-O-H bending vibration	1609	1616	1608	1609	1607	18
-C-H stretching vibration	2830	2854	2827	2826	2827	19
-O-H stretching vibration	3539	3442	3553	3609	3611	15

5.6.5 X-ray diffraction studies

The XRD patterns of FA, MFA, TFA and BaTFA are given in **Figure 5.8**. Quartz exhibits peaks at $2\theta = 20.7^\circ$, 26.5° , 40.66° and 49.96° (SiO_2 , ICDD pdf number 000-46-1045) while peaks at $2\theta = 33.4^\circ$ and 16.4° confirm the presence of calcite (CaCO_3 , ICDD pdf number, 47-1743) and mullite ($\text{Al}_6\text{Si}_2\text{O}_{13}$, ICDD pdf number 000-15-0776) respectively in all XRD patterns (**Figure 5.8**). After mechanical activation of FA peak intensities of crystalline phases like quartz, mullite and calcite get decreased (**Figure 5.8b**). Contrary on thermal activation respective peaks of different phases like quartz, mullite and calcite become more

intense and sharper while magnetite (Fe_3O_4 , ICDD pdf number, 19-0629) peak at $2\theta = 34.85^\circ$ (**Figure 5.8a-b**) tends to disappear and converts into hematite phase (Fe_2O_3 , ICDD pdf number, 33-0664) at high temperature treatment (**Figure 5.8c**). In BaTFA, presence of a broad peak at around $2\theta = 24^\circ$ confirms availability of witherite (BaCO_3 , JCPDS file no. 71-2394) [29] and hexacelsian ($\text{BaAl}_2\text{Si}_2\text{O}_8$, JCPDS files No 88-1049) [30,31]. Peaks around 24° , 42° , 45° and 47° are assigned to barium silicate ($\text{BaSi}_2\text{O}_5 \cdot (\text{H}_2\text{O})_3$) [32] while combined small peaks at $2\theta = 32.7^\circ$ and 33.04° are attributed to barium silicates (BaSi_2O_5 , Ba_2SiO_4) [26] and BaO [33]. The XRD results are in good agreement with the TEM, SEM and FTIR results.

5.6.6 SEM analysis results

Figure 5.9 shows the surface morphologies of FA, MFA, TFA and BaTFA samples. It can be seen that fly ash mainly consists of spherical particles with smooth outer surfaces and irregularly shaped unburned carbon particles [34]. During mechanical activation spherical shaped particles of FA break into irregular shaped particles as depicted in **Figure 5.9b**, which form clumps and convert into agglomerated particles during thermal activation **Figure 5.9c**, this agglomeration is the main reason of additional crystallinity which is clearly visible in the XRD pattern of TFA. Shiny clumps of hexacelsian, witherite and barium oxide on TFA surface (**Figure 5.9d**) confirm successful loading of Ba in the above mentioned forms on TFA surface.

5.6.7 TEM analysis results

TEM image of FA shows a completely spherical, fine and smooth particle of fly ash which has been reduced in size after mechanical activation (**Figure 5.10b**). So, mechanical activation is accountable for the complete removal of smoothness and sphericity. BaTFA (**Figure 5.10**) shows dark spots of loaded Ba species (**Figure 5.10c**) and rod like grains could be assigned to hexacelsian ($\text{BaAl}_2\text{Si}_2\text{O}_8$) (**Figure 5.10d**) [27, 28], BaCO_3 [35] and BaO [36] .

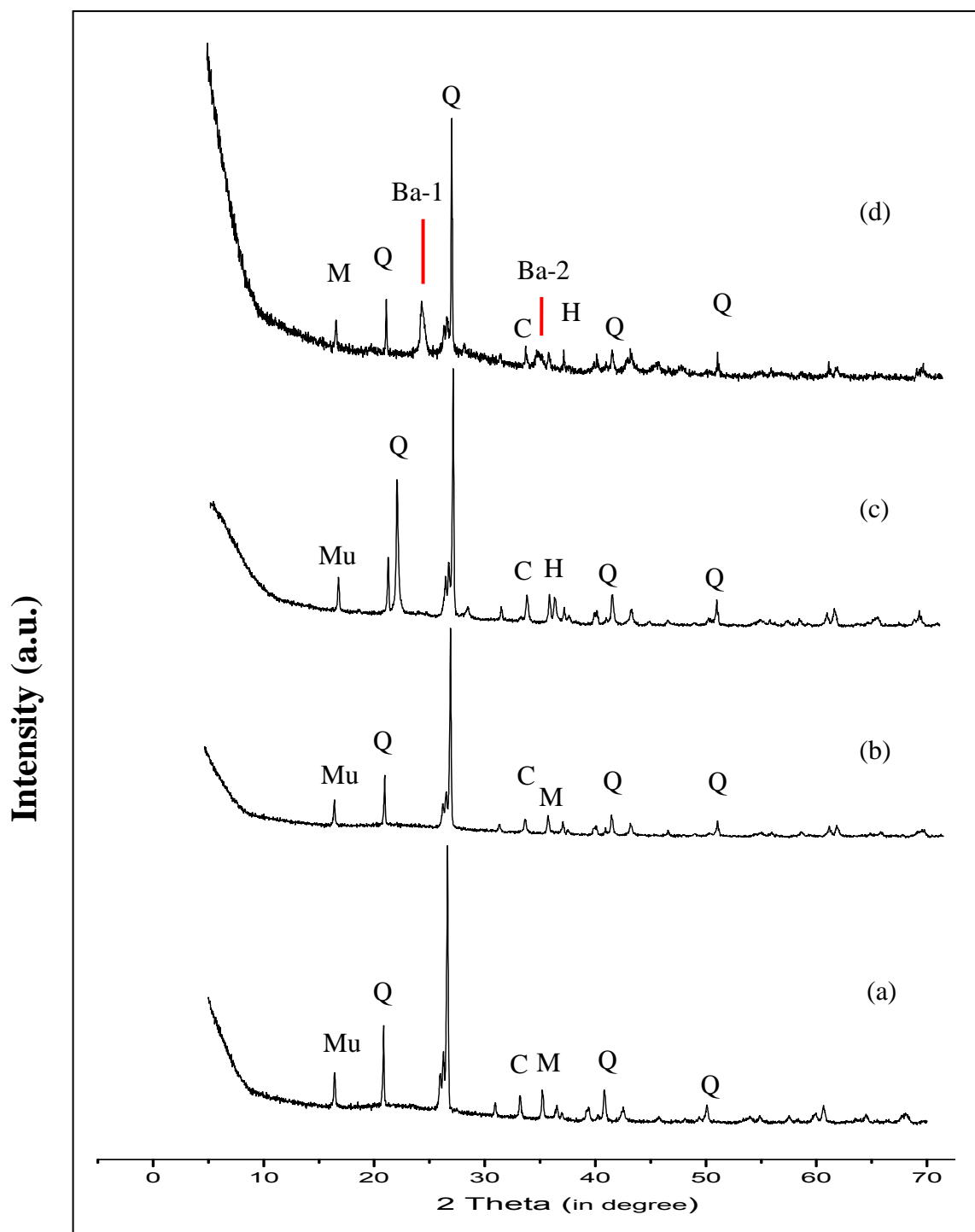


Figure 5.8: XRD patterns of (a) FA, (b) MFA, (c) TFA and (d) BaTFA.

[Mu = Mullite, Q = Quartz, C = Calcite, M = Magnetite, H = Hematite, Ba-1 = Hexacelsian ($\text{BaAl}_2\text{Si}_2\text{O}_8$), witherite (BaCO_3) and barium silicate ($\text{BaSi}_2\text{O}_5 \cdot (\text{H}_2\text{O})_3$), Ba-2 = Barium silicate (BaSi_2O_5 , Ba_2SiO_4) and BaO]

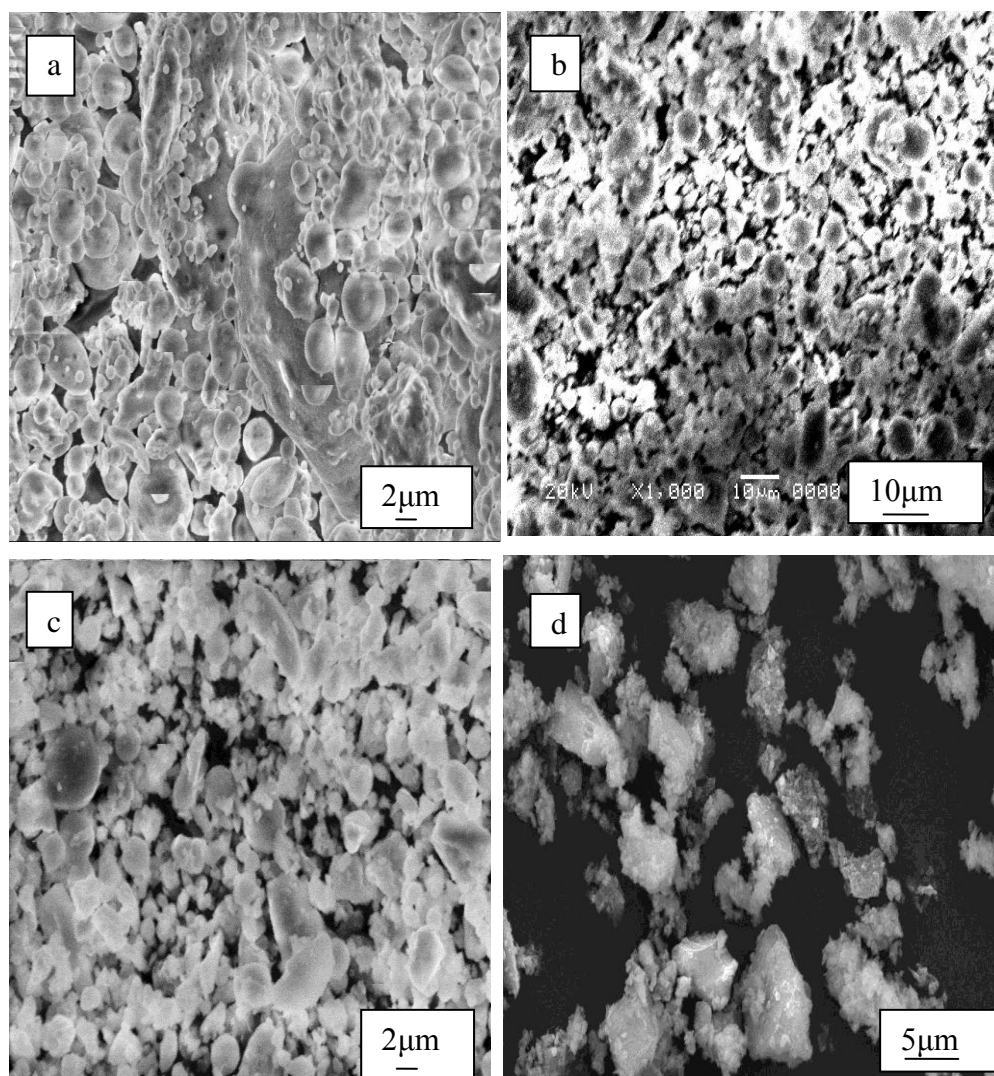


Figure 5.9: SEM micrographs of (a) FA, (b) MFA, (c) TFA and (d) BaTFA.

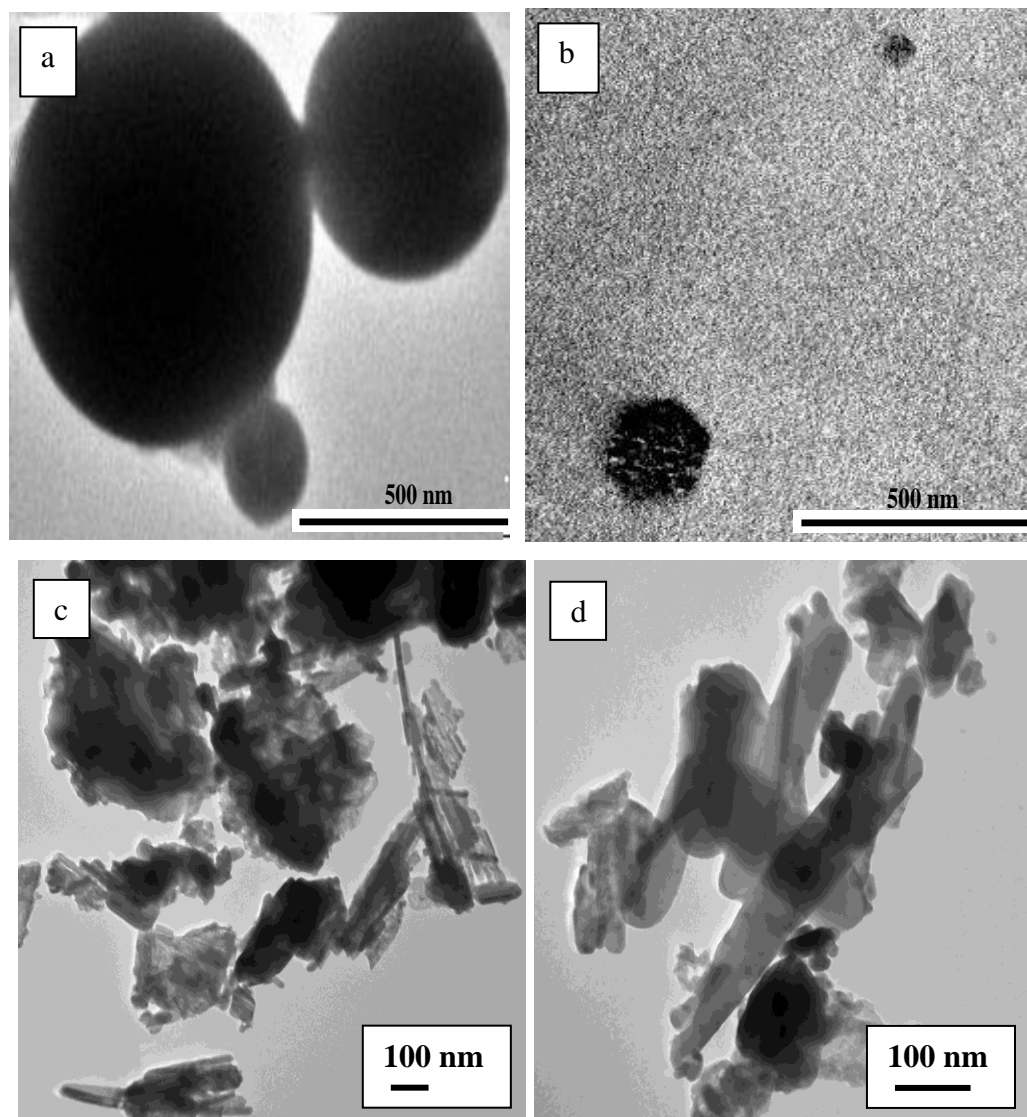


Figure 5.10: TEM images of (a) FA (b) MFA and (c-d) BaTFA.

5.6.8 Basic strength and basicity measurement

The base strength and basicity of BaTFA were determined by the Hammett indicator method. BaTFA shows basic strength $15 < H_a < 18.4$ and basicity 1.5 mmol/g.

5.7 Catalytic activity

The catalytic activity of BaTFA catalyst was investigated by Claisen-Schmidt condensation reaction of acetophenone with 4-chlorobenzaldehyde in batch reactor under optimized reaction conditions.

Results summarized in **Table 5.4** show that FA, MFA and TFA do not show any catalytic activity for Claisen-Schmidt condensation reaction while BaTFA catalyst under the given reaction conditions, showed maximum activity. On catalyst surface super basic sites $Ba^{2+}O^{2-}$ can exist at high temperature while Bronsted basic sites Ba-OH can exist at low temperature. Claisen-Schmidt condensation reaction is Bronsted base (-OH) catalyzed reaction. Therefore BaTFA catalyst is sufficiently active for the same reaction even at low calcination temperature at 400 °C, owing high amount of Bronsted basic sites Ba-OH [4]. Various parameters such as reactant molar ratio, amount of catalyst, reaction time and temperature were optimized, for getting the maximum catalytic activity, conversion and yield of desired product.

5.7.1 Effect of reaction time

The effect of reaction time variation on the conversion (%) of 4-chlorobenzaldehyde and product yield was studied in time range of 1-5 h at 130 °C by taking 4-chlorobenzaldehyde/acetophenone molar ratio 1:1 and acetophenone to catalyst weight ratio 5:1. The conversion continuously increased up to 90 % in initial 3 h and remained constant for the next 2 h (**Figure 5.11**). The optimized reaction time was found to be 3 h for the reaction.

Table 5.4: Catalytic activity of FA, MFA, TFA and BaTFA for Claisen-Schmidt condensation reaction of 4-chlorobenzaldehyde with acetophenone.

Catalyst	Conversion (%) of 4-chlorobenzaldehyde	Isolated yield (%) of 4-chloroalcone
FA	Nil	Nil
MFA	Nil	Nil
TFA	Nil	Nil
BaTFA	77	73

Reaction conditions: Temperature 130 °C, Time 3 h, 4-chlorobenzaldehyde/acetophenone molar ratio 1:1, substrate/catalyst weight ratio 5:1.

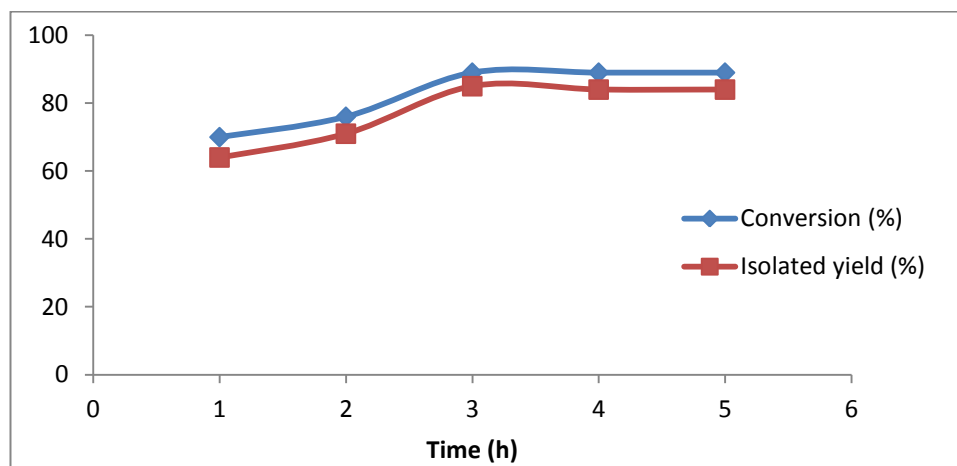


Figure 5.11: Variation in isolated yield (%) and conversion (%) of 4-chlorobenzaldehyde with time.

Reaction conditions: Temperature 130 °C, 4-chlorobenzaldehyde/acetophenone molar ratio 1:1, substrate/catalyst weight ratio 5:1.

5.7.2 Effect of reaction temperature

Optimization of reaction temperature for maximum conversion (%) and isolated yield (%) was carried out at temperature ranging from 90 °C to 150 °C for 3 h taking 4-chlorobenzaldehyde/acetophenone molar ratio of 1:1 while substrate

to catalyst weight ratio was 5:1. Conversion and yield were observed to increase on increasing reaction temperature ranging from 90 °C to 130 °C as depicted from **Figure 5.12**. The results show that the maximum conversion (90%) of 4-chlorobenzaldehyde and isolated yield (86%) of 4-chlorochalcone were found at 130 °C, after which conversion and isolated yield (%) remain almost steady till 150 °C.

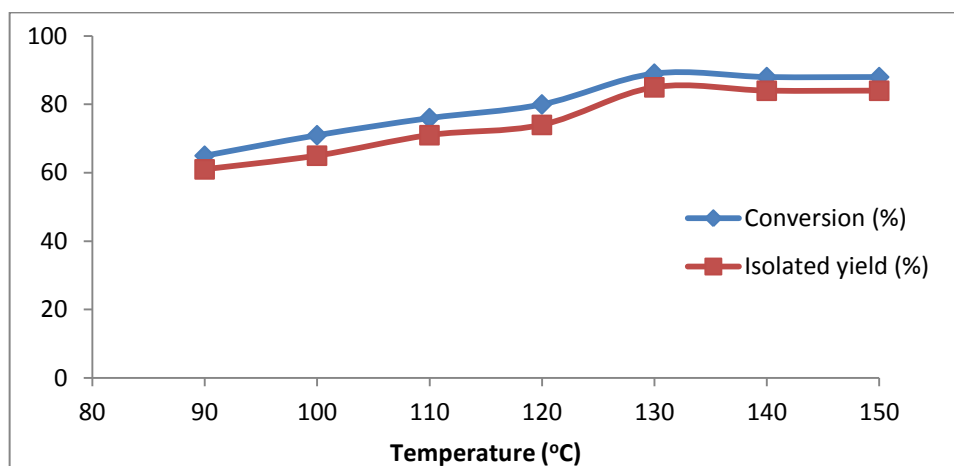


Figure 5.12: Variation in isolated yield (%) and conversion (%) of 4-chlorobenzaldehyde with temperature.

Reaction conditions: Time 3 h, 4-chlorobenzaldehyde/acetophenone molar ratio 1:1, substrate/catalyst weight ratio 5:1.

5.7.3 Effect of substrate/catalyst weight ratio

The influence of substrate to catalyst weight ratio on conversion and isolated yield (%) was studied by varying the amount of BaTFA catalyst under optimized reaction conditions. Only 77% conversion of 4-chlorobenzaldehyde is achieved at 2-cyclohexenone/BaTFA weight ratio 10:1 while conversion reached to 90% in case of 5:1 substrate/catalyst weight ratio. The increase in conversion, with increase in the catalyst weight can be attributed to an increase in the availability of number of catalytic active sites required for Claisen-Schmidt condensation reaction. On further increase in the amount of catalyst no changes in conversion and isolated yield (%) were observed (**Figure 5.13**).

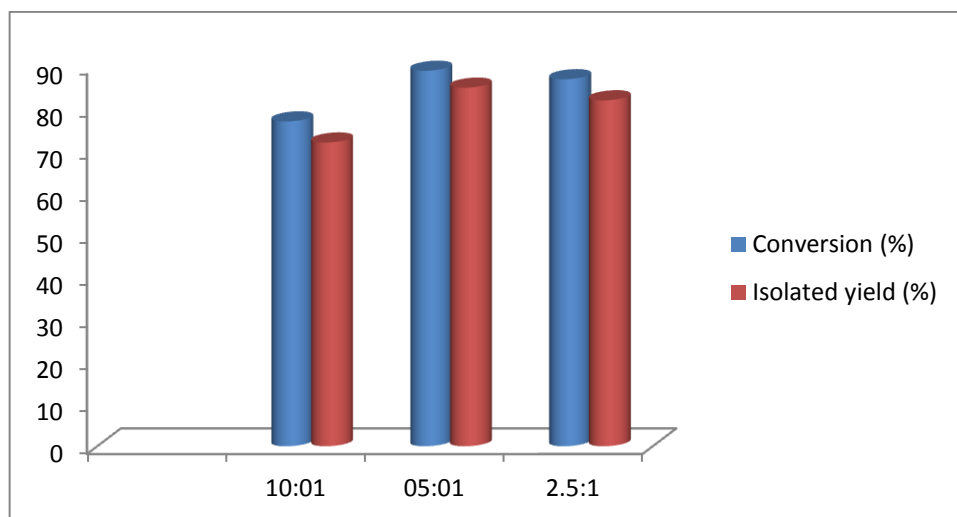


Figure 5.13: Effect of substrate/catalyst weight ratio on conversion (%) of 4-chlorobenzaldehyde and isolated yield (%) of 4-chlorochoalcone over BaTFA.

Reaction conditions: Temperature 130 °C, Time 3 h, 4-chlorobenzaldehyde/acetophenone molar ratio 1:1.

5.7.4 Effect of reactant molar ratio

The effect of reactant's molar ratio was studied in order to attain the most favorable molar ratio for the reaction. As indicated by **Figure 5.14**, 62 % conversion of 4-chlorobenzaldehyde was observed at 2:1 molar ratio of 4-chlorobenzaldehyde to 2-cyclohexenone. This may be due to insufficient quantity of the reactants to react with each other. There was an increase in conversion up to 90% at 1:1 molar ratio of 4-chlorobenzaldehyde to acetophenone at the same reaction conditions. This may be due to satisfactory reactant quantity on the basic sites of the BaTFA catalyst surface. The conversion decreased from 90-87% on further increasing the molar ratio from 1:2 to 1:3 which could be attributed to the lacking of 4-chlorobenzaldehyde or self condensation of acetophenone.

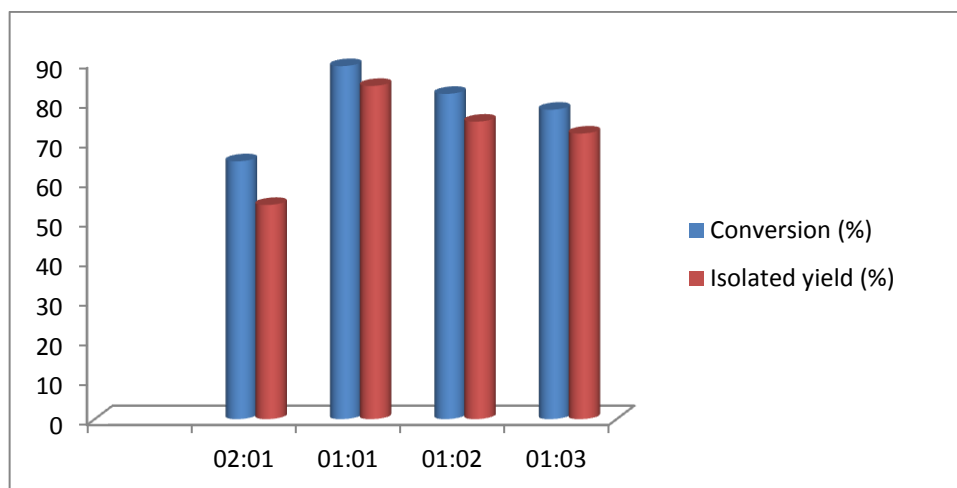


Figure 5.14: Effect of molar ratio of 4-chlorobenzaldehyde/acetophenone on conversion (%) of 4-chlorobenzaldehyde and isolated yield (%) of 4-chlorochalcone over BaTFA.

Reaction conditions: Temperature 130 °C, Time 3 h, substrate/catalyst weight ratio 5:1.

5.8 Reaction mechanism

The plausible structure of BaTFA catalyst surface is shown in **Scheme 5.3**. The reaction mechanism over BaTFA catalyst shows that Claisen-Schmidt is a condensation reaction (**Scheme 5.4**) [9]. Surface active Bronsted basic sites (-Ba-OH) abstract proton from acetophenone and form anion. The nucleophilic addition of the formed anion to the 4-chlorobenzaldehyde, followed by the successive protonation and dehydration produces 3-(4-chlorophenyl)-1-phenylprop-2-en-1-one or 4-chlorochalcone [37].

5.9 Catalyst regeneration

The regeneration reaction reflects that BaTFA catalyst can be regenerated by simple thermal regeneration method and retains the catalyst activity. The regenerated catalyst was found to be having similar activity as fresh catalyst for consecutive four reaction cycles, giving 86-79% yield (**Table 5.5**) for Claisen-Schmidt condensation of acetophenone with 4-chlorobenzaldehyde. The FTIR spectrum of reused BaTFA catalyst after five reaction cycles (**Figure 5.15b**) resembles that of fresh BaTFA catalyst (**Figure 5.15a**) indicating the stability of

surface hydroxyl groups responsible for Bronsted basic sites thus catalytic activity. Due to the stability of these basic sites BaTFA catalyst was found efficient up to five reaction cycles giving almost similar yield. The gradual decrease in yield after five reaction cycles is due to the deposition of carbonaceous material on the surface of the reused catalyst which may block the active basic sites of BaTFA catalyst.

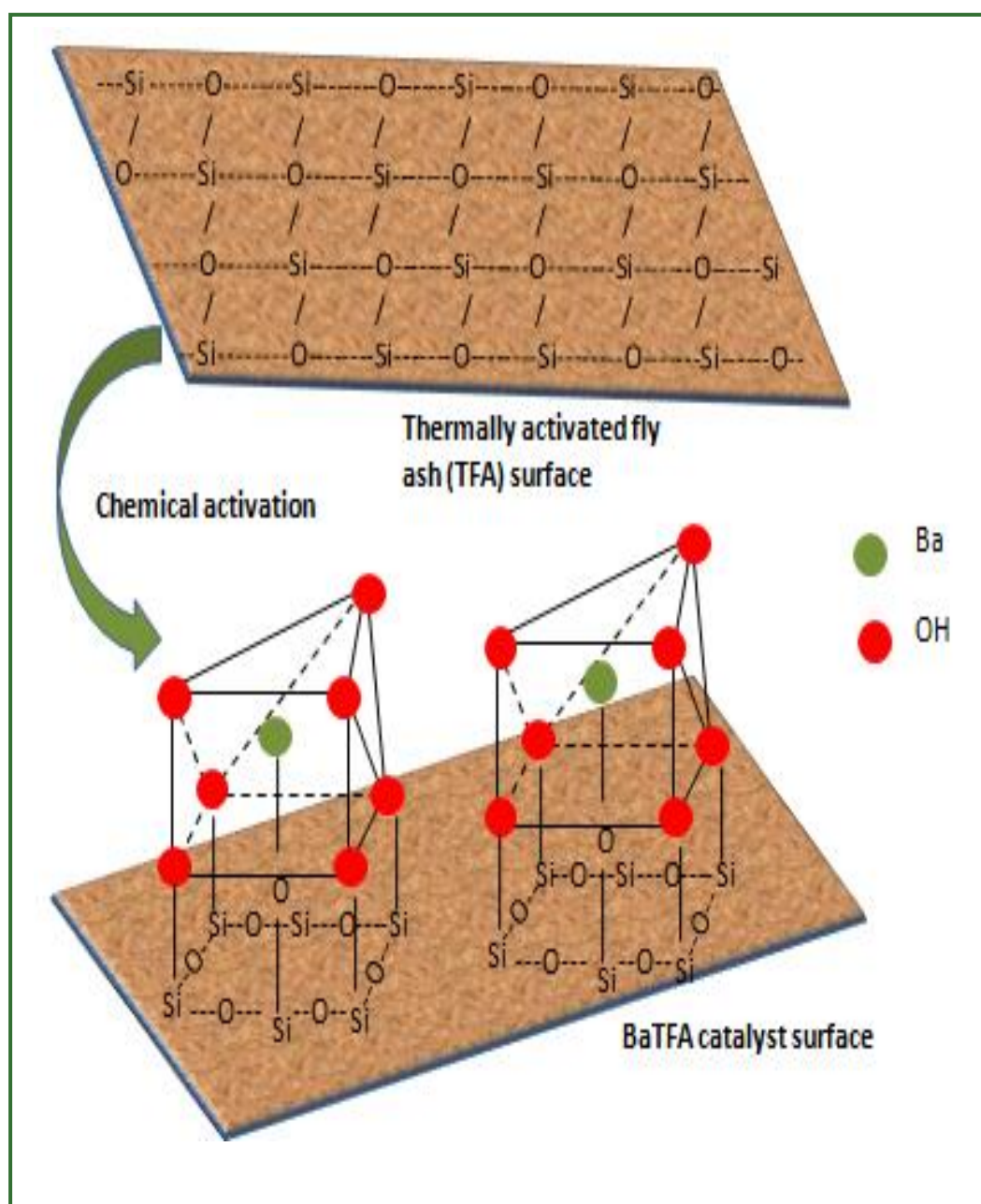
Leaching test was done using hot filtration technique. The catalyst was removed after 30 min and the reaction was continued to completion but no further product was formed. This led us to the conclusion that no leaching occurs with the catalysts used and under the conditions applied in the present investigation.

Table 5.5: Catalytic activity of fresh and regenerated BaTFA catalyst for Claisen-Schmidt condensation of 4-chlorobenzaldehyde with acetophenone.

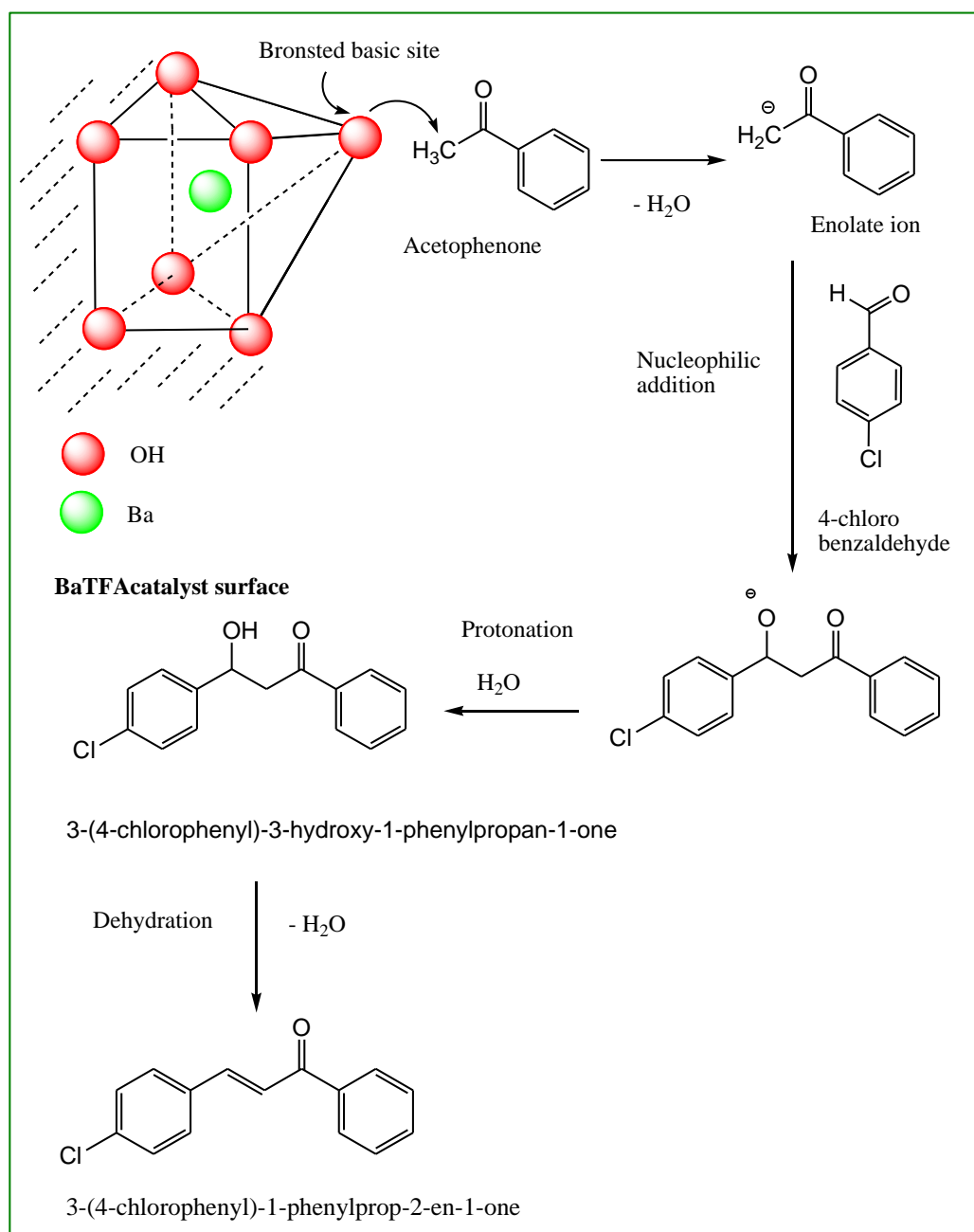
Reaction Cycle	Isolated yield (%)
I	86
II	83
III	80
IV	80
V	79

Reaction conditions: Temperature 130 °C, Time 3 h, substrate/catalyst weight ratio 5:1, 4-chlorobenzaldehyde/acetophenone molar ratio 1:1.

We extend the study of Claisen-Schmidt reaction to various substrates, including different aromatic aldehydes and ketone compounds. The results are listed in **Table 5.6**. All the reactions occurred in solvent free conditions within 3-3.5 h at 130 °C maintaining the reactant molar ratio 1:1, substrate/catalyst weight ratio 5:1.



Scheme 5.3: The schematic presentation of chemical activation of TFA with $\text{Ba}(\text{NO}_3)_2$ and proposed structure of BaTFA.



Scheme 5.4: Proposed mechanism for Claisen-Schmidt condensation reaction of 4-chlorobenzaldehyde with acetophenone over BaTFA.

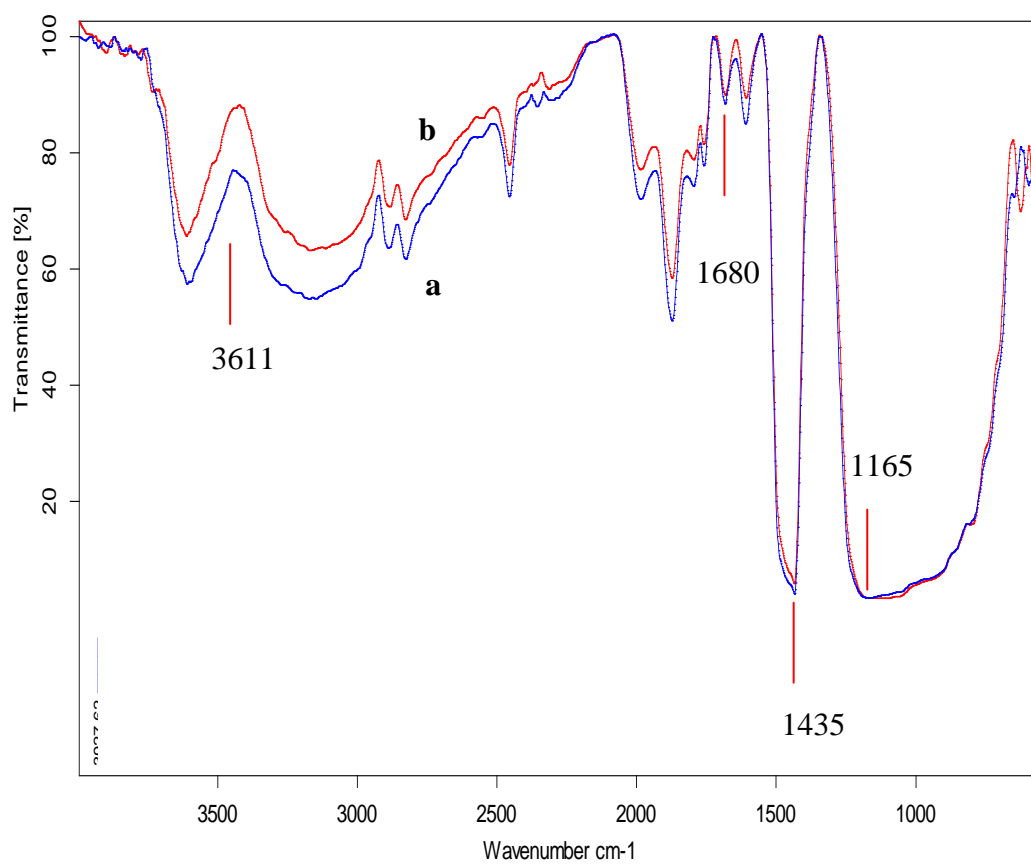


Figure 5.15: FTIR spectra of (a) BaTFA and (b) Reused BaTFA.

Table 5.6: Claisen-Schmidt condensation of various aromatic aldehyde with ketones in presence of BaTFA.

Entry	Ketone	Aromatic Aldehyde	Product	Time (h)	Isolated Yield (%)
1				3	85
2				3.5	94
3				3	85

Reaction conditions: Temperature 130 °C, substrate/catalyst weight ratio 5:1, 4-chlorobenzaldehyde/acetophenone molar ratio 1:1.

5.10 Conclusion

The recyclable solid base catalyst BaTFA has been synthesized in this chapter. The use of fly ash as solid support material makes the catalyst cost effective as well as provides a path for the utilization of fly ash, which is increasing day by day at an alarming rate. The characterization results prove the catalyst as efficient for base catalyzed reactions. The catalytic activity of BaTFA has been investigated by Claisen-Schmidt condensation reaction. The prepared catalyst has stable Bronsted basic sites i.e. -Ba-OH content, was recovered, regenerated and reused with no noticeable changes in the yield, confirming almost negligible leaching of active basic sites or slight deactivation of the catalyst under

the mentioned reaction conditions. So, the prepared BaTFA catalyst is stable, eco-friendly, cost effective, reusable, easily recoverable and suitable for the production of 4-chlorochalcone.

5.11 References

- [1] A. Gómez-rivera, H. Aguilar-mariscal, N. Romero-ceronio, L.F. Roa-de, C.E. Lobato-garcía, *Bioorg. Med. Chem. Lett.* 23 (2013) 5519.
- [2] A. Davoodnia, G. Yassaghi, *Chinese J. Catal.* 33 (2012) 1950.
- [3] J.K. Rajput, G. Kaur, *Tetrahedron Lett.* 53 (2012) 646.
- [4] G. Zhang, H. Hattori, K. Tanabe, *Appl. Catal.* 36 (1988) 189.
- [5] S. Sugiyama, T. Shono, E. Nitta, H. Hayashi, *Appl. Catal. A Gen.* 211 (2001) 123.
- [6] J. Park, Y. Cho, K. Yi, S. Han, S. Cho, *Appl. Surf. Sci.* 256 (2010) 5528.
- [7] S.G. Zavarukhin, A.S. Ivanova, R.G. Kukushkin, A.N. Simonov, O. V Sherstyuk, V.A. Yakovlev, L.I. Trusov, *Catal. Ind.* 5 (2013) 342.
- [8] W. Raróg-pilecka, E. Miskiewicz, L. Kepinski, Z. Kaszkur, K. Kielar, Z. Kowalczyk, *J. Catal.* 249 (2007) 24.
- [9] A. Aguilera, A.R. Alcantara, J.M. Marinas, J. V Sinisterra, *Can. J. Chem.* 65 (1987) 1165.
- [10] K. Kordatos, S. Gavela, A. Ntziouni, K.N. Pistiolas, A. Kyritsi, V.K. Rigopoulou, *Microporous Mesoporous Mater.* 115 (2008) 189.
- [11] R. Rahul, J.K. Satyarthi, D. Srinivas, *Indian J. Chem.* 50 (2011) 1017.
- [12] J.B. Condon, *Surface Area and Porosity Determinations by Physisorption Measurements and Theory*, First edit, Elsevier, Netherlands, 2006.
- [13] H. Ma, S. Li, B. Wang, R. Wang, S. Tian, *J. Am. Oil Chem. Soc.* 85 (2008) 263.
- [14] M.M.A. Sekkina, R.M. Issa, A.E.-D.M. Bastawisy, W.A. El Helece, *Int. J. Chem.* 2 (2010) 81.
- [15] D. Jain, A. Rani, *Am. Chem. Sci. J.* 1 (2011) 37.
- [16] C. Khatri, A. Rani, *Fuel* 87 (2008) 2886.
- [17] D. Jain, C. Khatri, A. Rani, *Fuel* 90 (2011) 2083.

- [18] S. Kabra, S. Katara, A. Rani, *Int. J. Innov. Res. Sci. Eng. Technol.* 2 (2013) 4319.
- [19] S. Katara, S. Kabra, A. Sharma, R. Hada, A. Rani, *Int. Res. J. Pure Appl. Chem.* 3 (2013) 299.
- [20] T. Sugama, L. Ecker, T. Butcher, in: *Energy Sci. Technol. Dep. Brookhaven Natl. Lab. ,Upton, NY 11973-5000, United States, 2010*, pp. 1–23.
- [21] H. Handa, T. Baba, H. Sugisawa, Y. Ono, *J. Mol. Catal. A Chem.* 134 (1998) 171.
- [22] B.J. Saikia, G. Parthasarathy, N.C. Sarmah, G.D. Baruah, *Indian Acad. Sci.* 31 (2008) 155.
- [23] M.E.G. Frances I. Hurwitz, Denisse V. Aranda, in: *Am. Chem. Soc. 236th Natl. Meet. Philadelphia, PA, August 20, 2008, 2008*.
- [24] D. Kishore, S. Kannan, *J. Mol. Catal. A Chem.* 223 (2004) 225.
- [25] A.P.S. Dias, J. Bernardo, P. Felizardo, M.J.N. Correia, *Fuel Process. Technol.* 102 (2012) 146.
- [26] E. Kaya, N. Oktar, G. Karakas, K. Murtezaoglu, *Turkish J. Chem.* 34 (2010) 935.
- [27] B. Yoosuk, P. Krasae, B. Puttasawat, P. Udomsap, N. Viriya-empikul, K. Faungnawakij, *Chem. Eng. J.* 162 (2010) 58.
- [28] A.M. Frey, J. Yang, C. Feche, N. Essayem, D.R. Stellwagen, F. Figueras, K.P. de Jong, J.H. Bitter, *J. Catal.* 305 (2013) 1.
- [29] M.R. Rezaie, H.R. Rezaie, R. Naghizadeh, *Ceram. Int.* 35 (2009) 2235.
- [30] C.M. López-badillo, J. López-cuevas, C.A. Gutiérrez-chavarría, *J. Eur. Ceram. Soc.* 33 (2013) 3287.
- [31] P. Namwong, N. Laorodphan, W. Thiemsorn, *Chiang Mai J. Sci.* 2010 37 (2010) 231.
- [32] E. Sadic, O. Taspinar, O. Ozcan, *Fresenius Environ. Bull.* 19 (2010) 2823.
- [33] J. Park, Y. Cho, K. Yi, S. Han, S. Cho, *Appl. Surf. Sci.* 256 (2010) 5528.
- [34] S.M. Nyale, O.O. Babajide, G.D. Birch, N. Böke, L.F. Petrik, *Procedia Environ. Sci.* 18 (2013) 722.

- [35] M. Shamsipur, S.M. Pourmortazavi, S.S. Hajimirsadeghic, M. Roushanid, Colloids Surfaces A Physicochem. Eng. Asp. 423 (2013) 35.
- [36] G. Suresh, P.N. Nirmala, Turkish J. Phys. 36 (2012) 392.
- [37] H. Hattori, Appl. Catal. A Gen. 222 (2001) 247.

*Silica Enrichment in Fly Ash and
Synthesis of Solid Base Catalyst
for Claisen-Schmidt
Condensation Reaction*

Abstract

Fly ash has been converted into silica enriched fly ash (SFA) and CaSFA catalyst by successively following mechanical, thermal and chemical activation. The prepared catalytic materials were characterized by using various analytical techniques viz. N_2 adsorption-desorption study, TGA, FTIR, XRD, SEM-EDX and TEM. The basic strength of the prepared CaSFA catalyst was determined by Hammett indicator method. The catalytic activity of catalyst was evaluated by Claisen-Schmidt condensation reaction of 4-methylbenzaldehyde with acetophenone under optimized reaction conditions. The catalyst gave high conversion (94%) of 4-methylbenzaldehyde. The CaSFA catalyst can be regenerated and reused up to four reaction cycles with almost equal efficiency. The conversion results show that the catalyst possesses sufficient stable active basic sites responsible for the catalytic activity. The work reports a novel application of abundantly available siliceous solid waste material fly ash in synthesis of silica enriched material and catalytic applications.

6.1 Introduction

Silica is a functional material that is used to improve surfaces and mechanical properties of many materials. Precipitated silica, is a white fluffy powder with amorphous nature, does not show a health hazard with respect to lung tumour or silicosis [1]. Generally, precipitated amorphous SiO_2 can be produced by chemical reaction between aqueous solution of sodium metasilicate and a mineral acid [2]. Precipitated silica has surface area in the range of 150-200 m^2/g , bulk density 120-200 g/litre and loss on ignition 3-6% [3]. Primary SiO_2 particles are ~15 to ~30 nm in size. These particles show a tendency to aggregate and form ~160 nm size secondary particles [2]. Precipitated SiO_2 has found various applications as absorbent, drying powder, support material for heterogeneous catalysts synthesis, anticorrosion agent, filler in rubber and plastics, additives in varnishes, paints and glues, insulation materials. In addition, amorphous silica is also used in the production of free-flowing powders for food stuffs, animal feeds, pharmaceuticals and cosmetics [2, 3]. Tetraethylorthosilicate (TEOS) is widely used in commercial silica synthesis, commercial silica is amorphous in nature [4]. Besides TEOS, amorphous silica has been extracted from a number of bio-wastes eg. rice husk ash [5], corn cob ash [6], bagasse ash [7] etc. Silica supported solid catalysts for catalyzing different organic reactions are well preceded in the literature viz. alkali metal supported silica for vapour phase O-methylation of 2-naphthol [8], silica supported ammonium acetate ($\text{NH}_4\text{OAc}/\text{SiO}_2$) catalyst for Knoevenagel condensation between aldehydes or ketones and active methylene compound [9], Li-Ba/ SiO_2 catalyst for conversion of methane [10] and silica supported cinchona alkaloids as heterogeneous catalysts for asymmetric Michael reaction [11].

The Claisen-Schmidt reaction is a condensation reaction of aldehydes and carbonyl compounds leading to chalcones. Chalcones are important synthetic intermediates for the preparation of flavonoids and various heterocyclic compounds. They also exhibit biological activities including antimitotic, antimalarial, anticancer and anti-inflammatory activity [12].

Fly ash is a aluminosilicate material, abundantly available by product of thermal power plants and having ~70% SiO_2 content, was thought to be explored

as a material for silica enrichment as well as for modification in surfacial properties by silica enrichment with removal of other accessory metal oxides. The physicochemical properties of prepared silica enriched fly ash (SFA) were characterized by using different characterization techniques. The prepared material has also been used to synthesize solid base catalyst by treating with $\text{Ca}(\text{NO}_3)_2$ solution. Catalytic activity of prepared silica catalyst was evaluated by Claisen-Schmidt condensation reaction of 4-methylbenzaldehyde with acetophenone in single step, liquid phase and solvent free reaction conditions. Thus the present work brings into light the use of fly ash for synthesis of silica enriched material which could be a significant alternative of commercial silica which can be utilized as support material for heterogeneous catalyst synthesis.

6.2 Experimental

6.2.1 Materials

Fly ash was collected from Jamshedpur Thermal Power Station, Jamshedpur (Jharkhand). All chemicals NaOH (98%), Na_2CO_3 (98%) $\text{Ca}(\text{NO}_3)_2$ (99%) were purchased from Sigma Aldrich and acetophenone and 4-methoxybenzaldehyde were purchased from S.D. Fine Chemical Ltd., India. All reagents used were of analytical grade and used as such.

6.2.2 Catalyst synthesis

As received FA was mechanically activated by using high energy planetary ball mill (Retsch PM-100, Germany) in an agate jar with 5mm diameter agate balls for 30 h at 250 rotation/minute speed to increase the surface area as well as surface active sites. Milled FA showed the higher specific surface area, also called as mechanically activated fly ash (MFA), was selected for further activations. MFA was thermally activated at 800 °C for 3 h to form thermally activated fly ash (TFA), consequently C, S, moisture and other impurities also get removed [13]. An aqueous solution of NaOH (6 M, 60 mL) was added into 10 g TFA. Then the mixture was constantly stirred for 3 days at 90 °C. Precipitation was done by dropwise addition of 5 N H_2SO_4 up to pH 7 in the above mixture at room temperature. The resultant slurry was aged for 24 h then filtered and washed

with double distilled water up to pH 7 to remove leached compounds and sodium sulphate. Now the silica enriched fly ash (SFA) was air dried at 110 °C for 24 h.

To prepare solid base catalyst from SFA, $\text{Ca}(\text{NO}_3)_2$ solution (15 wt%) was added into 10 g, 800 °C for 3 h thermally activated SFA. Then the mixture was constantly stirred for 1 h at 90 °C. Precipitation was done by dropwise addition of mixture of NaOH (3M) and Na_2CO_3 (2M) solution (in 1:1 ratio) up to pH 8 in the above mixture. The resultant slurry was aged for 24 h then filtered and washed with double distilled water up to pH 7 to remove leached compounds, air dried at 110 °C for 24 h and calcined at 500 °C for 3 h in a muffle furnace under static conditions to form CaSFA solid base catalyst.

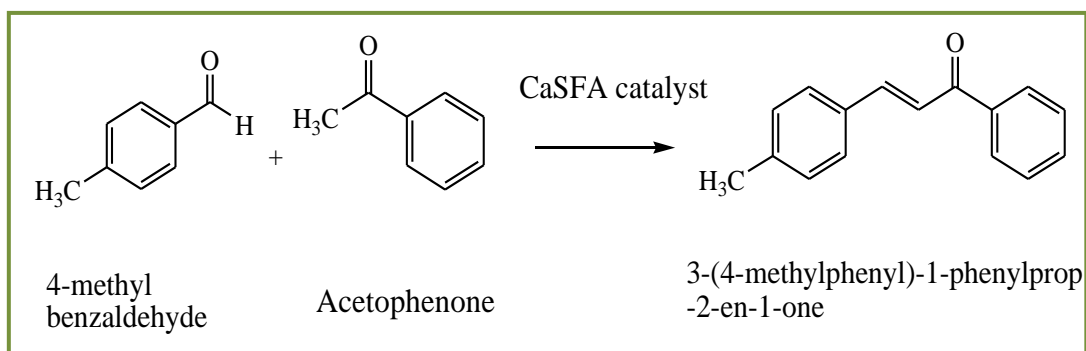
6.3 Catalyst characterization

The synthesized FA, MFA, TFA, SFA, thermally activated SFA and CaSFA were characterized by N_2 adsorption-desorption study, TGA, FTIR, XRD, SEM-EDX and TEM techniques. Instrumental details and operating conditions during the characterization are given in **Annexure I**.

Hammett indicator method was used to evaluate the basic strength of CaSFA catalyst. Basicity was measured by a benzoic acid titration method using phenolphthalein indicator [14]. The methods for evaluating basic strength and basicity are given in detail in **Chapter 2**.

6.4 Catalytic activity of CaSFA catalyst

The catalytic activity of CaSFA was investigated by Claisen-Schmidt condensation reaction of 4-methylbenzaldehyde with acetophenone as shown in **Scheme 6.1**. The reaction produces 3-(4-methylphenyl)-1-phenylprop-2-en-1-one also known as 4-methylchalcone. The reaction was carried out in a liquid phase batch reactor under optimized reaction conditions.



Scheme 6.1: Claisen-Schmidt condensation reaction of 4-methylbenzaldehyde with acetophenone over CaSFA.

The condensation of 4-methylbenzaldehyde with acetophenone was performed in a liquid phase batch reactor consisting of 250 mL round bottom flask equipped with digital magnetic stirrer and glass condenser, immersed in a constant temperature oil bath. In the procedure, 4-methylbenzaldehyde and acetophenone in 2:1 to 1:3 molar ratios were taken in a round bottom flask. The desired amount of CaSFA catalyst (preheated at 500 °C for 2 h), was taken according to substrate/catalyst weight ratio ranging from 10:1 to 2.5:1. The reaction mixture was heated at required reaction temperature ranging from 100-150 °C and time from 1-5 h at atmospheric pressure in solvent free liquid phase reaction conditions.

After completion of the reaction (TLC monitoring), the mixture was cooled and filtered to separate the catalyst. The product was analyzed by Gas Chromatograph.

The conversion of 4-methylbenzaldehyde and yield were calculated by using weight percent method.

$$\text{Conversion (wt\%)} = 100 \times (\text{Initial wt\%} - \text{Final wt\%}) / \text{Initial wt\%}$$

Yield % of 3-(4-methylphenyl)-1-phenylprop-2-en-1-one obtained =

$$100 \times \frac{\text{g of 3-(4-methylphenyl)-1-phenylprop-2-en-1-one obtained experimentally}}{\text{g of 3-(4-methylphenyl)-1-phenylprop-2-en-1-one obtained theoretically}}$$

6.5 Catalyst regeneration

After initial use, the spent catalyst was filtered out by simple filtration method, thoroughly washed with acetone and dried at 110 °C for 12 h followed by thermal activation at 500 °C for 2 h in muffle furnace before reuse in next reaction cycles under similar reaction conditions as earlier.

6.6 Results and discussion

6.6.1 Chemical composition of FA, SFA and CaSFA catalyst

The chemical compositions of FA, SFA and CaSFA as determined by SEM-EDX are given in **Table 6.1**. The LOI of FA is found to be 5 wt%, at 800 °C for 3 h. As it is clear from **Table 6.1** that in SFA, silica content increases from 59.42% to 76.63% while percentage of other metal oxides get decreased. It may be concluded that some other metal oxides are dissolved in NaOH solution and leach out during washing steps and results in increased silica content. After chemical treatment of SFA with Ca(NO₃)₂, CaO content increases in CaSFA 0.71% to 6.42%. The increased Ca generates basic sites in CaSFA as well as catalytic activity for Claisen-Schmidt condensation reaction.

6.6.2 Surface area results

Specific surface areas of all sample determined by N₂ adsorption-desorption are given in **Table 6.2**. Specific surface area of FA is 9.18 m²/g, considerably increases after mechanical activation and reaches up to 30.02 m²/g for MFA. The specific surface area again increases from TFA to SFA, from 28.47 m²/g to 65.78 m²/g, gets reduced after chemical activation with Ca(NO₃)₂ and reaches to 59.23 m²/g in CaSFA. The blockage of SFA small pores by loading of

different Ca species leads the reduction in surface area and confirms significant chemical activation by $\text{Ca}(\text{NO}_3)_2$.

Table 6.1: Chemical composition of FA, SFA and CaSFA.

Chemical components	FA (Wt%)	SFA (Wt%)	CaSFA (Wt%)
SiO₂	59.42	76.63	75.10
Al₂O₃	18.79	16.24	13.74
Fe₂O₃	6.91	3.18	1.89
CaO	2.56	0.71	6.42
MgO	1.84	0.46	0.30
K₂O	2.37	0.64	0.59
Na₂O	3.84	0.98	0.95
TiO₂	1.27	0.14	0.11
Other elements	3	1.2	0.9

Table 6.2: Surface area of all catalytic materials.

Catalyst	Specific surface area (m²/g)
FA	9.18
MFA	30.02
TFA	28.47
SFA	65.78
CaSFA	59.23

6.6.3 Thermogravimetric analysis

TGA curves of FA, SFA and CaSFA (**Figure 6.1**) show weight loss of 5.96% and 6.10% and 12.96% respectively, within the temperature range 50-1000°C, are attributed to water loss and burning of carbonaceous materials and volatilization of some trace metal oxides and other impurities [15]. Precursor

$\text{Ca}(\text{NO}_3)_2$ can attain any of the phases like $\text{Ca}(\text{OH})_2$, CaO , Ca-SiO_2 and CaCO_3 during the catalyst synthesis. So the slight weight loss in CaSFA may be assigned to the decomposition of these phases.

6.6.4 FTIR studies

The FTIR spectra of TFA, SFA and thermally activated SFA are given in the **Figure 6.2**. All spectra show a broad band between $3000\text{-}3600\text{ cm}^{-1}$, attributed to -O-H stretching vibration of surface silanol groups (Si-OH) [16]. Increase in intensity and broadness of this region in case of SFA is an evidence for the breaking of spherical silica particles and formation of Si-OH groups and the presence of strong H- bonding after precipitation. In case of thermally activated SFA, thermal activation causes the decrease in intensity and broadness due to loss of adsorbed water in SFA [17]. A peak centered around 1630 cm^{-1} , present in all samples is assigned to bending mode ($\delta_{\text{O-H}}$) of water molecules (**Figure 6.2, 6.3**) [18]. A small peak in TFA around 2827 cm^{-1} is assigned to -C-H stretching vibration of organic contaminants present in TFA (**Table 6.3**) [19]. Peaks centered at 1521 and 1679 cm^{-1} are due to $(\text{CO}_3)^{2-}$ stretching vibration, visible in all spectra [20, 21]. A broad band between $1129\text{-}1168\text{ cm}^{-1}$ is attributed to Si-O-Si asymmetric stretching vibration [21]. A peak at approx $\sim 600\text{ cm}^{-1}$ is attributed to Si-O-Al stretching vibration (**Figure 6.2, 6.3**) [22].

FTIR spectrum of CaSFA (**Figure 6.3c**) shows the broader and much intense band in the region of $3000\text{-}3600\text{ cm}^{-1}$ as compared to SFA samples. The increased intensity could be assigned to generation of Si-OH groups and Si/Al-O-Ca-OH groups during the chemical activation while H- bonding is responsible for the broadness of the band between these groups. The increased OH groups are responsible for the Bronsted basic sites which initiate the reaction by abstracting the proton from methyl group [23]. Loaded Ca could be present on thermally activated SFA surface in the forms of carbonate, hydroxide and oxide as well as in the form of silicate. $\text{Ca}(\text{OH})_2$ and CaCO_3 formation could be assigned due to the absorption of water vapour [24] and CO_2 from environment [25] by CaO compound or they may generate during the catalyst synthesis step.

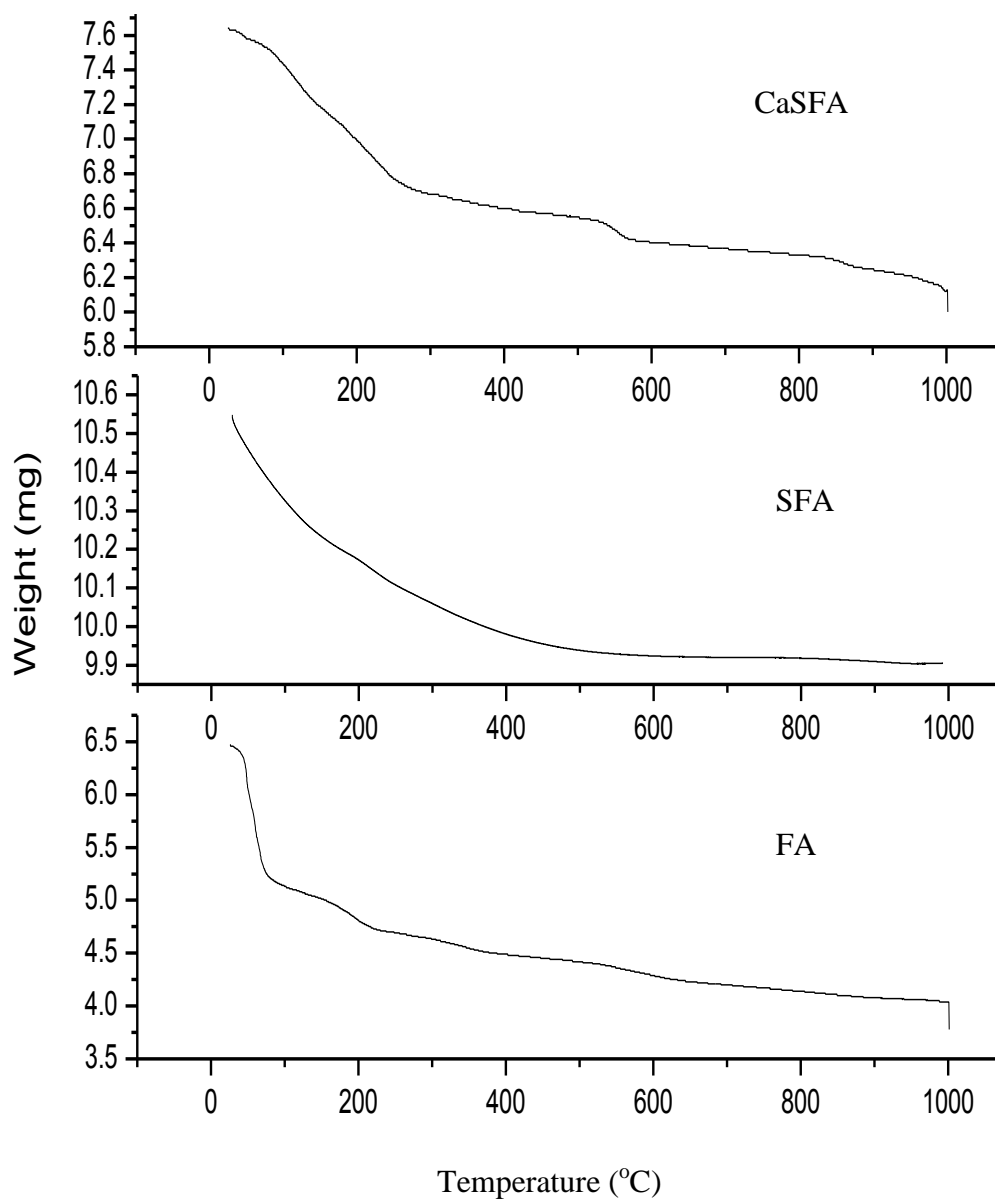


Figure 6.1: TGA curves of (a) FA, (b) SFA and (c) CaSFA.

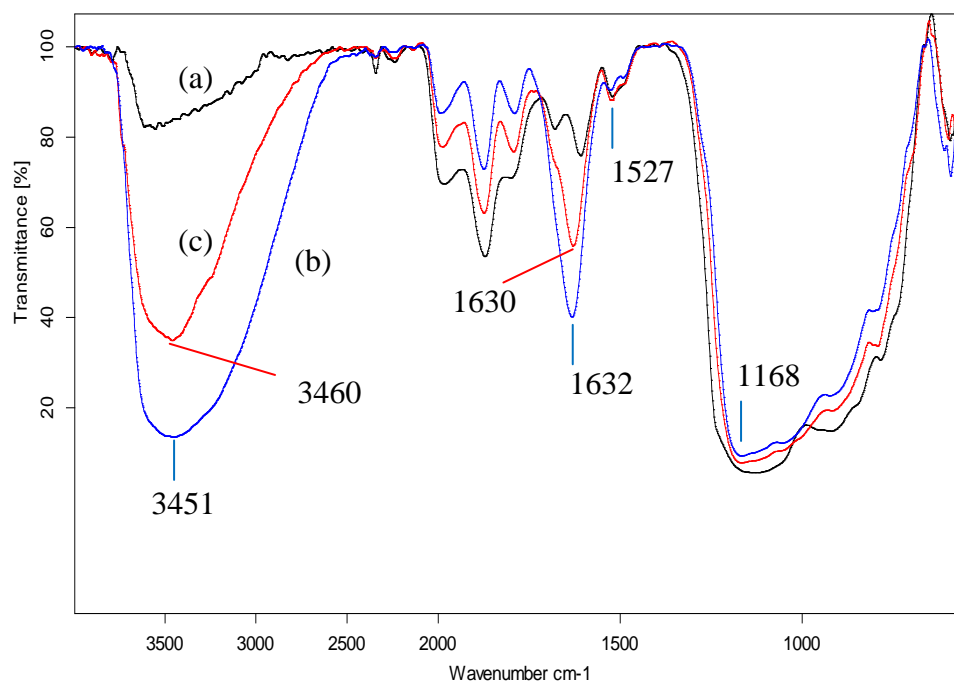


Figure 6.2: FTIR spectra of (a) TFA, (b) SFA and (c) Thermally activated SFA.

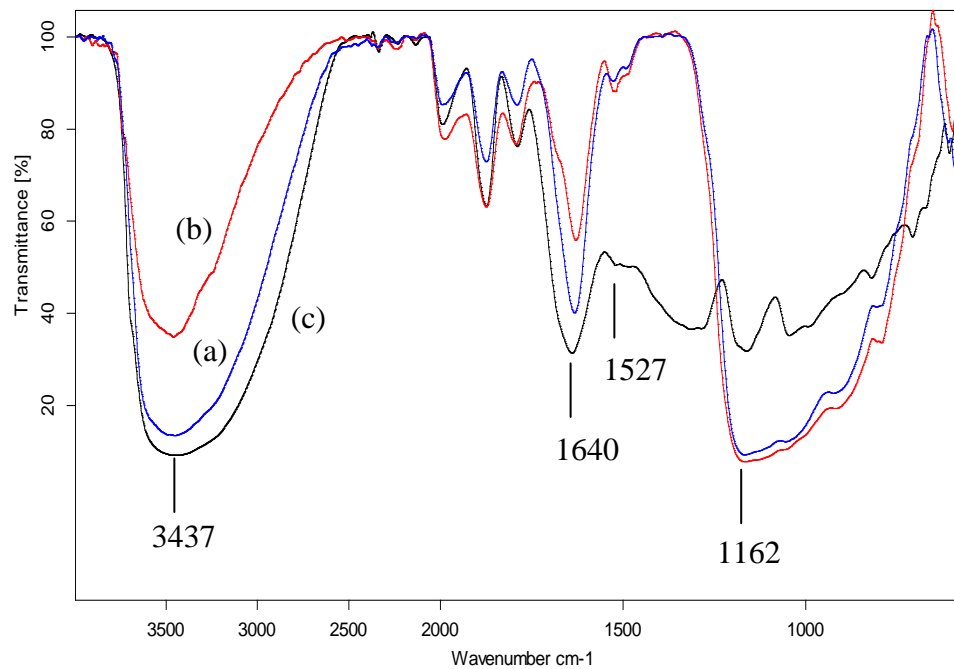


Figure 6.3: FTIR spectra of (a) SFA, (b) Thermally activated SFA and (c) CaSFA.

Table 6.3: The observed transmission frequencies (cm^{-1}) of Fourier transform infrared spectra of TFA, SFA, thermally activated SFA and CaSFA and their assignments.

Assignments	Thermally				Reference No.
	TFA	SFA	activated SFA	CaSFA	
Si-O-Al stretching vibration	594	593	599	607	22
Si-O-Si asymm. stretching vibration	1129	1168	1167	1162	21
(CO₃)²⁻ stretching vibration	1521, 1679	1527	1520	1527	20, 21
H-O-H bending vibration	1608	1632	1630	1640	18
-C-H stretching vibration	2827	-	-	-	19
-O-H stretching vibration	3553	3451	3460	3437	16

6.6.5 X-ray diffraction studies

The XRD patterns of TFA, SFA, thermally activated SFA and CaSFA are given in **Figure 6.4**. Quartz exhibits peaks at $2\theta = 20.7^\circ$, 26.5° , 40.66° and 49.96° (SiO₂, ICDD pdf number 000-46-1045) while peaks at $2\theta = 33.4^\circ$, 34.85° and 16.4° confirm the presence of calcite (CaCO₃, ICDD pdf number, 47-1743), hematite phase (Fe₂O₃, ICDD pdf number, 33-0664) and mullite (Al₆Si₂O₁₃, ICDD pdf number 000-15-0776) respectively in all XRD patterns (**Figure 6.4**). A

peak at around $2\theta = 41^\circ$ present only in CaSFA confirms increased amount of calcite (CaCO_3 , JCPDS card 05- 0586) [26],[27]. This increased amount of calcite generates active basic sites on SFA surface thus basicity in CaSFA catalyst.

6.6.6 SEM analysis results

Figure 6.5 shows the surface morphologies of FA, TFA, SFA and CaSFA samples. It can be seen that fly ash mainly consists of spherical particles with smooth outer surfaces and irregularly shaped unburned carbon particles [28] which form clumps and convert into agglomerated particles during thermal activation **Figure 6.5b**, this agglomeration is the main reason of additional crystallinity in TFA. During precipitation step, agglomerated particles of TFA break into irregular shape small particles as depicted in **Figure 6.5c, 6.6** which results in increased surface area of SFA. After chemical treatment with $\text{Ca}(\text{NO}_3)_2$, CaSFA particles show loaded Ca species in different forms, clearly visible in **Figure 6.5d**.

6.6.7 TEM analysis results

TEM image of FA shows a completely spherical, fine and smooth particle of fly ash which has been reduced in size after mechanical activation (**Figure 6.7b**). So, mechanical activation is accountable for the complete removal of smoothness and sphericity in FA particles. The TEM image of SFA shows < 100 nm particles of oval, rod and irregular shapes (**Figure 6.7c**). The clear difference in particle size and shape of SFA is responsible for increased surface area which facilitates the generation of surface active basic sites in CaSFA.

6.6.8 Basic strength and basicity measurement

The base strength and basicity of CaSFA was determined by the Hammett indicator method. CaSFA shows basic strength $9.8 < \text{pH} < 15$ and basicity was found to be 1.1 mmol/g.

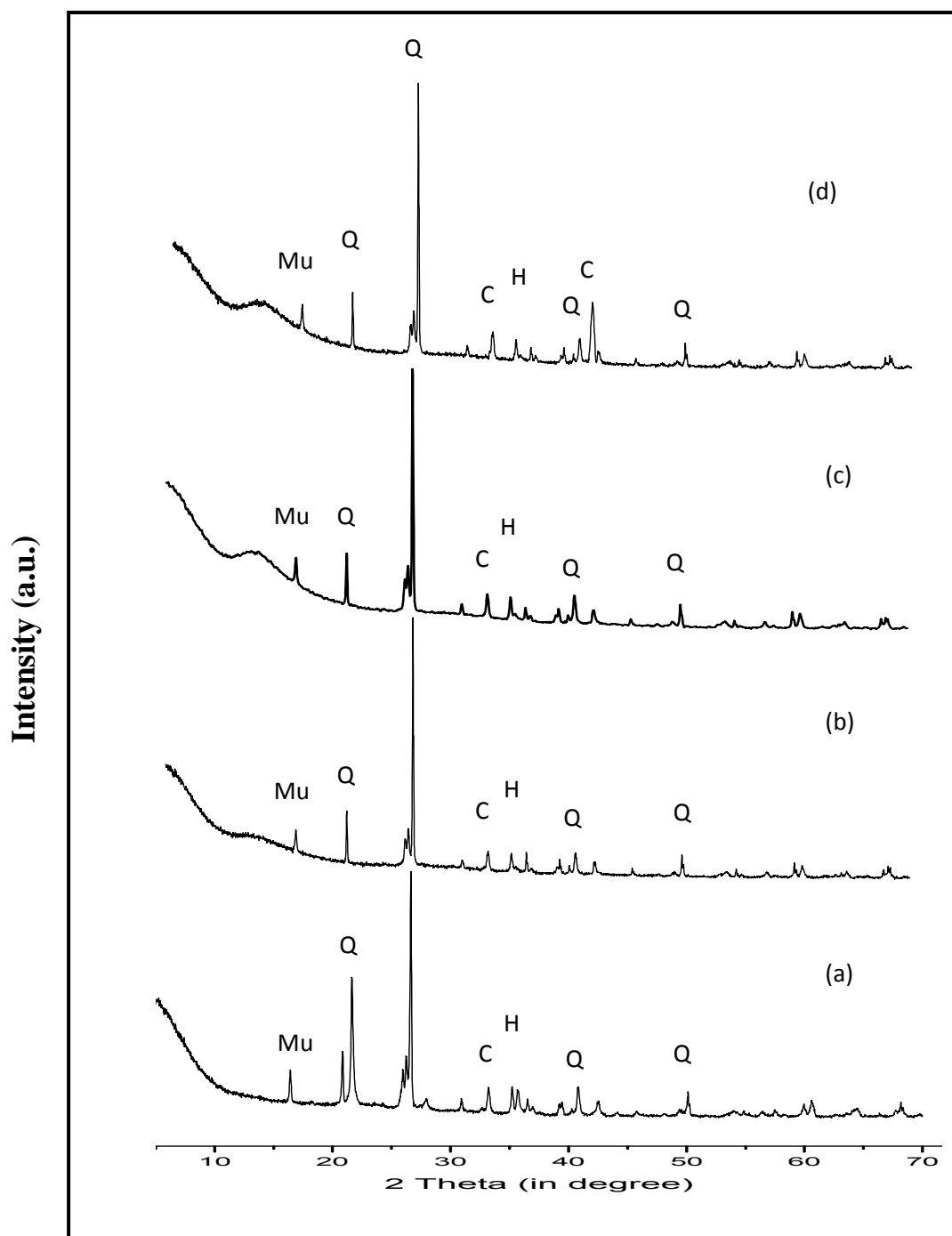


Figure 6.4: XRD patterns of (a) TFA, (b) SFA, (c) Thermally activated SFA and (d) CaSFA.

[Mu = Mullite, Q = Quartz, C = Calcite, H = Hematite]

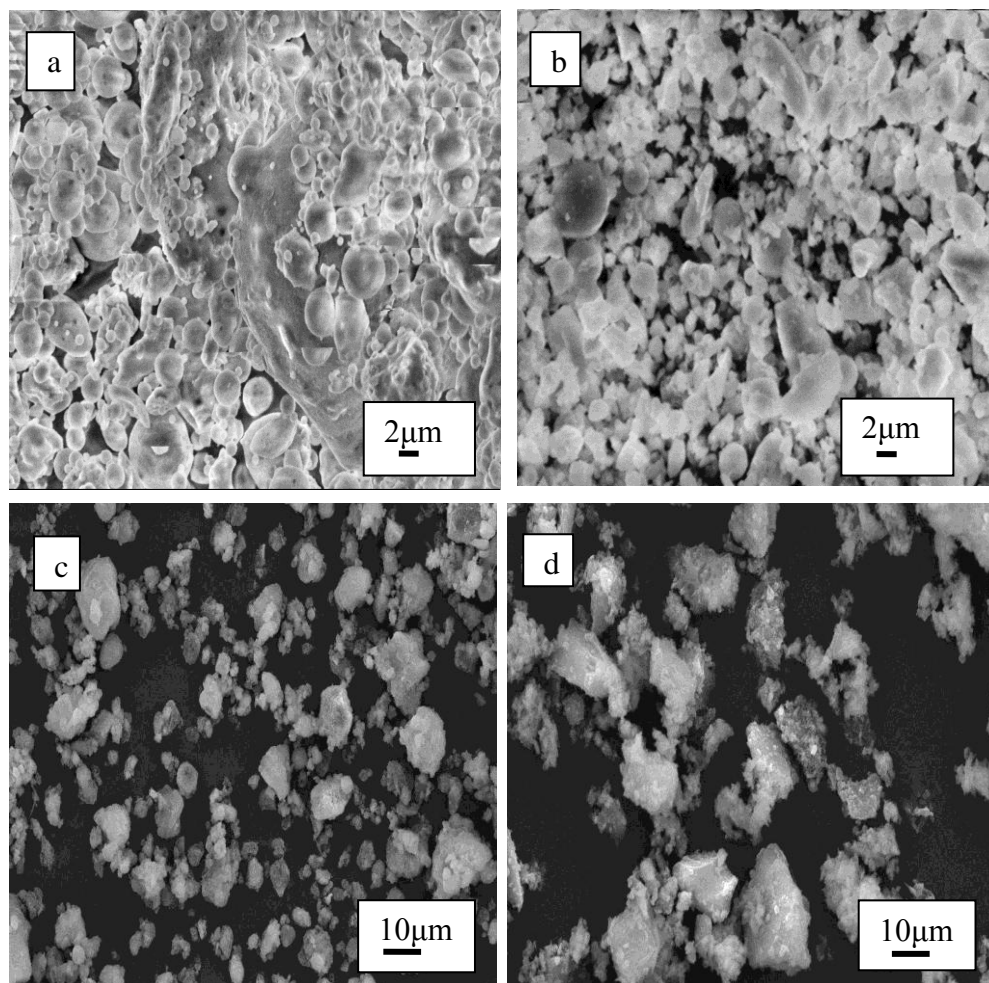


Figure 6.5: SEM micrographs of (a) FA, (b) TFA, (c) SFA and (d) CaSFA.

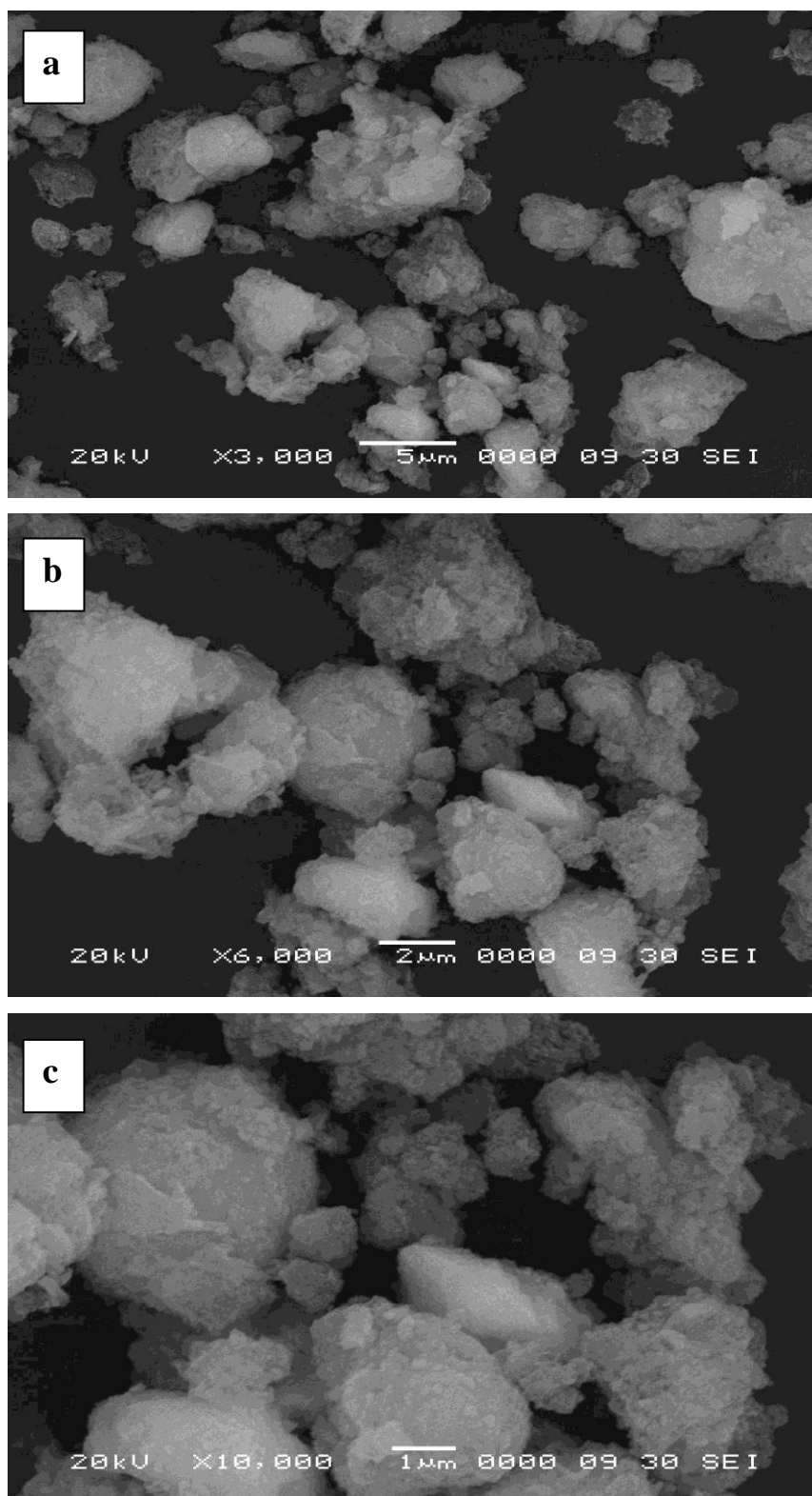


Figure 6.6: SEM micrographs of SFA in higher magnification.

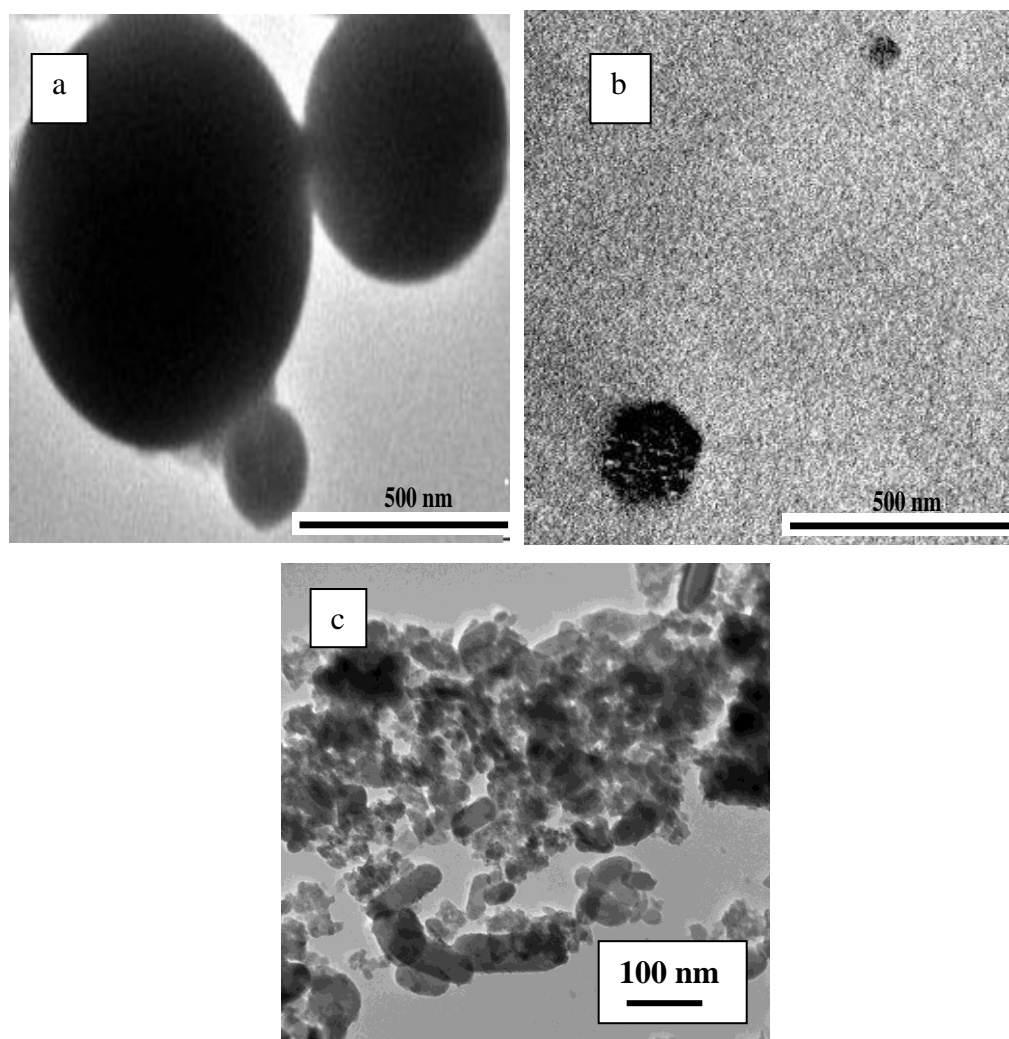


Figure 6.7: TEM images of (a) FA, (b) Mechanically activated FA and (c) SFA.

6.7 Catalytic activity

The catalytic activity of CaSFA catalyst was investigated by Claisen-Schmidt condensation reaction of acetophenone with 4-methylbenzaldehyde in batch reactor under optimized reaction conditions.

Results summarized in **Table 6.4** show that TFA, SFA and thermally activated SFA do not show any catalytic activity for Claisen-Schmidt condensation reaction while CaSFA catalyst under given reaction conditions, showed maximum activity. Bronsted basic sites Ca-OH exist on catalyst surface to catalyze Claisen-Schmidt condensation reaction. Various parameters such as reactant molar ratio, amount of catalyst, reaction time and temperature were optimized, for getting the maximum catalytic activity, conversion and yield of desired product.

Table 6.4: Catalytic activity of TFA, SFA, thermally activated SFA and CaSFA for Claisen-Schmidt condensation reaction of 4-methylbenzaldehyde with acetophenone.

Catalyst	Conversion (%) of 4-methylbenzaldehyde	Isolated yield (%) of 4-methylchalcone
TFA	Nil	Nil
SFA	Nil	Nil
Thermally activated SFA	Nil	Nil
CaSFA	75	71

Reaction conditions: Temperature 140 °C, Time 1.5 h, 4-methylbenzaldehyde/acetophenone molar ratio 1:1, substrate/catalyst weight ratio 5:1.

6.7.1 Effect of reaction time

The effect of reaction time on the conversion (%) of 4-methylbenzaldehyde and product yield was studied in time range of 1-5 h at 140 °C by taking 4-methylbenzaldehyde/acetophenone molar ratio 1:1 and

acetophenone to catalyst weight ratio 5:1. The conversion continuously increased up to 94 % in initial 3 h and remained constant for the next 2 h (**Figure 6.8**). The optimized reaction time was found to be 3 h, in which CaSFA catalyst gave highest conversion 94% of 4-methylbenzaldehyde to 4-methylchalcone with 89% yield.

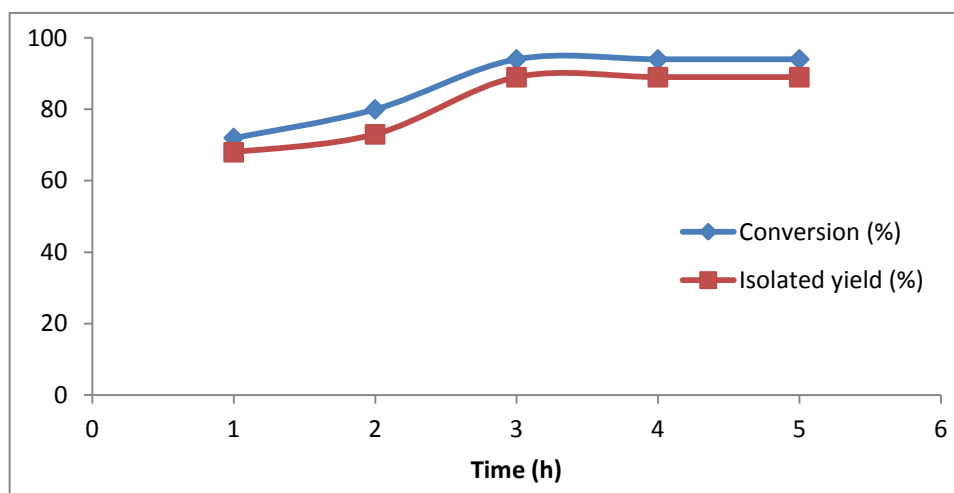


Figure 6.8: Variation in isolated yield (%) and conversion (%) of 4-methylbenzaldehyde with time.

Reaction conditions: Temperature 140 °C, 4-methylbenzaldehyde/acetophenone molar ratio 1:1, substrate/catalyst weight ratio 5:1.

6.7.2 Effect of reaction temperature

Optimization of reaction temperature for maximum conversion (%) and isolated yield (%) was carried out at temperature ranging from 100 °C to 150 °C for 3 h taking 4-methylbenzaldehyde/acetophenone molar ratio of 1:1 while substrate to catalyst weight ratio was 5:1. Conversion and yield were observed to increase on increasing reaction temperature ranging from 100 °C to 140 °C as depicted from **Figure 6.9**. The results show that the maximum conversion (94%) of 4-methylbenzaldehyde and isolated yield (89%) of 4-methylchalcone were found at 140 °C, after which conversion and isolated yield (%) remain almost steady till 150 °C.

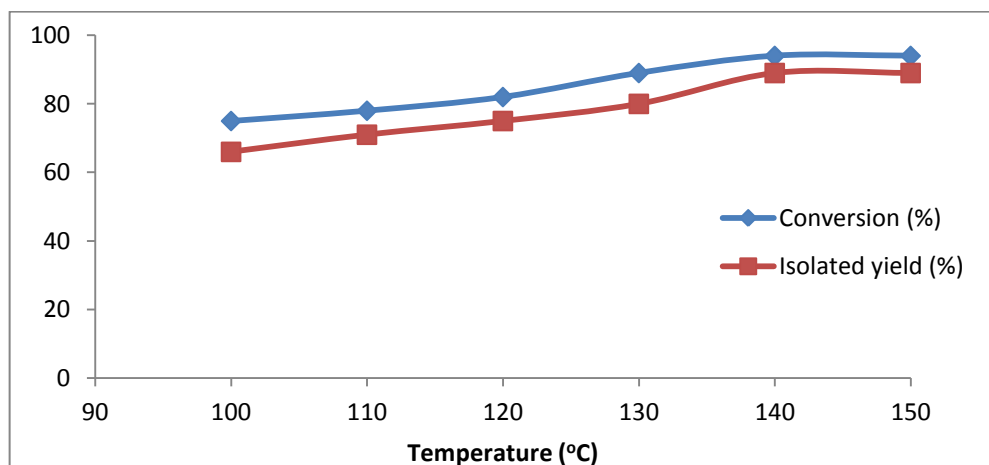


Figure 6.9: Variation in isolated yield (%) and conversion (%) of 4-methylbenzaldehyde with temperature.

Reaction conditions: Time 3 h, 4-methylbenzaldehyde/acetophenone molar ratio 1:1, substrate/catalyst weight ratio 5:1.

6.7.3 Effect of substrate/catalyst weight ratio

The influence of substrate to catalyst weight ratio on conversion and isolated yield (%) was studied by varying the amount of CaSFA catalyst under optimized reaction conditions. Only 79% conversion of 4-methylbenzaldehyde was achieved at acetophenone/CaSFA weight ratio 10:1 while conversion reached to 94% in case of 5:1 substrate/catalyst weight ratio which remained unchanged in 2.5:1 substrate/catalyst weight ratio. The increase in conversion, with increase in the catalyst weight can be attributed to an increase in the availability of number of catalytic active sites required for the reaction (**Figure 6.10**).

6.7.4 Effect of reactant molar ratio

The effect of reactant molar ratio was studied at different molar. As indicated by **Figure 6.11**, 62% conversion of 4-methylbenzaldehyde was observed at 2:1 molar ratio of 4-methylbenzaldehyde to acetophenone. This may be due to insufficient quantity of the reactants to react with each other. There was an increase in conversion up to 94% at 1:1 molar ratio due to satisfactory reactant quantity on the basic sites of the CaSFA catalyst surface. The conversion decreased on further increasing the molar ratio from 1:2 to 1:3 which could be

attributed to the lacking of 4-methylbenzaldehyde or self condensation of acetophenone.

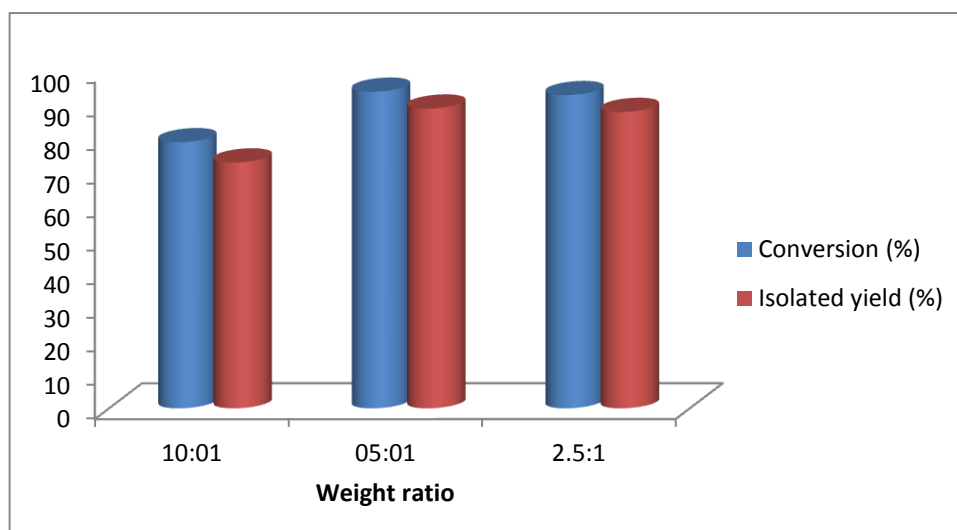


Figure 6.10: Effect of substrate/catalyst weight ratio on conversion (%) of 4-methylbenzaldehyde and isolated yield (%) of 4-methylchalcone over CaSFA.

Reaction conditions: Temperature 140 °C, Time 3 h, 4-methylbenzaldehyde/acetophenone molar ratio 1:1.

6.8 Reaction mechanism

The plausible structure of CaSFA catalyst surface is shown in **Scheme 6.2**. The reaction mechanism over CaSFA catalyst shows that Claisen-Schmidt is a condensation reaction (**Scheme 6.3**). Surface active Bronsted basic sites (–Ca–OH) abstract proton from acetophenone and form anion. The nucleophilic addition of the formed anion to the 4-methylbenzaldehyde, followed by the successive protonation and dehydration produces 3-(4-methylphenyl)-1-phenylprop-2-en-1-one or 4-methylchalcone.

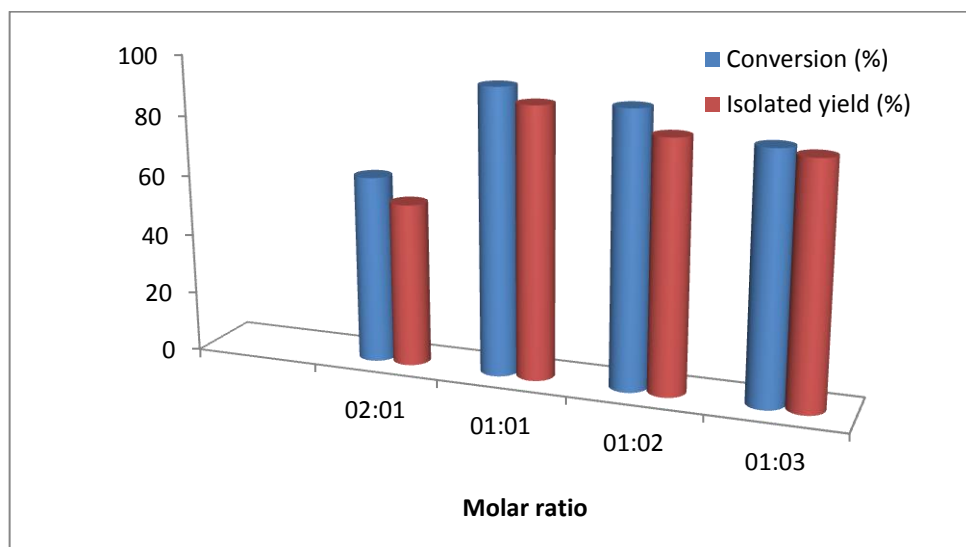
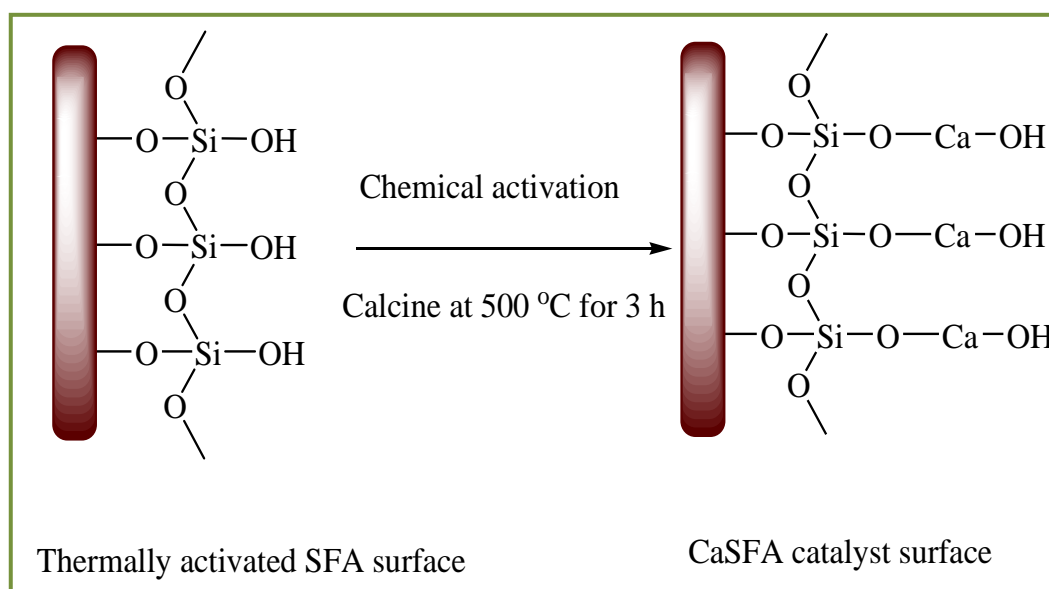
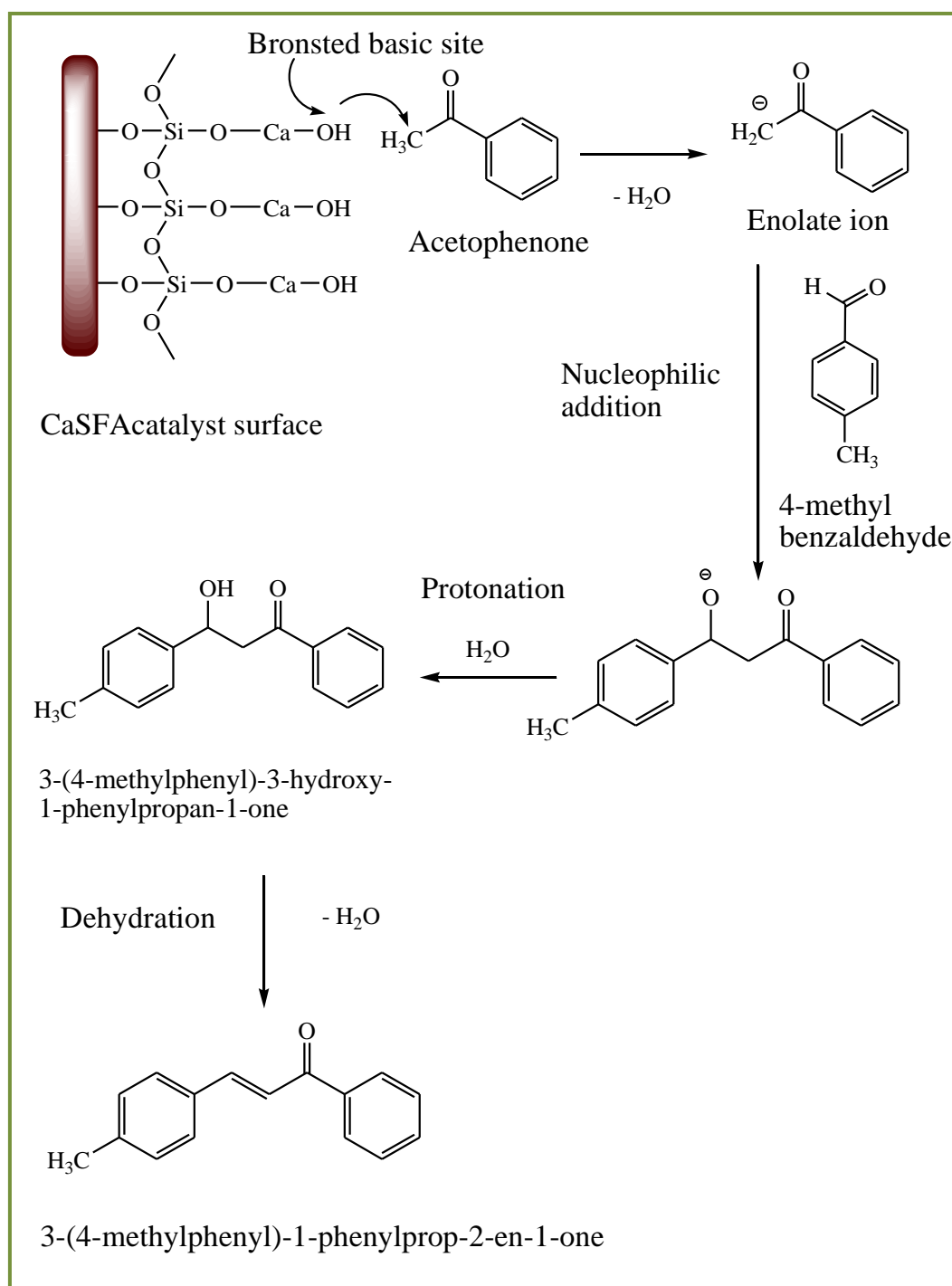


Figure 6.11: Effect of molar ratio of 4-methylbenzaldehyde/acetophenone on conversion (%) of 4-methylbenzaldehyde and isolated yield (%) of 4-methylchalcone over CaSFA.

Reaction conditions: Temperature 140 °C, Time 3 h, substrate/catalyst weight ratio 5:1.



Scheme 6.2: The schematic presentation of chemical activation of thermally activated SFA with $\text{Ca}(\text{NO}_3)_2$ and proposed structure of CaSFA.



Scheme 6.3: Proposed mechanism for Claisen-Schmidt condensation reaction of 4-methylbenzaldehyde with acetophenone over CaSFA .

6.9 Catalyst regeneration

The regeneration reaction reflects that CaSFA catalyst can be regenerated by simple thermal regeneration method and retains the catalyst activity. The regenerated catalyst was found to be having similar activity as fresh catalyst for consecutive four reaction cycles, giving 89-75% yield (**Table 6.5**) for Claisen-Schmidt condensation of acetophenone with 4-methylbenzaldehyde. Due to the stability of Ca-OH Bronsted basic sites, CaSFA catalyst was found efficient up to five reaction cycles giving almost similar yield. The gradual decrease in yield after five reaction cycles is due to the deposition of carbonaceous material on the surface of the reused catalyst which may block the active basic sites of CaSFA catalyst.

Leaching test was done using hot filtration technique. The catalyst was removed after 30 min and the reaction was continued to completion but no further product was formed. This led us to the conclusion that no leaching occurs with the catalysts used and under the conditions applied in the present investigation.

Table 6.5: Catalytic activity of fresh and regenerated CaSFA for Claisen-Schmidt condensation of 4-methylbenzaldehyde with acetophenone.

Reaction Cycle	Isolated yield (%)
I	89
II	85
III	82
IV	80
V	75

Reaction conditions: Temperature 140 °C, Time 3 h, substrate/catalyst weight ratio 5:1, 4-methylbenzaldehyde/acetophenone molar ratio 1:1.

6.10 Conclusion

The study provides CaSFA catalyst as an efficient solid base catalyst possessing significant amount of basicity and basic sites. Consecutive treatment of TFA with NaOH and H₂SO₄ result in increased amorphous silica content and converts fly ash into silica enriched fly ash (SFA). Further treatment with Ca(NO₃)₂ modify SFA surface by generating Bronsted basic sites i.e. -Ca-OH. These sites are responsible for catalytic activity of CaSFA, which has been investigated by Claisen-Schmidt condensation reaction. Catalyst was recovered, regenerated and reused with no noticeable changes in the yield, confirming almost negligible leaching of active basic sites or slight deactivation of the catalyst under the mentioned reaction conditions. The prepared CaSFA catalyst is stable, eco-friendly, cost effective, reusable, easily recoverable and suitable for the production of 4-methylchalcone. This study suggests that fly ash could be an economical source of silica for synthesizing novel solid base catalysts for catalyzing industrially important reactions in cost effective manner.

6.11 References

- [1] J. Schlomach, M. Kind, *J. Colloid Interface Sci.* 277 (2004) 316.
- [2] S. Music, N. Filipovic-Vincekovic, L. Sekovanic, *Brazilian J. Chem. Eng.* 28 (2011) 89.
- [3] R. Ghosh, S. Bhattacharjee, *J. Chem. Eng. Process Technol.* 04 (2013) 1.
- [4] A.E. Voinescu, M. Kellermeier, A.M. Carnerup, A. Larsson, D. Touraud, S.T. Hyde, W. Kunz, *J. Cryst. Growth* 306 (2007) 152.
- [5] F. Adam, J. Nelson, A. Iqbal, *Catal. Today* 190 (2012) 2.
- [6] E.A. Okoronkwo, P.E. Imoisili, S.O.O. Olusunle, *Chem. Mater. Res.* 3 (2013) 68.
- [7] V. Hariharan, G. Sivakumar, *Int. J. ChemTech Res.* 5 (2013) 1263.
- [8] R. Bal, K. Chaudhari, S. Sivasanker, *Catal. Letters* 70 (2000) 75.
- [9] R. Gupta, M. Gupta, S. Paul, R. Gupta, *Bull. Korean Chem. Soc.* 30 (2009) 2419.
- [10] S. Ahmed, J.B. Moffat, *Appl. Catal.* 58 (1990) 83.

-
- [11] W. Zhao, Y. Zhang, C. Qu, L. Zhang, J. Wang, Y. Cui, *Catal. Letters* (2014).
- [12] A. Davoodnia, G. Yassaghi, *Chinese J. Catal.* 33 (2012) 1950.
- [13] K. Kordatos, S. Gavela, A. Ntziouni, K.N. Pistiolas, A. Kyritsi, V.K. Rigopoulou, *Microporous Mesoporous Mater.* 115 (2008) 189.
- [14] R. Rahul, J.K. Satyarthi, D. Srinivas, *Indian J. Chem.* 50 (2011) 1017.
- [15] M.M.A. Sekkina, R.M. Issa, A.E.-D.M. Bastawisy, W.A. El Helece, *Int. J. Chem.* 2 (2010) 81.
- [16] D. Jain, A. Rani, *Am. Chem. Sci. J.* 1 (2011) 37.
- [17] D. Jain, C. Khatri, A. Rani, *Fuel* 90 (2011) 2083.
- [18] S. Kabra, S. Katara, A. Rani, *Int. J. Innov. Res. Sci. Eng. Technol.* 2 (2013) 4319.
- [19] S. Katara, S. Kabra, A. Sharma, R. Hada, A. Rani, *Int. Res. J. Pure Appl. Chem.* 3 (2013) 299.
- [20] H. Handa, T. Baba, H. Sugisawa, Y. Ono, *J. Mol. Catal. A Chem.* 134 (1998) 171.
- [21] B.J. Saikia, G. Parthasarathy, N.C. Sarmah, G.D. Baruah, *Indian Acad. Sci.* 31 (2008) 155.
- [22] M.E.G. Frances I. Hurwitz, Denisse V. Aranda, in: *Am. Chem. Soc. 236th Natl. Meet. Philadelphia, PA, August 20, 2008, 2008.*
- [23] D. Kishore, S. Kannan, *J. Mol. Catal. A Chem.* 223 (2004) 225.
- [24] B. Yoosuk, P. Krasae, B. Puttasawat, P. Udomsap, N. Viriya-empikul, K. Faungnawakij, *Chem. Eng. J.* 162 (2010) 58.
- [25] A.M. Frey, J. Yang, C. Feche, N. Essayem, D.R. Stellwagen, F. Figueras, K.P. de Jong, J.H. Bitter, *J. Catal.* 305 (2013) 1.
- [26] K.S. Hui, K.N. Hui, S.K. Lee, *World Acad. Sci. Eng. Technol.* 3 (2009) 174.
- [27] D. Jain, C. Khatri, A. Rani, *Fuel Process. Technol.* 91 (2010) 1015.
- [28] S.M. Nyale, O.O. Babajide, G.D. Birch, N. Böke, L.F. Petrik, *Procedia Environ. Sci.* 18 (2013) 722.

Annexure I and II

ANNEXURE I

Characterization Techniques

Physicochemical properties of all catalytic materials are studied by N₂ adsorption-desorption, TGA, FT-IR, XRD, SEM, SEM-EDX and TEM techniques. The reaction products are analyzed by ¹H NMR and gas chromatography.

1. BET analysis

Specific surface area and average pore diameter of samples are determined by N₂ adsorption-desorption, done by using Thermo Scientific™ Surfer surface area analyzer. The samples are degassed under vacuum at 120°C for 4 h, prior to adsorption in order to evacuate the physisorbed moisture. BET analysis is done at University of Pune, Pune.

2. Thermo-gravimetric analysis (TGA)

Thermo gravimetric analysis (TGA) of the samples is carried out using DTG-60-H- Shimadzu thermal analyzer (C-30574400175), by heating the samples in the range of 50–1000 °C with a heating rate of 10°C/min under nitrogen flow (50 cm³/min). TGA analysis of samples is done at University of Pune, Pune and IIT-Roorkee.

3. Fourier transform infra-red analysis (FT-IR)

FT-IR study is executed on Bruker FT-IR Spectrophotometer (TENSOR 27) in DRS (Diffuse Reflectance System) mode by mixing samples with KBr in 1:20 weight ratio. The spectra were recorded in the range of 550-4000 cm⁻¹ with a resolution of 4 cm⁻¹. FT-IR analysis is conducted at Department of Pure and Applied Chemistry, University of Kota, Kota.

4. X-ray diffraction analysis

The structural features of samples are analyzed by X-ray diffraction studies. X-ray diffraction (XRD) patterns are recorded by Bruker D8 Advance diffractometer, using Ni-filter and Cu K_α radiation (E = 8047.8 eV, λ = 1.5406Å°).

The samples are scanned in 2θ range of $5-75^\circ$ at a scanning rate of 0.04°s^{-1} . Crystallite size of the crystalline phase is determined from the peak of maximum intensity by using Scherrer formula with a shape factor (K) of 0.9 as below:

$$\text{Crystallite size} = K \cdot \lambda / W \cdot \cos \theta$$

Where, $W = W_b - W_s$; W_b is the broadened profile width of experimental sample and W_s is the standard profile width of reference sample. XRD analysis has been done at UGC-DAE CSR, Indore.

5. Scanning electron microscopy (SEM and SEM-EDX analysis)

The detailed imaging information about the morphology and surface topography is studied by Scanning electron microscope (SEM, Model-JEOL-JSM 5600). SEM analysis is done at UGC-DAE CSR Indore, University of Pune, Pune and IIT-Roorkee.

6. Transmission electron microscopy (TEM analysis)

The surface morphology and texture of samples is further confirmed by TEM analysis, Model: H-7500 (Hitachi Make). TEM analysis is done at SAIF-Chandigarh.

7. ^1H NMR analysis

^1H NMR analysis of reaction products is carried out on Bruker AvIII HD-300 NMR spectrometer. The analysis is done at CDRI Lucknow.

8. Mechanical activation

Mechanical activation of fly ash is carried out in a high energy planetary ball mill (Retsch PM-100, Germany). As received fly ash is mechanically activated in an agate jar using 5 mm agate balls with 10:1 ball to powder weight ratio (BPR). The mechanical activation was done at 250 rpm rotation speed for specified time period. Mechanical activation is at Department of Pure and Applied Chemistry, University of Kota, Kota.

9. Gas Chromatography

The products are analyzed by Gas Chromatograph (Agilent Technologies 7820A) having FID and Agilent J&W Advanced Capillary HP 5 GC Columns of 30 m length and 0.320 mm diameter, programmed oven temperature of 60–325°C and N₂ (1.5 ml/min) as a carrier gas. GC analysis is conducted at Department of Pure and Applied Chemistry, University of Kota, Kota.

ANNEXURE II

List of publications

In International and National Journals

1. Surface Modification of Fly Ash by Thermal Activation: A DR/FTIR Study, *Stuti Katara*, Sakshi Kabra, Anita Sharma, Renu Hada and Ashu Rani, International Research Journal of Pure & Applied Chemistry, 2013, 3(4), 299-307.
2. Characterization and Study of Turkish Perlite, Sakshi Kabra, *Stuti Katara* and Ashu Rani, International Journal of Innovative Research in Science, Engineering and Technology, 2013, 2(9), 4319-4326.
3. Acid Activated Fly Ash, as a Novel Solid Acid Catalyst for Esterification of Acetic Acid, Anita Sharma, *Stuti Katara*, Sakshi Kabra and Ashu Rani, Indian Journal of Applied Research, 2013, 3(4) 37-39.
4. Synthesis of Nanosized Titania by Sol Gel Route, Renu Hada, Sakshi Kabra, *Stuti Katara*, Ashu Rani, Vijay Devra and S. S. Amritphale, Indian Journal of Applied Research, 2013, 3(4), 49-50.
5. DRIFT- Spectroscopic Study of Modification of Surface Morphology of Perlite during Thermal Activation, Sakshi Kabra, Anita Sharma, *Stuti Katara*, Renu Hada and Ashu Rani, Indian Journal of Applied Research, 2013, 3(4), 40-42.
6. An Efficient and Cost-Effective Solid Base Catalyst for Cross-Aldol Condensation of Ketones with Aromatic Aldehydes under Solvent Free Condition. *Stuti Katara*, Sakshi Kabra, Renu Hada and Ashu Rani, Catalysis Communications (Communicated).
7. Fly Ash Supported Solid Base Catalyst for Microwave Assisted Michael Addition Reaction. *Stuti Katara*, Renu Hada, Sakshi Kabra and Ashu Rani, Fuel Processing Technology (Communicated).
8. Microwave Assisted Solution Combustion Synthesis of Activated Fly Ash Supported NiO Nanoparticles for Hydrogen Peroxide Decomposition, Renu Hada, *Stuti Katara*, Sakshi Kabra, Vijay Devra and Ashu Rani, Fuel (Communicated).

9. Perlite Supported Nickel Catalyst: Synthesis, Characterization and Catalytic Activity in Claisen-Schmidt Condensation Reactions, Sakshi Kabra, *Stuti Katara*, Renu Hada and Ashu Rani, Catalysis Communications (Communicated).
10. Non Aqueous Synthesis of Fly Ash Supported TiO₂ Nanoparticles for Enhanced Photo-Oxidation of Congo Red Dye, Renu Hada, Sakshi Kabra, *Stuti Katara*, Vijay Devra and Ashu Rani, Fuel Processing Technology (Communicated).
11. Fly Ash Supported Phosphomolybdic Acid as A Highly Efficient Solid Lewis Acid Catalyst for Microwave Assisted Friedel-Crafts Acylation Reactions, Sakshi Kabra, Renu Hada, *Stuti Katara* and Ashu Rani, Fuel (Communicated).

In International Conference/Workshop/Symposium –

1. An Abstract is accepted for Oral Presentation and three other abstracts are accepted for Poster Presentations at **World of Coal Ash Conference-2015** to be held in May at Nashville, Tennessee (U.S.).
2. Paper presentation as co-author and won “Best Presentation Award” in 3rd International Conference on **Advance Trends in Engineering, Technology and Research (ICATET-2014)** held on 23-24 December 2014 at Bal Krishna Institute of Technology, Kota.
3. Paper presentation as first author in International Conference on **Advanced Trends in Engineering, Technology and Research (ICATET-2014)** held on 23-24 December 2014 at Bal Krishna Institute of Technology, Kota.
4. Paper presentation in International Conference on **New Emerging Trends in Chemistry** held on 3-4 March 2013 at IIS University, Jaipur.
5. Poster presentation at International Conference on **Waste Wealth and Health (ICWWH-2013)** on 15-17 February 2013 at MPCST, Bhopal.
6. Poster presentation at International Workshop on **Green Initiatives on Energy, Environment & Health** held on 2-3 Dec 2013, organized by the Green Chemistry Centre of Excellence, The Energy and Resources Institute, Green Chemistry Network Centre, DU, Gautam Buddha University, Green Chemistry Network and sponsored by Royal Society of Chemistry London (North India Section) at Delhi.

7. Participated in **Indo – Swedish Symposium on Strategic Knowledge on climate Change** held on 9 October 2013 at the Department of Pure & Applied Chemistry, University of Kota, Kota.
8. Paper presentation as first author in International Conference on **Advanced Trends in Engineering and Technology (ICATET) 2013** held on 19-20 December 2013 at Arya College of Engineering & I. T., Jaipur.
9. Paper presentation as co-author in International Conference on **Advanced Trends in Engineering and Technology (ICATET) 2013** held on 19-20 December 2013 at Arya College of Engineering & I.T., Jaipur.

National Conference/ Workshop/ Symposium/School-

1. Participated in National Seminar on **Environmental Issues and Social Concerns** held on 21-22 March 2014 at Department of Social Sciences, University of Kota, Kota.
2. Participated in **Symposium of E-Resources** held on 16-17 December 2013 at Department of Library and Information Science, University of Kota, Kota.
3. Oral paper presentation in National Conference on **Frontiers in Physical, Chemical and Biological Sciences** held on 4-6 Oct 2013 at Department of Chemistry, University of Pune, Pune.
4. Participated in **5th National Academic Workshop on Organic Reaction Mechanisms & Analytical Techniques used in Chemical Sciences** held on 21-25 October 2013 at the Department of Pure & Applied Chemistry, University of Kota, Kota.
5. Participated in National Seminar on **Chemistry for Economic Growth and Human Comforts** held on 31 August 2013 at Department of Chemistry, University of Rajasthan, Jaipur.
6. Participated in **5th BRNS-AEACI Winter School on Analytical Chemistry-2012** held on 3-10 December 2012 at the Chemistry Department, IIT Roorkee.
7. Participated in **Brainstorming Workshop on Perspective of Fly Ash Characterization** held on 7 November 2012, organized by Center for Fly Ash Research & Management (C-Farm), New Delhi.

8. Poster presentation in a National Conference, **National Symposium on Recent Advances in Chemical Sciences** held on 7-8 January 2011 at University of Kota, Kota.
9. Paper presentation in a National Conference, **Emerging Views In Advanced Chemistry** held on 17-19 December 2010 at Govt. College, Bhilwara.



Surface Modification of Fly Ash by Thermal Activation: A DR/FTIR Study

Stuti Katara¹, Sakshi Kabra¹, Anita Sharma¹, Renu Hada¹
and Ashu Rani^{1*}

¹Department of Pure and Applied Chemistry, University of Kota, Kota, Rajasthan, India.

Authors' contributions

This work was carried out in collaboration between all authors. Authors SK and AR supervised and designed the study. Author SK (Stuti Katara) performed the experimental and analytical study, wrote the protocol, and wrote the first draft of the manuscript. Authors SK, AS and RH managed the literature searches and helped in analytical study. All authors read and approved the final manuscript.

Research Article

Received 31st March 2013
Accepted 12th July 2013
Published 24th July 2013

ABSTRACT

To acquire a deeper understanding of surface chemistry of fly ash along with thermal activation, the states of mineral phases, water and –OH groups on silica are studied in fly ash at different calcination temperatures by DR/FTIR spectroscopic technique. DR/FTIR spectroscopy allows differentiation of various types of bonds in a material on a molecular level. The spectroscopic results are also supported by XRF, XRD and SEM analysis. Studied fly ash was collected from Jamshedpur Thermal Power Station as an extremely fine ash, formed from the inorganic components of the coal, mainly silica and alumina which remain after combustion of the carbonaceous part of the coal. Distinguish changes were observed in fly ash IR bands regarding absorbed water, -OH group and Si-O-Si group with thermal activation. This investigation reveals that as the temperature increases, the physically adsorbed water begins to remove first, then silanol groups on surface is dehydrated. Increased temperature causes formation of different crystalline phases like quartz, mullite and hematite etc. and increased the crystallinity of the calcined samples.

*Corresponding author: Email: ashu.uok@gmail.com;

Keywords: DR/FTIR; thermal activation; silanol groups; fly ash.

1. INTRODUCTION

The coal fired power plant which consumes pulverized solid fuels composed of combustible organic matter with varying amount of inorganic mineral parts produce large amount of solid waste fly ash. Every year a crude estimation of 600 million tons of fly ash generated worldwide [1] and about 110 million tons only in India [2]. The combustible gasification takes place in coal fired boiler at an operative temperature 1450°C under reducing atmosphere. The mixture of effluent gases is cooled and fly ash gets solidify at temperature from 950°C to 400°C. In the form of spherical particles consisting of SiO₂, Al₂O₃, Fe₂O₃, CaO, MgO and alkali in varying amounts with some unburned activated carbon [3]. As per the ASTM C618-12a guideline [4] the fly ash containing >70% SiO₂, Al₂O₃ and Fe₂O₃ is classified as Class F type fly ash and those consists mainly of silica, alumina and calcium containing SiO₂, Al₂O₃ and Fe₂O₃ minimum upto 50 % are referred to as Class C fly ash. Class F type fly ash is used in agriculture, metal recovery, water and atmospheric pollution control [5] while class C type fly ash is used in cement production [6], steam cured bricks manufacturing [7] etc. Calcination temperature of fly ash before using as source material for synthesis of concrete material and geopolymer etc. is reported to be crucial for the end product [8]. Fly ash has a complex microstructure comprising of mixture of amorphous and crystalline components. The chemical and mineralogical compositions of fly ash vary with coal source as well as calcination temperature [9]. Fly ash also contains different amount of unburned carbon which may reach upto 17% [10] responsible for high ignition loss and undesirable constituents for geopolymerisation and concrete formation. Fly ash is also being used as heterogeneous catalytic support material due to high silica, surface mineralogy, morphology and surface silanol groups [11, 12]. Both the adsorbed water and silanol groups on surface may affect the surface modification process thus play important roles in catalytic application on silica surface. It is difficult to distinguish between the adsorbed moisture and actual surface hydroxyl groups in a form of crystalline water or amorphous silanol (Si-OH) [13]. Literature reports that high temperature calcination forms new crystalline phases on fly ash surface modifying siloxane groups (Si-O-Si) and different forms of silanol groups [8]. Therefore it is of interest to understand the modification of fly ash mineralogy and morphology with thermal activation by using Diffuse Reflectance Fourier Transform Infrared (DRIFTIR) spectroscopic technique, which is one of the advance techniques to illustrate the chemical structure of the bonding materials. The results of the DRIFTIR study are supported by other characterization tools such as X-ray Fluorescence (XRF), X-ray Diffraction (XRD) and Scanning Electron Microscopy (SEM).

2. EXPERIMENTAL DETAILS

2.1 Materials

The coal fly ash (Class F type with SiO₂ and Al₂O₃ > 70%) used in this study was collected from Jamshedpur Thermal Power Station (Jamshedpur, Jharkhand, India). Fly ash (FA) was thermally activated by calcining in muffle furnace at 400, 600, 800 and 1000°C for 3h and abbreviated as TFA-400, TFA-600, TFA-800 and TFA-1000 respectively (TFA –Thermally activated fly ash).

2.2 Sample Preparation and Characterization

DR/FTIR analysis of fly ash samples were carried out by diluting fly ash samples with KBr in 1:20 weight ratio and mixed gently with the help of mortar and pestle, being careful about atmospheric moisture absorption. In this study, FTIR spectra of the materials were recorded using FTIR Tensor 27 Bruker with DR (Diffuse Reflectance) accessory. The spectra were recorded in the range $550 - 4000 \text{ cm}^{-1}$ with a resolution of 4 cm^{-1} . The chemical composition was determined by wavelength dispersive X-ray fluorescence (WD-XRF) model Bruker S8 Tiger. The detailed imaging information about the morphology and surface texture of the sample was provided by SEM (Philips XL30 ESEM TMP). The XRD measurements were carried out using Bruker D8 Advance X-ray diffractometer with monochromatic $\text{CuK}\alpha$ radiation ($\lambda = 1.54056 \text{ \AA}$) in a 2θ range of $5-70^\circ$.

3. RESULTS AND DISCUSSION

The chemical composition of FA and all TFA samples reveals that major components of fly ash are SiO_2 and Al_2O_3 . Some minor components like Fe_2O_3 , CaO , MgO , TiO_2 , Na_2O , K_2O and trace elements around 1.5 wt% are also present in FA and all TFA samples (Table 1). The thermal activation of fly ash removes C, S, moisture and other adsorbed gases. The removal of moisture and co-existing unburned carbon increases with increasing temperature [14]. It can be concluded that all the compounds remained almost constant after thermal treatment, besides a reduction in Na_2O , K_2O and other elements in all TFA samples.

Table 1. Chemical composition of FA and all TFA samples

Sample	SiO_2 (wt%)	Al_2O_3 (wt%)	Fe_2O_3 (wt%)	CaO (wt%)	MgO (wt%)	TiO_2 (wt%)	Na_2O (wt%)	K_2O (wt%)	Other elements (wt%)
FA	62	30	3.0	0.4	0.3	1.4	0.4	0.8	1.7
TFA-400	62.3	30	3.2	0.4	0.3	1.4	0.3	0.5	1.6
TFA-600	62.5	30.1	3.2	0.3	0.3	1.4	0.3	0.3	1.6
TFA-800	62.8	30.3	3.2	0.3	0.2	1.3	0.2	0.2	1.5
TFA-1000	63	30.5	3.2	0.3	0.2	1.3	0.2	0.1	1.2

The FTIR spectra in Fig. 1 shows a broad band between $3400-3000 \text{ cm}^{-1}$, which is attributed to surface $-\text{OH}$ groups of silanol groups ($-\text{Si}-\text{OH}$) and adsorbed water molecules on the surface. The broadness of band indicates the presence of strong hydrogen bonding [11]. The gradual decrement in the intensity and broadness in this band, as shown in Fig. 1 confirms loss of water in all TFA samples during thermal activation. Most of the molecular water gets removed from the sample by heating up to 250°C , while crystalline $-\text{OH}$ remains in the sample till 700°C [15]. A peak around 1607 cm^{-1} (Fig. 1) is attributed to bending mode ($\delta\text{O}-\text{H}$) of water molecule [16] which is shown in all fly ash samples. A broad band ranging from 1070 cm^{-1} to 1170 cm^{-1} due to $\text{Si}-\text{O}-\text{Si}$ asymmetric stretching vibrations [17] of silica is present in FA and all TFA samples. FA shows $\text{Si}-\text{O}-\text{Si}$ asymmetric stretching vibration centered at 1100 cm^{-1} which get shifted towards higher wave number at 1162 cm^{-1} in case of TFA-1000. This high wave number shift is the result of loss of water thus transformation of Q^3 units $[\text{Si}(\text{OH})(\text{SiO}_4)_3]$ to Q^4 units $[\text{Si}(\text{SiO}_4)_4]$ thus decrease in silanol groups ($-\text{Si}-\text{OH}$). This phenomenon shows reverse accordance with the statement that an increase in the hydroxide concentration shifts the position of the maximum absorbance of $\text{Si}-\text{O}$ bands toward lower number, indicating the transformation of Q^4 units $[\text{Si}(\text{SiO}_4)_4]$ to Q^3 units $[\text{Si}(\text{OH})$

(SiO_4)₃] [18]. Peak at 2887 cm^{-1} could be assigned to C-H stretching vibration of organic contaminants which may be introduced during sample handling or some hydrocarbon present in fly ash [17.] This peak shows high intensity in FA while on thermal activation organic contaminants get removed from FA and show low intense peak in all TFA samples as compared to FA. Peaks appeared around 2343 cm^{-1} attributed to ν O-H stretching [19], 2241 cm^{-1} responsible for H-SiO₃ [20], 1984 cm^{-1} due to =Si-H monohydride [21], 1872 cm^{-1} due to calcium carbonate [22] present in FA and all TFA samples (Table 2). Peaks centered at 1521 cm^{-1} [23] and 1681 cm^{-1} [17] are due to $(\text{CO}_3)^{2-}$ stretching vibration show highest intensity in FA, which is reduced on thermal activation in all TFA samples conferring that during thermal activation C and C associated impurities like CO₂ are removed with increased temperature. A peak related to Al-O-Si stretching vibration appears around 600 cm^{-1} [24] and is present in FA and all TFA samples (Table 2) conferring that Si and Al are present in silico aluminate phase not affected by thermal activation [25].

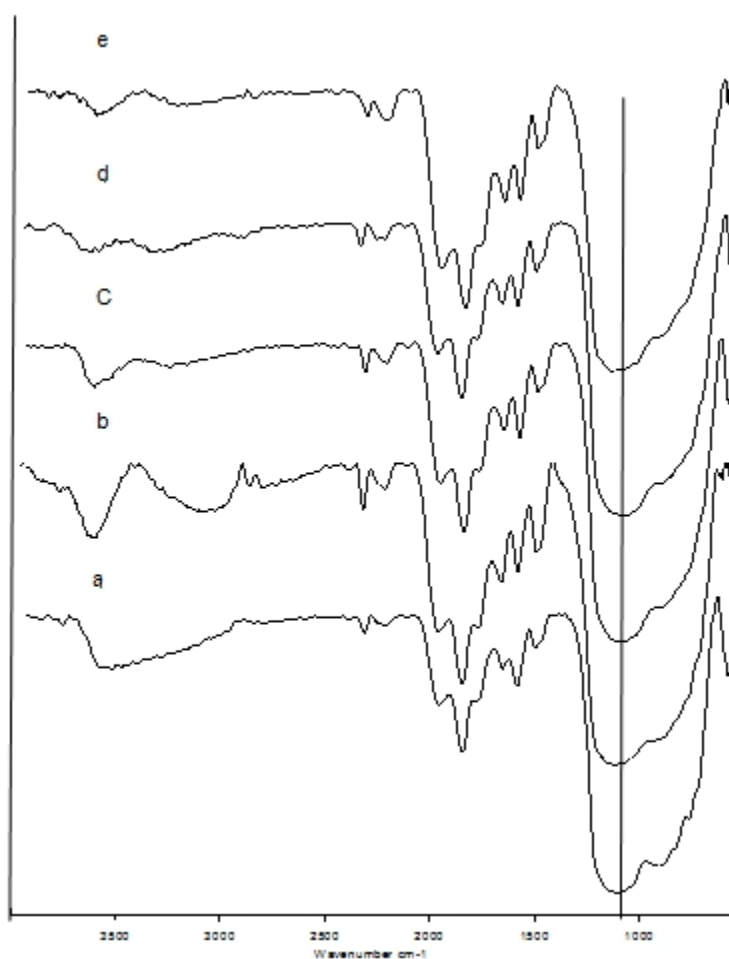


Fig. 1. DR/FTIR spectra of (a) FA (b) TFA-400 (c) TFA-600 (d) TFA-800 (e) TFA-1000
Table 2. Different DR/FTIR observed frequencies of (1.) FA (2.) TFA-400 (3.) TFA-600
(4.) TFA-800 (5.) TFA-1000 and their possible assignments

Assignments	FA	TFA-400	TFA-600	TFA-800	TFA-1000	Reference no.
Si-O-Al stretching vibration	600	611	589	592	603	24
Si-O-Si asymm. Stretching Vibration	1100	1102	1113	1148	1162	17
(CO₃)²⁻—stretching vibration	1521, 1679	1519, 1686	1519, 1680	1519, 1683	1521, 1681	23, 17
H-O-H bending Vibration	1608	1606	1606	1607	1607	16
Calcium Carbonate	1872	1872	1872	1872	1873	22
=Si-H (monohydride)	1984	1984	1986	1984	1987	21
H-SiO₃	2241	2240	2244	2236	2250	20
v -O-H stretching vibration	2343	2344	2341	2347	2345	19
-C—H stretching vibration	2827	2887	2886	2890	2895	17
-O-H stretching vibration	3553	3096	3276	3327	3260	11

The SEM image (Fig. 2) of FA demonstrates particles of different shapes and sizes, hollow cenospheres, irregularly shaped unburned carbon particles, miner aggregates and agglomerated particles whereas the typical SEM image of TFA-1000 shows different shape and size particles while irregular shaped unburned carbon is not seen. Some fused silica particles are showing which has been formed during thermal activation [11].

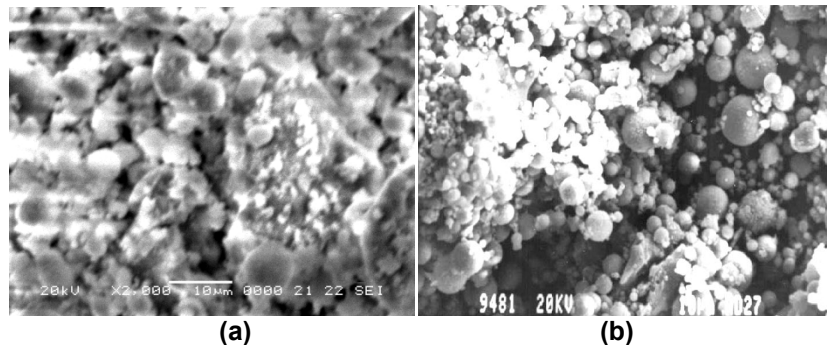


Fig. 2. SEM images of (a) FA (b) TFA-1000

The XRD patterns of FA and TFA-1000 are shown in Fig. 3. In both FA and TFA-1000, peaks at 2θ values of 16.4° , 25.9° and 26.2° show presence of mullite (alumino-silicate)

phases and quartz (silica) exhibits strong peaks at 20.7°, 26.5°, 26.66°, 40.66° and 49.96° of 2θ values [26] while calcite shows peaks at 33.4° of 2θ values [11]. TFA-1000 shows number of crystalline phases like quartz, hematite, mullite, calcite in higher intensities than FA, due to high temperature calcination. With thermal activation magnetite peak tends to disappear while a peak responsible for hematite begins to appear (Table 3) [27].

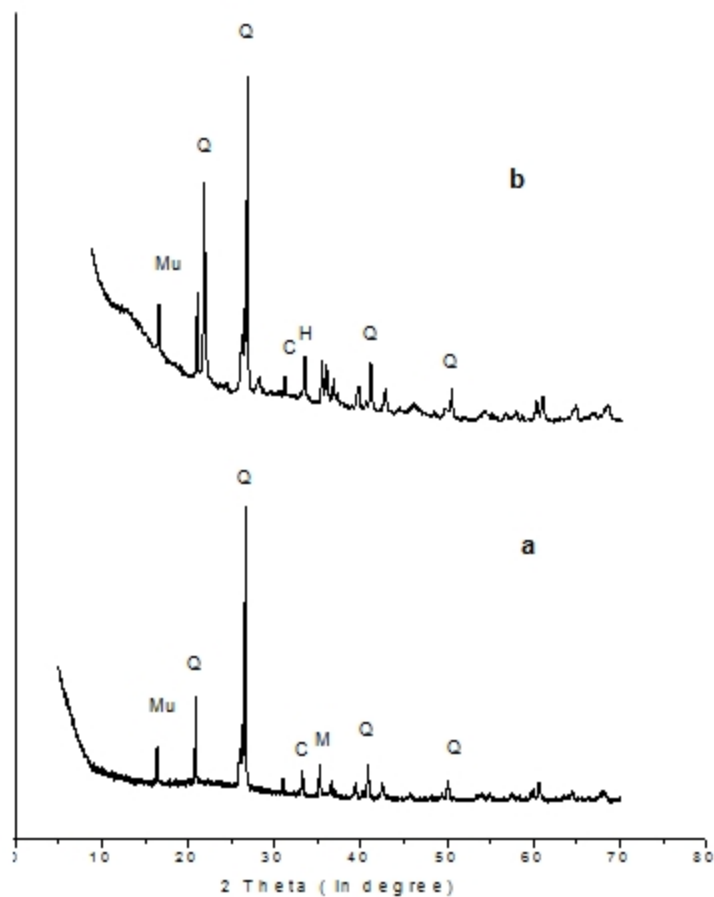


Fig. 3. XRD pattern of (a) FA (b) TFA-1000; (Q- Quartz, Mu- Mullite, M- Magnetite, H- Hematite, C- Calcite)

Table 3. Color and crystalline phases of FA and TFA samples

Sample	Color	Quartz	Magnetite	Hematite	Mullite	Calcite
FA	Grey	√	√	---	√	√
TFA-400	Light grey	√	√	---	√	√
TFA-600	Yellowish brown	√	√	---	√	√
TFA-800	Yellowish brown	√	---	√	√	---
TFA-1000	Reddish brown	√	---	√	√	---

(√ = Present, --- = Absent)

Variation of colors and crystalline phases of FA and TFA calcined at different temperatures is shown in Table 3. Initially fly ash was of grey color due to presence of unburned carbon content with increase in thermal activation temperature grey color of fly ash changes to yellowish brown and then finally red brown possibly due to hematite crystallization [8].

4. CONCLUSION

In each DR/FTIR spectrum broad band ranging from 3000-3400 cm^{-1} is showing a successive decrement in the intensity with increasing thermal activation temperature. It is thus revealed that as the temperature increases, physically adsorbed water is removed first, then silanol groups on surface is dehydrated resulting in transformation of Q^3 units $[\text{Si}(\text{OH})(\text{SiO}_4)_3]$ to Q^4 units $[\text{Si}(\text{SiO}_4)_4]$. Due to thermal activation of fly ash, SiO_2 , Al_2O_3 are increased which is also evidenced by increased intensity of quartz and mullite phases, the magnetite phases are converted into hematite phase at higher temperature. It can be concluded that modification in properties of fly ash with reference to Si-OH, intensity and crystallinity of crystalline phases can be achieved by thermal activation method to generate a solid support material for catalytic applications.

ACKNOWLEDGEMENT

SEM and XRD characterizations were performed at UGC-DAE Consortium for Scientific Research, Indore. The authors are thankful to Dr. D.M. Phase and Er. V.K. Ahiray for SEM-EDX analysis and Dr. Mukul Gupta for XRD analysis. The authors are also thankful to SAIF, Punjab University for their XRF facility. Stuti katara is thankful to University Grants Commission, New Delhi, India for their financial support through Senior Research Fellowship scheme.

COMPETING INTERESTS

Authors have declared that no competing interests exist.

REFERENCES

1. Yao ZT, Xia MS, Ye Y, Zhang L. Synthesis of zeolite Li-ABW from fly ash by fusion method. *J Hazard Mater.* 2009;170(2):639-44. doi:10.1016/j.bbr.2011.03.031.
2. Senapati MR. Fly ash from thermal power plants - waste management and overview. *Curr Sci.* 2011;100(12).
3. Kutchko BG, Kim AG. Fly ash characterization by SEM-EDS. *Fuel.* 2006;85(17):2537-44. doi:10.1016/j.fuel.2006.05.016.
4. American Society for Testing and Materials (ASTM), ASTM C618 – 12a, "Standard specification for coal fly ash and raw or calcined natural pozzolan for use in concrete", Annual book of ASTM standards, Vol.04.02, Philadelphia, Pennsylvania, 1994.
5. Blanco F, Garcia MP, Ayala J. The effect of mechanically and chemically activated fly ashes on mortar properties. *Fuel.* 2006;85(14):2018–26. doi:10.1016/j.fuel.2006.03.031.
6. Sahu S, Majling J. Preparation of sulphoaluminate belite cement from fly ash. *Cem Concr Res.* 1994;24(6):1065-72. doi:10.1016/0008-8846(94)90030-2.
7. Scheetz BE, Earle R. Utilization of fly ash. *Curr Opin Solid State Mater Sci.* 1998;3(5):510-20. doi:10.1016/S1359-0286(98)80017-X.

8. Temuujin J, Riessen AV. Effect of fly ash preliminary calcination on the properties of geopolymer. *J Hazard Mater*. 2009;164:634–39. doi:10.1016/j.jhazmat.2008.08.065.
9. Van Jaarsveld JSG, Van Deventer JSJ, Lukey GC. The characterisation of source materials in fly ash-based geopolymers. *Mater Lett*. 2003;57(7):1272–80. doi: 10.1016/S0167-577X(02)00971-0.
10. Gray ML, Champagne KJ, Soong Y, Killmeyer RP, Maroto-Valer MM, Andresen JM et al. Physical cleaning of high carbon fly ash. *Fuel Process Technol*. 2002;76(1):11–21. doi:10.1016/S0378-3820(02)00006-1.
11. Khatri C, Rani A. Synthesis of a nano-crystalline solid acid catalyst from fly ash and its catalytic performance. *Fuel*. 2008;87(13):2886–92. doi:10.1016/j.fuel.2008.04.011.
12. Jain D, Rani A. MgO enriched coal fly ash as highly active heterogeneous base catalyst for Claisen-Schmidt condensation reaction. *Am Chem Sci J*. 2011;1(2):37-49.
13. Peng L, Qisui W, Xi L, Chaocan Z. Investigation of the states of water and OH groups on the surface of silica. *Colloids and Surfaces A: Physicochem Eng Aspects*. 2009;334:112–15. doi:10.1016/j.colsurfa.2008.10.028.
14. Kordatos K, Gavela S, Ntziouni A, Pistiolas KN, Kyritsi A, Rigopoulou VK. Synthesis of highly siliceous ZSM-5 zeolite using silica from rice husk ash. *Micropor Mesopor Mater*. 2008;115(1-2):189-96. doi:10.1016/S0167-577X(02)00971-0.
15. Richardson IG. The calcium silicate hydrates. *Cem Concr Res*. 2008;38:137–58.
16. Palomo A, Grutzeck MW, Blanco MT. Alkali-activated fly ashes a cement for the future. *Cem Concr Res*. 1999;29:1323-29.
17. Saikia BJ, Parthasarthy G, Sarmah NC, Baruah GD. Fourier-transform infrared spectroscopic characterization of naturally occurring glassy fulgurites. *Bull Mater Sci*. 2008;31(2):155–58.
18. Morten ES, Camilla S, Li Z, Sogaard EG. Xps and Ft-Ir Investigation of Silicate Polymers. *J Mater Sci*. 2009;44:2079–88. doi:10.1007/s10853-009-3270-9.
19. Zaki MI, Knozinger H, Tese B, Mekhemer GAH. Influence of phosphonation and phosphation on surface acid–base and morphological properties of CaO as investigated by in situ FTIR spectroscopy and electron microscopy. *J colloid Interface Sci*. 2006;303(1):9-17. doi: 10.1016/j.jcis.2006.07.011.
20. Sun XH, Wang SD, Wong NB, Ma DDD, Lee ST, Teo BK. FTIR spectroscopic studies of the stabilities and reactivities of hydrogen-terminated surfaces of silicon nanowires. *Inorg Chem*. 2003;42(7):2398-404. doi:10.1021/ic020723e.
21. Blanco F, Garcia MP, Ayala J. Variation in fly ash properties with milling and acid leaching. *Fuel*. 2005;84(1):89-96. doi:10.1016/j.fuel.2004.05.010.
22. Jacox EM. Vibrational and Electronic Energy Levels of Polyatomic Transient Molecules Supplement B. *J Phys Chem Ref Data*. 2003;32(1). doi: 10.1063/1.1497629.
23. Handa H, Baba T, Sugisawa H, Ono Y. Highly efficient self-condensation of benzaldehyde to benzyl benzoate over KF-loaded alumina. *J Mol Catal A Chem*. 1998;134(1):171-77. doi:10.1016/S1381-1169(98)00033-8.
24. Frances IH, Denisse VA, Meghan EG. High temperature aerogels in the Al₂O₃-SiO₂ system. Presented at the American chemical society 236th national meeting Philadelphia, Pa, August 20, 2008. Accessed 24 May 2013. Available: <http://usrp.usra.edu/technicalPapers/glenn/arrandaAug08.pdf>.
25. Temuujin J, Okada K, Kenneth JDM. Preparation and properties of potassium aluminosilicate prepared from the waste solution of selectively leached calcined kaolinite. *Appl Clay Sci*. 2002;21:125–31. doi:10.1016/S0169-1317(01)00082-5.
26. Sharma A, Srivastava K, Devra V, Rani A. Modification in Properties of Fly Ash through Mechanical and Chemical Activation. *Am Chem Sci J*. 2012;2(4):177-87.

27. Fox JM. Changes in fly ash with thermal treatment. Presented in 2005 World of Coal Ash (WOCA), April 11-15,2005, Lexington, Kentucky, USA. Accessed 24 May 2013. Available: <http://www.flyash.info/2005/132fox.pdf>.

© 2013 Katara et al.; This is an Open Access article distributed under the terms of the Creative Commons Attribution License (<http://creativecommons.org/licenses/by/3.0>), which permits unrestricted use, distribution, and reproduction in any medium, provided the original work is properly cited.

Peer-review history:

The peer review history for this paper can be accessed here:
<http://www.sciencedomain.org/review-history.php?iid=245&id=7&aid=1733>

**International Journal of Innovative Research in Science,
Engineering and Technology**

(An ISO 3297: 2007 Certified Organization)

Vol. 2, Issue 9, September 2013

Characterization and Study of Turkish Perlite

Sakshi Kabra¹, Stuti Katara², Ashu Rani^{3*}

Research Scholar, Department of Pure and Applied Chemistry, University of Kota, Kota, Rajasthan, India¹

Research Scholar, Department of Pure and Applied Chemistry, University of Kota, Kota, Rajasthan, India²

Head, Department of Pure and Applied Chemistry, University of Kota, Kota, Rajasthan, India^{3*}

Abstract: An examination of the structural, morphological and mineralogical features of Turkish perlite sample was carried out by FT-IR, SEM, SEM-EDX, XRD, TGA and N₂-adsorption-desorption analytical techniques. Perlite is a natural, silica enriched igneous rock. This article features the primary step of study of basic characterization of perlite to investigate its utilization in different areas. Higher silica and alumina content was shown by EDX analysis. Both XRD and FT-IR studies reveal the presence of amorphous silica in perlite. TGA and LOI analysis illustrate the presence of water in the sample. The irregular morphology was exposed through SEM images. It was evident from the results that silica-enriched perlite could be developed further into a potential material in several area including catalyst synthesis by using various activation techniques.

Keywords: perlite, characterization, XRD, FT-IR.

I. INTRODUCTION

The basic objective of this paper is to provide the comprehensive characterization of Turkish perlite and suggest its suitability towards several fields of utilization. Perlite is a hydrated, widely occurring amorphous igneous rock formed by cooling of volcanic eruptions. Its unique structure consists of numerous concentric layers having SiO₂, Al₂O₃, K₂O and Na₂O as major constituents while TiO₂, CaO, MgO, Fe₂O₃ and hydrated water as well as unburned carbon remain present in varying quantities [1]. On heating the perlite to its softening range, i.e., above 850°C, crystalline water molecules vaporize and escape resulting in unusual expansion of perlite up to 7-16 times of its original volume, creating inert, non-toxic, lightweight particles with specific surface area of about 1.22 m²g⁻¹ [2], density in the range of 0.6 - 2.30 gm⁻¹ [3] and particle size in range of 0.2-4 mm. [4]. Physio-chemical properties of perlite need to be examined prior to evaluation of its possible utilization in various fields. As far as applications of perlite are concerned, it is mainly consumed as fillers, filter aids, in producing building construction materials [5], [6], adsorptive materials, precursor for geo-polymer formation [7], removal of heavy metal ions and other pollutants from atmosphere [8], in thermal insulation [9], removal of dyes [10], [11], in horticulture [12], sorption of oil [4] etc. Perlite is a naturally occurring waste, estimating about 700 million tons worldwide reserves. Turkey has rich resources of perlite, approximately 160 tons [13], since, domestic demand is very limited, so, most of the produced perlite is exported to various countries including India. Thus its effective, conducive and eco-friendly utilization has always been a challenge for scientific community. Above applications could thrive up to only some level in utilizing the huge reserves of perlite. However, the search of new applications of the perlite as either catalyst or catalyst support material is still enduring. Literature accounts only for the few applications of perlite as photo catalyst [14], pyrolysis catalyst [15] and catalyst used for different chemical reactions such as, immobilization [16], methacrolein production [17], zeolite synthesis [18], [19] etc.

The objective of the present work is to characterize perlite, in terms of structure, mineralogical composition, chemical behaviour, colour and morphology. This is the foundation stone in our research work to investigate the physio-chemical properties of perlite for its utilization in different fields. This paper mainly deals with identification of

International Journal of Innovative Research in Science, Engineering and Technology

(An ISO 3297: 2007 Certified Organization)

Vol. 2, Issue 9, September 2013

characteristics of perlite and their study using spectroscopic and microscopic analysis through FT-IR, SEM, SEM-EDX, XRD, TGA and N₂-adsorption-desorption techniques.

II. EXPERIMENTAL

A. Materials

Perlite sample was imported from Turkey and supplied to us by Indica Chem. Ind. Pvt. Ltd., India.

B. Procedure

Perlite sample was taken as such and thermally treated in a muffle furnace under static conditions at 800°C for 3 h and named as TAP.

C. Characterization

Physiochemical properties of perlite and TAP were studied by FT-IR, SEM and SEM-EDX, XRD, TGA, and N₂ adsorption-desorption studies.

The FT-IR study of the sample was done by Bruker FT-IR Spectrophotometer (TENSOR 27) in DRS mode by mixing samples with KBr in 1:20 weight ratio. The spectra were recorded in the range 550-4000 cm⁻¹ with a resolution of 4 cm⁻¹. SEM (Model-JEOL-JSM 5600) was used to investigate morphology and surface texture of the sample while elemental analysis was studied by SEM-EDX analysis (Model-INCA Oxford). X-ray diffraction study was done by X-ray powder diffractometer (Bruker D8 Advance) using Cu K_α radiation ($\lambda = 1.5406\text{\AA}$). The samples were scanned in 2 θ range of 5-65° at a scanning rate of 0.04°s⁻¹. TGA of the sample was carried out using Mettler Toledo thermal analyser (TGA/DSC1 SF/752), by heating the sample in the range of 50–850 °C with a heating rate of 10 °C/min under nitrogen flow (50 cm³/min). BET surface area of the samples was measured at liquid nitrogen temperature (77 K) using Quantachrome NOVA 1000e surface area analyser. The samples were degassed under vacuum at 120 °C for 2 h, prior to measurement.

III. RESULTS AND DISCUSSION

Perlite is white or light-gray coloured material which turns to light pinkish on thermal treatment. FT-IR spectrum of perlite and TAP (Fig. 1) shows a broad band between 3600-3300 cm⁻¹, which is attributed to surface –OH groups of –Si-OH and water molecules adsorbed on the surface. The broadness of band indicates the presence of strong hydrogen bonding in the sample [20]. The hydroxyl groups exist in higher degree of association with each other which results in extensive hydrogen bonding, while in FT-IR spectrum of TAP, the intensity and broadness of band is decreased which confirms the loss of water (Fig. 1b). The strong band at 1178 cm⁻¹ is due to the structural siloxane framework, which is the vibrational frequency of the Si-O-Si bond. The peak is shifted to higher wave number, i.e., 1192 cm⁻¹ after thermal treatment, which is normally observed in amorphous silica samples [21]. An intense peak at 1633 cm⁻¹ in the spectrum of perlite is attributed to bending mode ($\delta_{\text{O-H}}$) of water molecule [22], which is again highly decreased in case of TAP. The region around 805 cm⁻¹ is characteristic of Si-O-Si symmetric stretching modes [23], [24]. Amorphous silica exhibited a relatively strong peak at about 800 cm⁻¹ and it can be distinguished from the band of crystalline silicate [25]. The observed frequencies of IR bands of perlite and their possible assignments are summarized in Table 1.

**International Journal of Innovative Research in Science,
Engineering and Technology**

(An ISO 3297: 2007 Certified Organization)

Vol. 2, Issue 9, September 2013

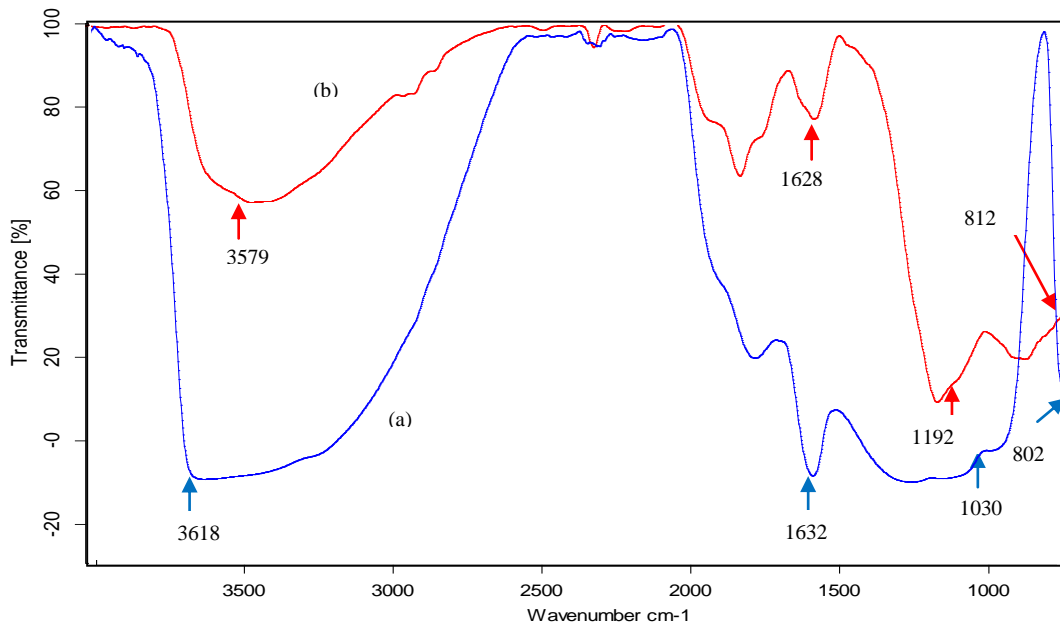


Fig 1. FT-IR spectrum of (a) perlite and (b) TAP

Table I. The Observed Frequencies of IR Bands of Perlite, TAP and their Possible Assignments

Assignments	Wave number(cm ⁻¹)	
	Perlite	TAP
Si-O-Si symm. stretching vib.	802	812
Si-O-Si asymm. stretching vib.	1030	1192
-O-H bending vib.	1632	1628
-O-H stretching vib.	3618	3579

SEM micrograph of perlite and its magnified view (Fig. 2 a and b) revealed the irregular morphology of perlite particles with broken or ragged edges. Similar pattern was observed in other reported micrographs of perlite [7]. SEM images of TAP and its magnified view (Fig. 3 a and b) are mainly fragmentic and random as a result of thermal activation [4]. But here, the morphology is less irregular which confirms the evaporation of water from the perlite sample on heating at high temperature.

**International Journal of Innovative Research in Science,
Engineering and Technology**

(An ISO 3297: 2007 Certified Organization)

Vol. 2, Issue 9, September 2013

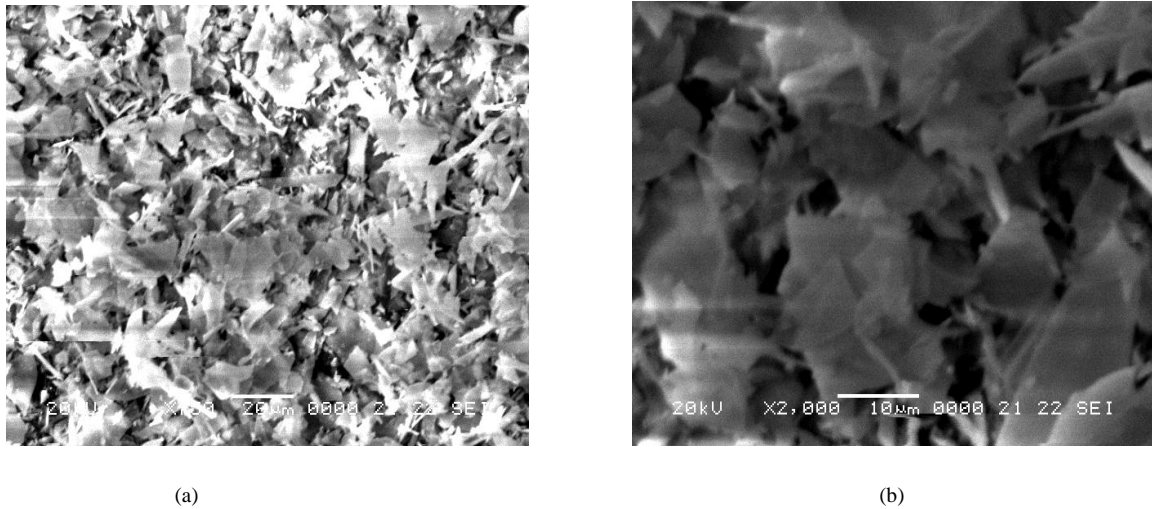


Fig 2. SEM micrograph of (a) perlite and (b) its magnified view

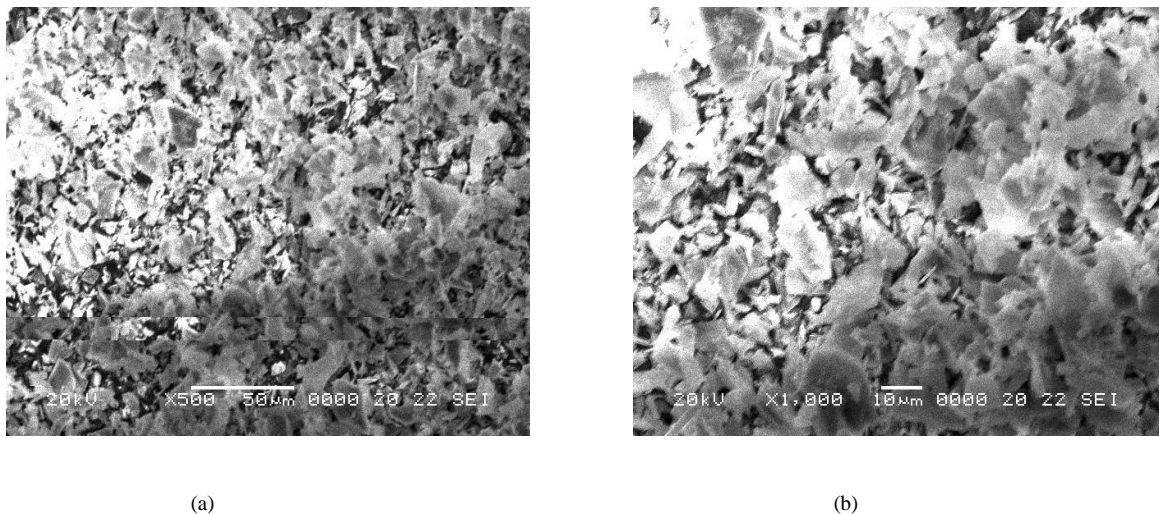


Fig 3. SEM micrograph of (a) TAP and (b) its magnified view

The chemical composition of perlite and TAP were determined by SEM-EDX technique which is shown in Table 2.

Table II. EDX Analysis of Perlite and TAP

Samples	O(wt%)	Si(wt%)	Al(wt%)	K(wt%)	Na(wt%)	Zn(wt%)	Fe(wt%)	Ti(wt%)	S(wt%)	LOI
Perlite	73.70	18.83	3.72	1.44	1.91	0.22	0.10	0.07	-	4.1
TAP	73.60	18.80	3.70	1.34	1.91	0.22	0.10	0.07	-	-

Loss on ignition (LOI) was determined by heating a certain weighed quantity of perlite in muffle furnace at 800°C for 3 h. The LOI amount was 4.1 wt % which corresponds to the removal of moisture and coexisting unburned carbon from sample [26]. The TGA curve of perlite, as shown in Fig. 4, shows continuous decrease in weight of sample from 50-

**International Journal of Innovative Research in Science,
Engineering and Technology**

(An ISO 3297: 2007 Certified Organization)

Vol. 2, Issue 9, September 2013

900°C. Weight loss in lower temperature range relates to the removal of moisture content of the sample together with some volatile materials. While, the weight loss of sample within range of 550-900°C would correspond to the burning of carbonaceous materials that were firmly adsorbed on the surface of the solid materials remaining or volatilization of some trace metal oxides [27].

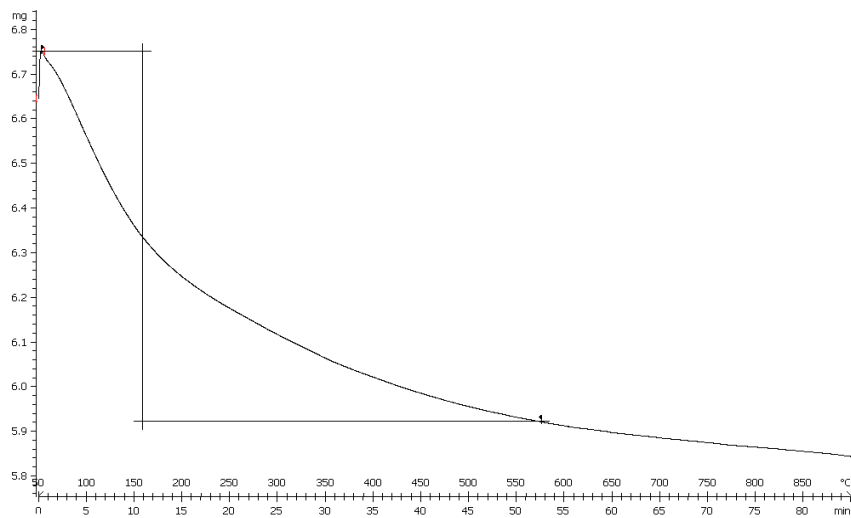


Fig 4. TGA curve of perlite

BET surface area of perlite and TAP samples were found to be 2.6 and 2.3 m²/g respectively.

The broad powder X-ray diffraction pattern of perlite (Fig. 5a), confirmed the absence of any ordered crystalline structure [28] which is typical for amorphous solids. However, heating of perlite at temperature over 800°C for 3 h could convert less ordered structure to a more highly ordered structure and a single crystalline peak appears at 2θ = 27.642° (Fig. 5b) which shows presence of quartz in the sample [29], along with a broad peak at 2θ = 22-23° confirming amorphous nature of silica [24], [30].

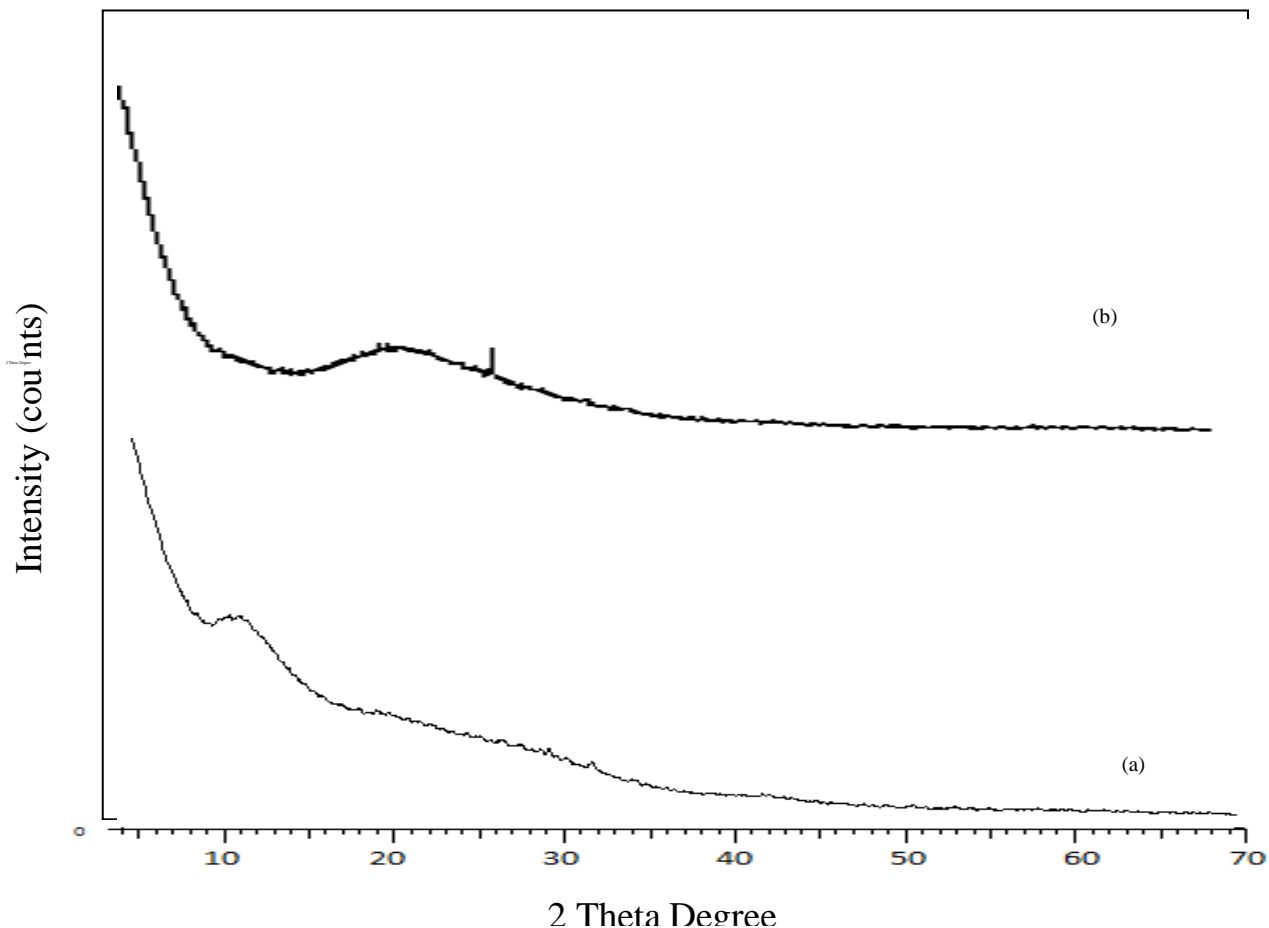


Fig 5. X-ray diffraction pattern of (a) Perlite and (b) TAP

IV. CONCLUSIONS

Results obtained in the present investigation confirm silica and alumina as major constituents of perlite. It is also observed that the nature of silica in perlite is mainly amorphous with irregular morphology and only a single crystalline peak appears on thermal treatment. On the basis of analysis, it can also be said that high number of hydroxyl groups and Si-O-Si network is also present in perlite. Moreover, comparison of perlite with TAP shows the effects of thermal treatment on structure, mineralogy, colour, surface area and morphology of perlite. The contemporary report aims at study of fundamental characteristics of perlite for its further applications in novel fields. The results like presence of amorphous silica network and surface hydroxyl groups in perlite indicate towards the potential capability of perlite as a support material in catalyst synthesis.

International Journal of Innovative Research in Science, Engineering and Technology

(An ISO 3297: 2007 Certified Organization)

Vol. 2, Issue 9, September 2013

ACKNOWLEDGEMENT

The authors are thankful to Dr. Mukul Gupta, Dr. D.M. Phase, Er. V.K. Ahiray from UGC-DAE CSR Lab, Indore, India for XRD and SEM, SEM-EDX respectively. The financial support was provided by Fly Ash Mission, DST, New Delhi, India. The authors are also grateful to UGC, New Delhi, India for their Junior Research Fellowship scheme.

REFERENCES

- [1] Dogan, M., Alkan, M., Cakir, U., "Electrokinetic Properties of Perlite", *J. Colloid Interface Sci.* Vol. 192, pp.114-18, 1997.
- [2] Dogan, M., Alkan, M., "Adsorption kinetics of methyl violet onto perlite", *Chemosphere*, Vol.50, pp.517-28, 2003.
- [3] Roulia, M., Chassapis, K., Kapoutsis, J.A., Kamitsos, E.L., Savvidis, T., "Influence of thermal treatment on the water release and the glassy structure of perlite", *J. Mater. Sci.*, Vol.41, pp.5870-81, 2006.
- [4] Bastani, D., Safekordi, A.A., Alihosseini, A., Taghikhani, V., "Study of oil sorption by expanded perlite at 298.15 K", *Sep. Purif. Technol.*, Vol.52, pp.295-300, 2006.
- [5] Morsy, M.S., Shebl, S.S., Abd El Gawad Saif, M., "Development of perlite-gypsum-slag-Lime sludge-composite system for building application", *Building Research Journal*, Vol.56, pp.49-58, 2008.
- [6] Aglan, H., Morsy, M., Allie, A., Fouad, F., "Evaluation of fiber reinforced nanostructured perlite-cementitious surface compounds for building skin applications", *Construction and Building Materials*, Vol.23 (1), pp.138-45, 2009.
- [7] Vance, E.R., Perera, D.S., Imperia, P., Cassidy, D.J., Davis, J., Gourley, J.T., "Perlite Waste as a Precursor for Geopolymer Formation", *Journal of the Australian Ceramic Society*, Vol.45 (1), pp.44-49, 2009.
- [8] Mostaedi, M.T., Ghassabzadeh, H., Maragheh, M.G., Ahmadi, S.J., Taheri, H., "Removal of cadmium and nickel from aqueous solution using expanded perlite", *Brazilian Journal of Chemical Engineering*, Vol.27 (2), pp. 299-308, 2010.
- [9] Vaou, V., Panias, D., "Thermal insulating foamy geopolymers from perlite", *Miner. Eng.*, Vol.23 (14), pp.1146-51, 2010.
- [10] Vijaykumar, G., Dharmendirakumar, M., Renganathan, S., Sivanesan, S., Baskar, G., Elango, K.P., "Removal of Congo Red from Aqueous Solutions by Perlite", *Clean- Soil, Air, Water*, Vol.37 (4-5), pp.355-64, 2009.
- [11] Dogan, M., Alkan, M., "Removal of methyl violet from aqueous solution by perlite", *J. Colloid Interface Sci.*, Vol.267 (1), pp. 32-41, 2003.
- [12] Silber, A., Bar-Yosef, B., Levkovitch, I., Kautzky, L., Minz, D., "Kinetics and mechanisms of pH-dependent Mn (II) reactions in plant-growth medium", *Soil Biol. Biochem.*, Vol. 40, pp. 2787-95, 2008.
- [13] Celik, A.G., Kilic, A.M., Cakal, G.O., "Expanded perlite aggregate characterization for use as a lightweight construction raw material", *Physicochem. Probl. Miner. Process.* Vol. 49 (2), pp. 689-700, 2013.
- [14] Hosseini, S.N., Borghei, S.M., Vossoughi, M., Taghavinia, N., "Immobilization of TiO₂ on perlite granules for photocatalytic degradation of phenol", *Appl. Catal., B*, Vol. 74 (1-2), pp. 53-62, 2007.
- [15] Balat, M., "Diesel-like Fuel Obtained by Catalytic Pyrolysis of Waste Engine Oil", *Energy, Exploration and Exploitation*, Vol. 26 (3), pp. 197-208, 2008.
- [16] Jafarzadeh, N.K., Sharifnia, S., Hosseini, S.N., Rahimpour, F., "Statistical optimization of process conditions for photocatalytic degradation of phenol with immobilization of nano TiO₂ on perlite granules", *Korean J. Chem. Eng.*, Vol. 28 (2), pp. 531-38, 2011.
- [17] Schlaefer, Francis, W., Hansen, A., "Methacrolein production utilizing novel Catalyst", George, *US Patent*, 05/428, pp. 150, 1978.
- [18] Kongkachuichay, P., Lohsoontorn, P., "Phase Diagram of Zeolite Synthesized from Perlite and Rice Husk Ash", *Science Asia*, Vol. 32, pp. 13-16, 2006.
- [19] Wang, P., Shen, B., Shen, D., Peng, T., Gao, "Synthesis of ZSM-5 zeolite from expanded perlite/kaolin and its catalytic performance for FCC naphtha aromatization", *J. Catal. Commun.*, Vol. 8 (10), pp. 1452-56, 2007.
- [20] Silverstein, R.M., Webster, F.X. *Spectrometric Identification of Organic Compounds*, Sixth ed., John Wiley Pub., Wiley India Pvt. Ltd., pp. 88., 2006.
- [21] Adam, F., Balakrishnan, S., Wong, P.L., "Rice Husk Ash Silica as a Support Material for Ruthenium based Heterogenous Catalyst", *Journal of Physical Science*, Vol. 17 (2), pp. 1-13, 2006.
- [22] Khatri, C., Rani, A., "Synthesis of a nano-crystalline solid acid catalyst from fly ash and its catalytic performance", *Fuel*, Vol. 87, pp. 2886-92, 2008.
- [23] Kabra, S., Sharma, A., Katara, S., Hada, R., Rani, A., "DRIFT- spectroscopic study of modification of surface morphology of perlite during thermal activation", *Indian Journal of Applied Research*, Vol. 3 (4), pp. 40-42, 2013.
- [24] Javed, S.H., Naveed, S., Feroze, N., Zafar, M., Shafaq, M., "Crystal and Amorphous Silica from KMnO₄ treated and untreated Rice Husk Ash", *Journal of Quality and Technology Management*, Vol. 6 (1), pp. 81-90, 2010.
- [25] Ojima, J., "Determining of Crystalline Silica in Respirable Dust Samples by Infrared Spectrophotometry in the Presence of Interferences", *J. Occup. Health*, Vol. 45, pp. 94-103, 2003.
- [26] Kordatos, K., Gavela, S., Ntziouni, A., Pistiolas, K.N., Kyritsi, A., Kasselouri-Rigopoulou, V., "Synthesis of highly siliceous ZSM-5 zeolite using silica from rice husk ash", *Microporous Mesoporous Mater.*, Vol. 115 (1-2), pp. 189-96, 2008.
- [27] Sekkina, M.M.A., Issa, R.M., El-Deen, A., Bastawisy, M., El-Helece, W.A., "Characterization and Evaluation of Thermodynamic Parameters for Egyptian Heap Fired Rice Straw Ash (RSA)", *Int. J. Chem.*, Vol. 2 (1), pp. 81-88, 2010.
- [28] Kalapathy, U., Proctor, A., Shultz, J., "A simple method for production of pure silica from rice hull ash", *Bioresour. Technol.*, Vol. 73, pp. 257-62, 2000.
- [29] Jain, D., Khatri, C., Rani, A., "Synthesis and characterization of novel solid base catalyst from fly ash", *Fuel*, Vol. 90, pp.2083-88, 2011.
- [30] Amutha, K., Ravibaskar, R., Sivakumar, G., "Extraction, Synthesis and Characterization of Nanosilica from Rice Husk Ash", *International Journal of Nanotechnology and Applications*, Vol. 4 (1), pp. 61-66, 2010.

**International Journal of Innovative Research in Science,
Engineering and Technology**

(An ISO 3297: 2007 Certified Organization)

Vol. 2, Issue 9, September 2013

BIOGRAPHY



Mrs. Sakshi Kabra is pursuing Ph.D. from Department of Pure and Applied Chemistry, University of Kota, Kota (Rajasthan). She secured All India Rank 385 in National Eligibility Test (June-2009) and acquired UGC-JRF. She is currently working as UGC-SRF in the department. Her research interests mainly include synthesis of heterogeneous acid catalysts and their various applications, solid waste management, material synthesis etc.



Ms. Stuti Katara is doing Ph.D. from Department of Pure and Applied Chemistry, University of Kota, Kota (Rajasthan). She got all India Rank 353 in National Eligibility Test (June-2009) and attained UGC-JRF. She is associated with solid base catalysis, green catalysis etc. and presently working as UGC-SRF in the department.



Prof. Ashu Rani is Head, Department of Pure and Applied Chemistry, Dean of post graduate departments and Convenor of various boards at University of Kota, Kota (Rajasthan). Several research scholars are pursuing M. Phil and Ph. D. under her guidance. Her wide research interests involve Heterogeneous Catalysis, Waste management, climate change, Lithospheric salt transport kinetics, Nanotechnology, Material Synthesis. She is associated with several National and International Collaborations and is a Principle Investigator of several projects funded by central and state governments.



Acid Activated fly Ash, as a Novel Solid Acid Catalyst for Esterification of Acetic Acid

KEYWORDS

Fly ash; Mechanical activation; Chemical activation; Acid treatment

Anita Sharma

Stuti Katara

Department of Pure and Applied Chemistry, University of Kota-324005, Rajasthan, India

Department of Pure and Applied Chemistry, University of Kota-324005, Rajasthan, India

Sakshi Kabra

Ashu Rani

Department of Pure and Applied Chemistry, University of Kota-324005, Rajasthan, India

Department of Pure and Applied Chemistry, University of Kota-324005, Rajasthan, India

ABSTRACT An efficient solid acid catalyst (AAFA) has been synthesized by mechanical and thermal activation of F-type fly ash (SiO_2 and $\text{Al}_2\text{O}_3 > 70\%$) followed by chemical activation using concentrated HCl at 110°C . The activation of fly ash resulted in increased silica content (79%) and surface area ($5.42 \text{ m}^2/\text{g}$) having sufficient silanol activity for esterification of n-butanol. The Catalyst was characterized by XRD, FT-IR, and SEM techniques. The product n-butyl acetate is an important fine chemical intermediate, widely used in pharmaceutical and as flavoring agent in confectionary. The catalyst was completely recyclable without significant loss in activity up to five reaction cycles, which confers its stability during reaction. The work reports an innovative use of solid waste fly ash as an effective solid acid catalyst.

1. Introduction

Acid catalyzed esterification is one of the most important industrial reactions, which are widely employed in synthetic organic process industries. Generally n-butyl esters of acetic acid are prepared under liquid phase, refluxing the reactant in the presence of small amount of concentrated H_2SO_4 , HCl , HI , AlCl_3 , BF_3 , ZnCl_2 , SbF_5 phosphoric acid and p-toluenesulfonic acid as the catalyst in homogenous systems [1]. The use of the above mentioned catalysts is undesirable from the environmental point of view as these chemicals are corrosive and generally encounter the problems of handling and transportation. Moreover reusability of the catalysts cannot be expected. For this purpose, the solid acid catalysts are employed as safe alternatives for conventional liquid acid catalysts in synthetic organic chemistry. Solid acids such as zeolites (ZSM-5), Metal oxides viz. Al_2O_3 , SiO_2 , ZrO_2 , ZrO_2 - Al_2O_3 , ZrO_2 - SiO_2 and their sulphated forms have been extensively studied as possible alternatives to conventional Lewis/Brønsted acid catalysts for esterification reaction [2,3].

A number of solid acids such as ion exchange resin eg. Amberlyst 15, smopex-101 [4,5], mesoporous molecular sieves like mesoporous Al-MCM-41, H-Mordenite [6], H-beta [7], H-ZSM-5 and HY zeolites [8,9], solid super acids [10] and heteropolyacids (salts), lipase, sulfonic acids supported on molecular sieves, active carbon [11-13], niobic acid and supported heteropoly acids (eg. $\text{H}_4\text{SiW}_{12}\text{O}_{40}/\text{ZrO}_2$), -alumina-supported vanadium oxide catalysts, sulfated zirconia and tetravalent metals acid salts [14], hafnium (IV) and zirconium (IV) salts [15], $\text{Zr}(\text{SO}_4)_2 \cdot 4\text{H}_2\text{O}$ [16] and modified zirconia catalyst have also been found to be acidic in nature and catalyze esterification, alkylation and condensation reactions [17,18]. In our previous work, fly ash has been used for developing several solid acid catalysts by loading cerium triflate, sulphated zirconia and used for the synthesis of aspirin, oil of wintergreen, 3, 4-dimethoxyacetophenone (anti neoplastic) and diphenylmethane [19-21].

The present work elaborates the synthesis of AAFA catalyst to have high acidity and catalytic activity for esterification reaction to produce n-butyl acetate with high yield and purity up to four reaction cycles. This investigation brings into light the structural aspects of a solid acid which exhibit good conversion and yield of an industrially important chemical "n-

butyl acetate" an important chemical intermediate, widely used in pharmaceutical and as flavoring agent in confectionary, under solvent free conditions and in low cost route.

2. Experimental methods

2.1 Materials

Class-F type fly ash was collected from Kota Thermal Power Plant, Kota (Rajasthan) HCl (98%); Acetic acid (98%) and n-butyl alcohol (99%) were purchased from S. D. Fine Chem. Ltd. and were used as such.

2.2 Catalyst Synthesis

As received fly ash was ball milled (1h at room temperature) followed by thermal activation at 900°C for 4h. The chemical activation of mechanically activated fly ash (MFA) was carried out in a stirred reactor by stirring 5M aqueous solution of mineral acid (HCl) in the ratio of 1:2 (FA: HCl) for 5 days at 110°C temperature followed by washing till pH 7.0 with complete removal of soluble ionic species (Cl^- , NO_3^- , SO_4^{2-} , ClO_4^- etc.) and drying at 110°C for 24h. The obtained solid acid catalyst (AAFA) was calcined at 500°C for 4h under static condition in a muffle furnace.

2.3 Characterization Techniques

2.3.1. Physicochemical properties of AAFA

The silica content of the fly ash samples after mechano-chemical activations were analyzed by X-ray fluorescence spectrometer (Philips PW1606). Powder X-ray diffraction studies were carried out by using (Philips X'pert) analytical diffractometer with monochromatic $\text{CuK}\alpha$ radiation ($k = 1.54056 \text{ \AA}$) in a 2θ range of 0 - 80° . The FT-IR study of the samples was done using FT-IR spectrophotometer (Tensor-27, Bruker, Germany) in DRS (Diffuse Reflectance Spectroscopy) system. The detailed imaging information about the morphology and surface texture of the sample was provided by SEM-EDAX (Philips XL30 ESEM TMP).

2.3.2. Catalytic activity

The esterification of n-butanol with acetic acid was performed in liquid phase batch reactor consisting of 50 ml round bottom flask with condenser in a constant temperature oil bath with magnetic stirring. A mixture of acetic acid and n-butanol (molar ratio of n-butanol and acetic acid is = 1:2)

were taken in a 50 ml round bottom flask. The catalyst (substrate to catalyst ratio = 10), activated at 500°C for 2h was added in the reaction mixture. After completion of the reaction the catalyst was filtered and the product was analyzed by Gas Chromatograph.

2.3.3 Catalyst regeneration

The spent catalyst was washed with acetone, dried in oven at 110°C for 12h followed by calcinations at 500°C for 2 h and reused for next reaction cycle under similar reaction conditions as earlier.

3. Result and Discussion

3.1 Catalyst Characterization

A comparison of FA, MFA, TFA and AAFA catalyst is given in Table 1, which shows that after mechanical activation BET surface area is increased from 0.97 m²/g to 2.57 m²/g, which is further increased to 5.42 m²/g after chemical activation. This result confirms that the AAFA catalyst has a higher specific surface area of 5.42 m²/g than the heat-treated fly ash with 2.99 m²/g [22, 23]. The particle diameter is reduced from 37.7 μm to 3.12 μm during milling, increased slightly (3.71 μm) after chemical activation [24]. The mechanical activation did not indicate any perceptible change in silica content of fly ash but the chemical activation increased the silica amount greatly (58% to 79%) [25].

Table 1: Physico-chemical properties of FA, MFA, TFA and AAFA catalyst.

Catalyst	Silica (Wt %)	Crystallite size (nm)	BET surface area (m ² /g)	Particle diameter (μm)
FA	58	33	0.97	37.7
MFA	59	21	2.57	3.12
TFA	70	18	2.99	3.10
AAFA	79	16	5.42	3.71

FA (Fly ash); MFA (mechanically activated fly ash); TFA (thermally activated fly ash) and AAFA (chemically activated fly ash).

The XRD pattern of the FA showed (figure 1a) the presences of quartz, mullite, iron oxide, hematite, sulfur oxide, small amounts of magnetite [26], CaO and amorphous phases. The XRD studies of milled fly ash (figure 1b) indicate that decrease in crystallite size from 33 to 21 nm results in increased amorphous content in it but after thermal activation the crystallinity is increased slightly as indicated by higher peak intensities in Figure 1b and c. [27]. After chemical activation of thermally activated fly ash, the crystallinity is further decreased due to removal of most of the crystalline components present in FA, thus increasing the amorphous nature [28, 29].

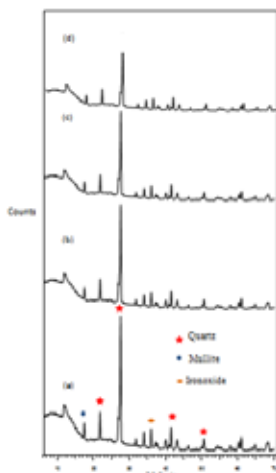


Figure 1: X-ray diffraction pattern of (a) FA (b) MFA (c) TFA and (d) AAFA catalyst.

The FT-IR spectra of FA, MFA, TFA and AAFA in Figure 2a-d show broad band between 3500-3000 cm⁻¹, which is attributed to surface -OH groups of Si-OH and adsorbed water molecules on the surface. The increment in broadness after ball milling is an evidence for the breaking down of the quartz structure and formation of Si-OH groups [30]. However, FT-IR studies clearly show changes in the broadening of IR peaks corresponding to Si-O-Si asymmetric stretching vibrations indicating structural rearrangement during mechanical milling.

The FT-IR spectra of AAFA shows the tremendous increment in broadness at 3500-3000 cm⁻¹ region as compared with FA, MFA and TFA which reflects strong hydrogen bonding between the hydroxyl groups due to increase in silica content and loss of significant amount of other components (Figure 2d). The increased amorphous silica in the activated fly ash can be characterized by an intense band in the range 1000-1300 cm⁻¹ corresponding to the valence vibrations of the silicate oxygen skeleton. The main absorption band of the valence oscillations of the groups Si-O-Si in quartz appears with a main absorption maximum at 1162 cm⁻¹ [20].

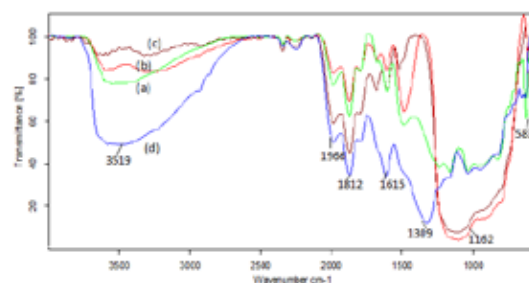


Figure 2: FT-IR of (a) FA (b) MFA (c) TFA and (d) AAFA catalyst.

SEM micrograph of the FA (Figure 3a) indicates that the most of the particles present in the fly ash are micro-particles in the shape of smooth balls (microspheres) with a relatively smooth surface grain. SEM image of MFA (Figure 3b) shows the structural break down of larger particles and increased surface roughness. The smooth spherical cenospheres are affected most resulting remarkable changes in morphology. After chemical activation with acid, rough cenospheres are transformed into agglomerations of more amorphous undefined shapes with no observation of crystal formation as seen in SEM micrographs presented in Figure 3a-d [31].

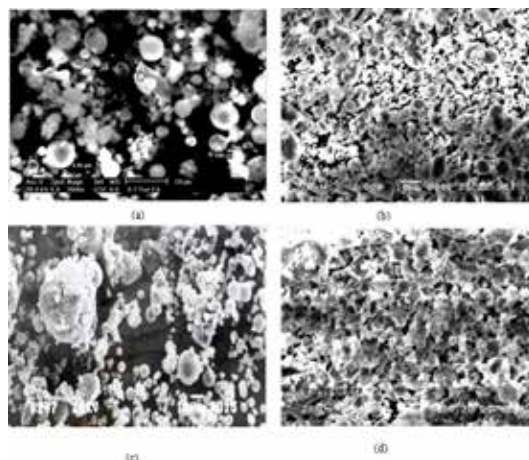


Figure 3: SEM images of (a) FA (b) MFA (c) TFA (d) AAFA.

4. Catalytic performance

To measure the catalytic performance of catalyst, esterification of acetic acid with 1-butanol over AAFA was carried out at 110°C for 4h, taking n-butanol/acetic acid molar ratio 1:2 and n-butanol to catalyst weight ratio of 10. The catalyst

AAFA was found highly active for esterification of acetic acid with 1-butanol giving high selectivity (99.6%) and yield of n-butyl acetate after 4h under optimized conditions, whereas both FA as well as MFA did not possess any catalytic activity.

The esterification of acetic acid with n-butanol was also carried out at different temperature ranging from 90°C to 130°C for 4h to optimize the reaction temperature giving maximum conversion of n-butanol to n-butyl acetate. The result shows that the maximum conversion (87.3%) of n-butanol to n-butyl acetate is found at 110°C, which remains almost, steady till 130°C. The spent catalyst from the reaction mixture was filtered, washed with acetone and regenerated at 450°C to use for the next reaction cycles. The catalyst was equally efficient up to five reaction cycles.

5. Conclusion

The study provides fly ash supported AAFA as an efficient solid acid catalyst possessing significant amount of acidity. The specific surface area of FA (0.97 m²/g) was greatly en-

hanced after mechanical, thermal and chemical activation using HCl. AAFA catalyst possessed surface area upto 5.42 m²/g with greater number of surface silanols responsible for surface acidity as evident by comparatively broad band at 3500-3000 cm⁻¹ in FT-IR spectra.

AAFA catalyst catalyzed the esterification of acetic acid with n-butanol giving high yield of the product n-butyl acetate in heterogeneous, solvent free optimized reaction conditions. It is concluded that the mechano-chemical activation can generate sufficient activity on fly ash surface rendering its potential application in heterogeneous catalysis.

6. Acknowledgement

The authors are thankful to Dr. D.D. Phase and Er. V.K. Ahiray for SEM-EDX analysis, conducted at UGC DAE-CSR Lab Indore. The financial support was provided by Fly Ash Unit, Department of Science and Technology, New Delhi, India, wide project sanction no. FAU/DST/600(23)/2009-10.

REFERENCE

1. Igbokwe, P.K., Ugonabo, V.I., Iwegbu, N.A., Akachukwu, P.C. and Olisa C.J., *Journal of university of chemical technology and metallurgy*, 43(3) (2008) 345-348.
2. Kuriakose, G., Nagaraju, N., *J. Mol. Cat. A: Chem.* 223 (2004) 155-159.
3. Mohamed Shamsuddin, S.Z., Nagaraju, N., *Cat. Comm.*, 7(2006) 593-599.
4. Blagova, S., Paradaa, S., Bailerb, O., Moritzb, P., Lamc, D., Weinandd, R., Hassea, H., *Chem. Eng. Sci.* 61 (2006) 753-765.
5. Zhang, Y., Ma L., Yang J., *React. Funct. Polym.* 6 (2004) 101-114.
6. Mbaraka, I.K., Shanks, B.H.J., *Cat.*, 229 (2005) 365-373.
7. Alvaro, M., Corma, A., Das D., Formés, V., Garcia, H., *J. Cat.*, 231 (2005) 48-55.
8. Kirumakki, S.R., Nagaraju, N., Narayanan, S., *Appl. Catal. A* 273 (2004) 1-9.
9. Rabindran, B., Jermy, A., *Journal of Molecular Catalysis A: Chemical* 237 (2005) 146-154.
10. Jiang, Y.X., Chen, X.M., Mo Y.F., Tong, Z.F., *J. Mol. Cat. A. Chem.*, 213 (2004) 231-234.
11. Abd, E.I., Wahab, M.M.M., Said A.A., *J. Mol. Catal. A. Chem.*, 240 (2005) 109-118.
12. Sepulveda, J.H., Yori J.C., Vera C.R., *Appl. Catal. A*, 288 (2005) 18-24.
13. Peres, C., Harper, N., Marco, D.R., da Silva, G., Bar reiros, S., *Enz. Micro. Tech.* 37(1) (2005) 145-149.
14. Mitran, G., Makó, E., Redey, A., Marcu, I. C., *Comptes Rendus Chimie*, 15(9) (2012) 793-798.
15. Ishihara, K., Nakayama, M., Ohara, S., Yamamoto, H., *Tetrahedron*, 58 (2002) 8179-8188.
16. Juan, J.C., Zhang, J.C., Yarmo, M.A., *Cat. Lett.* 117 (2007) 153-158.
17. Patel, H.K., Joshi, R.S., Chudasama, U.V., *Indian J. Chem.* 47 (2008) 348-352.
18. Dora, E., James, G., Goodwin, Jr., David, A., *Appl. Catal. A: Gen.* 339 (2008) 76-83.
19. Khatri, C., Jain, D., Rani, A., *Fuel*, 89(2012) 3853-3859.
20. Khatri, C., Mishra M., Rani, A., *Fuel Process. Technol.*, 91(10) (2010) 1288-1295.
21. Khatri, C., Rani, A., *Fuel* 87 (2008) 2886-2892.
22. Sarbak Z., Kramer-Wachowiak M., *Powder Technol.* 123 (2002) 53-8.
23. Penilla PR, Bustos AG, Elizalde SG. *Fuel* 85 (2006) 823-82.
24. Kumar S., Kumar R., (2010) The University of Wisconsin Milwaukee Centre for By-products Utilisation, Second International Conference on Sustainable Construction Materials and Technologies. June 28- June 30.
25. Blanco F, Garcia MP, Ayala J., *Fuel* 84 (2005) 89-96.
26. Bada S.O., Potgieter-Vermaak S., *J. Prac. Technol.* 12 (2008) 37-48.
27. John M.F., (2005), Changes in fly ash with thermal treatment. World of Coal Ash (WOCA), April 11-15; Kentucky, USA.
28. Blanco F, Garcia M.P., Ayala J., Mayoral G., Garcia M.A., *Fuel*, 85 (2006) 2018-2026.
29. Pengthamkeerati P., Satapanajaru T., Chularuengsoarn P., *Fuel*, 87 (2008) 2469-2476.
30. Patil, G.A., Anandhan, S., *International. J. Energy Eng.*, 2 (2012) 57-62.
31. Woolard, C.D., Petrus, K., van der Horst, M. *Water SA*, 26 (2002) 531-6.



DRIFT- Spectroscopic Study of Modification of Surface Morphology of Perlite During Thermal Activation

KEYWORDS

perlite, DRIFT, thermal activation.

Sakshi Kabra

Department of Pure and Applied Chemistry, University of Kota, Kota 324005, Rajasthan, India

Anita Sharma

Department of Pure and Applied Chemistry, University of Kota, Kota 324005, Rajasthan, India

Stuti Katara

Department of Pure and Applied Chemistry, University of Kota, Kota 324005, Rajasthan, India

Renu Hada

Department of Pure and Applied Chemistry, University of Kota, Kota 324005, Rajasthan, India

Ashu Rani

Department of Pure and Applied Chemistry, University of Kota, Kota 324005, Rajasthan, India

ABSTRACT

This article presents the use of diffuse reflectance infrared Fourier transform (DRIFT) spectroscopic technique in investigation of the effect of thermal activation on morphology of perlite. Perlite, a naturally occurring waste siliceous material formed by rapid cooling of volcanic eruptions was thermally treated over a range of temperatures. This study focuses on changes in both structure and chemical bonding of perlite due to thermal activation at different temperatures viz., 400, 600, 800, 1000°C for certain time period. The results reveal that on increasing temperature of thermal activation, loss of water occurs which is confirmed by decrease in intensity and broadness of the band, appears between 3600-3300 cm^{-1} , attributing to surface -OH groups. Other bands present in the DRIFT spectra shows the presence of Si-O-Si network and amorphous nature of silica in perlite.

Introduction

Infrared spectroscopy is a well established technique for the identification of chemical compounds and/or specific functional groups in compounds. An alternative is the use of Fourier Transform Infrared Spectroscopy (FTIR), which is both rapid, non-destructive and requires small, <1 mg, sized samples. Chemical bonds vibrate at a characteristic frequency representative of their structure, bond angle and length. Accordingly, individual molecules have the ability to interact with incident radiation by absorbing the radiation at specific wavelengths. FTIR spectroscopy takes advantage of this by recording the energy absorption of a sample over a range of frequencies. Diffuse reflectance infrared Fourier transform (DRIFT) spectroscopy in conjunction with other analytical techniques has been extensively applied over the years to explore the structure and bonding in amorphous siliceous materials [1]. This technique has proved to be a powerful method to identify the isolated and H-bonded hydroxyl groups on surface of silica [2,3].

R.L. Frost et al. [4] proposed that DRIFT spectroscopy is more applicable than transmission infrared spectroscopy for powdered samples because it provides a rapid technique for analyzing samples without any interference through sample preparation, suitable for the study on the hydroxyl stretching region of silicate minerals. DRIFT had several other advantages including ease of sample preparation, greater number of useful bands and the ability to detect both major and minor components from the same spectra.

Perlite is a hydrated, naturally occurring amorphous volcanic glass formed by cooling of volcanic eruptions, estimating about 700 million tonnes worldwide reserves. Its unique structure consists of numerous concentric layers having SiO_2 , Al_2O_3 , K_2O and Na_2O as major constituents while TiO_2 , CaO , MgO , Fe_2O_3 and hydrated water as well as unburned carbon remain present in varying quantities [5]. On heating the perlite to its softening range, i.e., above 850°C, water molecules vaporize and escape resulting in unusual expansion of perlite up to 7-16 times of its original volume,

creating inert, non-toxic, lightweight particles with specific surface area of about $1.22 \text{ m}^2\text{g}^{-1}$ [6], density in the range of 0.6 - 2.30 gml^{-1} [7] and particle size in range of 0.2-4 mm. [8]. As far as applications of perlite are concerned, it is mainly consumed as fillers, filter aids, in producing building construction materials [9,10].

In the current work, perlite was thermally treated at different temperatures viz., 400, 600, 800 and 1000°C for 3 h and then analyzed by DRIFT spectroscopy. The purpose of this investigation is to use DRIFT spectroscopy to characterize the structure and determine the chemical bonding of silica with other species present in the perlite, so that it can be further utilized for various applications in future.

Material

Perlite sample was supplied by Indica Chem. Ind. Pvt. Ltd., India.

Experimental

Perlite sample was then thermally treated in a muffle furnace under static conditions over a range of temperatures, 400, 600, 800 and 1000°C for 3h and abbreviated as TAP-400, TAP-600, TAP-800 and TAP-1000 respectively. The DRIFT spectroscopic study of the samples was done by Bruker FT-IR Spectrophotometer (SENSOR 27) in DRS (diffuse reflectance system) mode by homogenizing samples thoroughly with spectroscopic grade KBr in 1:20 weight ratio. The samples were crushed in an agate mortar. The spectra were recorded in the range $550\text{-}4000 \text{ cm}^{-1}$ with a resolution of 4 cm^{-1} .

Results and discussion

The colour change is seen in perlite from light grey to white-light pink on thermal treatment at higher temperature. The chemical composition of perlite was determined by EDX analysis which is shown in Table 1. Loss on ignition (LOI) was determined by heating a certain weighed quantity of perlite in muffle furnace at 1000°C for 3 h. The LOI amount was 4.4 wt % which corresponds to the removal of moisture and coexisting unburned carbon from sample [11].

Table 1. EDX analysis of perlite.

Samples	O(wt%)	Si(wt%)	Al(wt%)	K(wt%)	Na(wt%)	Zn(wt%)	Fe(wt%)	Ti(wt%)	S(wt%)	LOI
Perlite	73.70	18.83	3.72	1.44	1.91	0.22	0.10	0.07	-	4.4

LOI- Loss on ignition

The FT-IR spectrum of perlite and thermally activated perlite at different temperatures

(Fig. 1) confirmed that the calcination at any conditions in this experiment produced dehydroxylation in the perlite samples i.e. elimination of the -OH stretching from Si-OH [12,13]. In this fig., a broad band between 3600-3300 cm^{-1} is shown, which is attributed to surface -OH groups of -Si-OH and water molecules adsorbed on the surface. The broadness of band indicates the existence of hydroxyl groups in higher degree of association with each other which results in extensive hydrogen bonding [14], while in FT-IR spectra of thermally activated perlite samples, the intensity and broadness of band is decreased, confirming the loss of water, which is highest in case of TAP-1000 (Fig. 1e). The strong band at 1030 cm^{-1} is due to the structural siloxane framework, which is the vibrational frequency of the Si-O-Si bond. The peak gets shifted to higher wave number, i.e., 1227 cm^{-1} after thermal treatment in TAP-1000 (fig. 1e), normally observed in amorphous silica samples [15]. An intense peak at 1632 cm^{-1} in the spectrum of perlite is attributed to bending mode (δ_{OH}) of water molecule, is again highly decreased in case of TAP-1000. The shoulder at about 3200 cm^{-1} (fig. 1a) could be assigned to the stretching vibrations of Si-OH groups in the structure of amorphous SiO_2 [16]. An intense band in the range of 1300-1100 cm^{-1} , corresponding to valence vibrations of the silicate oxygen skeleton is usually assigned to the amorphous silica content. The region around 805 cm^{-1} is characteristic of Si-O-Si symmetric stretching modes [17,18,19]. In the Si-O stretching vibration region (800–1195 cm^{-1}), the bands at 802, 808, 812, 942, 1050 cm^{-1} are identical to the bands at 800, 958, 1088 cm^{-1} due to amorphous silica [20]. Amorphous silica exhibited a relatively strong peak at about 800 cm^{-1} and it can be distinguished from the band of crystalline silicate [20]. The structure of most SiO_2 is polymorphous, both crystalline and amorphous, based on tetrahedral unit of silicon coordinated to four oxygen atoms. In the Si-O-Si bending vibration region (400–700 cm^{-1}) of quartz, the band at 695 cm^{-1} is determinative whether it is crystalline or amorphous [21]. The band at 695 cm^{-1} appears due to the vibrations in octahedral site symmetry [22]. In the amorphous state this band will be missing. In the perlite samples, we did not get this band which indicates that the silica mineral in this sample is in amorphous form. Another evidence of the presence of amorphous silica in perlite sample is the appearance of a peak at about 1100 cm^{-1} , which is normally assumed to be formed by continuous network of Q^4 species, characteristic in case of amorphous silica [23].

The major component of perlite is silica and untreated silica is totally hydroxylated and the hydroxyl layer is covered with physically adsorbed water. Thermal treatment of the support leads first to removal of water (dehydration) and then to combination of adjacent hydroxyl groups to form water (dehydroxylation) [24].

Fig. 2 shows the magnified FT-IR spectra of all studied samples in the range between 550-1750 cm^{-1} .

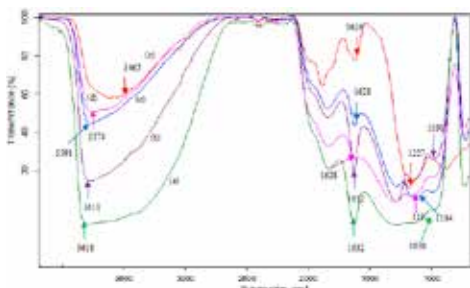


Fig 1. FT-IR spectrum of (a) perlite, (b) TAP-400, (c) TAP-600, (d) TAP-800 and (e) TAP-1000.

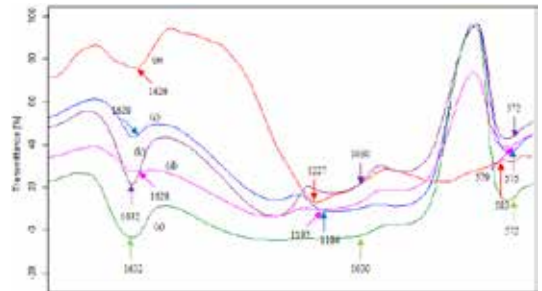


Fig 2. Magnified FT-IR spectrum of (a) perlite (b) TAP-400 (c) TAP-600 (d) TAP-800 and (e) TAP-1000

The observed frequencies of IR bands of all samples and their possible assignments are summarized in Table 2.

Table 2. The observed frequencies of IR Bands of all samples and their possible assignments

Assignments	Perlite	TAP-400	TAP-600	TAP-800	TAP-1000
Si-O-Si symm. stretching vib.	802	802	808	812	942
Si-O-Si asymm. stretching vib.	1030	1030	1184	1192	1227
Si-O-Si bending vib.	572	572	575	579	583
-O-H bending vib. H-O-H bending vib.	1632	1632	1628	1628	1626 1626
-O-H stretching vib. -O-H stretching vib.	3618	3611	3591	3579	3465

Conclusions

Results found in this paper showed that DRIFT can be successfully employed in investigation of the effect of thermal treatment on perlite morphology. After calcination, physically adsorbed water gets driven away from the surface, so intensity of -OH stretching and bending bands decreases. The present spectroscopic study could be useful in understanding characteristic features of amorphous silica, changes occurred in its structure and chemical bonding because of thermal treatment. This knowledge may be employed in further utilization of perlite for several applications.

Acknowledgement

The authors are thankful to DST Lab, Deptt. Of Pure & Applied Chemistry, University of Kota, for providing DRIFT spectroscopic facility. The authors are also grateful to University Grants Commission, New Delhi, India for their Junior Research Fellowship scheme.

REFERENCE

1. A. Hamoudi, L. Khouchaf, C. Depecker, B. Revel, L. Montagne and P. Cordier, *J. Non-crystalline Solids*, 354 (2008) 5074–78. | 2. R.K. Iller, *The Chemistry of Silica*, John Wiley & Sons, New York, 1979. | 3. H. E. Bergna. In *the colloid chemistry of silica* (ed. H.E. Bergna), American Chemical Society, 1994. | 4. R. L. Frost, U. Johansson, *Clays and Clay Minerals* 46 (1998) 466. | 5. M. Dogan, M. Alkan, U. Cakir, *J. Colloid Interface Sci.* 192 (1997) 114-118. | 6. M. Dogan, M. Alkan, *Chemosphere*, 50 (2003) 517-528. | 7. M. Roulia, K. Chassapis, J. A. Kapoutsis, E. I. Kamitsos, T. Savvidis, *J. Mater. Sci.*, 41 (2006) 5870-81. | 8. D. Bastani, A.A. Safekordi, A. Alihosseini, V. Taghikhani, *Sep. Purif. Technol.*, 52 (2006) 295-300. | 9. M.S. Morsy, S.S. Shebl SS, M. Abd El Gawad Saif, *Building Research Journal*, 56 (2008) 49-58. | 10. H. Aglan, M. Morsy, A. Allie, F. Fouad, *Construction and Building Materials*, 23(1) (2009) 138-145. | 11. K. Kordatos, S. Gavala, A. Ntziouni, K.N. Pistiolas, A. Kyritsi, V. Kasselouri-Rigopoulou, *Microporous Mesoporous Mater.*, 115(1-2) (2008) 189-196. | 12. C. Belver, M.A.B Munoz and M.A.Vicente. *Chem. Mater.*, 14 (2002) 2,033-43. | 13. R.A. Shawabkeh and M.F. Tutunji. *Clay Sci.*, 24 (2003) 111-120. | 14. R.M. Silverstein, F.X. Webster, *Spectrometric Identification of Organic Compounds*, Sixth ed., John Wiley Pub., 2006, pp. 88. | 15. F. Adam, S. Balakrishnan, P.L. Wong, *Journal of Physical Science*, 17(2) (2006) 1–13. | 16. S. Music, N.F. Vincekovic, L. Sekovanic, *Brazilian Journal of Chemical Engineering*, 28(1) (2011) 89-94. | 17. S.H. Javed, S. Naveed, N. Feroze, M. Zafar, M. Shafaq, *Journal of Quality and Technology Management*, 6(1) (2010) 81-90. | 18. K. Amutha, R. Ravibaskar, G. Sivakumar, *International Journal of Nanotechnology and Applications*, 4(1) (2010) 61-66. | 19. J.P. Nayak, J. Bera, *Trans. Indian Ceram. Soc.*, 68 (2) (2009) 1-4. | 20. J. Ojima, *J. Occup. Health* 45 (2003) 94-103. | 21. G. Parthasarathy, A.C. Kunwar and R. Srinivasan, *Eur. J. Mineral.* 13 (2001) 127. | 22. H. Schneider, *Contrib. Miner. Petr.* 43 (1974) 233. | 23. F.I. Hurwitz, D.V. Aranda and M.E. Gallagher, Presented at the 236th National Meeting, American Chemical Society, Philadelphia, PA (2008) | 24. B.M. Reddy, G.K. Reddy, K.N. Rao, A. Khan, I. Ganesh, *J. Mol. Catal. A: Chem.*, 265 (2007) 276-82.



Synthesis of Nanosized Titania by sol Gel Route

KEYWORDS

Titania; Sol gel; Ethylene glycol; Anatase

Renu Hada

Department of Pure and applied Chemistry, University of Kota, Kota (Raj), India

Sakshi Kabra

Department of Pure and applied Chemistry, University of Kota, Kota (Raj), India

Stuti Katara

Department of Pure and applied Chemistry, University of Kota, Kota (Raj), India

Ashu Rani

Department of Pure and applied Chemistry, University of Kota, Kota (Raj), India

Vijay Devra

Jankidevi Bajaj Government Girls College, Kota (Raj), India.

S. S. Amritphale

Advanced Materials & Processes Research Institute (CSIR), Hoshangabad Road, Bhopal (M.P), India.

ABSTRACT The main objective of this work was to prepare anti-pollutant and photocatalyst. Titanium dioxide nanoparticles by simple ethylene glycol route to synthesize titanium dioxide nanoparticles at industrial level. In this work TiO_2 was prepared by sol-gel route in presence of titanium n-butoxide (TNBT) as TiO_2 precursor, n-butanol as dilutant and EG as solvent and chelating agent. The X-ray diffraction and scanning electron microscopy studies show that the product has anatase crystal structure with average particle size 20-50 nm. The nanoparticles thus prepared can be used for gas sensing and biological applications, also as photo-electrodes for dye-sensitized solar cells and in removing the organic chemicals which occur as pollutants in wastewater effluents from industrial and domestic sources.

Introduction

Nanosized titania has been the subject of a great deal of research because of their unique physicochemical properties and applications in the areas of pigments, catalysts and supports, cosmetics, gas sensors, inorganic membranes, environmental purification, and dielectric materials [1-9]. Much interest has been shown in photochemical reactions on nanosized titania particles due to their potential application in the conversion of solar energy into chemical energy [10-13] and electric energy [14, 15]. When titania powder is irradiated with photon energy larger than the band-gap energy, electrons (e^-) and holes (h^+) are generated in the conduction band and the valence band, respectively. These electrons and holes are thought to have the respective abilities to reduce and oxidize chemical species adsorbed on the surfaces of titania particles [16]. The uses and performance for a given application are, however, strongly influenced by the crystalline structure, the morphology, and the size of the particles. It is well known that titania exists in three kinds of crystal structures namely anatase, rutile and brookite. Anatase and brookite phases are thermodynamically metastable and can be transformed exothermally and irreversibly to the rutile phase at higher temperatures. The transition temperatures reported in the literature ranges from 450 to 1200 °C. The transformation temperature depends on the nature and structure of the precursor and the preparation conditions [17, 18]. Among the three kinds of crystal structures of Titania, anatase TiO_2 has been widely used as a well known catalyst, because of its various merits, such as electronic and optical properties, non-toxicity, high photocatalytic activity, low cost, and chemical stability [19-23]. A number of methods for the synthesis of TiO_2 nanoparticle have been reported, such as chemical precipitation [24], microemulsion [25], hydrothermal crystallization [26] and sol-gel [27]. The sol-gel process is the most successful for preparing nanosized metal oxide semiconductors. For example, sol-gel derived TiO_2 powders have been reported to show high catalytic activity due to their fine structure, wide surface area and high porosity. Thus in this research work we have prepared titania by sol gel route using ethylene glycol as gelling agent and titanium n-butoxide as titania precursor.

Experimental Work

Titanium (IV)-n-butoxide (TNBT) (20 g) was added to n-butanol (16 g) and the mixture was stirred for 5 min using a magnetic stirrer operating at 2000 rpm. After stirring, above mixture was added to Ethylene glycol (100 ml) and mixture was stirred with heating at 850 °C till sol converted to gel then gel was dried in oven at 500 °C. Dried sample was calcined at 5000 °C for 3 h.

Results and discussion

The XRD pattern and SEM image of nanosized Titanium Oxide particles, prepared by EG route is shown in figure 1 and 2.

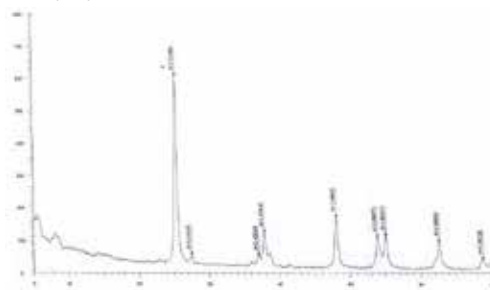


Figure 1. XRD patterns of nanosized titania obtained from sol gel route at 500 °C

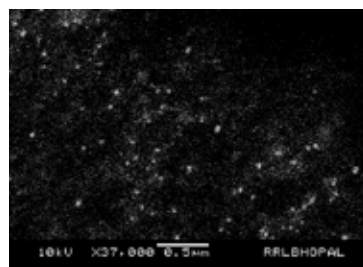


Figure 2. SEM photograph of nanosized titania obtained from sol gel route at 500 °C

The XRD patterns of the calcined sample of nanosized titania powder prepared using sol gel route is given in Figure 1. The presence of peaks of anatase titania at d' values 3.49, 1.88, 2.35 have been observed in XRD pattern. The d -values of the pattern recorded were compared and matched with the standard d -values along with the intensity given in JCPDS manuals. The average crystalline size of nanosized titania has been calculated by applying Scherrer's equation ($d = k / \cos \theta$) to the 100 % intensity peak and is found 19 nm. The prepared nanosized powder of TiO₂ was fired at 500 °C, leads to its conversion from amorphous phase to anatase phase.

The crystal size of the powder sample of TiO₂ is of 19 nm size as estimated by Scherrer equation. SEM photograph shows that particles are strongly aggregated which is typical for particles with a size less than 50 nm, so the particle size was estimated to be 20-50 nm.

Conclusion

We synthesized TiO₂ nanoparticles by sol gel route using ethylene glycol as gelling agent. The physical properties, such as crystallite size and crystallinity were investigated by XRD, and SEM. X-ray diffraction pattern shows that TiO₂ particles calcined at 500°C have a stable anatase phase with 19 nm average crystallite size, determined according to the Scherrer equation. The SEM image shows that particles have spherical shape. The yield of the prepared photocatalyst was comparatively higher than other methods used for nanoparticles preparation i.e. microemulsion route.

Acknowledgement

The authors are grateful to the Director, AMPRI, CSIR, Bhopal for encouragement of the present research work. The financial support was provided by Fly Ash Mission, Department of Science and Technology, New Delhi, India.

REFERENCE

1. T. Moritz, J. Reiss, K. Diesner, D. Su and A. Chemseddine, *J. Phys. Chem. B*, 1997, 101, 8052-8053.
2. J. Karch, R. Birrigger and H. Gleiter, *Nature*, 1987, 330, 556-558.
3. M. R. Hoffmann, S. T. Martin, W. Choi and D. W. Bahnemann, *Chem. Rev.*, 1995, 95, 69-96.
4. A. Fujishima and K. Honda, *Nature*, 1972, 238, 37-38.
5. M. A. Fox and M. T. Dulay, *Chem. Rev.*, 1993, 93, 341-357.
6. R. J. Gonzalez, R. Zallen and H. Berger, *Phys. Rev. B*, 1997, 55, 7014-7017.
7. K.-N. P. Kumar, K. Keizer and A. J. Burggraaf, *J. Mater. Chem.*, 1993, 3, 1141 - 1149.
8. R. Wang, K. Hashimoto, A. Fujishima, M. Chikuni, E. Kojima, A. Kitamura, M. Shimohigoshi and T. Watanabe, *Nature*, 1997, 388, 431-443.
9. P. A. Mandelbaum, A. E. Regazzoni, M. A. Blesa and S. A. Bilmes, *J. Phys. Chem. B*, 1999, 103, 5505-5511.
10. K. Fujiwara, T. Ohno, M. Matsumura, *J. Chem. Soc., Faraday Trans.*, 1998, 94, 3705-3709.
11. T. Ohno, K. Fujihara, K. Sarukawa, F. Tanigawa, M. Matsumura, *Z. Phys. Chem.*, 1999, 213, 165-174.
12. Z.G. Zou, H. Arakawa, *J. Photochem. Photobiol. A: Chem.*, 2003, 158, 145-162.
13. R. Abe, K. Sayama, H. Arakawa, *Chem. Phys. Lett.*, 2003, 371, 360-364.
14. J. Ye, Z. Zou, H. Arakawa, M. Oshikiri, M. Shimoda, A. Matsushita, T. Shishido, *J. Photochem. Photobiol. A: Chem.*, 2002, 148, 79-83.
15. B. O'Regan, M. Grätzel, *Nature*, 1991, 353, 737-740.
16. S. Kambe, S. Nakade, T. Kitamura, Y. Wada, S. Yanagida, *J. Phys. Chem. B*, 2002, 106, 2967-2972.
17. H. Goto, Y. Hanada, T. Ohno, M. Matsumura, *J. Catal.*, 2004, 225, 223-229.
18. V. Chhabra, V. Pillai, B.K. Mishra, A. Morrone, D.O. Shah, *Langmuir*, 1995, 11, 3307-3311.
19. A. Rammal, F. Brisach and M. Henry, *C. R. Chimie*, 2002, 5, 59-66.
20. P.V. Kamat, *Chem. Rev.*, 1999, 93, 267-300.
21. A. Mills, G. Hill, S. Bhopal, I.P. Parkin and S.A. O'Neill, *J. Photochem. Photobiol. A: Chemistry*, 2003, 160, 185-194.
22. P.S. Awati, S.V. Awate, P.P. Shah and V. Ramaswamy, *Catal. Comm.*, 2003, 4, 393-400.
23. R. Zhang, L. Gao and Q. Zhang, *Chemosphere*, 2004, 54, 405-411.
24. S. Jeon and P.V. Braun, *Chem. Mater.*, 2003, 15, 1256-1263.
25. Y. Bessekhoud, D. Robert and J.W. Veber, *J. Photochem. Photobiol. A: Chemistry*, 2003, 157, 47-53.
26. M.M. Yusuf, H. Imai and H. Hirashima, *J. Sol-Gel Sci. Technol.*, 2002, 25, 65-74.
27. Y. Diaoued, S. Badilescu, P.V. Ashirt, D. Bersani, P.P. Lottici and J. Robichaud, *J. Sol-Gel Sci. Technol.*, 2002, 24, 255-264.